Ontario

ONTARIO GEOLOGICAL SURVEY

Open File Report 6095

Precambrian Geology of Kitto, Eva, Summers, Dorothea and Sandra Townships, Northwestern Ontario: Phoenix Bedrock Mapping Project

by

T.R. Hart, M. terMeer and C. Jolette

2002

Parts of this publication may be quoted if credit is given. It is recommended that reference to this publication be made in the following form:

Hart, T.R., terMeer, M. and Jolette, C. 2002. Precambrian geology of Kitto, Eva, Summers, Dorothea and Sandra townships, northwestern Ontario: Phoenix Bedrock Mapping Project; Ontario Geological Survey, Open File Report 6095, 206p.

© Queen's Printer for Ontario, 2002

In partnership with FedNor and
En partenariat avec FedNor et
Industry Canada Industrie Canada
Canada

The Phoenix Bedrock Mapping Project is an economic development initiative supported by Industry Canada (FedNor), administered by the Lake Nipigon Heritage Authority and conducted by the Precambrian Geoscience Section of the Ontario Geological Survey.

© Queen's Printer for Ontario, 2002.

Open File Reports of the Ontario Geological Survey are available for viewing at the Mines Library in Sudbury, at the Mines and Minerals Information Centre in Toronto, and at the regional Mines and Minerals office whose district includes the area covered by the report (see below).

Copies can be purchased at Publication Sales and the office whose district includes the area covered by the report. Although a particular report may not be in stock at locations other than the Publication Sales office in Sudbury, they can generally be obtained within 3 working days. All telephone, fax, mail and e-mail orders should be directed to the Publication Sales office in Sudbury. Use of VISA or MasterCard ensures the fastest possible service. Cheques or money orders should be made payable to the *Minister of Finance*.

Mines and Minerals Information Centre (MMIC)
Macdonald Block, Room M2-17
900 Bay St.
Toronto, Ontario M7A 1C3
Tel: (416) 314-3800
1-800-665-4480(toll free inside Ontario)

Mines Library
933 Ramsey Lake Road, Level A3
Sudbury, Ontario P3E 6B5
Tel: (705) 670-5615

Publication Sales
933 Ramsey Lake Rd., Level A3
Sudbury, Ontario P3E 6B5
Tel: (705) 670-5691(local)
1-888-415-9845(toll-free)
Fax: (705) 670-5770
E-mail: pubsales@ndm.gov.on.ca

Regional Mines and Minerals Offices:

Kenora - Suite 104, 810 Robertson St., Kenora P9N 4J2
Kirkland Lake - 10 Government Rd. E., Kirkland Lake P2N 1A8
Red Lake - Box 324, Ontario Government Building, Red Lake P0V 2M0
Sault Ste. Marie - 70 Foster Dr., Ste. 200, Sault Ste. Marie P6A 6V8
Southern Ontario - P.O. Bag Service 43, Old Troy Rd., Tweed K0K 3J0
Sudbury - Level B3, 933 Ramsey Lake Rd., Sudbury P3E 6B5
Thunder Bay - Suite B002, 435 James St. S., Thunder Bay P7E 6S7
Timmins - Ontario Government Complex, P.O. Bag 3060, Hwy. 101 East, South Porcupine P0N 1H0
Toronto - MMIC, Macdonald Block, Room M2-17, 900 Bay St., Toronto M7A 1C3

This report has not received a technical edit. Discrepancies may occur for which the Ontario Ministry of Northern Development and Mines does not assume any liability. Source references are included in the report and users are urged to verify critical information. Recommendations and statements of opinions expressed are those of the author or authors and are not to be construed as statements of government policy.

If you wish to reproduce any of the text, tables or illustrations in this report, please write for permission to the Team Leader, Publication Services, Ministry of Northern Development and Mines, 933 Ramsey Lake Road, Level B4, Sudbury, Ontario P3E 6B5.

Cette publication est disponible en anglais seulement.

Parts of this report may be quoted if credit is given. It is recommended that reference be made in the following form:

Hart, T.R., terMeer, M. and Jolette, C. 2002. Precambrian geology of Kitto, Eva, Summers, Dorothea and Sandra townships, northwestern Ontario: Phoenix Bedrock Mapping Project; Ontario Geological Survey, Open File Report 6095, 206p.

Contents

Abstract xxiii

Introduction 1
- Acknowledgments 2
- Access 2
- Previous Geological Work 3
- Present Geological Survey 3
- Prospecting and Mining Exploration 4
- Physiography 7

General Geology 9
- Precambrian 12
  - Neoarchean 12
    - Mafic Metavolcanic Rocks 12
      - Massive Flows 12
      - Pillowed Flows 13
      - Volcaniclastic Rocks 14
      - Depositional Environment 15
    - Intermediate to Mafic Metavolcanic Rocks 15
      - Massive Flows 15
      - Pillowed Flows 16
      - Volcaniclastic Rocks 16
      - Depositional Environment 19
    - Intermediate to Felsic Metavolcanic Rocks 20
      - Massive Flows 20
      - Dikes 21
      - Volcaniclastic Rocks 22
      - Depositional Environment 22
    - Chemical Metasedimentary Rocks 22
      - Oxide-Facies Iron Formation (Magnetite-Chert) 22
      - Clastic-Magnetite-Argillite Iron Formation 23
      - Jasper-Hematite Banded Iron Formation 24
      - Chert 24
      - Actinolite-Magnetite Hornfels 25
    - Clastic Metasedimentary Rocks 25
      - Feldspathic Wacke 25
      - Lithic Wacke 26
      - Quartzose Wacke 26
      - Lithic Arenite 26
      - Siltstone and Argillite 27
      - Conglomerate 27
      - Depositional Environment 28
      - Quetico Subprovince 28
        - Depositional Environment 29

Synvolcanic to Syntectonic Mafic Intrusive Rocks 29
Synvolcanic to Syntectonic Intermediate to Felsic Intrusive Rocks 30
Posttectonic Mafic Intrusive Rocks 32
Proterozoic 34
Sibley Group Sedimentary Rocks 34
Ultramafic to Mafic Intrusive Rocks 34
Diabase Dikes 34
Ultramafic Intrusive Rocks 36
Wehrlite 37
Lherzolite 37
Olivine Gabbro 38
Nipigon Diabase Sills 38
Cenozoic 43
Quaternary 43
Pleistocene 43
Recent 43

Structural Geology 45
Primary Structures 45
Joints and Igneous Contacts 47
Tectonic Foliations 47
Folding 49
Faulting 53
North-Striking Faults 53
Regional Deformation Zones 53
Blackwater River Fault 53
Empire Fault and Princess Lake Fault 53
Standingstone Fault 54
Sandy Creek – Sandra Lake Fault 54
Poplar Point Assemblage Faults 54
Paint Lake Fault 55
Musca Lake Fault 55

Alteration and Metamorphism 56
Alteration 56
Axinite 59
Mineral Chemistry and Genesis 59
Discussion 61
Conclusions 64
Metamorphism 64

Geochemistry 67
Mafic Metavolcanic Rocks 67
Intermediate to Mafic Metavolcanic Rocks 74
Intermediate to Felsic Metavolcanic Rocks 76
Synvolcanic Mafic Intrusive Rocks 79
Synvolcanic Intermediate to Felsic Intrusive Rocks 80
Posttectonic Mafic Intrusive Rocks 81

103-00675/

- Proterozoic Mafic Intrusive Rocks 83
  - Diabase Dikes 83
  - Ultramafic Intrusive Rocks 85
    - Peridotite 85
    - Olivine Gabbro 92
  - Mafic Intrusive Rocks 95
    - Diabase Sills 95

Geochronology 100

Economic Geology 102
- Gold 103
- Sulphide Mineralization 104
  - Base Metals 104
    - Southern Metavolcanic Subbelt 105
    - Central Metavolcanic Subbelt 105
    - Northern Metavolcanic Subbelt 107
    - Southern Metasedimentary Subbelt 108
    - Proterozoic Ultramafic and Mafic Intrusive Rocks 108
  - Nickel–Copper 108
    - Diabase Sills 109
    - Peridotite – Olivine Gabbro 113
- Molybdenum 113
- Magnetite 113
- Hematite 114
- Platinum Group Elements 115

Mineral Occurrences 118
- Gold 120
  - Southern Metavolcanic Subbelt 121
    - Speke Point South 121
    - Speke Point Central 121
    - Speke Point North 122
    - C.J. Morgan 122
    - Gold Fields 123
    - Morgan South Extension 124
    - Rentz 124
    - Buffalo–Beardmore 125
    - Anglo–Beardmore 125
    - Holt 126
    - Summers Pipeline 126
  - Southern Metasedimentary Subbelt 126
    - Undersill Claims 126
    - Creek Vein 127
    - Sand River Mine 128
    - Leitch Mine 128

- Central Metavolcanic Subbelt ... 129
  - Calhet ... 129
  - Minnow Lake ... 129
  - Candela ... 130
  - Archie Lake ... 131
  - Coté–Archie Lake ... 131
- Northern Metavolcanic Subbelt ... 132
  - Dorothea Gold Property ... 132
- Poplar Point Assemblage ... 133
  - Johnson–Hopkins ... 133
  - Lawrence–McKirdy ... 133
- Paint Lake Deformation Zone ... 133
  - Placer Dome–Metalore ... 133
  - Holm ... 134
  - Mill City Gold ... 134

Base Metals ... 134
- Central Metavolcanic Subbelt ... 135
  - Eva Lake Property ... 135
- Southern Metasedimentary Subbelt ... 136
  - Princess Property ... 136

Molybdenum ... 136
- Northern Metavolcanic Subbelt ... 136
  - Tyson #3 ... 136

Platinum Group Elements ... 136
- Phoenix Occurrence ... 136

Recommendations For Mineral Exploration ... 137
- Gold Mineralization ... 137
- Volcanogenic Massive Sulphide Mineralization ... 138
  - Base Metals ... 138
- Base Metals and Gold Mineralization ... 138
- Platinum Group Element Mineralization ... 139

Appendix 1: Analytical Methods and Detection Limits ... 140

Appendix 2: Whole Rock Geochemical Analyses ... 142

Appendix 3: Normative Calculations ... 153

Appendix 4: Assay Results for Gold-Related Sampling. ... 159

Appendix 5: Assay Results for Base Metals-Related Sampling. ... 168

Appendix 6: Assay Results for Platinum Group-Related Sampling. ... 174

Appendix 7: Glossary of Abbreviations and Acronyms Used in This Report. ... 190

References ... 194

Metric Conversion Table ... 206

FIGURES

1. Map showing location of project area. The shaded area represents the approximate area that was burnt during a major forest fire in 1999. 1
2. Regional geology of the Beardmore–Geraldton Belt 2
3. Location of mineral occurrences in the southern metavolcanic subbelt, Summers and Kitto townships.... 4
4. Location of mineral occurrences in the southern metasedimentary subbelt and central metavolcanic subbelt, Eva and Summers townships 5
5. Location of mineral occurrences in Dorothea and Sandra townships 6
6. General geology of Kitto, Eva, Summers, Dorothea and Sandra townships, in the Beardmore–Geraldton area 8
7. Vertical longitudinal section showing attitude of diabase, Northern Empire Mine 35
8. Stereographic plots of S_0 bedding for a) metasedimentary rocks and b) volcanic rocks.......... 44
9. Stereographic plot of S_2 for a) cleavage and b) foliation 48
10. Detailed mapping near the Leitch Mine suggests a third tectonic fabric 49
11. Geographic sketch map showing location of major faults in the Beardmore–Geraldton Belt with respect to historical gold showings. 52
12. Location of axinite occurrences in the map area. 60
13. Location of geochemical samples within Kitto Township and from the ultramafic to mafic intrusions in Eva and Kitto townships 66
14. Location of lithogeochemical samples within Eva, Dorothea, and parts of Summers and Sandra townships collected during this mapping program, with additional unlabelled samples.......... 68
15. Nb/Y versus Zr/TiO_2 rock classification diagram with mafic, intermediate and felsic metavolcanic rocks and associated synvolcanic and posttectonic intrusive rocks 69
16. Ytterbium versus lanthanum chondrite-normalized diagram of mafic, intermediate and felsic metavolcanic rocks and associated synvolcanic and posttectonic mafic intrusive rocks 69
17. Mantle-normalized extended element diagram of mafic metavolcanic rocks 70
18. Nb/Y versus Zr/TiO_2 rock classification diagram with mafic and intermediate metavolcanic rocks.......... 70
19. Ytterbium versus lanthanum chondrite-normalized diagram of mafic and intermediate metavolcanic rocks overlain on the mafic, intermediate and felsic metavolcanic rocks and associated synvolcanic and posttectonic mafic intrusive rocks for comparison.......... 71
20. Mantle-normalized extended element diagram of mafic metavolcanic rocks 72
21. Ta/Yb versus Th/Yb tectonic discrimination diagram of mafic, intermediate and felsic metavolcanic rocks, the associated synvolcanic and the posttectonic mafic intrusive rocks.......... 72
22. Ta/Yb versus Th/Yb tectonic discrimination diagram of mafic and intermediate metavolcanic rocks....... 73
23. Mantle-normalized extended element diagram of the intermediate metavolcanic rocks 75
24. Mantle-normalized extended element diagram of intermediate metavolcanic rocks 75
25. Ytterbium versus La/Yb chondrite-normalized diagram with fields for felsic volcanic rocks.......... 77
26. Mantle-normalized extended element diagram of felsic metavolcanic rocks and felsic intrusive rocks..... 77
27. Continental-crust normalized extended element diagram of felsic metavolcanic and felsic intrusive rocks 78

28. Ta/Yb versus Th/Yb tectonic discrimination diagram of felsic metavolcanic and felsic intrusive rocks.... 78

29. Mantle-normalized extended element diagram of synvolcanic to syntectonic mafic intrusive rocks 79

30. Mantle-normalized extended element diagram of posttectonic mafic intrusive rocks 82

31. Nb/Y versus Zr/TiO_2 rock classification diagram with the Proterozoic diabase dikes, peridotite, olivine gabbro, and diabase sills 82

32. Ytterbium versus lanthanum chondrite-normalized diagram of the Proterozoic diabase dikes, peridotite, olivine gabbro, and diabase sills, overlain on the mafic, intermediate and felsic metavolcanic rocks and associated synvolcanic and posttectonic mafic intrusive rocks for comparison........ 84

33. Mantle-normalized extended element diagram of diabase dike rocks........ 84

34. Log zirconium versus log niobium diagram of the Proterozoic diabase dikes, peridotite, olivine gabbro, and diabase sills (this study), with the diabase (dolerite) samples overlain on the mafic, intermediate and felsic metavolcanic rocks and associated synvolcanic and posttectonic mafic intrusive rocks (this study) for comparison. 86

35. MgO versus CaO of the Proterozoic diabase dikes, peridotite, olivine gabbro, and diabase sills with ideal mineral chemistries, and the fields for diabase and peridotite 86

36. SiO_2 versus Al_2O_3 of the Proterozoic diabase dikes, peridotite, olivine gabbro, and diabase sills with the ideal mineral chemistries........ 87

37. Al_2O_3 versus Na_2O of the Proterozoic diabase dikes, peridotite, olivine gabbro, and diabase sills with the ideal mineral chemistries........ 87

38. Gd/Yb versus La/Sm diagram of the Proterozoic diabase dikes, peridotite, olivine gabbro, and diabase sills, and a feldspathic wacke of the southern metasedimentary belt (this study) with the fields for the Lower, Central and Upper suite basalts of the Osler Group........ 88

39. Ta/Yb versus Th/Yb tectonic discrimination diagram of the Proterozoic diabase dikes, peridotite, olivine gabbro, and diabase sills 88

40. Mantle-normalized extended element diagram of the peridotite and olivine gabbro........ 89

41. Zirconium versus yttrium diagram of the peridotites from Disreali, Seagull and Fox Mountain and the diabase samples, the samples for the Hele Township melanogabbro and olivine gabbro, and the fields for the Kitto Township diabase, peridotite and olivine gabbro........ 90

42. Gd/Yb versus La/Sm diagram of the diabase and Hele Township melanogabbro and olivine gabbro, and the fields for the Lower, Central and Upper suite basalts of the Osler Group........ 91

43. Mantle-normalized extended element diagram of the Hele Township melanogabbro and olivine gabbro with the fields for the Kitto Township peridotite and olivine gabbro 91

44. Thorium versus Th/Yb diagram with the Proterozoic diabase dikes, peridotite, olivine gabbro, and diabase sills, and a feldspathic wacke of the southern metasedimentary belt with the fields for the Lower, Central and Upper suite basalts of the Osler Group and trends for igneous processes 92

45. MgO, SiO_2, TiO_2, La/Sm, and Th/Nb versus approximate stratigraphic height for the eastern stratigraphic section through the peridotite and olivine gabbro 93

46. MgO, SiO_2, TiO_2, La/Sm, and Th/Nb versus approximate stratigraphic height for the western stratigraphic section through the peridotite and olivine gabbro 94

47. MgO, SiO_2, TiO_2, La/Sm, and Th/Nb versus approximate stratigraphic height for the southern stratigraphic section through the peridotite........ 94

48. Mantle-normalized extended element diagram of the diabase sills........ 96

49. MgO, SiO_2, TiO_2, La/Sm, and Th/Nb versus approximate stratigraphic height for the highway stratigraphic section through the diabase sill 97

50. MgO, SiO_2, TiO_2, La/Sm, and Th/Nb versus approximate stratigraphic height for the quarry stratigraphic section through the diabase sill 97
51. Mantle-normalized extended element diagram of the diabase sills chill samples 98
52. Mantle-normalized extended element diagram of the diabase sills chill samples 98
53. Location map of samples collected for radiometric age determinations 100
54. $^{207}Pb/^{235}U$ versus $^{206}Pb/^{238}U$ isochrons for sample 225 and for sample 229 101
55. Locations of significant base metal results discovered in Kitto Township 104
56. Locations of significant base metal results discovered in Eva and Summers townships 105
57. Locations of significant base metal results discovered in Dorothea and Sandra townships 106
58. SiO_2 versus La/Sm diagram with the Proterozoic diabase dikes, peridotite, olivine gabbro, and diabase sills, and a feldspathic wacke of the southern metasedimentary subbelt 110
59. MgO versus nickel diagram for the Proterozoic diabase dikes, peridotite, olivine gabbro, and diabase sills, and a feldspathic wacke of the southern metasedimentary subbelt with the igneous fractionation trend for an idealized sulphur-unsaturated magma 110
60. MgO versus log nickel diagram with the Proterozoic diabase dikes, olivine gabbro, and diabase sills, and a feldspathic wacke of the southern metasedimentary subbelt with the trends for sulphur-unsaturated within-plate basalt and upper crust 111
61. MgO versus copper diagram with the Proterozoic diabase dikes, peridotite, olivine gabbro, and diabase sills, and a feldspathic wacke of the southern metasedimentary subbelt 111
62. MgO, nickel and copper versus approximate stratigraphic height for the highway stratigraphic section through the diabase sill 112
63. MgO, nickel and copper versus approximate stratigraphic height for the eastern stratigraphic section through the peridotite and olivine gabbro 112
64. Metal mantle-normalized element diagram for the peridotite 114
65. Metal mantle-normalized element diagram for the olivine gabbro 115
66. Metal mantle-normalized element diagram for the diabase sills 116
67. Log Ni/Cu versus log Pd/Ir diagram with the Proterozoic diabase dikes, olivine gabbro, and diabase sills with the fields for layered intrusions and flood basalts and an olivine cumulate from a komatiite flow 117
68. Log Cu/Ir versus log Ni/Pd diagram with the Proterozoic diabase dikes, olivine gabbro, and diabase sills with the fields for platinum group element reef deposits and an olivine cumulate from a komatiite flow 117
69. Log palladium versus log Cu/Pd diagram with the Proterozoic diabase dikes, olivine gabbro, and diabase sills with the fields for platinum group element reef deposits and mantle 118
70. Location of diamond-drill holes and associated properties in Eva, Summers, Dorothea and Sandra townships, Beardmore area 119
71. Surface plan of the trace of the Sand River Mine vein, Leitch Mine No. 2 vein, No. 1 vein, No. 3 vein and No. 4 vein with composite long section of the veins projected to surface and shifted 150 m northwest for clarity .... Chart A, back pocket
72. Composite longitudinal section of the Sand River Mine vein, Leitch Mine No. 2 vein, No. 1 vein, No. 3 vein and No. 4 vein .... Chart A, back pocket
73. Composite longitudinal section of the Leitch Mine No. 4 vein, No. 1 vein, No. 3 vein, No. 2 vein and Sand River Mine vein .... Chart A, back pocket

PHOTOS

1. Coarse-grained, gabbroic-textured plagioclase megacrystic basalt flow, SVB, containing compositionally zoned euhedral plagioclase up to 5 cm in length........ 13
2. Concentric flow laminae in pillowed andesite, Poplar Point assemblage, NVB........ 16
3. Pillow fragment breccia with subangular, rounded, or amoeboid-shaped fragments in hyaloclastite matrix, Poplar Point assemblage, NVB........ 18
4. Heterolithic breccia, Poplar Point assemblage, NVB, containing clasts of vesicular intermediate metavolcanic rocks with minor feldspar porphyritic felsic metavolcanic rocks, cherts, and mafic metavolcanic clasts........ 18
5. Heterolithic breccia, Poplar Point assemblage, NVB, containing mafic clasts that display silicified reaction rims in a highly chloritized matrix........ 20
6. Peperitic textured feldspar-quartz porphyritic felsic feeder dike fragments in a heterolithic tuff breccia, Poplar Point assemblage, NVB........ 21
7. Folded horizon of clastic-magnetite-argillite iron formation, SSB, interpreted to indicate large-scale structural repetition of iron formations........ 24
8. Coarse-grained, leucocratic, synvolcanic gabbro crosscut by diabase dike, SVB........ 30
9. Synvolcanic to syntectonic intrusive granodiorite with a weak to moderate tectonic foliation highlighted by silicification and chloritization along fractures........ 31
10. Medium-grained porphyritic pyroxene peridotite with randomly oriented, medium- to coarse-grained pyroxene phenocrysts, from a Proterozoic ultramafic intrusion in Kitto Township........ 36
11. The edge of a irregular coarse-grained pod located near the upper contact of a diabase sill, in Kitto Township, interpreted to represent the last fluid-rich phase of the magma........ 39
12. Medium-grained magnetite-porphyritic diabase, an example of the lithologic variability in diabase sills, Highway 11 section, Kitto Township........ 40
13. Aplite dikelet in diabase sill, with continuous to discontinuous bleached alteration rims up to 5 cm wide, and alteration-filled fractures in diabase, Warneford quarry section........ 41
14. Xenoliths of coarse- to medium-grained quartz and feldspar and rounded, metasedimentary rocks in a biotite-rich diabase matrix, interpreted to reflect partial assimilation of Quetico Subprovince metasedimentary rocks by the diabase sills, in northeast Kitto Township........ 42
15. Crudely graded bedding in pebble conglomerate with occasional pebble-sized jasper clast, central metasedimentary subbelt........ 46
16. Arcuate cooling fractures-joints and later linear structures in diabase sill, in the CNR ballast quarry, Kitto Township........ 46
17. Well-developed crenulation cleavage in the jasper-hematite iron formation, Leitch Mine, Highway 580. 50
18. Well-developed S_3 spaced cleavage; jasper-hematite iron formation, Leitch Mine, Highway 580........ 50
19. F_2 fold, in jasper-hematite banded iron formation adjacent to the Leitch Mine, Highway 580........ 51
20. Mylonitic shear zone, defining the Paint Lake deformation zone, in a felsic to intermediate metavolcanic rock of the Onaman–Tashota terrane........ 55
21. Intense chlorite alteration of the matrix in a brecciated pillowed basalt flow with fragments of chilled granodiorite, adjacent to granodiorite dike in the Poplar Point assemblage, NVB........ 58
22. Intense silicification along a crosscutting fracture in a monolithic tuff breccia of the Poplar Point assemblage, NVB........ 58

TABLES

1. Lithological units for the Beardmore–Geraldton Belt 10
2. Axinite locations with associated mine and commodity type 62
3. Mineral Deposit Inventory (MDIII) property location information .... back pocket
4. Mineral Deposit Inventory (MDIII) assessment work types .... back pocket
5. Mineral Deposit Inventory (MDIII) geology table .... back pocket
6. Mineral occurrences with no recent work 120
7. Mineral Deposit Inventory (MDIII) production and mineral resources .... back pocket

GEOLOGICAL MAPS

Map P.3512 Precambrian geology of Kitto Township, Beardmore area, northwestern Ontario ...... back pocket
Map P.3513 Precambrian geology of Eva and Summers townships, Beardmore area, northwestern Ontario .... back pocket
Map P.3514 Precambrian geology of Dorothea and Sandra townships, Beardmore area, northwestern Ontario .... back pocket

CHART

A. Figures 71, 72 and 73. Composite surface plan and longitudinal sections of the veins of the Leitch Mine and Sand River Mine .... back pocket

Abstract

The Phoenix Bedrock Mapping Project is an economic development initiative supported by FedNor, administered by the Lake Nipigon Heritage Authority and conducted by the Precambrian Geoscience Section of the Ontario Geological Survey. The objective of the project is to conduct bedrock mapping at 1:20 000 scale, east of Lake Nipigon and west of Beardmore, in an area that was burnt during a major forest fire in 1999. The fire has enhanced outcrop exposure in most of Kitto, Eva and Dorothea townships and parts of Summers and Sandra townships, providing an opportunity to collect new geoscience information. The Beardmore area has mineral resource potential for gold, volcanogenic massive sulphide (VMS) mineralization and magmatic platinum group element (PGE) mineralization.

The Phoenix map area is located approximately 190 km northeast of Thunder Bay, and east of Lake Nipigon. The area mapped during 2001 encompassed all of Kitto, Eva, and Dorothea townships and portions of Summers and Sandra townships. Within the map area, the Beardmore–Geraldton Belt (BGB) is approximately 20 km wide in a northerly direction and was mapped for about 10 km along an east strike. The BGB forms the southern margin of the eastern Wabigoon Subprovince, and is bounded, to the south, by metasedimentary rocks of the Quetico Subprovince and, to the north, by metavolcanic rocks of the Onaman–Tashota terrane.

The BGB was subdivided into a series of 3, northeast-striking metasedimentary and metavolcanic subbelts. The southern metavolcanic subbelt (SVB) and the northern Bish Bay assemblage of the northern metavolcanic subbelt (NVB) consist of massive and pillowed flows with minor volcaniclastic rocks and interflow chert-magnetite iron formation. Wacke, conglomerate, and argillite with argillite-magnetite iron formation and jasper-hematite iron formation providing stratigraphic markers form the southern metasedimentary subbelt (SSB). The central metavolcanic subbelt (CVB), and the southern Poplar Point assemblage of the NVB consist of intermediate massive and pillowed flows with significant tuffs, lapilli tuffs and tuff breccias, and minor interflow chert-magnetite iron formation. Exposures of the central metasedimentary subbelt (CSB) consist of conglomerate, arenite and argillite-magnetite iron formation. To the southeast, wackes, argillite and conglomerate of the Quetico Subprovince resemble metamorphosed equivalents of the metasedimentary rocks of the BGB. Felsic to intermediate flows, volcaniclastic rocks of the Onaman–Tashota terrane are exposed to the north. The synvolcanic gabbroic rocks form generally thin sills in the SVB and the Bish Bay assemblage. A series of granodiorite to quartz porphyritic, feldspar porphyritic and feldspar-quartz porphyritic dikes intrude the metavolcanic rocks of the Poplar Point assemblage. Late posttectonic diorite sills predominantly occur in the units along the SSB–CVB and the CSB–NVB contacts.

A swarm of narrow, generally north-striking diabase dikes intrude the supracrustal rocks and appear to be predominantly Paleoproterozoic in age. A crudely zoned ultramafic intrusion has an upper zone of olivine gabbro granophyre along the upper western contact and a main body of massive to pyroxene porphyritic peridotite consisting of lherzolite and wehrlite composition. A series of undulating, generally shallow-dipping diabase sills forming part of the Nipigon sills intrude all other rock types in the map area. Proterozoic diabase sills overlie both the ultramafic intrusion and Sibley Group sedimentary rocks, but the relative ages of the ultramafic rocks and Sibley Group are not known. Locally, the diabase and peridotite have xenolith-rich contacts adjacent to the metasedimentary rocks.

The metavolcanic and metasedimentary rocks of the BGB are generally weakly carbonatized, with localized areas of intense carbonatization generally associated with fracturing or intense shearing often related to regional-scale deformation zones. Intense silicification is associated with units that had a higher original permeability and may represent synvolcanic hydrothermal alteration. Widespread axinite

occurs in quartz-carbonate veins located in dilatant fractures hosted by carbonatized metavolcanic rocks near the SSB–CVB contact and the contact between the Poplar Point and Bish Bay assemblages. The BGB exhibits a relatively uniform low to middle greenschist-facies metamorphism, and the metasedimentary rocks of the Quetico Subprovince have a middle to upper greenschist-facies metamorphism. Hornfels metamorphism is restricted to a small area along the contact of the Proterozoic ultramafic intrusion.

Supracrustal rocks of the BGB generally face to the north, though local reversals result in south-facing panels that have been interpreted to have formed as an imbricated thrust wedge developed by the collision between the Wabigoon and Wawa subprovinces, or a large-scale high-amplitude folding event. In general, deformation within the belt decreases to the west resulting in well-preserved primary textures, but deformation tends to be inhomogeneous and concentrated within the ironstone beds. Foliations are moderate to well developed, and are oriented 0 to 15° counterclockwise to the primary structures. Three folding events may be present, including sporadically exposed F_1 folds, southeast-trending, west-plunging F_2 folds evident in the large-scale fold of the SSB–CVB contact; and northeast-trending F_3 folds. North-striking faults and east-striking fault and/or deformation zones are present, and the age relationship between the 2 structures is not known and both were probably active at multiple times. A number of regionally significant east-striking fault systems, or deformation zones, are generally delineated in the field by highly carbonatized and silicified units and the intense shear fabrics are generally associated, but not necessarily coincident, with the subbelt boundaries.

Gold production in the Beardmore area totalled greater than one million ounces, and the area has the potential to host additional gold mineralization, as well as base metal VMS and PGE mineralization. There is the potential for additional gold mineralization in quartz veins hosted by structures subparallel to parallel to the Sand River Mine vein – Leitch Mine No. 2 vein, both within the immediate area of the No. 2 vein and within the SSB and CVB to the northeast. The southwest portion of the SVB in western Kitto Township has not been extensively explored, and has the potential to host gold mineralization similar to the iron formation associated brittle fracture hosted quartz stringers of the Northern Empire Mine. Anomalous assays of copper, zine and molybdenum were found in structures related to faulting and closely associated with posttectonic diorite intrusions indicating that these structures have the potential to host copper and/or molybdenum, as well as gold mineralization, along the contact between the Bish Bay and Poplar Point assemblages and along the CVB–SSB contact. Anomalous zinc values in chloritized tuff breccia intruded by FII-type, peperitic textured felsic feeder dikes indicate that the Poplar Point assemblage has the potential to host VMS mineralization. Anomalous PGE and nickel values indicate that the basal contact of the peridotite and the adjacent diabase are the areas that have a high potential to host PGE mineralization.

Precambrian Geology of Kitto, Eva, Summers, Dorothea and Sandra Townships, Beardmore Area, Northwestern Ontario

T.R. Hart[1], M. terMeer and C. Jolette

Ontario Geological Survey
Open File Report 6095
2002

---

[1] Precambrian Geoscience Section, Ontario Geological Survey
Ministry of Northern Development and Mines, Sudbury, Ontario, Canada P3E 6B5

Introduction

The Phoenix Bedrock Mapping Project is an economic development initiative supported by FedNor, administered by the Lake Nipigon Heritage Authority and conducted by the Precambrian Geoscience Section of the Ontario Geological Survey. The objective of the project was to conduct bedrock mapping at 1:20 000 scale in an area east of Lake Nipigon and west of Beardmore that was burnt during a major forest fire in 1999 (Figure 1). The fire enhanced outcrop exposure in most of Kitto, Eva and Dorothea townships and in parts of Summers and Sandra townships, providing an opportunity to collect new geoscience information. The Beardmore area has mineral resource potential for gold, volcanogenic massive sulphide (VMS) mineralization and magmatic platinum group element (PGE) mineralization. It is hoped that this new information will generate interest in prospecting, mineral exploration and investment and create and/or maintain community-based jobs and opportunities for the Municipality of Greenstone and the surrounding area.

The Phoenix map area is located approximately 190 km northeast of Thunder Bay, and east of Lake Nipigon. The area mapped during 2001 encompassed all of Kitto, Eva, and Dorothea townships and portions of Summers and Sandra townships, bounded roughly by latitudes 49°45′09″ and 49°29′27″N and by longitudes 87°53′27″ and 88°09′54″W. Within the map area, the Beardmore–Geraldton Belt (BGB) is approximately 20 km wide in a northerly direction and was mapped for about 10 km along an east strike. The eastern end of the BGB is located more than 100 km to the east, in the area of Long Lac (Figure 2). The western extent of the BGB supracrustal rocks is not known as the rocks continue under Lake Nipigon. The airborne magnetic survey (Gupta 1991) appears to indicate that the iron formations of the metasedimentary subbelt(s) can be traced to the Max Lake greenstone belt, in the Legris Lake – Lac des Iles area.

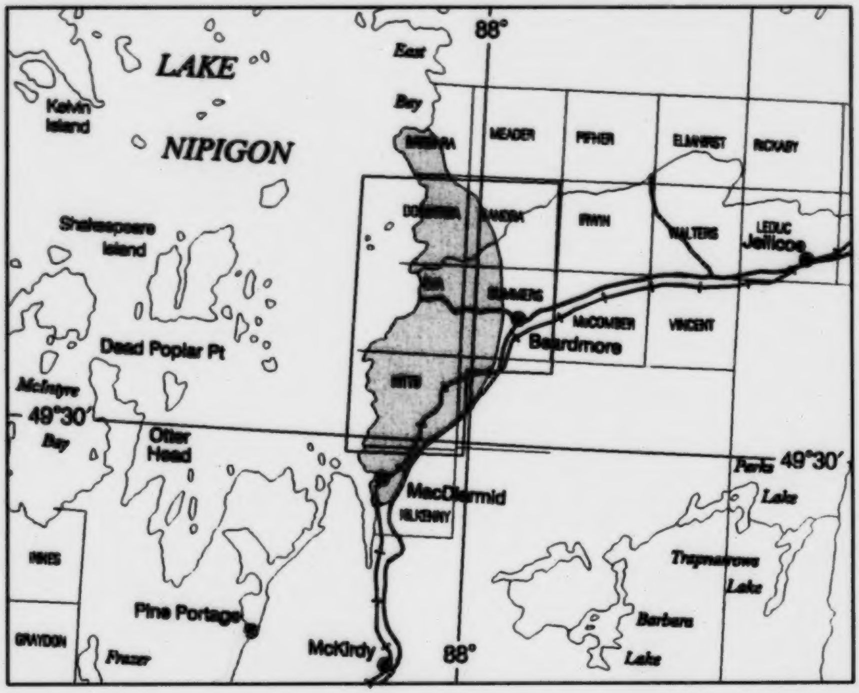
88°
LAKE
NIPIGON
East
Bay
Kelvin
Island
MEADER
PIFHER
ELMHIRST
RICKABY
IRWIN
WALTERS
LEDUC
Jellicoe
Shakespeare
Island
SUMMERS
McCOMBER
VINCENT
Beardmore
Dead Poplar Pt
McIntyre
49°30′
Bay
Otter
Head
Poria
49°30′
Lake
MacDiarmid
KILKENNY
Trapnarrows
Lake
INNES
Pine Portage
Barbara
Lake
GRAYDON
Frazer
McKirdy
88°

Figure 1. Map showing location of project area. The shaded area represents the approximate area that was burnt during a major forest fire in 1999.

ACKNOWLEDGMENTS

The author was assisted by senior assistants Mariska terMeer and Chantal Jolette, and by junior assistants Barbara Duggan, Riku Metsaranta, Myndi Quirion, Adrian Van Rythoven, Stephanie Thibeault, and Amy Robinson. Ms. terMeer and Ms. Jolette were each responsible for approximately one third of all mapping, with Ms. Duggan, Ms. Thibeault and Ms. Robinson assisting in some areas. Ms. Duggan is in the process of completing an BSc (Hons) thesis, at Queen's University, Kingston, Ontario, examining the Proterozoic ultramafic intrusion in Kitto Township. Mr. Gerry White, Resource Geologist with the Resident Geologist's Office, Thunder Bay, provided background information on mineral occurrences and logistical assistance during the course of the project.

ACCESS

Access to a large portion of the map area and to the Town of Beardmore is provided by Highway 11 and by the roads and trails that branch off the highway. Highway 580, which begins at Highway 11 north of the Town of Beardmore, extends west to Poplar Point Park on the east shore of Lake Nipigon. The logging roads and trails branching from this highway provide access to the western half of the map area. The 72 Road extends north from Highway 580, accessing Sandra, Dorothea and the northwest side of Summers townships. The Mary-Jane, Sand-River and High Hill Harbour roads extend south of Highway 580 and provide access to Eva Township and the northern part of Kitto Township. The CNR rail line and Trans-Canada gas pipeline are parallel to Highway 11 and provide additional access to the area. Lake Nipigon, and the lower portions of the Blackwater and Namewaminikan rivers, provide access to the extreme western portion of the map area. Local boats were chartered to supply waterborne access. A lack of roads in central Kitto and Dorothea townships required the use of a helicopter for access.

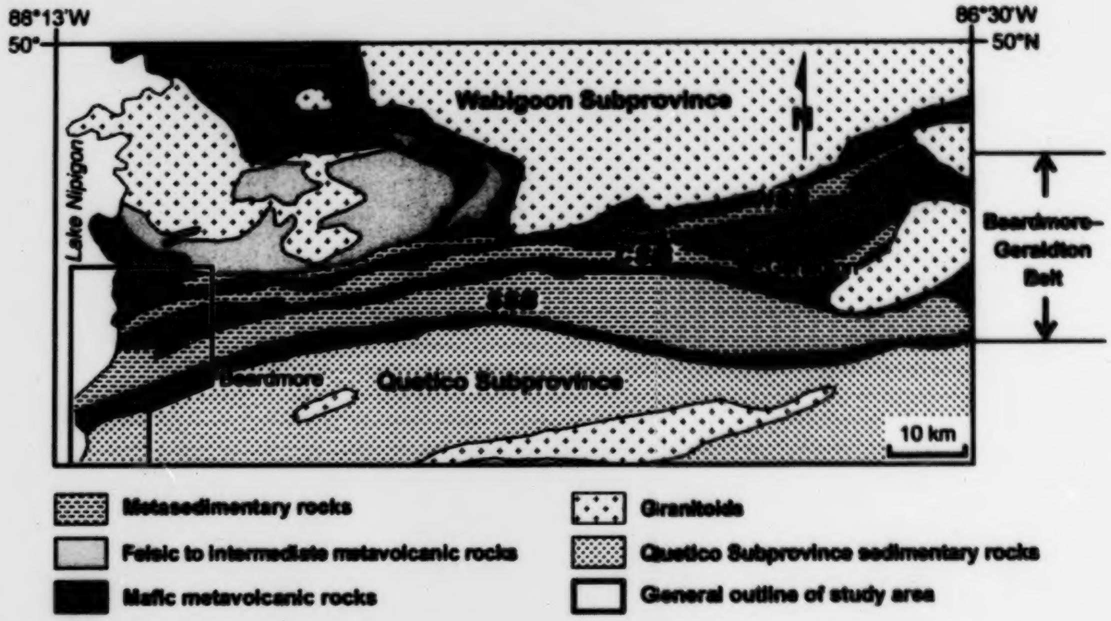
88°13'W
50°
86°30'W
50°N
Wabigoon Subprovince
N
Lake Nipigon
Beardmore–Geraldton Belt
SSB
Beardmore
Quetico Subprovince
10 km
Metasedimentary rocks
Felsic to intermediate metavolcanic rocks
Mafic metavolcanic rocks
Granitoids
Quetico Subprovince sedimentary rocks
General outline of study area

Figure 2. Regional geology of the Beardmore–Geraldton Belt (BGB); abbreviations: CSB, central metasedimentary subbelt; NSB, northern metasedimentary subbelt; SSB, southern metasedimentary subbelt.

PREVIOUS GEOLOGICAL WORK

Initial geological mapping was by conducted by the Geological Survey of Canada by R. Bell in 1867–1869 (Bell 1870, p.339-363 and accompanying Map No. 78), and by W. McInnes and D.B. Dowling in 1894, as reported by G.M. Dawson (Dawson 1895, p.48A-51A; and 1901, p.94A-99A). Details of these works can be found in *Geology of the Nipigon Basin* (Wilson 1910). The first detailed work in the area was by Parks in 1901, who traversed both north and south of the Sturgeon River (Laird 1937). The Sturgeon River area was mapped at a scale of 1:63 360 (1 mile = 1 inch) scale by Laird (1937). In 1948, the Canadian Institute of Mining and Metallurgy published the Jubilee Volume *Structural Geology of Canadian Ore Deposits*, which contained detailed descriptions of the Leitch (McKay, Cormie and Coulson 1948) and Northern Empire mines (Benedict and Titcomb 1948). Geological compilation maps by Pye et al. (1966), at a scale of 1:253 440, and by Stott (1984), at a scale of 1:126 720, include all or part of the present map area. Bedrock mapping by Mackasey (1975), at a scale of 1:31 680 (1 inch to ½ mile), was conducted in Dorothea, Sandra, Eva and Summers townships in 1970 (Mackasey 1970a, 1970b). Sutcliffe (1981, 1982a, 1982b, 1982c, 1982d) and Sutcliffe and Greenwood (1985) concentrated on mapping the Proterozoic rocks around Lake Nipigon, at a scale of 1:50 000, as part of a PhD thesis (Sutcliffe 1986). A compilation of the mineral exploration and prospecting activity in the surrounding Beardmore–Geraldton Belt was completed by Mason and White (1986), with additional historical data compiled by Speed and Craig (1992). The structural development of the Beardmore–Geraldton Belt was studied by Williams (1986, 1987a, 1987b, 1989) and by Kehlenbeck (1983). Eva and Summers townships were mapped by Shanks (1993) at a scale of 1:20 000. Detailed lithogeochemistry of the metavolcanic rocks of the Beardmore–Geraldton Belt was completed by Tomlinson (1996) and Tomlinson et al. (1996). A preliminary investigation of the potential for structurally controlled mesothermal gold mineralization was completed by DeWolfe (2001) as part of a MSc thesis at Laurentian University, Sudbury, Ontario.

PRESENT GEOLOGICAL SURVEY

The area was mapped during the summer and early fall of 2001. Whenever possible, pace and compass traverses were conducted perpendicular to the regional trend of stratigraphy at approximately 400 to 500 m line spacing. The outcrops were located in Universal Transverse Mercator (UTM) co-ordinates in the North American Datum 1983 (NAD83) on a scale of 1:20 000 using an averaged position acquired by a Garmin® GPS 12XL™ global positioning system. Geological field data, with UTM co-ordinates, were recorded in a database using FieldWorker software, from Fieldworker Products Limited, running on an Apple® Newton® handheld computer. These digital data were downloaded to Fieldlog–ACAD™ software running on an IBM® compatible computer and geo-referenced using the UTM co-ordinates or by digitizing closely spaced outcrops. The geological data were overlain on a 1:20 000 scale digital base map derived from the Ontario Basic Mapping Program, Surveys, Mapping and Remote Sensing Branch, Ontario Ministry of Natural Resources. Additional trail and logging road positions were acquired by downloading the track files of the road from the Garmin® GPS 12XL™.

Exploration information, such as mineral deposit locations, assay results and diamond-drill holes, were obtained from the Earth and Resources Land Information System (ERLIS) and the assessment files at the Resident Geologist's Office, Thunder Bay. Diamond-drill hole locations were initially obtained from the Diamond Drill Hole Database in ERLIS, and were corrected based on data obtained from the assessment files. Showing and assay locations were also initially acquired from the Mineral Deposit Inventory (MDI II) (OGS 2000), and were similarly corrected based on an examination of the assessment files. These data were plotted with the field geological information and aided in the development of the geological interpretation.

The geological interpretation was also enhanced by the use of airborne geophysical data, a side-scan radar image and a Landsat image. A subset of the total field and second vertical derivative magnetic and electromagnetic data (EM) were acquired from the regional airborne geophysical survey (OGS 1998). The side-scan radar image was regional in scale and particularly useful in the delineation of large-scale structures. A Landsat 7 composite of the image of the area from the spring of 2001 provided information on access and ground conditions as well as being useful in the geological interpretation.

PROSPECTING AND MINING EXPLORATION

Bell (1870) initially discovered the "Nipigon Iron Ranges" around 1870, but serious exploration of the iron ranges began in 1901 in the area of the Standingstone River (Coleman 1907). Interest in the iron deposits was not sustained, but prospecting activity continued in the area.

Gold was discovered in 1925 in an auriferous quartz-carbonate vein located east of Beardmore by T.G. Powers and P. Silam (Mason and White 1986). This discovery led to the development of the Northern Empire Mine and later discoveries, by R. Cryderman, led to the development of the Sand River and Leitch mines in the early 1930s.

The Northern Empire Mine (Figure 3) was discovered by Powers and Silam in 1925 and work began on the property in 1926. The gold was located in an *en échelon* quartz vein system. The Northern Empire Mine produced 149 492 ounces of gold and 19 803 ounces of silver in the period from 1934 to 1949.

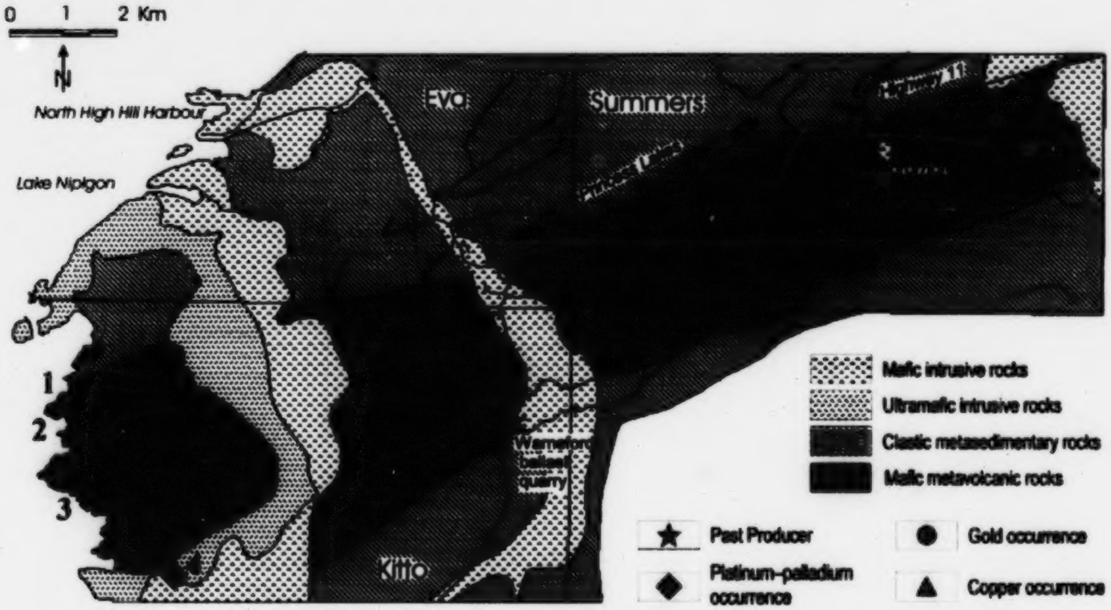
0 1 2 Km
N
North High Hill Harbour
Lake Nipigon
Eva
Summers
Kitto
quarry
1
2
3
Mafic intrusive rocks
Ultramafic intrusive rocks
Clastic metasedimentary rocks
Mafic metavolcanic rocks
★ Past Producer
● Gold occurrence
◆ Platinum–palladium occurrence
▲ Copper occurrence

1 Speke Point North
2 Speke Point Central
3 Speke Point South
4 Phoenix occurrence
5 C.J. Morgan
6 Gold Fields
7 Morgan South Extension
8 Rentz
9 Canadian–Beardmore
10 Buffalo–Beardmore
11 Holt
12 Summers pipeline
13 Anglo–Beardmore
14 Hac–Craig
15 McWilliams–Beardmore
16 Northern Empire
17 Pauline Lake
18 Spooner
19 Banner

Figure 3. Location of mineral occurrences in the southern metavolcanic subbelt, Summers and Kitto townships.

Exploration has been conducted since that time along strike with the Northern Empire Mine in an attempt to find similar gold mineralization. Examples include the Spooner property and McWilliams–Beardmore property to the east, the Buffalo–Beardmore, Gold Fields, Anglo–Beardmore, Holt and the Summers Pipeline properties to the west (*see* Figure 3). To date, work on these properties has outlined only sub-economic gold mineralization of a similar style to the Northern Empire Mine.

The Leitch property (Figure 4) was initially explored for iron by a number companies in the early 1900s. R. Cryderman discovered an auriferous quartz vein in 1934 on a topographic high that became the Sand River gold mine. The Cryderman brothers ran a picket line from the Sand River No. 1 vein onto the adjacent Leitch property resulting in the discovery of additional auriferous quartz veins. Total production from the Sand River Mine No. 1 and Leitch Mine No. 2 veins, with a number of other veins on the Leitch property, was 847 690 ounces of gold at an average grade of 0.92 ounce of gold per ton (Mason and White 1986). Additional exploration along strike with the Leitch and Sand River mines has outlined a number of auriferous quartz veins. East of the Leitch Mine, the Wilport showing was explored in 1935 for gold along a 300-foot quartz vein reported to contain visible gold and was optioned to Northern Empire in 1940 (*see* Figure 4, property #9). The Creek vein and Sand River Mine were initially explored in the 1930s (*see* Figure 4, properties # 1 and 5). The Creek vein was re-examined in the 1980s with ground geophysical magnetic surveys and diamond drilling. The results indicate that the Creek vein represents a complex system of auriferous, pyritized, quartz-carbonate shear zones within a diorite dike and possibly extending beyond the limits of the dike (Rennick 1988).

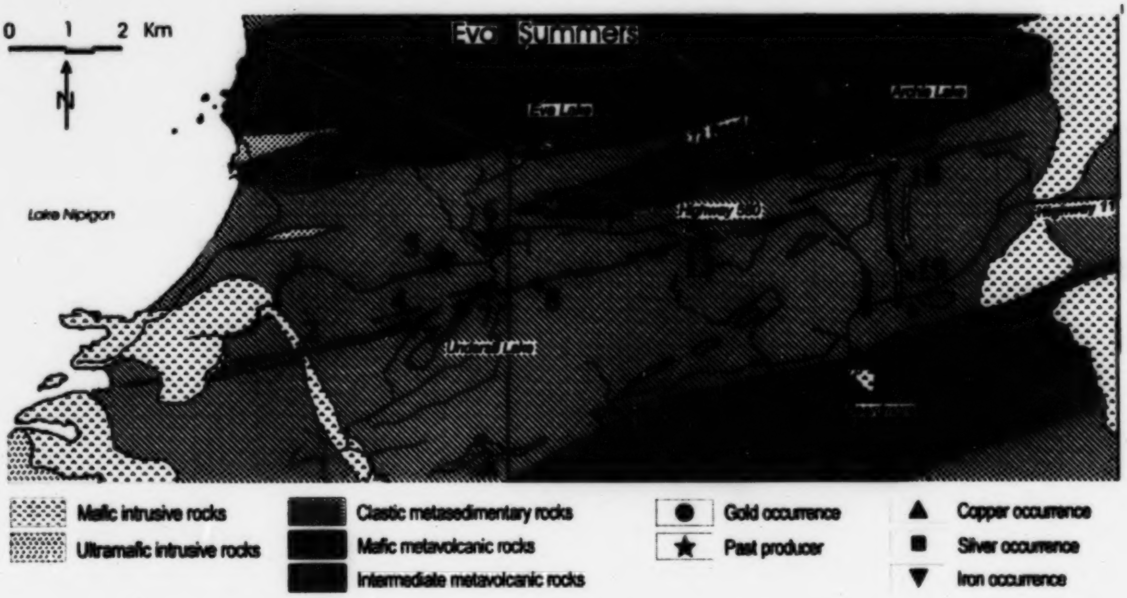
0 1 2 Km
N
Eva
Summers
Eva Lake
Lake Nipigon
Mafic intrusive rocks
Ultramafic intrusive rocks
Clastic metasedimentary rocks
Mafic metavolcanic rocks
Intermediate metavolcanic rocks
● Gold occurrence
★ Past producer
▲ Copper occurrence
■ Silver occurrence
▼ Iron occurrence

1 Creek vein
2 Undersill claim
3 Princess property
4 Lake Nipigon Central
5 Sand River Mine
6 Leitch Mine
7 Murphy claims
8 Undersill Lake property
9 Wilport
10 Eva Lake property
11 Candela
12 Ardmore
13 Long Lac Superior West
14 Coté–Archie Lake
15 Calhet
16 Minnow Lake
17 Archie Lake
18 Long Lac Superior 2
19 Empire Contact

Figure 4. Location of mineral occurrences in the southern metasedimentary subbelt and central metavolcanic subbelt, Eva and Summers townships.

Areas peripheral to the Leitch / Sand River trend have also been actively explored for gold mineralization (*see* Figure 4). The area to the south of Sand River Mine, along the iron range, was explored for gold in 1989 by Mingold Resources Inc. with ground geophysical surveys, diamond drilling and rock sampling (Nelson 1989). The sheared and carbonatized metavolcanic rocks of the central metavolcanic subbelt north of the regional fold hinges have been explored since the 1950s by Candela Development Company, and Calhet occurrence – Freewest Resources Canada Inc., and Minnow Lake occurrence – A. Lafontaine (*see* Figure 4). Currently, R. Coté is actively exploring the Archie Lake gold occurrence west of the 72 Road located along this same trend (*see* Figure 4).

Sandra and Dorothea townships were examined during the initial exploration for iron, and have since been explored for gold, base metals and molybdenum. Gold and base metal exploration has been conducted in the northeastern portion of Sandra Township by Cyril Knight Prospecting Company Ltd. (west claims) and by H.M. Holm (Figure 5). Molybdenite was discovered in a number of locations in Dorothea Township in 1935 by Amorada Gold Mines Ltd. (Laird 1937; Mackasey 1975; *see* Figure 5). Subsequently, the property was examined by a number of prospectors and companies (e.g., Nortoba Mines Ltd. in 1958–1959, A.E. Tyson in 1963, Houghton and Cox (1995) and Lassila (1995, 2000)). In 1959, Lamble (1959) reported that the occurrence contained a total of 7500 tons grading at least 1.5% MoS_2 to a depth of 40 feet. A number of molybdenum occurrences are associated with the felsic to intermediate dikes (Hopkins 1959) located in the western portion of the Poplar Point assemblage (*see* Figure 5, area of property #7).

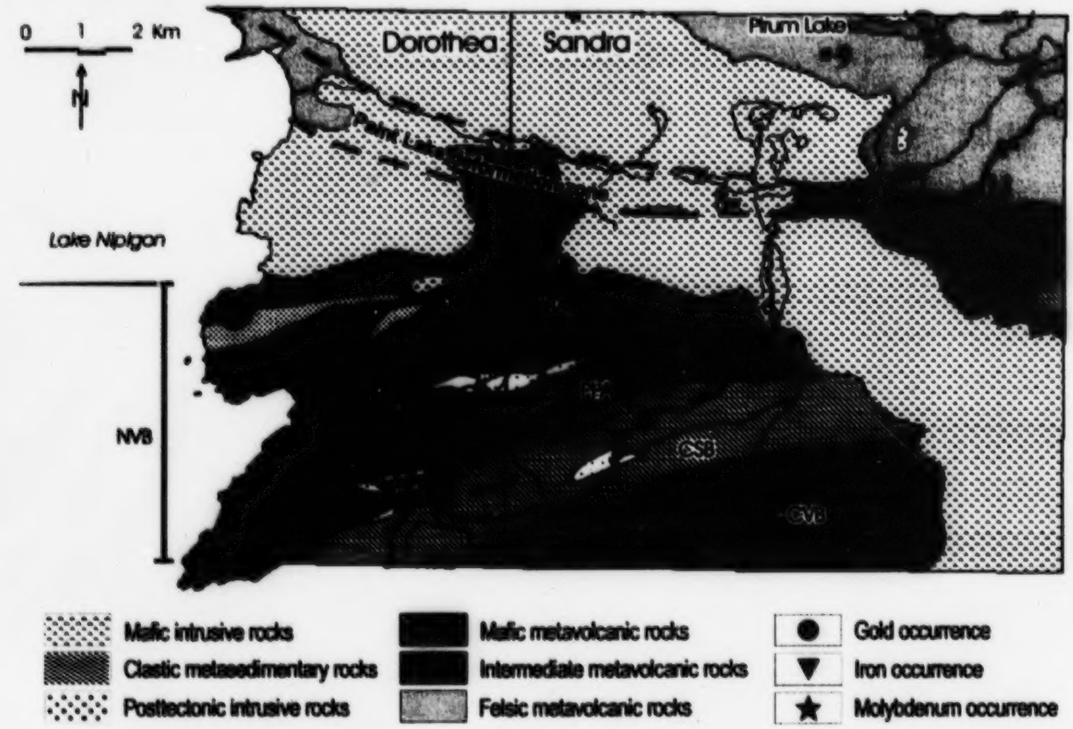

0 1 2 Km
N
Dorothea
Sandra
Pirum Lake
Lake Nipigon
NVB
PPA
CSB
CVB
Mafic intrusive rocks
Clastic metasedimentary rocks
Posttectonic intrusive rocks
Mafic metavolcanic rocks
Intermediate metavolcanic rocks
Felsic metavolcanic rocks
● Gold occurrence
▼ Iron occurrence
★ Molybdenum occurrence

1 Montmorr 2
2 Johnson–Hopkins
3 Lawrence–McKirdy
4 Dorothea Gold
5 C.L. Craig
6 Tyson #1
7 Tyson #3
8 Mill City Gold
9 Cyril Knight West
10 Holm
11 Placer Dome – Metalore

Figure 5. Location of mineral occurrences in Dorothea and Sandra townships. Abbreviations: BBA, Bish Bay assemblage; CSB, central metasedimentary subbelt; CVB, central metavolcanic subbelt; PPA, Poplar Point assemblage.

Initial exploration for platinum group elements was done by East–West Resources Corporation and Maple Minerals Inc. on the mafic to ultramafic intrusive complex located in Eva and Kitto townships in 2000. The area was prospected and ground geophysical induced polarization, resistivity and magnetic surveys were completed. The property is currently optioned by Kennecott Canada Exploration Inc. with a field program planned for the summer of 2002 (http://www.eastwestres.com (web site accessed July 31, 2002); D. Rossell, Kennecott Exploration, personal communication, 2002).

PHYSIOGRAPHY

Topographic relief is varied and most of the topographic highs are associated with diabase ridges that generally have steep cliffs on one side and talus slopes on the other. The best example of the cliff and talus is in Kitto Township along the railroad where hills grade approximately 5° over 1.5 km then abruptly terminate in a 100 m cliff. Some of these diabase ridges have a semicircular shape that becomes progressively smaller on a regional scale toward Lake Nipigon. The outer arc is located east of the Town of Beardmore, a second arc in eastern Kitto Township, and a third in western Kitto Township (Preliminary Maps P.3512, P.3513 and P.3514, *see* back pocket). In areas underlain by supracrustal rocks, the topography may be an expression of the underlying structures. A series of north- to northwest-trending ridges in the Poplar Point assemblage (PPA) correlate with the northwest strike of the metavolcanic rocks (Figure 6). Similarly, in Summers Township within the southern metavolcanic subbelt (SVB) and the southern metasedimentary subbelt (SSB), the northeast-trending ridges correlate with east-striking bedding fabrics and fold axes of the underlying metavolcanic and metasedimentary rocks.

The area is drained by a number of rivers and streams, the largest of which are the Namewaminikan, Standingstone and Blackwater rivers. A combination of bedrock, structural and glacial features control the pattern of lakes and rivers producing an overall west flow into Lake Nipigon.

Outcrop distribution is generally abundant due to the 1999 forest fire that burnt 30 000 hectares in Kitto, Eva, Dorothea and parts of Sandra and Summers townships. The exceptions are an approximately 3 km wide area in central Kitto Township bordering the Blackwater River and a 2 km wide section bordering the Namewaminikan River in Dorothea and Sandra townships that are overlain by greater than 75 m of subaqueous outwash and associated glaciolacustrine sediments.

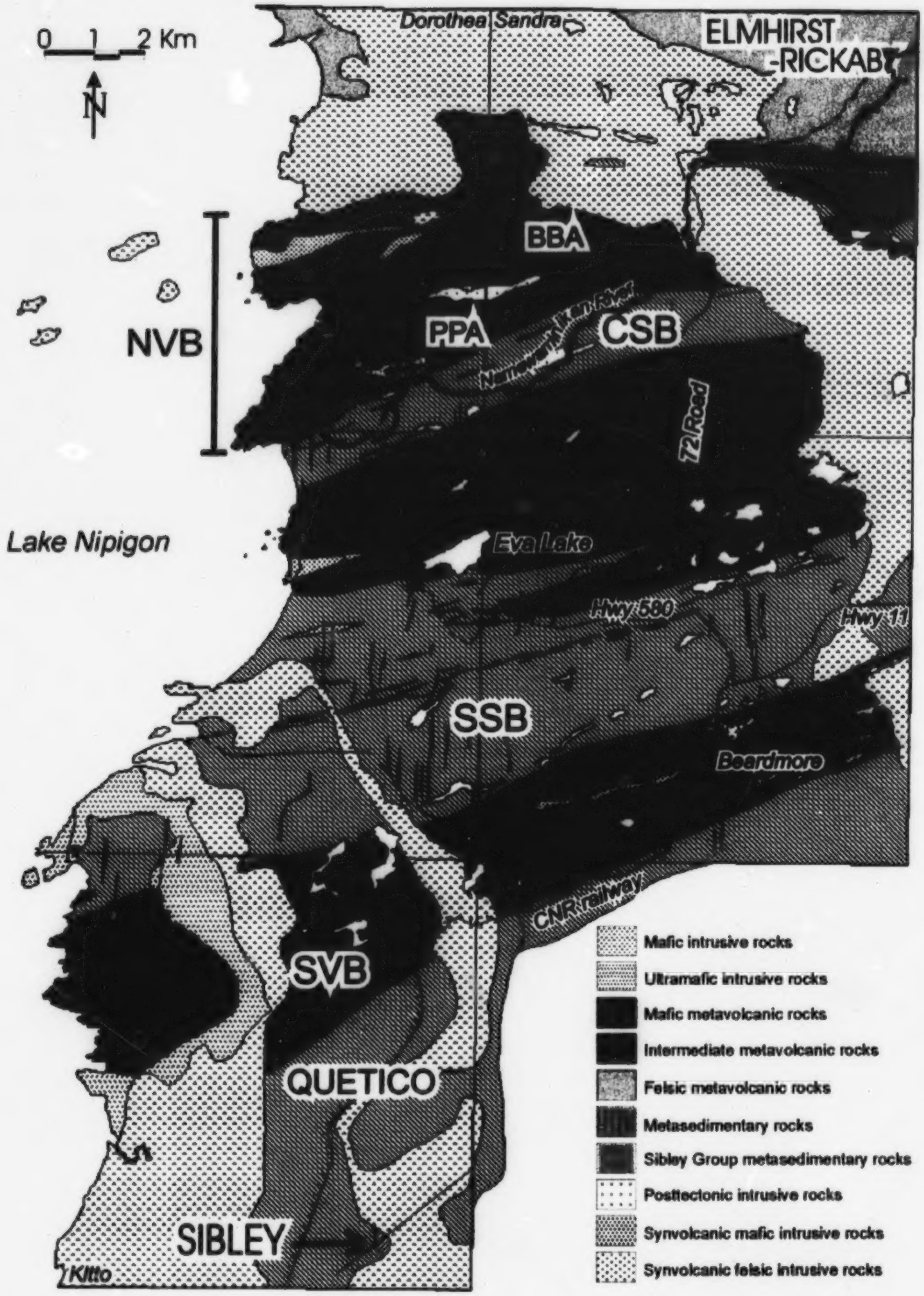
0 1 2 Km
N
Dorothea
Sandra
ELMHIRST
-RICKAB
BBA
NVB
PPA
CSB
Namewaminikan River
72 Road
Lake Nipigon
Eva Lake
Hwy 580
Hwy 11
SSB
Beardmore
CNR railway
SVB
QUETICO
SIBLEY
Kitto
Mafic intrusive rocks
Ultramafic intrusive rocks
Mafic metavolcanic rocks
Intermediate metavolcanic rocks
Felsic metavolcanic rocks
Metasedimentary rocks
Sibley Group metasedimentary rocks
Posttectonic intrusive rocks
Synvolcanic mafic intrusive rocks
Synvolcanic felsic intrusive rocks

Figure 6. General geology of Kitto, Eva, Summers, Dorothea and Sandra townships, in the Beardmore–Geraldton area. Abbreviations: NVB, northern metavolcanic subbelt; CVB, central metavolcanic subbelt; SVB, southern metavolcanic subbelt; SSB, southern metasedimentary subbelt; CSB, central metasedimentary subbelt; PPA, Poplar Point assemblage (part of the NVB); BBA, Bish Bay assemblage (part of the NVB).

General Geology

The Phoenix project area is underlain by Archean metasedimentary and metavolcanic rocks of the Beardmore–Geraldton Belt (BGB), which form the southern margin of the eastern Wabigoon Subprovince (Table 1). The BGB is bounded to the south by metasedimentary rocks of the Quetico Subprovince and, to the north, by metavolcanic rocks of the Onaman–Tashota terrane (*see* Figure 2). Previous workers (Devaney and Williams 1989; Shanks 1993; Tomlinson et al. 1996) have interpreted the BGB to represent the collisional zone formed between the Wabigoon and Wawa subprovinces.

The Beardmore–Geraldton Belt was subdivided into a series of 3, northeast-striking metasedimentary and 3 volcanic belts by Devaney and Williams (1989). For the purposes of this report, to differentiate these belts from the Beardmore–Geraldton Belt, the smaller belts will be referred to as "subbelts". In addition, the names have been changed slightly from Devaney and Williams (1989) to indicate the metamorphism of the volcanic rocks. Thus, the 6 belts of Devaney and Williams (1989) will be referred to herein as the northern, central and southern metasedimentary subbelts and the northern, central and southern metavolcanic subbelts. Mafic metavolcanic rocks of the southern metavolcanic subbelt (SVB) consist of massive and pillowed flows with minor tuffs, lapilli tuffs, and tuff breccias and interflow chert-magnetite iron formations. The southern metasedimentary subbelt (SSB) is composed of thinly to thickly bedded feldspathic wacke, lithic wacke, siltstone, polymictic conglomerate, and mudstone and/or argillite with argillite-magnetite iron formation and jasper-hematite iron formation providing stratigraphic markers within the SSB. The central metavolcanic subbelt (CVB) consists of intermediate massive and pillowed flows with significant tuffs, lapilli tuffs and tuff breccias, and minor interflow chert-magnetite iron formation. Exposures of the central metasedimentary subbelt (CSB) consist of polymictic conglomerate, lithic arenite and argillite-magnetite iron formation. The northern metavolcanic subbelt (NVB) is subdivided into the northern Bish Bay assemblage and the southern Poplar Point assemblage. The Bish Bay assemblage is composed of east-striking mafic pillowed to massive flows and rare tuffs resembling the SVB. The Poplar Point assemblage consists of northwest-striking, intermediate flows, tuff breccias and tuffs resembling the CVB, with subordinate mafic massive and pillowed flows (*see* Figure 6).

Thinly bedded feldspathic wacke, siltstone, argillite and conglomerate of the Quetico Subprovince are exposed in the southeastern corner of the map area and resemble metamorphosed equivalents of the metasedimentary rocks of the BGB. Felsic to intermediate flows, tuff and tuff breccias of the Onaman–Tashota terrane are exposed in the northeast and northwest corners of the map area.

A number of rock types intrude the supracrustal rocks, including a series of mafic to ultramafic synvolcanic, intermediate to felsic synvolcanic, mafic posttectonic intrusive rocks and diabase dikes. The synvolcanic gabbroic rocks form thin sills subparallel to the strike of the mafic metavolcanic rocks of the SVB and the Bish Bay assemblage (BBA). A large intrusive body located in the BBA is a composite intrusion with gabbroic phases and peridotitic phases in the south and north parts of the intrusion, respectively. A series of intermediate to felsic dikes and sills ranging from massive granodiorite to quartz porphyritic, feldspar porphyritic and feldspar-quartz porphyritic phases occur within the metavolcanic rocks of the Poplar Point assemblage (PPA). These units appear to have been emplaced along the regional foliation, although some bodies are subhorizontal in orientation. A feldspar porphyritic granodiorite dike intrudes the mafic flows of the SVB and resembles the dikes of the PPA. Late posttectonic diorite sills predominantly occur within the metasedimentary and metavolcanic rocks along the contact between the SSB and CVB. Additional intrusions are located along the northern and southern contacts of the PPA. These diorite sills are generally undeformed and have chilled contacts with the metasedimentary rocks. A swarm of narrow, generally north-striking diabase dikes intrude the supracrustal rocks and appear to be predominantly Paleoproterozoic in age.

Table 1. Lithological units for the Beardmore–Geraldton Belt.

PHANEROZOIC
- **CENOZOIC**
  - **QUATERNARY**
    - **RECENT**
      - Lake, stream, and swamp deposits (unconsolidated)
    - **PLEISTOCENE**
      - Glacial deposits, sand, gravel, till (unconsolidated)

UNCONFORMITY

PRECAMBRIAN
- **PROTEROZOIC**
  - Mafic Intrusive Rocks
    - Nipigon sill complex diabase, medium-grained diabase, magnetite-porphyritic diabase, coarse-grained diabase[a], diabase dike[b], hybrid contact zone[c]

INTRUSIVE CONTACT

  - Sibley Group Metasedimentary Rocks
    - Feldspathic wacke, and argillite and/or slate

UNCONFORMITY

  - Ultramafic Intrusive Rocks
    - Olivine-gabbro hybrid[c], olivine gabbro, pyroxenite[d], porphyritic pyroxenite[d]

INTRUSIVE CONTACT

ARCHEAN
- **NEOARCHEAN**
  - Posttectonic Mafic Intrusive Rocks
    - Diorite, gabbro

INTRUSIVE CONTACT

  - Synvolcanic or Syntectonic Intermediate to Felsic Intrusive Rocks
    - Granodiorite, quartz diorite, quartz porphyry, quartz feldspar porphyry, feldspar porphyry

INTRUSIVE CONTACT

  - Synvolcanic or Syntectonic Mafic Intrusive Rocks
    - Diorite, gabbro[e]

INTRUSIVE CONTACT

  - Clastic Metasedimentary Rocks[f]
    - Quartzose arenite, lithic arenite, quartzose wacke, feldspathic wacke, lithic wacke, siltstone, argillite, polymictic conglomerate

UNCONFORMITY

  - Chemical Metasedimentary Rocks
    - Oxide-facies iron formation (magnetite–chert), clastic-magnetite-argillite iron formation[g,h], jasper-hematite banded iron formation[h], chert, actinolite-magnetite hornfels[i]
  - Intermediate to Felsic Metavolcanic Rocks[j]
    - Massive flow, dike, tuff, monolithic tuff breccia
  - Intermediate to Mafic Metavolcanic Rocks[k]
    - Massive flow, feldspar-porphyritic pillowed flow, feldspar-porphyritic massive flow, pillowed flow, pillowed fragment breccia, dike, tuff, lapilli tuff, monolithic tuff breccia, heterolithic tuff breccia
  - Mafic Metavolcanic Rocks
    - Massive flow, feldspar megacrystic flow, pillowed flow, pillow fragment breccia, dike, tuff, lapilli tuff

---

[a] This is, in part, granophyre, based on petrographic examination

[b] Lithology of dikes is variable, suggesting this subunit may include both Archean and Proterozoic diabase dikes

[c] Biotite-rich matrix and contains blocks of older metasediment and metavolcanic xenoliths

[d] Petrology indicates this unit is probably a wehrlite and/or lherzolite

[e] Contacts with units "Mafic Metavolcanic Rocks" and "Intermediate to Mafic Metavolcanic Rocks" generally not observed; may be, in part, posttectonic mafic intrusive rocks

[f] This unit includes metasedimentary rocks of the Beardmore–Geraldton Belt and the Quetico Subprovince

[g] Generally contains less than 5% lenses of jasper; assumed to be clastic in origin

[h] These units are probably contemporaneous with the "Clastic Metasedimentary Rocks" unit

[i] May be composed of units "Chemical Metasedimentary Rocks: oxide-facies iron formation (magnetite–chert)" and "Mafic Metavolcanic Rocks: lapilli tuff"

[j] More felsic than other metavolcanic units, but commonly no quartz phenocrysts are observed

[k] Commonly contains abundant fine feldspar phenocrysts; assumed to be intermediate in composition

The Proterozoic diabase sills overlie both the ultramafic intrusion and Sibley Group sedimentary rocks, but the relative ages of the ultramafic rocks and Sibley Group are not known. Sedimentary rocks of the Sibley Group unconformably overlie the Quetico Subprovince metasedimentary rocks and are, in turn, overlain by the diabase sills. A single outcrop of carbonaceous feldspathic arenite units is located on Highway 11 in southeast Kitto Township (*see* Preliminary Map P.3512). The ultramafic intrusion is crudely zoned, with an olivine gabbro granophyre along the upper western contact of a massive to pyroxene porphyritic peridotite of lherzolite and wehrlite composition. The peridotite forms a semicircular body located along the SVB–SSB and BGB–Quetico Subprovince contacts in western Kitto Township (*see* Figure 6). A series of undulating, generally flat-lying to shallow-dipping mafic sills containing diabasic textures form part of the Nipigon sills. The sills are generally 100 m thick, and vary by 50 to 60 m in elevation over distances of 400 to 500 m. A 185 m thick sill was intersected in the workings of the Leitch, Sand River and Northern Empire mines. Sill stratigraphy is varied, and coarse-grained granophyric zones were observed toward the base of the sill and near the sill top underlying a magnetite porphyritic phase. Contacts are commonly polygonal jointed, aphanitic chills or xenolith-rich hybrid contacts adjacent to the metasedimentary rocks.

Quaternary raised beach sand deposits form an extensive cover along Lake Nipigon, with the best examples located south of Poplar Point Park and along the Devil's Walk. Thick glaciolacustrine deposits cover much of central Kitto Township along the Blackwater River. The rest of the map area is covered by differing thicknesses of till.

The metavolcanic and metasedimentary rocks of the BGB are generally weakly carbonatized, predominantly calcite, with localized areas of more intense carbonatization generally associated with either a high degree of fracturing or intense shearing that is often related to regional-scale deformation zones. Intense silicification is associated with units that had a higher original permeability, specifically in the CVB east of Eva Lake and in the SVB adjacent to Lake Nipigon. This silicification may represent synvolcanic hydrothermal alteration. Minor to moderate epidote and hematite alteration is observed throughout the BGB and is generally associated with local late fractures in the metavolcanic and metasedimentary rocks. Intense localized epidote and quartz-epidote alteration occurs as open-space fracture fillings and is associated with some of the less altered north-striking diabase dikes. Serpentine veins are present in the peridotite intrusion in the Bish Bay assemblage. Widespread axinite occurs in dilatant fractures with quartz and calcite and is hosted by mafic metavolcanic rocks near the SSB–CVB contact and near the gabbroic intrusions of the Bish Bay assemblage.

The majority of Archean metavolcanic and metasedimentary rocks of the BGB exhibit a relatively uniform low to middle greenschist-facies metamorphism. The sedimentary rocks of the Quetico Subprovince are at a slightly higher metamorphic grade than rocks of the BGB and contain a typical mineral assemblage of biotite + plagioclase + quartz ± carbonate. Hornfels metamorphism is restricted to a small area along the SVB–SSB contact in an area situated west of the Proterozoic ultramafic intrusion. Middle to upper greenschist-facies rocks were observed in thermal aureoles adjacent to the diabase sills.

Supracrustal rocks of the BGB have experienced multiple phases of deformation. In general, deformation within the belt decreases to the west resulting in well-preserved primary textures, such as graded bedding, flame structures and load casts. In the SVB and SSB, inhomogeneous deformation tends to be concentrated within the ironstone beds and relatively large portions of stratigraphy were not affected by major reworking. Beds generally face to the north, though local reversals result in south-facing panels that may be interpreted to either suggest an imbricated thrust wedge developed by the collision between the Wabigoon and Wawa subprovinces (Williams 1987a), or a large-scale high-amplitude folding event (Shanks 1993). Foliations are moderate to well developed, and are oriented 0 to 15° counterclockwise to the primary structures. Three folding events may be present, including F_1 folds that were only observed within a few sporadic outcrops near the Leitch Mine; F_2 folds with west-plunging, southeast-trending axes evident in the large-scale fold of the SSB–CVB contact; and F_3 folds with northeast-trending axes. Faulting in the Beardmore portion of the BGB may be subdivided into discrete north-striking faults and east-striking fault or deformation zones. The age relationship between the 2 structural systems is not known and both were probably active at multiple times. Small-scale north-striking faults may have locally offset iron formations and acted as conduits for magma during emplacement of the diabase dike swarm. A number of regionally significant east-striking fault systems, or deformation zones, are generally delineated in the field by highly carbonatized and silicified units and the intense shear fabrics are generally associated, but not necessarily coincident, with the subbelt boundaries.

PRECAMBRIAN

Neoarchean

MAFIC METAVOLCANIC ROCKS

Mafic metavolcanic rocks are the dominant rock type of the southern metavolcanic subbelt (SVB) and the Bish Bay assemblage (BBA) of the northern metavolcanic subbelt (NVB), but is a minor rock type in the central metavolcanic subbelt (CVB) and the Poplar Point assemblage (PPA) of the NVB. In the Poplar Point assemblage, mafic metavolcanic rocks are restricted to a central band that is bounded by intermediate metavolcanic rocks. The mafic metavolcanic rocks in the CVB are confined to a band that is located along the southern contact between the CVB and the southern metasedimentary subbelt (SSB) that was only recognized geochemically (*see* "Geochemistry"), but was otherwise indistinguishable from the intermediate metavolcanic rocks. Mafic metavolcanic rocks consist of massive and pillowed flows with minor tuff, lapilli tuff and pillow breccia. An actinolite-magnetite hornfels horizon, composed of lapilli tuff and chert-magnetite iron formation, occurs along the contact between the SVB and the olivine gabbro in western Kitto Township (*see* "Chemical Metasedimentary Rocks"). Deformation decreases toward the west with the result that primary textures are better preserved.

The mafic metavolcanic rocks are composed of a mineral assemblage consisting of amphibole, plagioclase, chlorite and epidote with minor amounts of carbonate, quartz and opaque minerals. The amphibole occurs as laths and masses that appear to be of the tremolite-actinolite series. Plagioclase is generally saussuratized, with minor, transparent, secondary albite. Quartz and larger carbonate grains are usually less than 2% of the total rock and occur in amygdules. Mafic and intermediate metavolcanic rocks were distinguished in the field by using the colour index, with the mafic metavolcanic rocks generally being darker due to a higher chlorite and or amphibole content. Intermediate flows are usually lighter grey-green with up to 10% fine-grained, white feldspar phenocrysts, with the exception of some darker intermediate flows of the CVB exposed along the shore of Lake Nipigon. The mafic metavolcanic rocks may be distinguished from the mafic intrusions by the lack of subhedral amphibole.

Massive Flows

Massive flows vary from aphanitic to fine-grained to medium-grained, with minor coarse-grained amphibole-rich flows. The flows range from dark to medium green to grey-green on weathered surfaces, and dark to medium green on fresh surfaces. Individual flow thickness is difficult to determine due to a lack of recognizable primary features, such as flow-top breccias or pillowed flows, with which to separate individual flows. Based on a few well-exposed examples, the individual flows appear to be on the order of metres thick. A single variolitic, massive flow was observed near the SVB–SSB contact in western Kitto Township. White to beige, roughly circular varioles up to 1 cm in diameter form coalescing masses of irregular to ovoid shapes. Darker bands may represent ruptured pillow selvages and this unit could be interpreted to represent the flow front of a pillowed flow. Coarse-grained amphibole-rich flows are rare and may be either metamorphosed massive flows or synvolcanic mafic intrusive rocks (*see* "Synvolcanic to Syntectonic Mafic Intrusive Rocks"). A series of coarse-grained, gabbroic-textured, plagioclase megacrystic flows occur in 2 separate horizons near the southern edge of the SVB. The most prominent occurrence probably represents a series of porphyritic flows with an aggregate thickness of up to 100 m that are best exposed in southwest Kitto Township, east of Lion Bay. The plagioclase occurs as euhedral, white, compositionally zoned phenocrysts up to 5 cm in diameter (Photo 1). These phenocrysts are usually randomly distributed throughout the flow, but may form random aggregations of crystals or crudely defined bands striking southeast. These feldspar porphyritic flows resemble plagioclase megacrystic feeder flows interbedded with flow-top breccias and pillowed flows in the Whitton assemblage of the Heaven Lake greenstone belt (Hart and MacDonald 2000). However, these flows could be shallow-level gabbroic feeder sills for overlying flows.

Pillowed Flows

The pillowed flows are dark to medium green to grey-green, aphanitic to fine-grained, with occasional amygdaloidal to vesicular or variolitic textures. Pillowed flow thickness, as with the massive flows, was difficult to determine, but appears to be on the order of metres thick, although occasionally flows may be tens of metres thick. The amygdule content of the flows is varied, but larger amygdules are observed closer to Lake Nipigon and within the relatively undeformed flows of the Poplar Point assemblage (PPA). Amygdules are commonly 3 to 5 mm in diameter and filled with quartz and/or carbonate. Flows within the PPA have amygdules up to 1.5 cm in diameter that are filled with quartz and epidote or quartz and chlorite. Occasionally flows have variolitic textures consisting of 0.5 to 1 cm white to light grey varioles clustering or coalescing along the pillow selvage. Variolitic textures are present in pillowed flows of both the SVB and the PPA.

Photo 1. Coarse-grained, gabbroic-textured plagioclase megacrystic basalt flow, southern metavolcanic subbelt, containing compositionally zoned euhedral plagioclase up to 5 cm in length. Tip of pen is approximately 1.5 cm in length.

Weakly deformed pillows are generally less than 0.3 m in length, with roughly a 1:3 (height:length) aspect ratio. Deformation increases to the east where pillows exposed in the Highway 11 roadcuts are flattened to a 1:20 (height:length) aspect ratio. There are a limited number of reliable top determinations due to the level of deformation, poorly developed pillow shapes and lack of internal structures. Pillow selvages are usually less than 1 cm wide, dark green, with little to no hyaloclastite. The exceptions are the undeformed pillowed flows in the PPA that may be 1.0 m or more in diameter, with up to 3 cm wide selvages and minor interpillow hyaloclastite. These pillows may contain drainage shelves, occurring as open cavities partially filled with quartz and chlorite, that indicate that the flows are close to their original orientation.

Volcaniclastic Rocks

Volcaniclastic mafic metavolcanic rocks are volumetrically insignificant, with the tuffs forming beds tens of centimetres thick and lapilli tuffs forming beds up to a few metres in thickness. The tuffs and lapilli tuffs have been classified as volcaniclastic due to a lack of primary features supporting a pyroclastic origin. The volcaniclastic rocks are medium to dark grey-green on weathered surfaces. Tuffs within the SVB are moderately foliated, finer grained rocks that are mineralogically similar to the massive flows. Primary structures were not observed, and provided no useful top indicators in the tuffs of the SVB. In thin section, the tuffs in the SVB generally have less actinolite and more plagioclase than the massive and pillowed flows, however, they are lithogeochemically indistinguishable from the flows (*see* "Geochemistry").

Mafic lapilli tuffs are rare and difficult to distinguish in the field due to the compositional similarity between the matrix and the scoria lapilli. The few mafic lapilli tuffs present in the area are located in the Bish Bay assemblage of the NVB and could not be traced along strike. A hornfelsed mafic metavolcanic rock and iron formation, located along the contact with the olivine gabbro granophyre of the Proterozoic ultramafic intrusion, contains lapilli-sized scoriacous clasts of mafic metavolcanic rock in a matrix of very coarse-grained tremolite with 5 to 10% magnetite (*see* "Chemical Metasedimentary Rocks"). Some of the volcaniclastic units may, in part, be the products of intense deformation and shearing of massive or pillowed flows. An example of the intense deformation is observed in a unit located along the northern contact of the PPA that was interpreted in the field to represent a reworked tuff with grey chert clasts. This unit could also be interpreted to represent an intensely deformed massive flow and interflow chert, or possibly a deformed conglomerate of the NSB, although it lacks the variety of clasts common to the other conglomerates of the area.

Hyaloclastite, pillow fragment breccias in the SVB, and interpillow hyaloclastite in the PPA, are rare in the mafic metavolcanic rocks of the area and are not significant enough to be distinguished as separate map units. Pillow fragment breccias are generally only recognized in the better exposures along Lake Nipigon and the stripped areas to the west of Beardmore. The breccias are composed of subrounded to rounded, amoeboid-shaped clasts up to 10 cm in size in a very fine-grained chlorite-rich matrix. The clasts commonly have chloritic selvages less than 0.5 cm thick and are chloritized and silicified. The breccias form beds less than 1 m in thickness and appear to be discontinuous along strike. Interpillow hyaloclastite is only recognizable in the PPA and consists of irregular fragments up to 2 cm in length. These fragments are probably spalled pieces of the pillow selvage.

Depositional Environment

Flow morphology and textures in the mafic flows, with abundant pillows, are interpreted to indicate a subaqueous eruptive environment. Thinner massive flow thickness, compared to the pillowed flows and lack of volcaniclastic rocks, in the SVB and BBA is interpreted to indicate deposition distal to the vent. The higher hyaloclastite content and interbedding with tuff breccias in the PPA is interpreted to indicate deposition in a more vent proximal environment than the SVB.

INTERMEDIATE TO MAFIC METAVOLCANIC ROCKS

Intermediate to mafic metavolcanic rocks are predominant in the CVB and the Poplar Point assemblage (PPA) of the NVB. The intermediate metavolcanic rocks consist of massive and pillowed flows, tuffs, lapilli tuffs, pillow breccias, and tuff breccias. These units are commonly distinguished from the mafic metavolcanic rocks by their colour index, with the intermediate metavolcanic rocks generally weathering to a lighter green, except for the darker shoreline exposures. These shoreline outcrops have weathered surface colouration that closely resembles the fresh surface colour. Some flows, and clasts in tuff breccias, contain up to 10% fine-grained, white feldspar phenocrysts that are not present in the mafic metavolcanic rocks. The intermediate metavolcanic rocks also lack the variolitic textures observed in some mafic metavolcanic flows. The CVB does not display the same increase in deformation progressing from west to east that is evident in the mafic metavolcanic rocks of the SVB and NVB, resulting in better preservation of primary textures. The exceptions are narrow zones of higher deformation along the CVB–SSB contact and the Sandy Creek fault.

The intermediate metavolcanic rocks consist of plagioclase, epidote, and chlorite with minor amounts of sericite, amphibole, carbonate, quartz and opaque minerals. Plagioclase is saussuratized to different degrees, occurring both in a fine-grained groundmass and as relict phenocrysts in some flows. The dominant mafic mineral is chlorite, which occurs as groundmass material and as amygdule fillings. The minor amount of amphibole that is present appears to be of the tremolite-actinolite series. Quartz is generally less than 1%, but is more common than in the mafic metavolcanic rocks. This mineral assemblage produces a lighter colour that distinguishes the intermediate from the mafic metavolcanic rocks and an andesitic composition that contrasts with the basaltic composition of the mafic metavolcanic rocks (*see* "Geochemistry").

Massive Flows

Massive intermediate flows are fine to medium grained, and range from medium to light green or grey-green on weathered surfaces and medium grey green or grey on fresh surfaces. Individual flow thickness are difficult to determine, but appear to be on the order of metres based on the presence of interbedded pillowed flows and tuff breccias. Textures range from vesicular or amygdaloidal to feldspar porphyritic. Amygdules may be up to 0.75 cm in diameter, and filled with quartz, quartz-carbonate or quartz-epidote. A weakly silicified and carbonatized flow in the Poplar Point assemblage (PPA) hosts pyrite- and pyrrhotite-filled amygdules. Small chlorite-filled amygdules were observed in thin section. The feldspar porphyritic flows contain euhedral, 2 to 4 mm, white to light grey feldspar crystals in a very fine-grained to aphanitic groundmass. The phenocrysts may be difficult to identify unless the groundmass has weathered to a light green to pale green. These porphyritic flows are most prominent in the area of the 72 Road and in the PPA, where individual flows may be traceable on a map scale of less than 1:20 000. Some of the feldspar porphyritic flows of the PPA that are interbedded with pillowed flows have up to 5% vesicles and/or amygdules.

Pillowed Flows

Pillowed flows are medium to light green to grey-green on weathered surfaces and are aphanitic to fine grained. Individual flows are commonly a few metres thick, with a few examples that are tens of metres thick. Pillows are generally weakly deformed to undeformed, and approximately 0.5 m in diameter with some flows exposed along the shore of Lake Nipigon containing well-formed pillows greater than 1 m in diameter. Pillowed flows provided a number of reliable top determinations, which were particularly useful in the identification of folding in the area of the 72 Road. Pillow selvages are generally thicker than in the mafic metavolcanic rocks, ranging from 1 to 4 cm in width. Internal features include amygdaloidal and vesicular flow lamina textures and feldspar phenocrysts. The amygdules are filled with quartz, quartz-carbonate and/or quartz-epidote and are randomly distributed within the pillows. Locally, some pillows contained concentric flow laminae defined by the alignment of about 1 mm vesicles, with the best examples exposed along Lake Nipigon in Eva Township and in the eastern portion of the PPA (Photo 2). Some pillowed flows are feldspar porphyritic, with the same general appearance as the feldspar porphyritic massive flows. The feldspar porphyritic pillowed flows may be nonvesicular or vesicular, as is the flow shown in Photo 2. Feldspar porphyritic pillowed flows may also be traced on a map scale of less than 1:20 000.

Volcaniclastic Rocks

Volcaniclastic intermediate metavolcanic rocks include tuffs, lapilli tuffs, pillow breccias and tuff breccias. The tuffs and lapilli tuffs have been classified as volcaniclastic due to a lack of primary features supporting a pyroclastic origin, which is particularly difficult in the case of waterlain pyroclastic textures and subaqueous reworked volcaniclastic textures (e.g., Fisher and Schminke 1984). The pillow breccias exposed in the map area are composite units consisting of pillow breccia, pillow fragment breccia and

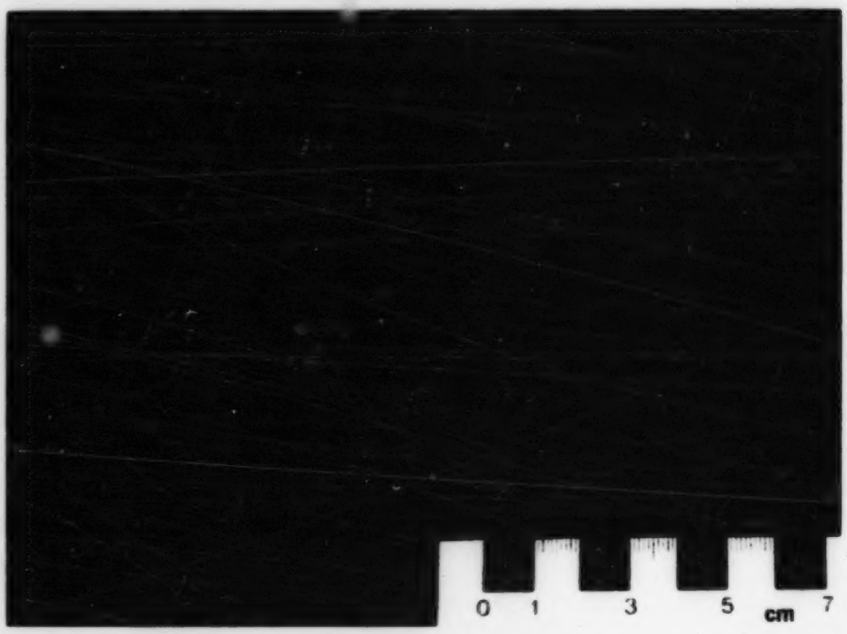

Photo 2. Flow laminae, resulting from alignment of approximately 1 mm vesicles, surrounded by alteration; detail to right: concentric flow laminae in pillowed andesite, Poplar Point assemblage, northern metavolcanic subbelt. Pen magnet is approximately 14 cm in length.

hyaloclastite-rich pillow fragment breccia best exposed along the shore of Lake Nipigon and in the PPA. Tuff breccias form a major portion of the volcanic stratigraphy in the eastern part of the CVB and in the PPA and have been subdivided into monolithic and heterolithic subtypes, with the monolithic breccias containing less than 5% mafic clasts.

The tuffs are generally insignificant and occur as interflow units less than 1 m thick. These rocks are well foliated, light grey-green on weathered surfaces and lack any primary internal structures. This lack of primary structures means that there is the possibility that some tuffs may represent thin, intensely foliated flow-top breccias that have been differentially deformed due to greater heterogeneity and much lower competency. Tuffs may contain white to light grey subhedral feldspar crystals and may be classified as crystal tuffs, but these beds are not thick enough to distinguish on a map scale. Primary bedding textures are present in 3 relatively undeformed tuffs, exposed in the PPA, that are composed of well-bedded, graded beds. These tuffs occur as interflow units, which, in one case, consists of a series of beds approximately 30 cm thick that are draped over the underlying mafic pillowed flows. However, the other 2 examples are thicker than the other tuffs in the map area, with 1 unit consisting of multiple beds forming a unit greater than 25 m thick. These tuffs could be classified as well-bedded, waterlain pyroclastic units rather than volcaniclastic rocks.

Lapilli tuffs consist of subrounded to well-rounded and flattened, light grey to grey-green scoria and pumice clasts in a fine- to very fine-grained, medium to light green chloritic groundmass. These tuffs form beds a few metres thick and are interbedded with massive and pillowed flows. The best examples of lapilli tuffs are exposed along the southern contact of the CVB, south of the 72 Road. The generally ellipsoid lapilli vary from 5 to 15 cm long and are elongated along the foliation, possibly indicating a higher degree of deformation than the flows. Some tuffs contain abundant lapilli with 2 to 3 mm subrounded to rounded quartz that are interpreted to represent quartz-filled amygdules, but may be quartz phenocrysts. The darker colour of the matrix is interpreted to be a result of a higher chlorite content, due to a greater degree of alteration related to an originally higher porosity. Lapilli tuffs are generally interbedded with pillowed flows indicating a subaqueous depositional environment, but as with the other volcaniclastic rocks, it is difficult to distinguish primary waterlain pyroclastic material from reworked volcaniclastic textures.

Pillow breccias occur as a transition from the pillowed flows to the hyaloclastite-rich pillow fragment breccias (e.g., Batiza and White 2000). The pillow breccia portion of the units are generally 1 m wide, with the pillows very rapidly diminishing in size away from the main body of the flow. Pillow fragment breccia forms the major part of the unit, and is generally a few metres in width adjacent to the flow front. Fragments generally consist of subangular parts of pillows and rounded fragments or amoeboid-shaped fragments and small pillows in hyaloclastite matrix. In one location, the flow front has a ropy transition to the breccia suggesting that the magma was intruding or supported by the hyaloclastite. The hyaloclastite is commonly dark green and highly chloritic, which obscures the glass and finer pillow fragments. The hyaloclastite-rich portion forms the outer edge of the unit, but the total thickness is difficult to determine due to increased alteration that obscures the contact with the overlying flow (Photo 3). The best examples are well exposed along the shore of Lake Nipigon and the central portion of the Poplar Point assemblage, where the pillow breccias are observed to overly the pillow flow front. Although the pillow breccias have been classified as volcaniclastic rocks, a portion of the units could be classified as hyaloclastite or rocks that are the result of fragmentation of the magma due to interaction with water (e.g., Cas and Wright 1987; Batiza and White 2000). There is no depth restriction to the formation of the pillow breccias, as the breccias have been observed in both shallow water and seafloor sites.

The monolithic tuff breccias usually form units a few metres thick, and are most prominent in the Poplar Point assemblage as beds that are tens of metres thick. This greater bed thickness may be due to

Photo 3. Pillow fragment breccia with subangular, rounded, or amoeboid-shaped fragments in hyaloclastite matrix, Poplar Point assemblage, northern metavolcanic subbelt. The hyaloclastite is highly silicified with replacement of hyaloclastite fragments with silica. Hammer is approximately 30 cm in length.

Photo 4. Heterolithic breccia, Poplar Point assemblage, northern metavolcanic subbelt, containing clasts of vesicular intermediate metavolcanic rocks with minor feldspar porphyritic felsic metavolcanic rocks, cherts, and mafic metavolcanic clasts.

the shallower dips of the units in this assemblage. The breccias were classified based on the dominant clast population, with the monolithic breccias containing less than 5% mafic or lithic clasts. Subangular to angular clasts in the monolithic breccias range from 0.5 to 10 cm in length, are a medium to light grey on the weathered surface and are set in a light to medium grey, fine-grained matrix. There is a bimodal clast size distribution, with the majority of the larger clasts ranging from 5 to 10 cm or finer clasts from 0.5 to 1.0 cm. The finer clasts are often difficult to distinguish from the matrix. The clasts are usually massive and fine grained with rare examples containing fine-grained feldspar phenocrysts. These units appear to overlie massive intermediate flows, but the stratigraphic relationship is not clear in all examples, as some breccias appear to occur in pillow flow sequences. These breccias are usually only identified on weathered surfaces, as the lack of contrast between the clasts and matrix on fresh surfaces could result in the classification of the unit as a massive flow.

The heterolithic breccias generally form beds a few metres thick and, as with the monolithic breccias, form thicker beds in the Poplar Point assemblage. The clasts are predominantly intermediate metavolcanic rocks, but a variety of feldspar porphyritic felsic metavolcanic rocks, cherts and mafic metavolcanic clasts are scattered through the beds. Generally, the breccias lack any internal structure, and although occasional areas appeared to have bedding structures, they generally could not be traced for any distance. Clasts of intermediate composition are medium to light grey on weathered surfaces, subangular to angular, and range from 0.5 to 10 cm, with a similar bimodal clast size distribution as observed in the monolithic breccias. These clasts are massive to vesicular, with some massive clasts containing fine-grained, white laths of feldspar and some vesicular clasts consisting of medium-grained, quartz-filled amygdules (Photo 4). Elongation of the quartz-filled amygdules may represent a flow foliation in the source magma. Feldspar to feldspar-quartz porphyritic clasts generally occur within 3 m of a contact with a felsic metavolcanic dike with peperitic textures along the margins of the clasts (*see* "Intermediate to Felsic Metavolcanic Rocks"). Mafic clasts are usually less than 5 cm in size and commonly form the majority of the finer clasts in the breccia. The matrix of the heterolithic breccias are generally highly chloritized and some of the smaller, more porous clasts may have been totally chloritized. Reaction rims were observed in outcrop and appear to be related to a higher degree of alteration (Photo 5). Irregular pods to disseminated medium- to coarse-grained pyrite occur in some of the breccias with a highly altered chloritized matrix (*see* "Alteration"). The difference between the heterolithic and monolithic breccias is, at least in part, due to the higher degree of alteration in the heterolithic breccias.

Depositional Environment

Flow morphology and textures in the intermediate to mafic flows, with abundant pillowed flows, are interpreted to indicate a subaqueous eruptive environment. The moderate massive flow thickness compared to the pillowed flows, and the greater abundance of volcaniclastic rocks compared to the mafic metavolcanic rocks, are interpreted to indicate a more vent proximal environment. Although the greater abundance of amygdules and abundant tuff breccias in the Poplar Point assemblage may be indicative of a higher volatile content rather than proximity to the vent. Both the monolithic and heterolithic breccias have been classified as volcaniclastic deposits as the breccias are usually matrix supported and contain some subangular clasts. However, some of the monolithic breccias could be classified as clast supported and may represent autobreccias formed by the adjacent massive, amygdaloidal flows (e.g., Cas 1992). The preservation of vesicular textures in the clasts of the heterolithic breccia and the lack of bedding or other primary sedimentary structures indicates that these clasts have not been extensively reworked. The lack of quench textures and glassy rimmed clasts suggest that most of the breccias are not hyaloclastite, although the alteration rims in some breccias may represent alteration of original glass rims. Therefore, there is the possibility that some of the breccias may be hyaloclastite or reworked hyaloclastite that originally formed as either autobreccia or as hyaloclastite from the adjacent subaqueous flows (e.g., Cas and Wright 1987; Cas 1992).

INTERMEDIATE TO FELSIC METAVOLCANIC ROCKS

Intermediate to felsic metavolcanic rocks are volumetrically insignificant in the BGB and are most prominent in the Elmhirst–Rickaby volcanic centre, Onaman–Tashota terrane, located in the northeast corner of the map area. A number of thin felsic metavolcanic units are interbedded with the intermediate flows of the CVB, with the thickest unit exposed in exploration trenches north of Eva Lake. A number of felsic dikes interpreted to be feeder dikes or synvolcanic intrusive rocks intrude the intermediate flows and tuff breccias of the Poplar Point assemblage (PPA). The felsic metavolcanic rocks of the Elmhirst–Rickaby volcanic centre were only observed within the Paint Lake deformation zone, along the shore of Lake Nipigon, with the majority of the data for the rocks compiled from Mackasey (1975).

Massive Flows

Massive, felsic to intermediate flows within the CVB form units usually a few metres thick that are interbedded with the intermediate metavolcanic flows. The best example is exposed in an exploration trench located within a topographic low, north of Eva Lake (*see* Figure 6). The flow is fine to very fine grained, light grey to a mottled pinkish grey on weathered surfaces and light grey on fresh surfaces. The mottled pinkish grey colour is interpreted to be the result of sporadic, weak hematitic alteration. In thin section, the rock is composed of subhedral laths of twinned feldspar, filled with inclusions, in a fine- to very fine-grained massive groundmass of cloudy feldspar, quartz and sericite, with 1%, disseminated, euhedral carbonate. This unit was named the Eva Lake quartz-feldspar porphyry by Shanks (1993) and was interpreted to be a hypabyssal rock unit. Contact relationships are not well exposed and are slightly ambiguous due to the alteration of the surrounding rocks, but due to a lack of textures indicative of a shallow crustal intrusive depth (e.g., mariolitic cavities), this unit is interpreted to be extrusive in origin. A sample of this unit was collected for a U/Pb radiometric age determination (*see* "Geochronology").

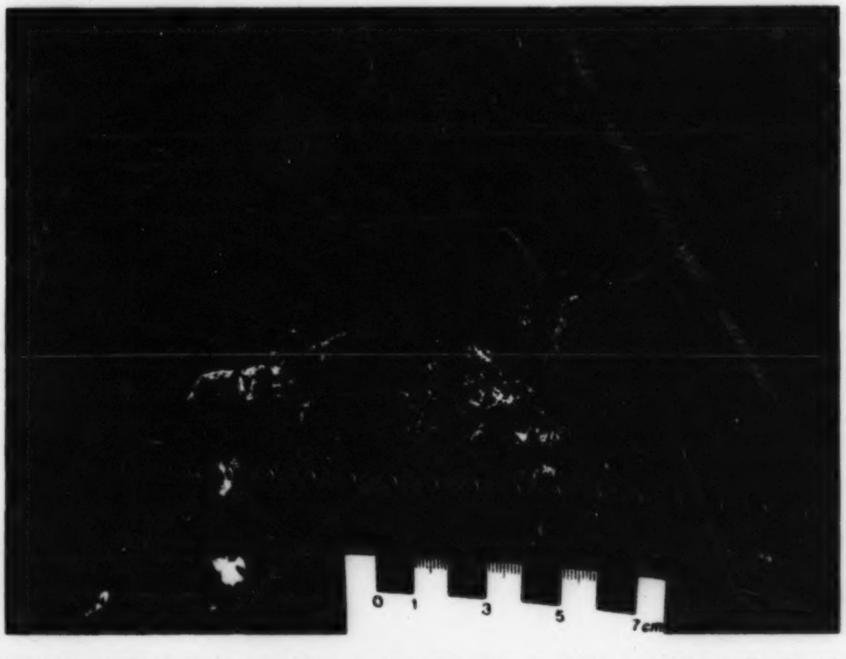

Photo 5. Heterolithic breccia, Poplar Point assemblage, northern metavolcanic subbelt, containing mafic clasts that display silicified reaction rims in a highly chloritized matrix.

This unit has the appearance of a silicified intermediate to mafic massive flow making it difficult to properly define without the exposure provided by the exploration trenches. There are probably more of these felsic units interbedded with the intermediate metavolcanic rocks of the CVB in less exposed areas.

Massive flows of the Elmhirst–Rickaby volcanic centre are located within the Paint Lake deformation zone along the shore of Lake Nipigon. These rocks are strongly to intensely sheared and have no recognizable primary textures. The flows are a few metres thick and interbedded with felsic to intermediate volcaniclastic rocks and intruded by a mafic intrusion. Flows are light grey to light greenish grey on weathered surfaces and medium to light grey or greenish grey on fresh surfaces. In thin section, the rocks consist of feldspar, quartz, chlorite, and sericite with bands of quartz-carbonate along the foliation. Descriptions of the massive flows by Mackasey (1975), in the northeast portion of Sandra Township, are comparable to the flows observed along the shore of Lake Nipigon.

Dikes

A number of fine- to medium-grained, massive, feldspar-quartz porphyritic felsic feeder dikes intrude the intermediate heterolithic tuff breccias of the central portion of the Poplar Point assemblage. The dikes are light grey to white with occasional pinkish grey patches on weathered surfaces and medium to light grey on fresh surfaces. The phenocryst content is varied with generally 10% white feldspar phenocrysts and 3 to 5% quartz phenocrysts, although occasionally the feldspar content decreases to approximately 1%. In thin section, the dikes consist of 1 to 3 mm subhedral laths of feldspar and 1 mm rounded quartz grains in a very fine-grained massive groundmass of feldspar, quartz and sericite with minor chlorite. The feldspar phenocrysts are twinned, but are nearly totally replaced by sericite. Contacts with the tuff breccia are very irregular and are marked by an approximately 2 m wide zone of tuff breccia containing up to 25% felsic dike clasts with irregular margins (Photo 6). These textures are interpreted to be peperites, which are indicative of synvolcanic formation as either subvolcanic felsic feeder dikes or

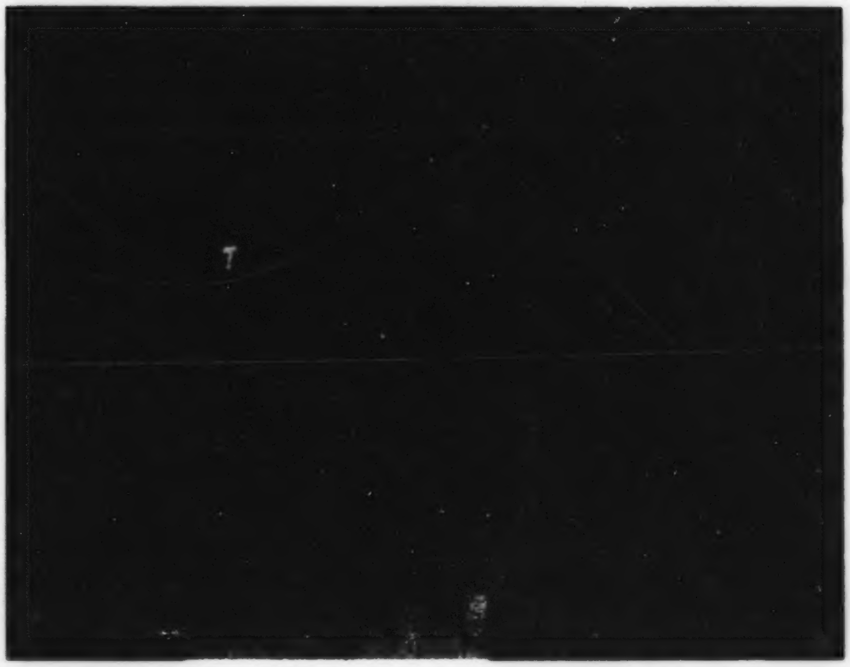

Photo 6. Peperitic textured feldspar-quartz porphyritic felsic feeder dike fragments in a heterolithic tuff breccia, Poplar Point assemblage, northern metavolcanic subbelt. Percentage of dike fragments decreases away from dike contact.

portions of felsic cryptodomes resulting from the intrusion of hot magma into a wet, unconsolidated volcaniclastic pile. This texture was observed along the contact of a number of dikes in this assemblage. A sample of one of these dikes was collected for geochronology (*see* "Geochronology").

Volcaniclastic Rocks

There appears to be a number of volcaniclastic intermediate metavolcanic rocks interbedded with the massive flows. However, the near total destruction of primary textures hinders an accurate description, and, in some locations, the volcaniclastic textures may be a result of intense deformation. The rocks observed along the Lake Nipigon shore appear to be lapilli tuffs or monolithic tuff breccias with flattened, lapilli-size fragments in a fine- to very fine-grained matrix. The rocks are light grey to greenish grey on weathered surfaces and light to medium greenish grey to grey on fresh surfaces. The greenish tint of some of the rocks is probably a result of high sericite ± chlorite content. The descriptions presented by Mackasey (1975) for the felsic to intermediate pyroclastic rocks would appear to encompass lapilli tuffs and monolithic tuff breccias. Primary textures are generally moderately well preserved further to the east as seen in Photos 5, 6, 7, and 8 in the report by Mackasey (1975, p.12, 14).

Depositional Environment

The low number of felsic metavolcanic rocks exposed in the map area and the intense deformation of some of the units means that an accurate interpretation of the depositional environment is difficult. The peperitic textures of the dikes in the Poplar Point assemblage indicate intrusion of the dikes into a wet unconsolidated volcanic pile suggesting a subaqueous depositional environment.

CHEMICAL METASEDIMENTARY ROCKS

The chemical metasedimentary rocks in the BGB include oxide-facies, clastic magnetite-argillite and jasper-hematite iron formations, cherts and an actinolite-magnetite hornfels unit. Oxide-facies iron formations, consisting of interbedded magnetite-chert beds, occur interbedded with the metavolcanic rocks of the SVB and CVB. Clastic iron formations, composed of magnetite interbedded with argillite, form multiple horizons within the SSB and CSB. Well-banded jasper-hematite iron formation horizons occur within the northern portion of the SSB close to the contact with the CVB. The cherts are relatively minor lithologic units in the map area and may represent variations on the oxide-facies iron formation. The actinolite-magnetite hornfels unit is restricted to the area immediately adjacent to the Proterozoic ultramafic intrusion.

Oxide-Facies Iron Formation (Magnetite-Chert)

Magnetite-chert iron formations exposed in the SVB are composed of units up to 2 m thick consisting of thinly bedded magnetite and chert. A number of iron formations are well exposed along the shoreline of Lake Nipigon in Kitto Township. These units are generally less then 1 m in thickness, but vary along strike, so that it is difficult to trace individual units for more than a few tens of metres. Alteration is characterized by moderate to patchy development of hematite. Iron formation is also exposed in the exploration trenches in southern Summers Township. The iron formation may be up to 2 m thick, but the thickness varies along strike. Alteration is intense with the development of hematite and minor sulphidization along quartz stringers, the formation of arsenopyrite and the deposition of gold. There are approximately 5 stratigraphically stacked iron formations in the SVB that can be trace intermittently along the length of the subbelt using the regional airborne magnetic survey (OGS 1998).

Within the CVB, magnetite-chert iron formations have 2 distinct forms, brecciated and magnetite-chert-bearing pyroclastic rocks. Exposures of either unit are rare and interpretation of the mode of formation is hindered since adjacent rock types are poorly exposed. A brecciated magnetite-chert iron formation occurs approximately 1 km north of Eva Lake, adjacent to the Eva Lake property (*see* Preliminary Map P.3513), as a small, circular hill. It is composed of brecciated magnetite (~60%) and chert (~40%) with trace amounts of fine-grained pyrite. The brecciation is probably the result of late tectonic deformation although no regional or local fault is interpreted to occur in the area. The lack of exposed contacts with adjacent rock units hinders a detailed interpretation and the lateral continuity of this unit is not known. In the southern CVB, the iron formation generally occurs as highly disrupted, weakly magnetic beds that are intercalated with thin chert layers. The magnetite may also occur in the matrix of a pyroclastic lapilli tuff suggesting that this unit may have been affected by diffuse hydrothermal discharge of iron-rich fluids. The magnetite is almost always highly altered to hematite. The iron formations of the CVB are discontinuous on the ground and define laterally restricted units that are difficult to correlate using the regional airborne magnetic survey (OGS 1998).

Clastic-Magnetite-Argillite Iron Formation

Clastic-magnetite-argillite iron formations occur as multiple horizons within the SSB, south of the Standingstone fault, and extend east to the Geraldton area. These units range from magnetite to clastic dominated. The magnetite-dominated iron formations consist of 0.05 to 0.3 m (may be up to 1 m) thick magnetite beds intercalated with 0.1 to 0.2 m thick argillite and rare siltstone beds forming units up to 25 m thick. Locally, the iron formation may contain less than 5% jasper lenses. A good example of one of the thicker units is exposed to the west of Undersill Lake. The clastic sediment dominated iron formations form units up to 1 m thick consisting of 1 to 5 cm thick magnetite beds interbedded with 1 to 20 cm thick feldspathic wacke, argillite and rare siltstone beds. These units may overlie or underlie the magnetite-dominated units as observed in the area west of Undersill Lake. The variability of the clastic sediment content of these units, and the lack of prominent jasper or chert, is interpreted to indicate that these units were formed by a resedimentation of pre-existing chemical sediments. The magnetite-dominated units may represent the main channels and the clastic-dominated units may represent the levée facies.

Generally, only one horizon of iron formation was observed in a traverse across the SSB, hindering lateral correlation of magnetite- and clastic-dominated units. However, a series of exploration trenches south of Highway 580 on the Long Lac Superior property have exposed a stratigraphic section with 4 separate iron formation horizons that range from magnetite- to clastic-dominated varieties. Deformation within the iron formations and blocks of rip-up clasts in the adjacent clastic metasedimentary rocks are interpreted to be the result of soft sediment deformation. This suggests that the iron formations may be an original stratigraphic succession. However, the highly folded nature of one clastic-dominated iron formation indicates that this stratigraphic stacking may be the result of large-scale structural repetition (Photo 7). Minor discontinuities in the regional airborne magnetic data could be interpreted to be the result of structural repetition or may represent a series of isolated depositional channels (OGS 1998). The channel interpretation is partially supported by the turbidite model proposed by Barrett and Fralick (1986). In this model, variations in the coarseness and thickness of clastic beds in different sections within the iron formations are interpreted to reflect proximal to distal locations relative to the channel-feed systems on a turbidite deltaic fan located on the paleoseafloor.

In the CSB, approximately 1 km north of the Namewaminikan River, magnetite-chert iron formation at least 25 m thick is exposed close to the contact with the metavolcanic rocks of the Poplar Point assemblage. The iron formation is composed of 5 to 10 cm thick chert beds intercalated with 1 to 5 cm thick magnetite beds. Chert beds are generally medium to light grey and occasionally light green. The magnetite beds occasionally display intense alteration to hematite that can be mistaken as jasper horizons. Contacts vary from sharp to gradational with the surrounding clastic metasedimentary rocks.

Jasper-Hematite Banded Iron Formation

Jasper-hematite banded iron formations occur in the SSB, along the contact with the CVB, with the best exposures in the area near the Leitch Mine. The units range from 10 cm to over 3 m in thickness, and are composed of 0.5 to 1.0 cm jasper beds intercalated with 0.3 to 2.0 cm specular hematite beds and 0.5 to 4 cm mudstone beds. These iron formations are interbedded with feldspathic wacke, siltstone and argillite of the SSB. Some thicker occurrences of the iron formation are likely due to fold repetition, with up to 3 phases of folding observed at an outcrop scale near the Leitch Mine. This unit can be traced along the strike of the folded SSB–CVB contact before disappearing to the west due to overburden cover. To the east, this unit appears to terminate against the Standingstone fault. The presence of jasper-hematite iron formation north of the Standingstone fault, in contrast to clastic magnetite-argillite iron formation south of the fault, suggests that this fault may represent a major structural discontinuity.

Chert

Sporadic, discontinuous horizons of chert occur within the metavolcanic units of the Beardmore–Geraldton Belt, with the most prominent examples located within the Poplar Point assemblage of the NVB and throughout the CVB. The chert occurs as 1 to 5 cm thick interflow units that are laterally discontinuous. Many of the units display intense hematitic alteration suggesting a very low magnetite content.

Photo 7. Folded horizon of clastic-magnetite-argillite iron formation, southern metasedimentary subbelt, interpreted to indicate large-scale structural repetition of iron formations. Hammer is approximately 30 cm in length.

A single occurrence of isoclinally folded, banded jasper-chert occurs in the SSB, exposed in the exploration trenches south of Highway 580. This unit is about 2 m thick and composed of 0.5 to 1.0 cm thick jasper beds intercalated with 0.3 to 1.0 cm thick light to medium grey chert beds. Although, this unit indicates some hydrothermal activity within the SSB, south of the Standingstone fault, this activity was probably restricted due to the lack of chert in the clastic iron formations. The significance of this unit is not known as it was observed in only a single location.

Actinolite-Magnetite Hornfels

A hornfels unit composed of alternating beds of magnetite and actinolite and/or tremolite is located along the contact between the olivine gabbro portion of the ultramafic intrusion and the mafic metavolcanic rocks of the SVB in western Kitto Township (*see* Figure 6; *see* Preliminary Map P.3512). The magnetite-rich beds are medium grey and composed of coarse-grained actinolite and/or tremolite and fine-grained magnetite with an irregular ribbon texture. The actinolite-rich beds consist of a light grey to grey-green matrix of coarse-grained actinolite and/or tremolite and disseminated magnetite containing light brown, lapilli-sized vesicular clasts of mafic metavolcanic rock and dark grey irregular-shaped clasts of magnetite-rich material. The metavolcanic clasts may occasionally have light-grey reaction rims. These units are interpreted to be derived from the mafic metavolcanic rocks and magnetite-chert iron formation observed along strike and subsequently metamorphosed in the thermal aureole of the ultramafic intrusion.

CLASTIC METASEDIMENTARY ROCKS

The clastic metasedimentary rocks of the Beardmore–Geraldton Belt form 3 northeast- to east-northeast-striking subbelts, of which only the southern metasedimentary subbelt (SSB) and portions of the central metasedimentary subbelt (CSB) crop out in the map area. The SSB is composed of thinly to thickly bedded feldspathic wacke, lithic wacke, siltstone, polymictic conglomerate and mudstone and/or argillite with a clastic-argillite-magnetite iron formation and a jasper-hematite iron formation providing stratigraphic markers within the subbelt. Exposures of the CSB are less diverse than the SSB and consist of polymictic conglomerate, lithic arenite and an argillite-magnetite iron formation.

Feldspathic Wacke

Feldspathic wacke is the dominant clastic sediment in the BGB, forming units ranging in thickness from less than 0.3 cm to greater than 1 m and are composed of beds averaging between 0.3 and 30 cm thick. The wacke weathers to a pale greyish brown, medium green, or buff white, and are medium grey to pale greyish brown on fresh surfaces. Beds generally consist of sand- to granule-sized material that is poorly sorted to moderately well graded. Grain gradation and rare cross-beds were used to define original stratigraphic top directions and were useful in delineating panels of opposing facing directions that are interpreted to result from folding. Bedding is steeply dipping (65 to 90°), commonly overturned, and strikes east (240 to 284°), although a change in the orientation of graded bedding in the area southwest of the Leitch Mine suggests a reversal in top directions. Locally, some beds contain greater than 15 cm long rip-up clasts of siltstone and/or argillite and coarse-grained feldspar clasts up to 2 cm in length. A good example of the rip-up clasts of the finer clastic metasedimentary rocks in a wacke matrix are exposed in the exploration trenches south of Highway 580. Load casts, cross-beds and flame structures may be present along contacts with argillite beds and some channel scours were observed. These structures are well exposed on the logging road system in the area of Undersill Lake. It is unclear whether these structures are primary sedimentological features or if they are false sedimentary structures produced by layer-parallel shear.

The feldspathic wacke is composed of subequal amounts of plagioclase and feldspar in a matrix of predominantly fine-grained chlorite with varied amounts of carbonate and sericite. Opaque minerals include pyrite and ilmenite. Matrix content ranges from 60 to 85% indicating a wacke composition. However, in hand samples, it is difficult to accurately determine the matrix content, and some wacke may have been incorrectly identified as arenite in the field. One sample, located approximately 100 m south of the metavolcanic inlier along the shore of Lake Nipigon in northwestern Kitto Township, contains anomalous amounts of biotite (>5%) comparable to that observed in a sample from the Quetico Subprovince. A high biotite content is also common in the matrix of the diabase and olivine gabbro located along the contact with the metasedimentary rocks. This high biotite content is interpreted to be due to contact metamorphism during the intrusion of the adjacent ultramafic body.

Lithic Wacke

The lithic wacke is restricted to the SSB, and appears to represent less than 5% of the clastic metasedimentary rocks exposed in the subbelt. These units are distinguished by the presence of greater than 10% lithic fragments that are difficult to identify except on the best outcrop exposures. Therefore, some of the lithic wacke was probably misidentified in the field as feldspathic wacke. The wacke weathers to pale greyish brown, medium green, or buff white, and is medium grey to pale greyish brown on fresh surfaces. These units are intercalated at a scale of tens of centimetres with feldspathic wacke, siltstone, and mudstone and/or argillite. Lithic wacke consists of both massive and well-graded beds 1 to 3 cm thick that commonly form bedsets that are 10 to 20 cm thick. The beds are composed of angular to subangular sand- to granule-sized quartz, feldspar and lithic clasts. Within the map area, this lithology seems to be restricted to rocks of the SSB, although this may be due to the restricted number of exposures of the CSB. No samples were collected for petrographic analysis.

Quartzose Wacke

Quartzose wacke occurs immediately adjacent to a polymictic conglomerate in the upper portion of the CSB. Massive beds range from 30 to 100 cm in thickness, although, due to limited field exposures, it is unclear as to the thickness of bedsets or to the strike extent of the unit in general. The beds weather a distinctive reddish orange to grey, and are pinkish grey on fresh surfaces. The wacke is extremely fine grained, matrix supported and composed predominantly of quartz with minor plagioclase phenocrysts. The wacke has been affected by the strain in the CSB and contains a well-developed slatey cleavage that overprints primary bedding features. A thin section was not made for this lithology.

Lithic Arenite

The lithic arenite is restricted to the CSB and is distinguished from lithic wacke by the presence of angular, sand-sized clasts of jasper (<2 to 10%). The arenite occurs as massive beds greater than 4 m thick, although thinner bed thicknesses may have been overlooked on larger exposures as the bed definition between arenite and wacke is very indistinct. The lithic arenite is located along the south side of a polymictic conglomerate in the northern portion of the CSB. Beds are composed of angular to subangular sand- to granule-sized quartz and plagioclase, with rare jasper clasts and less than 1% pebble-sized clasts of siltstone observed on the larger exposures of the lithic arenite. The lithic arenite may be more correctly termed a sublitharenite (following Pettijohn 1975). The arenite weathers a light reddish grey and is light to medium grey on fresh surface. Some misidentification of lithic arenite as lithic wacke may have occurred due to the difficulty in determining the percentage of matrix without the aid of thin section petrography. For example, 1 hand sample, identified in the field as a lithic wacke, was subsequently renamed a lithic arenite by the presence of angular jasper clasts. However, the percentage of matrix is varied and it is possible that either all units mapped as lithic arenite are actually lithic wacke or this package of rocks ranges from wacke to arenite in composition.

Siltstone and Argillite

Exposures of siltstone are generally restricted to the SSB where it is interbedded with wacke and argillite. The only exception is an occurrence in the CSB where thin beds of siltstone are intercalated with argillite in a clastic-magnetite-argillite iron formation. Siltstone weathers buff-white to whitish and are a powdery white on fresh surface. The siltstone forms thin 0.3 to 3 cm thick beds intercalated with wacke or wacke–argillite bedsets ranging from 3 to 10 cm thick. Flame structures and load casts are generally microscopic. Rare flame structures may be up to 8 cm in diameter (1.5 cm in height) and form locally along contacts with the feldspathic wacke. Limited bedsets display a crude fining-upward sequence of wacke, argillite and siltstone, suggesting transition from a high-energy depositional environment to a low-energy environment.

Similar to the siltstone, argillite generally occurs within the SSB, with the exception of sporadic occurrences associated with iron formations in the CSB. Argillite weathers dark greenish grey to brown and are dark greyish brown to charcoal on fresh surfaces. The argillite beds are generally less than 0.3 to 3 cm thick and, together with siltstone beds, form 0.1 to 1.0 m thick bedsets interbedded with feldspathic and lithic wacke beds. Occasional rip-up clasts of argillite and siltstone occur locally within feldspathic wacke.

Conglomerate

The conglomerate units in both the CSB and SSB are polymictic, matrix supported and occur in 10 to 30 cm thick beds. The conglomerate units in the SSB may occur as individual beds or bedsets up to 3 m thick, whereas, in the CSB, the units occur as a horizon of multiple bedsets greater than 25 m thick. In the SSB, the conglomerate beds range from 10 to 30 cm up to 3 m in thickness and are generally interlayered with feldspathic wacke on a scale of metres to tens of metres. Volumetrically, the conglomerate comprises only a small percentage of the outcrop exposure. The conglomerate is composed of granule- to cobble-sized granitoid, quartz and volcanic clasts and rare chert and jasper clasts in a chloritic wacke matrix. An average point count, over a 1 m^2 area, on an outcrop east of the Leitch Mine, contained approximately 40% coarse-grained, 2 to 5 cm, unfoliated granitoid clasts; 30% coarse-grained, 2 to 5 cm, quartz-porphyritic clasts; 15% well-foliated, fine- to medium-grained, 2 to 3 cm, felsic metavolcanic clasts; approximately 15% highly foliated, fine- to medium-grained (1 to 4 cm) mafic metavolcanic clasts; greater than 1% jasper pebbles; and greater than 1% chert pebbles. The conglomerate is generally poorly sorted and matrix supported, although immediately north of the Leitch Mine along Highway 580, the conglomerate is interbedded with feldspathic wacke which displays graded bedding overturned to the south. Excluding granitoid and quartz-porphyritic clasts, most of the clasts are moderate to highly strained. With the exception of an anomalous thicker bedset north of the Leitch Mine, the SSB conglomerate generally occurs as single beds with a strike length of approximately 5 to 10 m, as exposed in an exploration trench south of Highway 580, north of the Standingstone fault. These thinner, laterally restricted beds are interpreted to have formed as channel deposits.

In the northern portion of the CSB, polymictic conglomerate occurs as 0.3 to 2.0 m thick beds in a horizon greater than 25 m thick. The conglomerate is generally matrix supported, although portions seem to be clast supported. The conglomerate consists of mafic metavolcanic, felsic to intermediate metavolcanic, felsic metavolcanic, feldspar-porphyritic, granitoid, quartz and minor chert, magnetite and jasper clasts. The pebble- to cobble-sized clasts are subrounded to rounded and, in places, display crude pseudograded beds up to 30 cm thick. However, grading commonly reverses both along strike and vertically within adjacent beds and thin, discontinuous horizons of silty sandstone and clast-poor beds are commonly intercalated within the polymictic conglomerate. These features are interpreted to be related to the conglomerate forming as individual channel flows.

Depositional Environment

The SSB displays no systematic variation in either bedding thickness or composition with the exception of the conglomerate, which was only observed in the northern portion of the subbelt. Locally, feldspathic wacke beds near Undersill Lake were observed to be coarser grained and thicker toward the north, though similar beds also occur elsewhere in the subbelt so that this variation may not be significant. A detailed petrographic study of the sequence through the Leitch Mine was interpreted by Barrett and Fralick (1985) to represent progradation of clastic-rich sediment lobes on a submarine fan into relatively quiet, low-energy depositional environments. The conglomerate forms channel deposits of up to 10 m in strike length along the south side of a clastic-argillite-magnetite iron formation and along the north boundary of the SSB. The metasedimentary rocks of the SSB have been interpreted, by Shanks (1993), to represent deep-water turbidites (Bouma A + E).

The CSB displays a similar south to north variation from the lithic arenite into the conglomerate. Lithic arenite generally forms in short transport and/or intraformational environments, such as a large drainage basin with diverse bedrock lithology (Pettijohn 1975). Lithic arenite of the CSB are interpreted to be deposited by either an alluvial or deltaic river. The conglomerate beds of the CSB are commonly lensoidal, which may be interpreted to represent a series of overlapping channel deposits supporting the deltaic river model (after Pettijohn 1975).

Quetico Subprovince

Metasedimentary rocks of the Quetico Subprovince are exposed along the southeast and east side of Kitto Township. The rocks consist of feldspathic wacke, lithic wacke, siltstone and local polymictic conglomerate that are distinguished from the metasedimentary rocks of the Beardmore–Geraldton Belt by the presence of biotite. The feldspathic wacke is generally moderately to well sorted with 3 to 30 cm thick beds and weathers to a pale greyish brown or buff-white. Locally, feldspathic wacke displays minor amounts of hematite alteration. In thin section, the rock contains 30 to 35% medium- to coarse-grained, subhedral biotite in a fine-grained matrix of quartz, plagioclase and muscovite. The biotite displays weak to moderate chlorite alteration and contains abundant pleochroic haloes. Thick (0.5 to 2 cm) biotite-rich layers may represent relict primary bedding. A moderate to strong foliation is defined by the alignment of biotite and by the undulatory extinction of matrix quartz. The rock contains weak to moderate quartz ribbons that are dominantly oriented subparallel to the main fabric. These units are similar to the metasedimentary rocks of the SSB and probably represent comparable but more highly deformed and metamorphosed units.

Feldspathic wacke is interbedded with lithic wacke, siltstone and mudstone and/or argillite. Lithic wacke forms 1 to 3 cm thick horizons composed of sand- and granule-size clasts. Some lithic wacke may have been misidentified in the field as feldspathic wacke due to the difficulty in identifying the lithic clasts. Siltstone weathers buff-white to whitish and forms thin horizons that are 0.3 to 1 cm thick. The argillite generally occurs in 0.3 to 3 cm thick beds, and together with siltstone, form 0.1 to 1.0 m thick bed sets within the feldspathic and lithic wacke. One outcrop of polymictic conglomerate was observed in southeastern Kitto Township. It is matrix supported, containing subangular to subrounded pebble- and cobble-sized clasts of felsic and intermediate metavolcanic rock. The conglomerate grades to the north, forms 10 to 30 cm thick beds, and is interlayered on a scale of tens of centimetres with feldspathic wacke.

DEPOSITIONAL ENVIRONMENT

The metasedimentary rocks of the Quetico Subprovince generally consist of felsic and mafic turbidite sequences that were likely accumulated in the trench environment of an accretionary complex (Williams 1989; Percival and Sullivan 1988). The felsic turbidites dominate the subbelt and have been interpreted to represent a Bouma A, AB and ABC sequence reflecting deposition in a ramp-like environment (Fralick, Wu and Williams 1992). Minor mafic turbidites occur as isolated pods within the subbelt and display possible shallow water reworked intervals (Fralick, Wu and Williams 1992). The Quetico Subprovince displays a similar depositional environment to that of the Beardmore–Geraldton Belt as both basins dominantly consist of unstructured turbidite sequences.

SYNVOLCANIC TO SYNTECTONIC MAFIC INTRUSIVE ROCKS

A number of 10 to 130 m thick, medium-grained, massive, mafic sills intrude the metavolcanic rocks of the SVB and Bish Bay assemblage of the NVB. The mafic intrusion within the intermediate to felsic rocks along the shore of Lake Nipigon, transected by the Paint Lake fault, has been included in this group of rocks (*see* Figure 6). The age of these intrusions is difficult to determine because contact relationships are rarely observed. However, these intrusions have been interpreted to be synvolcanic to syntectonic as they are oriented subparallel to bedding, have a weak tectonic foliation, do not have obvious metamorphic haloes, and have not been identified as intruding the SSB or CSB.

The mafic intrusions located in the SVB in Kitto and Summers townships strike approximately 035°, or subparallel to the bedding of the mafic metavolcanic rocks. These intrusions are generally about 1 km long and 100 m wide. The intrusions are white to pink and dark green on weathered surfaces and greenish grey on fresh surfaces. The rocks have a fine-grained to aphanitic grey groundmass with fine- to medium-grained, euhedral to subhedral green hornblende phenocrysts and were mapped as gabbro. In thin section, the gabbroic rocks are characterized by 30 to 60% euhedral to subhedral fibrous hornblende phenocrysts, 10 to 30% anhedral feldspar crystals, 2 to 10% anhedral opaque minerals and up to 30% fine-grained groundmass composed of chlorite, epidote and sericite alteration. The gabbroic rocks have a higher amphibole content than the mafic metavolcanic rocks, providing a useful discriminator between the rock types. Alteration varies between intrusions, with the degree of alteration estimated from the amount of fresh feldspar present. Two intrusions within the SSB are more leucocratic than most of the gabbroic rocks. One leucocratic gabbro is located in Kitto Township, and is in contact with the ultramafic intrusive rocks (*see* Figure 6; *see* Preliminary Map P.3512). This gabbro has a pale green weathered surface resulting from the epidotization of the plagioclase, and contains only about 30% mafic minerals. This unit is most deformed than most of the mafic intrusions with the hornblende phenocrysts aligned along a foliation. The second leucocratic gabbro is located in Summers Township near the contact between the SVB and the SSB (*see* Figure 6; *see* Preliminary Map P.3513). This gabbro contains about 25% coarse-grained hornblende phenocrysts in a fine-grained, white feldspar-rich groundmass (Photo 8).

The mafic intrusions located in the Bish Bay assemblage of the NVB have a varied amphibole and feldspar content and range from gabbro to diorite in composition. These intrusions are about 100 m wide, 0.5 to 1.0 km long and strike approximately 075°. Weathered surfaces vary from light pink-white to green and rusty-orange with fresh surfaces varying from medium to dark green. The intrusions are fine to medium grained with phenocrysts of amphibole from 1 to 5 mm in length. Thin sections indicate that these rocks consist of 10 to 40% anhedral to subhedral hornblende phenocrysts, up to 5% opaque minerals, trace amounts of quartz and a fine-grained groundmass of chlorite, sericite and epidote. The large intrusion, interpreted to extend from the lakeshore of Lake Nipigon for approximately 3500 m to the east, has a width of 500 m. A sample has a chlorite groundmass with hornblende phenocrysts replaced by actinolite. Further to the east, the intrusion contains hornblende and plagioclase laths with significant amounts of chlorite in both the groundmass and fracture fillings in the hornblende phenocrysts. The easternmost samples collected from this intrusion are composed of zoned and twinned plagioclase phenocrysts in a plagioclase and chlorite groundmass. This intrusion is interpreted to be a fractionated gabbro sill with a peridotite phase in the north and a gabbro to diorite phase in the southern part of the intrusion. The gabbroic rocks from both the SVB and the NVB have similar mineralogy, but the NVB intrusions are more altered and metamorphosed.

The mafic intrusion within the intermediate to felsic metavolcanic rocks of the Elmhirst–Rickaby volcanic centre and transected by the Paint Lake fault has been grouped with this series of mafic intrusions. The intrusion is moderately foliated, medium to coarse grained with very coarse-grained amphibole. The rock is dark green to grey green on weathered surfaces and dark green on fresh surfaces. This intrusion is slightly oblique to the structural fabric and is much less deformed than the adjacent metavolcanic rocks. This is interpreted to be the result of the intrusion being more competent during deformation. Thin section analysis indicates that the rock consists of 30% (2.5 mm in diameter) hornblende phenocrysts with dark inclusions. The remainder of the section consists of a fine-grained groundmass of sericite, chlorite ± epidote.

SYNVOLCANIC TO SYNTECTONIC INTERMEDIATE TO FELSIC INTRUSIVE ROCKS

A number of intermediate to felsic intrusive rocks occur in the metavolcanic rocks of the Beardmore–Geraldton Belt. Most of the intrusions are granodiorite in composition, but include minor feldspar, quartz and quartz-feldspar porphyry and quartz diorite phases. Large, granodioritic sills and dikes occur throughout the metavolcanic rocks of the Poplar Point assemblage (PPA) of the NVB. Numerous feldspar porphyritic dikes intrude the intermediate to mafic metavolcanic rocks of the PPA and the CVB, and one feldspar porphyritic dike was observed in mafic metavolcanic rocks of the SVB. Two quartz porphyry dikes are exposed within intermediate to mafic metavolcanic rocks of the PPA and the CVB. Some of these units were grouped together based on petrographic similarities, but have been subdivided due to lithogeochemical differences. Many of these intrusive rocks were observed in the relatively undeformed PPA, complicating the determination of the relative ages.

Photo 8. Coarse-grained, leucocratic, synvolcanic gabbro crosscut by diabase dike, southern metavolcanic subbelt.

The majority of granodiorite intrusions in the PPA intrude intermediate to mafic, pillowed to massive flows and tuff breccia (*see* Figure 6), generally as dikes that are subparallel to the regional tectonic fabric. On outcrop, the rock is a distinctive light pink-grey on weathered surfaces (*see* Photo 6), and contains 3 to 5 cm thick chill margins favouring a syntectonic intrusive event. A weak to moderate tectonic foliation is defined by the orientation of biotite and chlorite grains within the intrusion (Photo 9). The granodiorite contains weak, 0.3 to 3.0 cm wide fault-fill quartz veins and trace to weak, 0.3 to 1.0 cm wide epidote, calcite and ankerite veins. Generally, the quartz veins and fractures do not contain sulphide minerals. An intrusion located along the lakeshore of Lake Nipigon, in northern Dorothea Township, contains 1% coarse-grained disseminated pyrite along fractures associated with chlorite alteration. In places, the granodiorite displays very weak to weak sericitic, hematitic and chloritic alteration, generally as fracture fillings throughout the rock. In thin section, the granodiorite is comprised of medium-grained quartz (55%), medium-grained, subhedral to euhedral plagioclase (30%), medium-grained, anhedral to subhedral potassium feldspar (orthoclase?, 10%), fine- to medium-grained, subhedral biotite (<5%), with trace amounts of titanite. Hypidomorphic and equigranular quartz, plagioclase and potassium feldspar crystals indicate a classic granitic texture. Individual plagioclase crystals are 80 to 90% altered to sericite. Biotite contains a moderate amount of pleochroic haloes, and displays moderate to intense alteration to chlorite. Quartz diorite locally intrudes adjacent to the granodiorite. It is a massive unit that displays moderate carbonate and trace epidote alteration, and contains less than 0.3 cm wide extensional quartz calcite veins.

Numerous feldspar porphyritic dikes were observed in the western portion of the intermediate to mafic metavolcanic rocks of the PPA and throughout the CVB, and one feldspar porphyritic dike was noted in the SVB near Lion Bay (*see* Preliminary Map P.3512). The dikes weather white to light greyish pink and usually do not display chill margins with the host rocks. An exception to this occurs northeast of the Placer Dome–Metalore property (*see* Figure 5, #11) where a series of metre-scale feldspar porphyritic dikes display 3 to 5 cm thick chill margins against the massive metavolcanic host rock.

Photo 9. Synvolcanic to syntectonic intrusive granodiorite with a weak to moderate tectonic foliation highlighted by silicification and chloritization along fractures. Pen magnet is approximately 14 cm in length.

Contacts are straight, in comparison with the granodioritic bodies that generally display irregular peperitic contacts (*see* Photo 6). In general, although dikes have undergone a high degree of alteration to sericite, they remain relatively undeformed. A thin section from a dike in Kitto Township contains approximately 15% subhedral plagioclase phenocrysts. The phenocrysts are 10 to 15% altered to fine-grained sericite. The matrix consists of a fine-grained mixture of plagioclase and quartz and displays a weak to moderate amount of sericite, calcite and chlorite alteration. The chlorite grains define a very weak tectonic foliation. In the PPA, the feldspar porphyritic dikes contain up to 35% subhedral, medium-grained to coarse-grained plagioclase phenocrysts in a fine-grained mixture of plagioclase and feldspar. Alteration is varied with the feldspar intensely altered to sericite and chlorite, but some dikes contain relict amphibole grains. No geochronology has been completed for the feldspar porphyritic dikes intruding into either the NVB or the SVB, and it is unclear whether the dikes reflect multiple phases of one intrusive event related to the granodiorite or if they belong to separate intrusive events.

Quartz-feldspar dikes were observed within the intermediate to mafic metavolcanic rocks of the PPA (*see* Figure 6). The dikes are massive, quartz-feldspar porphyritic bodies that weather white-pink to greyish-green. They commonly contain up to 5 to 10% circular to oval quartz eyes that are 2 to 3 mm in size and 1 to 3 mm anhedral plagioclase laths. Some dikes contain 0.3 to 1.0 cm thick epidote-filled fractures with associated trace to weak pyrite mineralization and display a moderate to intense amount of pervasive alteration to fine-grained sericite, calcite and chlorite. The dikes consist of coarse-grained, subhedral phenocrysts of plagioclase (20%) and medium- to coarse-grained, subrounded phenocrysts of quartz (5 to 10%) in a fine-grained, randomly oriented matrix of quartz and plagioclase. Plagioclase phenocrysts display moderate to intense pervasive alteration to sericite, whereas discrete rims of sericite alteration occur locally around quartz phenocrysts. Fibrous chlorite occurs adjacent to plagioclase phenocrysts. The matrix is intensely altered to sericite and minor calcite with recrystallized quartz lenses occurring locally throughout the matrix. Locally, quartz-feldspar dikes contain less than 2% opaque minerals.

Minor quartz porphyritic dikes occur within intermediate to mafic metavolcanic rocks of the PPA, the NVB and the CVB. These dikes are generally approximately 2 m in width and have pale white to light green weathered surfaces and grey fresh surfaces. The quartz porphyry is comprised of a very fine-grained to aphanitic matrix of quartz and feldspar that may contain up to 10% circular to oval quartz eyes that are 2 to 3 mm in size. Locally, the rock contains 3 to 5% disseminated grains of pyrite. The dikes have undergone moderate to intense sericitization.

The majority of felsic intrusive rocks occur in outcrops that are laterally discontinuous with contacts not well exposed, resulting in unclear intrusive and tectonic relationships. In general, the granodoritic bodies have irregular contacts with the tuff breccia, which is marked by a zone of tuff breccia containing up to 25% felsic dike clasts with irregular margins (*see* Photo 6). These peperitic textures are indicative of synvolcanic formation as either subvolcanic felsic feeder dikes or portions of felsic cryptodomes resulting from the intrusion of hot magma into a wet, unconsolidated volcaniclastic pile. In contrast, the feldspar, quartz and quartz-feldspar porphyries generally display sharp contacts, suggesting that the volcanic pile was already consolidated when the dikes were intruded. The compositional range of the intrusions is interpreted to reflect multiple phases related to one intrusive event, though it also allows for small-scale individual intrusive events.

POSTTECTONIC MAFIC INTRUSIVE ROCKS

Several massive, diorite and gabbro sills intrude the metavolcanic and the metasedimentary rocks along the contact between the CVB and the SSB, and the northern and southern boundaries of the Poplar Point assemblage (PPA) of the NVB. These intrusions are generally elongate along the regional strike, but are relatively undeformed. A chilled contact was observed between one of the intrusions and the metasedimentary rocks of the SSB. Based on these differences, these intrusions are interpreted to have been emplaced during a posttectonic igneous event in contrast to the deformed synvolcanic mafic intrusions. The intrusions are approximately 40 m up to 2 km wide and extend for approximately 300 to 3000 m along strike.

The intrusions are generally massive, fine to medium grained with a surface that weathers white-pink to white-green. Fresh surfaces are grey to green with green phenocrysts and noticeable white minerals (probably plagioclase) that are absent in synvolcanic mafic intrusions. In thin section, the average mineralogical composition is 35 to 70% fine-grained groundmass of chlorite and sericite, 5 to 45% secondary chlorite that fills open space, and trace to 5% opaque minerals and quartz. Hornblende phenocrysts are present in a few samples and are totally or partially replaced by chlorite or actinolite. One intrusion, located on the shore of Lake Nipigon in central Eva Township, appears to be a composite intrusion. In thin section, the rocks on shore have remnant hornblende crystals replaced by chlorite, 10% feldspar and an average of 50% fine-grained groundmass consisting of sericite and chlorite and trace amounts of quartz and opaque minerals. About 600 m to the east of the lakeshore, a sample was collected from the intrusion that contains relatively fresh hornblende phenocrysts with chlorite and sericite restricted to the groundmass. The easternmost sample within this composite intrusion contains hornblende phenocrysts replaced by actinolite in a fine- to very fine-grained matrix that is very dark grey with completely altered primary minerals. This intrusion was interpreted to be a single unit, but may represent 2 or more separate intrusive phases of similar age. There are slight mineralogical difference seen in thin section. In general, the synvolcanic intrusions contain hornblende phenocrysts, whereas posttectonic intrusions do not contain hornblende phenocrysts, contain only minor amounts, or contain completely altered hornblende.

Two intrusions are located along the northern and southern boundaries of the PPA (*see* Figure 6; *see* Preliminary Map P.3514). The intrusion located along the northern contact of the PPA hosts the Tyson gold and molybdenum showings. The intrusion is dark brownish green on weathered surfaces and dark green on fresh surfaces. Hand samples contain 35% white sericitized feldspar phenocrysts approximately 2 mm in diameter. A thin section of sample 413 consists of 40% secondary chlorite that fills open spaces, 3% anhedral quartz and 3% subhedral opaque minerals. The remainder of the section is a brown, sericitic, fine-grained groundmass with relict unidentifiable phenocrysts. In addition, the thin section contains quartz-feldspar intergrowth textures that suggests shallow rapid cooling, and superimposed calcite rhomboids indicative of intense carbonate alteration. The intrusion located at the falls on the Namewaminikan River (*see* Figure 6; *see* Preliminary Map P.3514) is situated within the CSB. This sample is medium grey on weathered surfaces and dark grey to green on fresh surfaces with medium- to coarse-grained amphibole phenocrysts and a fine-grained groundmass. The thin section of sample 2185 consists of 50% plagioclase with 90% altered to sericite with pseudomorphs of altered minerals, 20% amphibole pseudomorphs replaced by chlorite and sericite, 3% opaque minerals, and 20% recrystallized chlorite in the matrix. Both of these intrusions are geochemically similar to the diorite intrusions of the CVB and the SSB.

A sample, collected from a dike located in north-central Summers Township, is dark brown to grey on weathered surfaces and grey green on fresh surfaces. The dike intrudes the andesite of the CVB close to the CVB–SSB contact (*see* Figure 6). The dike is aphanitic and contains fine-grained phenocrysts of amphibole or pyroxene. In thin section, sample 444 consists of 10% anhedral, opaque minerals that are 0.5 to 1 mm in diameter, 10% chlorite filling open spaces, 2% quartz, 35% amphibole phenocrysts that are altered to chlorite along rims and fractures in a fine-grained chlorite-sericite groundmass. This rock is very geochemically different from other posttectonic intrusions in the area (*see* "Geochemistry").

Proterozoic

SIBLEY GROUP SEDIMENTARY ROCKS

The Sibley Group sedimentary rocks are red bed sequences preserved in north-striking, elongated, fault-bounded basins. It consists of red shale and mudstone (Kama Hill Formation), sandy dolostone (Rossport Formation), and quartz sandstone and conglomerate (Pass Lake Formation). The rocks are Mesoproterozoic in age, with a Rb/Sr age of 1340 ± 33 Ma (Wanless and Loveridge 1978) and overlie the Archean supracrustal and intrusive rocks.

In the Beardmore area, the Sibley Group sedimentary rocks are exposed in 2 outcrops located along Highway 11, in southeast Kitto Township (*see* Preliminary Map P.3512). The sedimentary rocks comprise a flat-lying, basal, calcareous mudstone to sandy dolostone unconformably overlying the steeply dipping Quetico Subprovince metasedimentary rocks. The calcareous unit is overlain by a poorly sorted, matrix-supported sandstone that weathers greyish brown and is medium to light grey on fresh surfaces. The sandstone is a 30 to 40 cm thick, shallow-dipping to flat-lying horizon.

ULTRAMAFIC TO MAFIC INTRUSIVE ROCKS

Diabase Dikes

A swarm of north-striking, 2 to 10 m wide diabase dikes intrude metasedimentary and metavolcanic units of the Beardmore–Geraldton Belt. Previous references to north-striking dikes in the area north of Lake Superior have interpreted that they are all part of the Nipigon dike swarm, although it has also been suggested that some of these dikes are feeders to, or branches off, the Nipigon sills (Osmani 1991). However, some of the dikes are much more altered than would be expected for the Mesoproterozoic-age Nipigon dike swarm, and it has been interpreted that there are at least 2 generations of dikes in the map area. A significant number of the dikes contain quartz rather than olivine and are probably Paleoproterozoic in age, with a lesser number of dikes related to the diabase sills. Classification of the dikes is complicated by a south to north decrease in the metamorphic grade of the dikes with the southern dikes resembling the Archean gabbroic rocks and the northern dikes more closely resembling the diabase sills.

The southern dikes are commonly 2 to 4 m wide diabase dikes and composed of fine- to medium-grained, massive diabase, with rare plagioclase porphyritic textures. These dikes are massive, medium green to green-grey to pinkish brown on weathered surfaces and medium grey-green to grey on fresh surfaces. Rare dikes may contain medium-grained, subhedral plagioclase phenocrysts. In thin section, the diabase is composed of 40 to 50% subhedral plagioclase laths, 30 to 40% subhedral to anhedral hornblende, 5 to 10% skeletal opaque crystals of magnetite or ilmenite, and 2 to 3% anhedral quartz. The plagioclase is moderately to highly altered to sericite and epidote, and the hornblende is weakly to moderately altered to chlorite with abundant opaque inclusions. Rare myrmekitic intergrowths of plagioclase and quartz are present. The dikes may contain chill margins along their contacts ranging from 5 to 15 cm wide, and some dikes contain epidote and quartz patches in open-space fillings with associated epidote-quartz alteration in the adjacent country rock. The epidote alteration is similar to that described as a halo around the diabase sills (e.g., Benedict and Titcomb 1948). However, the presence of this alteration could not be correlated with proximity to a diabase sill. A plagioclase porphyritic dike, north of the Creek Zone, contains multiple chill zones within the interior of the dike that are interpreted to indicate multiple magma injections along the same conduit (*see* Figures 4 and 6). The northern dikes, particularly those in Dorothea Township, are much less altered, lack the wall rock alteration haloes, and more closely resemble the Proterozoic sills. In thin section, these dikes are composed of 40 to 50% subhedral plagioclase laths, 30 to 40% subhedral pyroxene, 5 to 10% skeletal opaque crystals of magnetite or ilmenite, and 1% anhedral quartz. The plagioclase is moderately altered to sericite and epidote, and the pyroxene is weakly to moderately altered to amphibole and chlorite. Rare myrmekitic intergrowths of plagioclase and quartz are present usually with the plagioclase totally replaced by sericite. However, the southern and northern dikes are geochemically similar and the cause of the change in their appearance is not known.

A dike, situated east of Beardmore, contains very coarse-grained megacrysts of plagioclase not observed elsewhere in the map area. Sericitization of plagioclase in the megacrystic dike imparts a distinctive pale green hue to the feldspars previously referred to as greenspar (Shanks 1993). This dike is truncated by the diabase sill located in the underground workings of the Northern Empire Mine (Benedict and Titcomb 1947; Figure 7). The plagioclase megacrystic dike is texturally similar to Matachewan dikes in the Abitibi Subprovince and could be similar in age (2473 Ma: Heaman 1997).

The relative ages of the dikes in the map area is difficult to determine and is hindered by the variation in alteration. The northern dikes resemble the diabase sills and could be interpreted to be related to the sills. However, these dikes are much wider than the dike offshoots connected to the sills observed southwest of Undersill Lake, which are less than 1 m in width, and the offshoots observed in the Northern Empire Mine were referred to as dikelets by Benedict and Titcomb (1948). The southern dikes are more highly altered and resemble the Archean mafic intrusive rocks, which may be interpreted to indicate an age older than the sills. A diabase dike in western Kitto Township is cut by ultramafic intrusive rocks, indicating that some of the dikes are unrelated to the Mesoproterozoic intrusive event. However, there is the possiblity that some of the dikes are related to the same intrusive event as the sills, with the presence of quartz rather than olivine indicating that the sills are granophyric phases of the magma. Thus, there is the possibility that there is a mixture of Matachewan (2473 Ma), Marathon (circa 2170 or circa 1960 Ma: Osmani 1991), and Nipigon (1113 Ma: Tomlinson et al. 1999) diabase dikes in the map area.

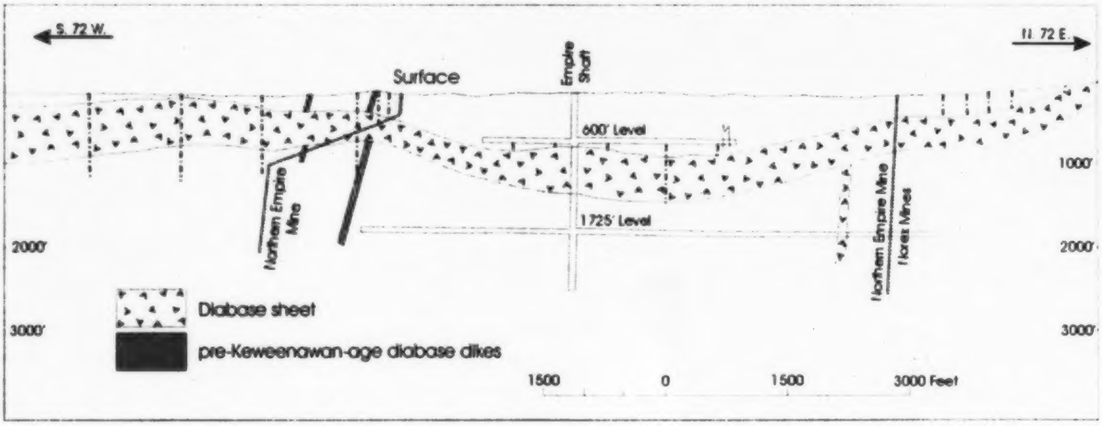

Figure 7. Vertical longitudinal section showing attitude of diabase, Northern Empire Mine (*modified from* Benedict and Titcomb 1948).

Ultramafic Intrusive Rocks

A peridotite forms a horseshoe-shaped intrusion approximately 6 km in diameter surrounded by a diabase sill, along the shore of Lake Nipigon. The peridotite intrudes the metasedimentary and metavolcanic rocks of the SSB and the SVB in western Kitto and southwest Eva townships, and is one of a number of ultramafic intrusions that have been assumed to be Proterozoic in age (Sutcliffe 1991). The peridotite is overlain by a diabase sill, but was not observed in contact with the Sibley Group sedimentary rocks, so that the relative ages of the peridotite and Sibley Group are not known.

The lithological classifications used in the field subdivided the intrusion into an inner zone of olivine gabbro, a central zone of massive peridotite and an outer zone of pyroxene porphyritic peridotite. The massive pyroxene peridotite is medium grained, massive with a medium brown to dark brown weathered surface, a few very coarse-grained, poikilitic (oikiocrystic) pyroxene grains and 1% fine-grained reddish brown biotite. The pyroxene porphyritic peridotite is similar in appearance to the massive pyroxenite, except for the presence of approximately 5% coarse-grained, subhedral, black pyroxene phenocrysts (Photo 10) and irregular leucocratic patches with increased plagioclase content. Outcrop exposure is sparse, probably due to the weathering of the olivine, and internal and external contacts are not commonly observed.

Detailed examination of the thin sections by Duggan (2002) indicates that the intrusion is crudely zoned, with a lherzolite outer zone, a wehrlite core and a granophyric olivine gabbro inner zone. This subdivision is based on petrography as well as calculated CIPW normative mineralogy (*see* Appendix 3). The wehrlite–lherzolite subdivision is not equivalent to the massive–porphyritic field subdivision, as both the wehrlite and the lherzolite can be massive or porphyritic. Average mineral compositions of olivine (Fo_{82-69}), clinopyroxene ($Wo_{38-46}En_{44-54}Fs_{7-14}$), orthopyroxene ($Wo_{2-4}En_{76-80}Fs_{17-21}$), and plagioclase ($An_{70}$) for the ultramafic rocks are from microprobe work by Sutcliffe (1987). The following lithological descriptions are taken extensively from notes by Duggan (2002) with some elaboration by the authors.

Photo 10. Medium-grained porphyritic pyroxene peridotite with randomly oriented, medium- to coarse-grained pyroxene phenocrysts, from a Proterozoic ultramafic intrusion in Kitto Township.

WEHRLITE

Wehrlite forms the main portion of the ultramafic intrusion, occurring as a massive and pyroxene porphyritic phase. The average mineral composition of the massive wehrlite is 58% olivine, 20% clinopyroxene, 9% plagioclase, 4% orthopyroxene and accessory hornblende, biotite, apatite, and opaque minerals. Olivine is the main cumulate mineral phase with orthopyroxene and clinopyroxene occurring as intercumulus minerals. Plagioclase, hornblende and biotite are late-stage igneous minerals. The pyroxene porphyritic wehrlite contains mostly subhedral, 3.5 to 8.0 mm poikilitic orthopyroxene with inclusions of opaque minerals, olivine and biotite. Alteration mainly affects pyroxene and plagioclase and, to a lesser extent, olivine, resulting in the formation of serpentine, chlorite and minor sericite.

Olivine crystals are euhedral to subhedral with an average size of 2.5 mm, and may form large aggregates with adcumulate textures. Smaller olivine crystals may be enclosed by biotite, clinopyroxene and/or plagioclase. Clinopyroxene occurs as phenocrysts, intercumulus groundmass and crystal aggregates. Subhedral, poikilitic phenocrysts, 2.0 to 3.0 mm in size, may enclose olivine and opaque minerals. Intercumulus clinopyroxene crystals are generally subhedral, with an average size of 1.5 mm, or as anhedral crystal aggregates of grains less than 0.75 mm in size. Orthopyroxene commonly occurs as subhedral, poikilitic, 0.5 to 2.0 mm phenocrysts averaging 3.5 mm, with inclusions of olivine, opaque minerals and biotite. Plagioclase forms anhedral grains ranging from 1.5 to 3.0 mm, with grains greater than 9.0 mm occurring as intercumulus minerals. Opaque minerals occur as disseminated grains or crystal aggregates closely associated with biotite and olivine. Individual grains are generally euhedral, less than 0.1 mm in size with cubic and rectangular forms indicative of magnetite and ilmenite. The crystal aggregates are anhedral and up to 1.5 mm in diameter.

The accessory phases include hornblende, biotite and apatite. Hornblende is present in some samples as euhedral grains less than 0.4 mm in size and as smaller anhedral grains. The hornblende is usually surrounded by biotite. Biotite occurs in fractures or in the smaller void spaces between pyroxene and olivine crystals. The grains are anhedral, 0.5 to 1.2 mm in size, ranging from dark brown to tan-brown to reddish. Apatite is present in a few samples, as euhedral, 0.5 to 1.5 mm grains that occur as inclusions in the biotite and hornblende.

The common alteration minerals are serpentine and chlorite occurring along fractures in both olivine and pyroxene crystals and as pseudomorphs after olivine. The fractures may be zoned with serpentine cores and chlorite rims classified as iddingsite by Shanks (1993). Minor biotite ± sericite may also occur along the fractures. The plagioclase may be very weakly altered to sericite. Chlorite may partially replace biotite.

LHERZOLITE

The lherzolite has an average mineral composition of 43% olivine, 23% clinopyroxene, 20% plagioclase and 9% orthopyroxene. The accessory minerals consist of biotite, hornblende, apatite and opaque minerals. Orthopyroxene, clinopyroxene and plagioclase are intercumulus mineral phases. Alteration minerals are serpentine, chlorite and sericite.

Olivine forms euhedral phenocrysts and groundmass grains ranging from 0.3 to 2.0 mm in size. Orthopyroxene forms euhedral grains averaging 3.0 mm in size that generally occur as phenocrysts and occasionally as subhedral grains in the groundmass. Orthopyroxene crystals occur mainly as poikilitic grains enclosing opaque minerals, olivine, biotite and a minor amount of clinopyroxene. Clinopyroxene forms subhedral, 0.3 to 4.0 mm poikilitic phenocrysts containing olivine, opaque minerals and alteration minerals. Smaller clinopyroxene grains are present as anhedral aggregates in the groundmass with olivine. Plagioclase forms subhedral to anhedral grains averaging 3.5 mm, but the size of the plagioclase crystals increase with plagioclase abundance with some grains greater than 7.0 mm in size. Plagioclase may form poikilitic crystals enclosing olivine, opaque minerals and minor pyroxenes. The opaque minerals consist of magnetite and ilmenite, forming subhedral to euhedral disseminated grains to aggregates. The disseminated crystals range from less than 0.1 to 1.1 mm, and the larger crystal aggregates are 1.0 to 1.5 mm. Crystal aggregates are commonly surrounded by biotite.

Accessory minerals include hornblende, biotite and apatite. Hornblende occurs as subhedral 0.3 to 1.3 mm grains in the groundmass. Subhedral, 0.3 to 4.5 mm biotite grains may have perfect basal cleavages. Some of the biotite appears to be a primary igneous mineral, but the biotite is also associated with the alteration minerals. Apatite forms euhedral inclusions approximately 1.0 mm in length in the biotite crystals.

The main alteration minerals are serpentine and chlorite which commonly replace olivine and, to a lesser extent, pyroxene. The alteration usually occurs along fractures with serpentine cores and chlorite rims. Occasionally, the olivine grains are completely replaced by serpentine. The clinopyroxene grains commonly have highly altered rims with relatively unaltered cores. Inclusions of serpentine and chlorite, with minor sericite and biotite, may occur in olivine and pyroxenes. Biotite may be, in part, an alteration mineral, replacing hornblende and occurring with serpentine and chlorite. Plagioclase is weakly altered to sericite.

The peridotite is interpreted to have formed by the progressive crystallization of an initial olivine, followed sequentially by clinopyroxene, orthopyroxene and, finally, plagioclase. Cumulate textures in the ultramafic intrusions of the Nipigon Plate were interpreted to indicate that these intrusions formed by accumulation of olivine at shallow crustal depths (Sutcliffe 1987).

OLIVINE GABBRO

An olivine gabbro is located along the inner contact of the wehrlite, in the area of the SSB–SVB contact. The gabbro is medium brown to grey brown with areas that are pinkish grey with small white patches. The massive and medium-grained gabbro is composed of plagioclase, pyroxenes, olivine and magnetite and generally resembles the diabase of the sills. The pinkish grey areas are massive, medium to coarse grained and are composed of plagioclase with lesser pyroxene and 3 to 4 mm irregular vugs that may be mariolitic cavities. These areas resemble the coarse-grained pods in the upper portion of the sills. In thin section, the main portion of the gabbro consists of 40% plagioclase, 25% pyroxenes and 5% subhedral, skeletal opaque minerals, 5 to 10% biotite, and 1 to 5% olivine with minor chlorite. The feldspar-rich areas contain 5 to 10% myrmekite, a wormy quartz-alkali feldspar intergrowth. Although resembling the diabase in the field, the olivine gabbro is geochemically similar to the wehrlite.

The contact with the metasedimentary rocks of the SSB resembles the contact between the diabase sills and Quetico Subprovince metasedimentary rocks. An olivine gabbro hybrid with up to 10% fine-grained black biotite contains angular to subangular blocks composed of fragments of metasedimentary rocks, which, in 1 example, appears to have broken along bedding planes. The presence of country rock xenoliths in a biotite-rich gabbro matrix is indicative of the assimilation of the country rocks by the intruding diabase. The olivine gabbro is located immediately to the north of the hornfels zone within the metavolcanic-chemical metasedimentary rocks of the SVB.

Nipigon Diabase Sills

A series of undulating, generally flat-lying to shallow-dipping Proterozoic diabase sills intrude the supracrustal rocks of the Beardmore area. The sills form 3 semicircular ridges of highly varied relief that are open to the west. The shallow west, highly varied dip results in ridge widths that vary from 20 to 3000 m. Commonly, the sills have one side with a gradual slope and a cliff to the other side. A good example of this topography is the sill located between the Canadian National Railway and Highway 11, in eastern Kitto Township (*see* Figure 6). This sill forms a ridge with a gradual eastern slope reaching a maximum height of 180 m above the surrounding area, and terminates in a cliff to the west. Less commonly, the sills form mesa-like ridges as occurs on the shore of Lake Nipigon in South High Hill Harbour, where the sill has a height of 150 m. Talus slopes occur at the base of all of the cliffs, and the talus obscures the basal contact relationships of the sills hindering the determination of the sill thickness. The 185 m thick sill intersected in the shafts of the Leitch, Sand River and Northern Empire mines may be the best approximation of the original thickness of the sills.

Correlation of the different sills in the map area is difficult, and the 3 ridges may not represent 3 unrelated sills. A longitudinal section from the Northern Empire Mine indicates that the sill varies greatly in dip and may resurface in other locations (Benedict and Titcomb 1947; *see* Figure 7). The extent of the eastern sills is evident from the airborne magnetic data, which indicates that the metavolcanic and metasedimentary rocks in the area east of the Town of Beardmore and central Dorothea and Sandra townships are underlain by a diabase sill. The potential exists that the easternmost sill may be contiguous with the middle sill or even the western sill depending on where the sill breached the surface and how much sill material has been eroded (*see* Figures 6 and 7).

The diabase sills are massive, range from fine to coarse grained and consist of feldspar, pyroxene, trace to 5% fine-grained olivine and magnetite. The diabase weathers a medium brown to grey-brown and is medium grey on fresh surfaces. In thin section, diabase consists of 25 to 40% clinopyroxene and/or orthopyroxene, 35 to 50% plagioclase, trace to 5% olivine, trace to 5% opaque minerals and 2 to 3% biotite. Although generally massive, a sample from north of High Hill Harbour, in Eva Township, is composed of medium-grained plagioclase laths aligned subparallel to the sill contact. This alignment is interpreted to represent an igneous flow foliation indicating that some portions of the sills had a dynamic flow history. Irregularly shaped, coarse-grained to pegmatitic pods containing a pinkish feldspar are common within the upper portion of the sills (Photo 11).

Photo 11. The edge of a irregular coarse-grained pod located near the upper contact of a diabase sill, in Kitto Township, interpreted to represent the last fluid-rich phase of the magma. Pen is approximately 10 cm in length.

There are 3 common phases that could be distinguished in the more highly weathered outcrops: a medium-grained phase, a coarse-grained phase, and a magnetite porphyritic phase. The medium-grained diabase is the most common phase and is the type lithology for the sills. The coarse-grained diabase appears to be simply a grain size variation, and should not be confused with the coarse-grained to pegmatitic pods and patches common to the upper portion of the sills. This coarse-grained phase forms a major portion of the sills in some locations, as in the Highway 11 section and along the road to High Hill Harbour. The magnetite porphyritic diabase is a medium-grained diabase containing 5 to 10%, subhedral magnetite (Photo 12). This phase was observed in a number of locations overlying the coarse-grained diabase in the Highway 11 sections, the High Hill Harbour Road, and the sill in western Kitto Township. The difficulty in identification of the different phases, due to the high degree of weathering of many outcrops, hinders detailed interpretation. Systematic grain size variation related to igneous processes could not be consistently mapped in the field, except in a single detailed stratigraphic section along Highway 11, which is described below.

A well-exposed, relatively unweathered stratigraphic section through the central sill located on Highway 11 in southeastern Kitto Township provides a possible stratigraphic type section for some of the various lithologies observed elsewhere in the sill. This section was subdivided into 3 subunits: 1) diabase (upper and lower), 2) magnetite-porphyritic diabase (closer to top), and 3) coarse-grained diabase (closer to bottom). The first subunit is typically massive and is the predominant phase. It is dark grey, medium grained (1 to 5 mm) and weathers to pinkish brown. It is commonly composed of massive, medium- to fine-grained feldspar and pyroxene with trace to 5% fine-grained olivine and magnetite. In some locations, there are accumulations of mafic minerals making the rock appear melanocratic and, in some areas, contain abundant coarse-grained plagioclase imparting a leucocratic appearance. The second subunit, magnetite porphyritic diabase, is the second most abundant phase. This phase differs from the typical diabase in that it contains magnetite phenocrysts. The third subunit, coarse-grained diabase, has the same mineralogy, but the mineral grains are larger than 5 mm and it is olivine and pyroxene rich.

Photo 12. Medium-grained magnetite-porphyritic diabase, an example of the lithologic variability in diabase sills, Highway 11 section, Kitto Township. Pen is approximately 10 cm in length.

This subunit contains small 3 to 4 mm vugs that may represent mariolitic cavities. The first subunit underlies the coarse-grained phase and probably represents a decrease in grain size toward the lower contact. Occasional coarse-grained to pegmatitic pods containing pinkish feldspar are present within the upper subunit. Although these units were observed in other locations, this stratigraphic variation is not present in all portions of the sills as a composite stratigraphic section at the CNR ballast quarry is not as varied in lithology as elsewhere and is dominantly composed of massive medium-grained diabase.

Irregular-shaped pods and patches of coarse to pegmatitic pyroxene and pinkish feldspar are common along the upper contact of the sills. These patches vary in size from a few centimetres to tens of centimetres in diameter and have irregular amoeboid shapes on horizontal surfaces. Thin section analysis has shown that these pods contain myrmekitic textures and are interpreted to represent the last magmatic phase to crystallize (Sutcliffe 1991).

White, 5 to 10 cm wide aplite dikelets intrude the diabase within the CNR ballast quarry in Kitto Township. The dikelets consist of very fine-grained plagioclase and quartz and commonly have irregular discontinuous bleached alteration haloes (Photo 13). Myrmekitic intergrowth of the quartz and plagioclase is common, and the plagioclase is highly altered to sericite. Amphibole and sphene occur as minor accessory minerals. Some of the alteration-related fracture fillings containing wollastonite and amphibole have a similar bleached margins comparable to the aplite (*see* "Alteration"). These dikelets are interpreted to be a late fraction of the diabase magma, possibly overprinted by the later alteration that produced the fracture fillings.

Two styles of diabase contacts, polygonal and hybrid, are observed in the area. Polygonal contacts consist of polygonal-jointed, aphanitic diabase with a very fine-grained amphibole occurring along the joints. A vertical section through a diabase basal chill zone consists of a 2 cm aphanitic zone that grades stratigraphically upward and increases in grain size over a distance of 1.5 m. The hybrid contact consists of fine-grained diabase containing up to 10% fine-grained black biotite with blocks and/or pebble-sized xenoliths. The angular to subangular blocks are composed of coarse-grained quartz and white to pinkish feldspar that resembles granite to granodiorite intrusive rock. In 1 well-exposed area, pebble xenoliths

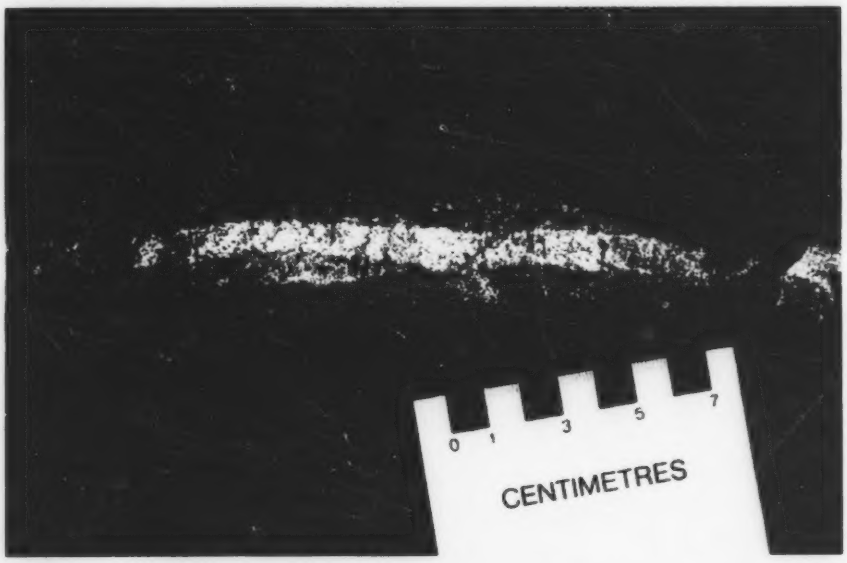

Photo 13. Aplite dikelet in diabase sill, with continuous to discontinuous bleached alteration rims up to 5 cm wide, and alteration-filled fractures in diabase, Warneford quarry section.

and irregular-shaped quartz-rich xenoliths, both with fine rims of biotite, were observed (Photo 14). The irregular xenoliths may be mariolitic cavities indicating a significant fluid and/or volatile phase in the magma. The presence of country rock xenoliths in a biotite-rich diabase matrix is indicative of the assimilation of the country rocks by the intruding diabase.

Myrmekitic textures are formed by simultaneous and rapid crystallization of quartz and plagioclase from the late-stage liquid trapped between the earlier formed crystals (e.g., Cox, Bell and Pankhurst, 1978). The myrmekitic textures present in the coarse-grained pods of the upper portion of the diabase sills were referred to as granophyric by Sutcliffe (1991) and were interpreted to indicate that these pods are a late, more evolved magmatic phase in the sills. In other intrusions, granophyric gabbroic rocks are often interpreted to represent the extreme differentiate of a basaltic magma with probable incorporation of partially melted sediments (Smith and Silver 1975). However, a number of possible processes were considered for the origin of granophyre in Mesozoic diabase intrusions in eastern North America including fractional crystallization, segregation during flow or contamination (Dudas and Rogan 1997). The occurrence of myrmekitic textures, combined with mariolitic cavities, in the coarser grained diabase in the lower portion of the Highway 11 section, suggests a more complex fractionation and contamination within the sills than previously interpreted. The source of myrmekite in the lower portion of the highway section may represent the most differentiated portion of an initial diabase sill representing a magma conduit that was subsequently reused by the second upper pulse of magma.

Photo 14. Xenoliths of coarse- to medium-grained quartz and feldspar and rounded, metasedimentary rocks in a biotite-rich diabase matrix, interpreted to reflect partial assimilation of Quetico Subprovince metasedimentary rocks by the diabase sills, in northeast Kitto Township.

CENOZOIC

Quaternary

PLEISTOCENE

The Quaternary cover in the Beardmore–Geraldton Belt includes both glacial and postglacial environments. Zoltai (1967) interpreted glacial straie, drumlins and eskers as indicating ice flow generally toward the southwest, but fanning to the west in the area east of Lake Nipigon (230 to 260°). Detailed studies by Kristjansson and Thorleifson (1987) suggest 2 glacial advances, an early advance to the south as evidenced by rare glacial straie trending approximately 190°, and a more recent advance to the southwest, where glacial striae measured in the Beardmore–Geraldton Belt trends between 240 and 255°.

Much of the area is covered by thin till (bedrock–drift complex) and is described by Kristjansson and Thorleifson (1991) as predominantly gravel, silt and sand, with thin sand and gravel in areas adjacent to glaciofluvial and glaciolacustrine deposits. Locally, it may cover anywhere from 25 to 85% of the map area. It is generally 1 m in thickness, and is interpreted to be a largely locally derived sandy till deposited beneath and by sliding glacial ice (Kristjansson and Thorleifson 1991).

Subaqueous outwash and associated glaciolacustrine sediments cover a large portion of the map area, including an approximately 3 km wide swath in central Kitto Township and a 2 km wide section bordering the Namewaminikan River in Dorothea and Sandra townships. It ranges from 1 to 75 m in thickness and is comprised of silty, very fine sand and fine sand interbedded on a scale of centimetres to a few metres with 1 cm thick silt and clay layers (Kristjansson and Thorleifson 1991). Kristjansson and Thorleifson (1991) interpret these sediments to have been deposited in a proglacial lake, with ripple cross-laminated sand present at the mouth of the Namewaminikan River indicating deposition in an underflow current. Stabilized eolian dunes, generally oriented to the northwest and a few hundred metres in length, are common in these areas, and consist of fine to medium sand (Kristjansson and Thorleifson 1991).

A moderate portion of Summers Township, and a small portion of Sandra Township, is overlain by ice-contact glaciofluvial deposits interpreted by Kristjansson and Thorleifson (1991) on the basis of gravelly texture, the presence of esker ridges, and an array of kettle holes and relief. Eskers generally grade vertically and horizontally from massive to crudely bedded pebble, cobble and gravel to gravelly sand or sand, range upward of 30 m in height, and are oriented southwestward, parallel to the direction of final ice flow (Kristjansson and Thorleifson 1991). Carbonate content is less than 1% in eskers northeast of Beardmore, interpreted by Kristjansson and Thorleifson (1991) to indicate that the glacial process carried out the majority of transport. The predominance of glaciofluvial ice-contact as opposed to glaciofluvial outwash sediments, with the absence of end moraines, has been interpreted by Kristjansson and Thorleifson (1987) to imply rapid deglaciation and a relatively thin ice mass.

RECENT

Alluvial deposits occur adjacent to the Blackwater River in Kitto and Summers townships and adjacent to the Namewaminikan River in Sandra Township, in present-day floodplain environments and early Holocene terrains. The deposits comprise silt, sand, gravelly sand and/or organic material (Kristjansson and Thorleifson 1991). Small, sporadic organic deposits occur throughout the map area as thin patches of peak and muck less than 1 m thick, and are commonly associated with areas of open water and swamp (Kristjansson and Thorleifson 1991). Recent deposits of organic-rich unconsolidated swamp, lake and stream sediments are common, but of limited, extent.

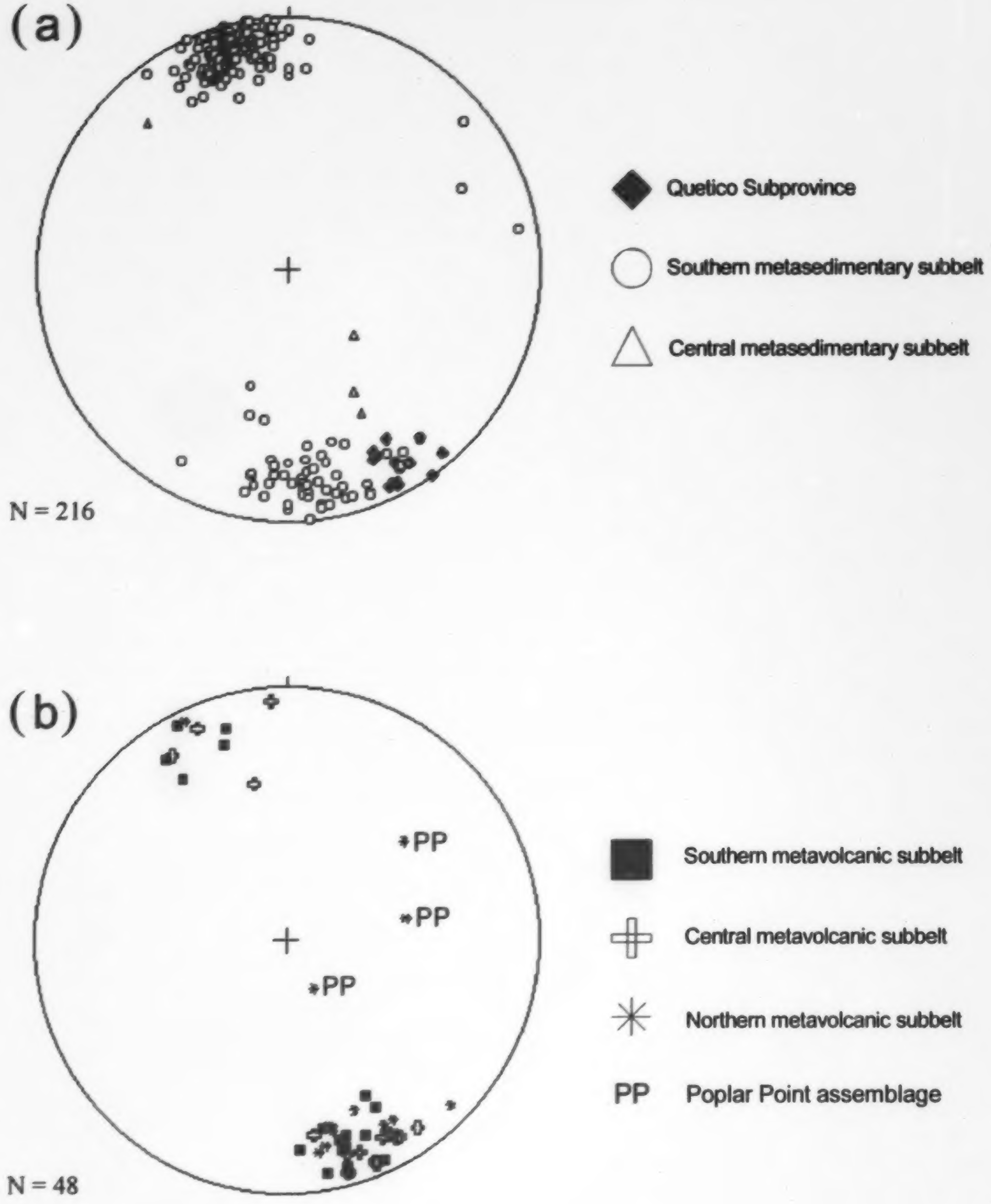

Figure 8. Stereographic plots of S_0 bedding for **a)** metasedimentary rocks and **b)** volcanic rocks. Beds generally strike easterly, with steeply north to steeply south dips. Approximately north-striking beds occur within the Poplar Point assemblage, NVB.

Structural Geology

Metasedimentary and metavolcanic units of the Beardmore–Geraldton Belt (BGB) within Kitto, Eva, Summers, Dorothea, and Sandra townships (*see* Figure 6) have experienced multiple phases of deformation. In general, deformation within the belt decreases to the west, resulting in well-preserved primary textures, such as graded bedding, pillows, flame structures, and load casts. Heterogeneous deformation tends to be concentrated within iron formation units, whereas more competent lithologies are relatively undeformed.

PRIMARY STRUCTURES

Bedding (S_0) within the belt generally strikes east at 240 to 284° and dips steeply to the north and south (Figure 8). Stratigraphic facing directions are defined by pillow tops that generally face to the northwest within the metavolcanic subbelts. The exception is the Poplar Point Assemblage (PPA), which has pillow tops, drainage shelves, and grading in tuff beds that strike approximately 140 to 170° and dip 30 to 50° northwest. This variation in strike and dip, along with geochemical data, is interpreted to indicate that the PPA is an allochthonous block within the northern metavolcanic subbelt (NVB).

Within the southern metasedimentary subbelt (SSB), graded bedding and rare cross-beds dominantly indicate overturned bedding that is north facing. However, younging directions are reversed immediately north of the Standingstone fault, and are locally reversed in areas spatially associated with shear transposition, as observed in the area around Undersill Lake. These reversals may either be related to juxtaposition of 2 sedimentary "slices" due to major faulting, or to folding within a single sedimentary package (Anglin and Franklin 1985).

Well-developed bedding is rarely observed in the arenite and conglomerate of the central metasedimentary subbelt (CSB), with the arenite forming massive, generally featureless, units and the conglomerate occurring as less than 1 m thick overlapping channel deposits. Crude grading observed in conglomerate appears to indicate facing to the south (Photo 15).

A number of small-scale sedimentary and soft-sediment features occur in metasedimentary rocks, including flame structures, rip-up clasts and channel scours. These are interpreted to be primary features useful for determining original bedding orientation. Flame structures generally occur along the contacts between siltstone and argillite, with the best examples observed in the area of Undersill Lake. However, pseudo-flame structures were observed in the Quetico Subprovince metasedimentary rocks, and are interpreted to result from displacement of the bedding by an oblique foliation. Rip-up clasts, ranging in size from pebbles to cobbles, are present in both clastic and chemical metasedimentary rocks. Rip-up clasts of wacke in a siltstone matrix are well exposed in the exploration trenches near the Long Lac Superior property, south of Highway 580. Williams (1987a, 1989) observed wispy to lensoid clasts within wackes that were characterized by the destruction of bedding, and this was interpreted to suggest that the shear deformation caused total disruption of the bedded units along the shear planes. Channel scours are well developed in the conglomerates of the CSB and the clastic metasedimentary rocks of the SSB, south of Highway 580 and the Standingstone fault. Discontinuities along lithological contrasts observed by Williams (1987a) within the CVB, east of the map area, are interpreted to be the equivalent to channel scours observed during mapping, and were interpreted by Williams (1987a) to represent an early D_1 deformation that occurred prior to fold-related fabric formation.

Photo 15. Crudely graded bedding in pebble conglomerate with occasional pebble-sized jasper clast, central metasedimentary subbelt. Hammer is approximately 30 cm in length, and faces north.

Photo 16. Arcuate cooling fractures-joints vary from approximately 30 to 90°, and later linear structures in diabase sill, in the CNR ballast quarry, Kitto Township.

JOINTS AND IGNEOUS CONTACTS

Jointing is common in both the diabase sills and pyroxenite. In the diabase, arcuate and linear joints are well exposed in the face of the CNR ballast quarry in Kitto Township. The arcuate joints can be traced from an approximately 30° dip at the bottom of the face to a 90° orientation, and are interpreted to be cooling fractures. Arcuate joints were also observed on horizontal outcrop surfaces. There is 1 example of a series of arcuate joints outlining a possible flow tube in the north face of the quarry (Photo 16). Linear joints are late structures that transect the cooling fractures and may be related to regional structures. Accurate measurement of the orientation of the joints in the magnetic diabase required the use of sun angles to calculate the joint azimuth. This method limited measurements to sunny days. More importantly, the arcuate nature of some joints limits their use for interpreting the internal structure of the sills.

The diabase sill contacts that have been observed generally dip less than 30° and are oriented in many different directions. However, in eastern Kitto Township, the contacts generally dip to the east. The nearly flat-lying, outwardly dipping contact orientations do not fit the previously suggested cone sheet model for the diabase (Sutcliffe 1991), and the distribution of the diabase may be a result of erosion as the diabase sills generally form topographic highs (e.g., *see* Figure 7).

Jointing is common in the pyroxenite, and the shallow-dipping joints could be interpreted to be an indication of an originally shallow-dipping orientation to the pyroxenite sill. However, these joints may also be cooling joints, and cooling joint could have a similar arcuate trace as those observed in the diabase. The use of joints to predict the original orientation of the pyroxenite may not be valid.

Although the pyroxenite appears to form a ring-shaped body, the orientation of the intrusion cannot be defined due to the lack of definitive contact relationships. Possible orientations range from a near vertical circular dike to a shallow west-dipping sill. Controls on the location of both the diabase and the pyroxenite intrusion are complex as they transect both the SVB–SSB contact and the Wabigoon–Quetico subprovincial boundary. There are also late north-striking fault systems that may have also influenced the orientation of the intrusion.

TECTONIC FOLIATIONS

A bedding-parallel fabric is generally recognizable in finer grained metasedimentary and metavolcanic rocks. This fabric is defined as a weak to moderate slaty cleavage within the argillite and iron formations and as a weak phylitic cleavage, or general foliation, within the mafic flows. The term "cleavage", as used during this project, was defined as a fabric plane along which a rock would break, whereas a foliation was defined as a penetrative, nonfissile fabric. The timing of this fabric is not known, and may have developed as an expression of sedimentary compaction, as evidenced by its affinity to develop within the argillites, or may be a bedding-parallel fabric developed during the first phase of deformation.

A S_1 fabric was tentatively identified on a limited number of outcrops in the area south of the Leitch Mine (B. Lafrance, Laurentian University, personal communication, 2002). This fabric strikes northwest and was based on the recognition of small, refolded folds observed within larger scale F_2 folds. Although more detailed mapping is required to verify this interpretation, all subsequently developed fabrics have been named consecutively based on an early S_1 fabric.

A subvertical to vertical tectonic fabric (S_2) generally strikes 245 to 275°, and is slightly counterclockwise (<15°) to S_0 bedding (Figures 8 and 9). The S_2 fabric is axial planar to F_2 folds. The S_2 fabric is generally defined by a slaty to phylitic continuous cleavage, but also occurs as a spaced cleavage

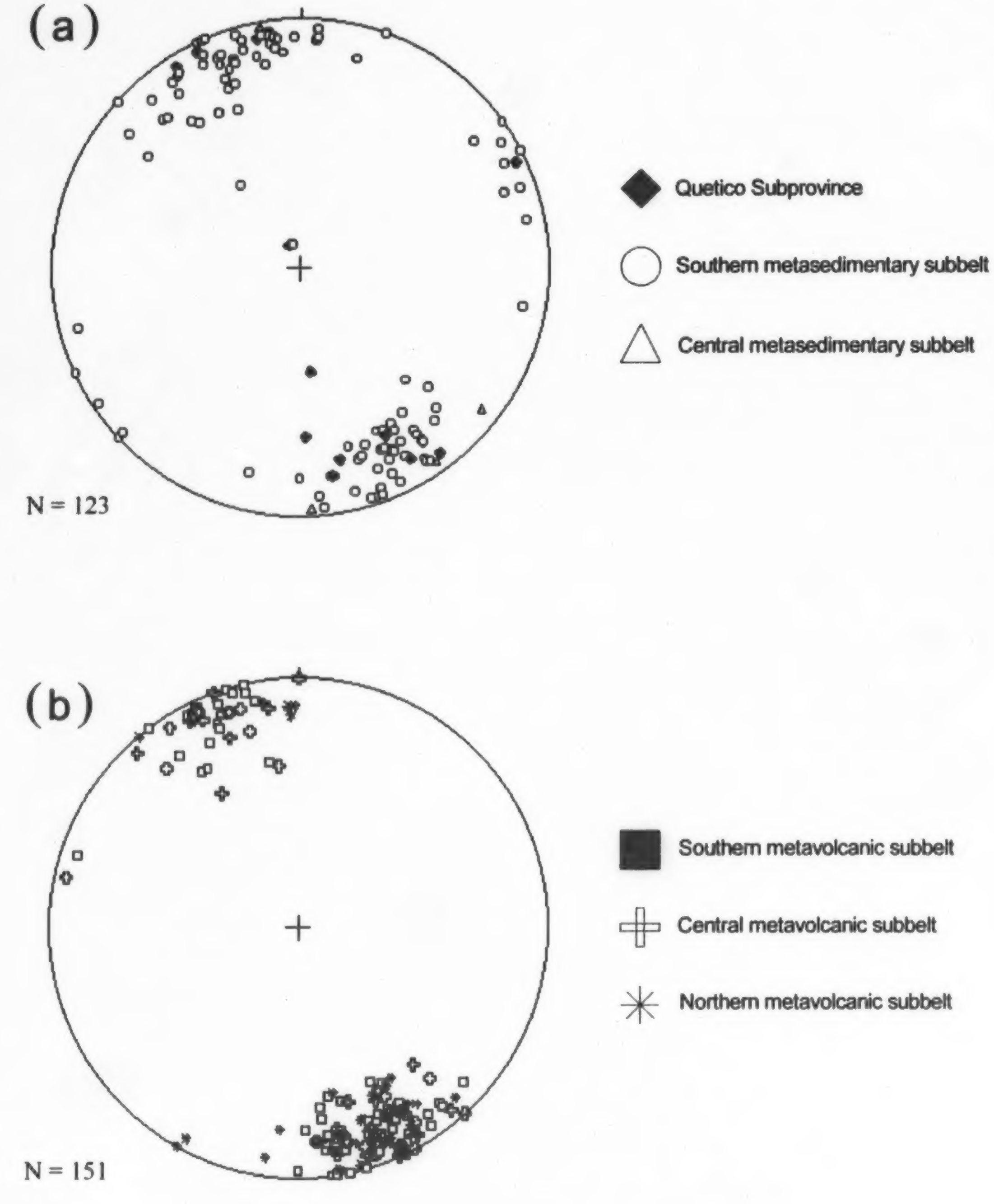

Figure 9. Stereographic plot of S_2 for **a)** cleavage and **b)** foliation. Rocks generally strike easterly, with steeply north to steeply south dips. Anomalous north-striking cleavages are interpreted to be due to local folding.

in finer clastic metasedimentary rocks and mafic flows. Transposition of the S_2 fabric into a bedding-parallel tectonic fabric occurs in zones that have experienced intense deformation, and is spatially associated with both major and minor lithological boundaries. In the field, it is often difficult to distinguish between a transposed fabric, S_2 fabric and original sedimentary structures (S_0). In some locations, intense fabrics can result in false cross-bedding structures. Sinistral displacement was observed along this fabric in one location, within the iron formations south of the Sand River Mine.

Detailed mapping near the Leitch Mine suggests a third tectonic fabric, S_3, which strikes 220 to 235° and dips about 65° northwest (Figure 10). It is a well-developed crenulation cleavage and an associated spaced cleavage (Photos 17 and 18) is preserved within both banded iron formation and feldspathic wacke. The S_3 fabric is axial planar to macroscopic crenulation folds and is best developed along the limbs of F_2 folds. Stereonet projections comparing detailed mapping at the Leitch Mine with regional mapping (*see* Figures 9 and 10) suggest that the S_3 fabric was difficult to identify and was rarely distinguished from the S_2 fabric during regional mapping. The S_3 fabric may anastamose into the S_2 fabric.

FOLDING

Three folding events were identified in this portion of the Beardmore–Geraldton Belt. The F_1 folds were only observed within a few outcrops near the Leitch Mine. Centimetre-scale refolded folds within banded iron formation are interpreted to represent F_1 folding and are refolded by F_2 folding. The F_1 folds trend between 310 to 325° and plunge shallowly to the northwest. It is unclear whether the F_1 event is local or regional in scale, and further detailed mapping is required in order to fully relate the various fabrics and folding events.

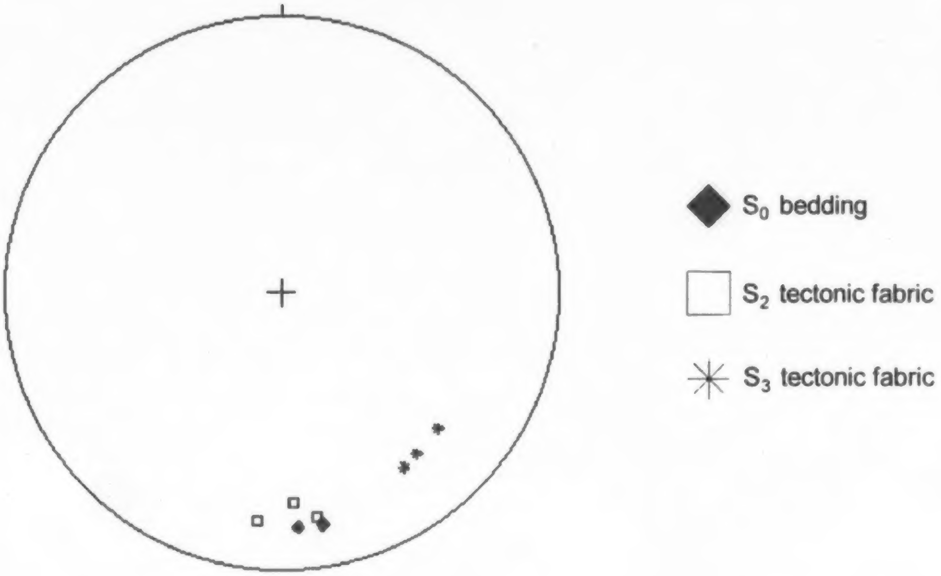

Figure 10. Detailed mapping near the Leitch Mine suggests a third tectonic fabric. S_0 = bedding, S_2 = penetrative cleavage, S_3 = crenulation cleavage, spaced cleavage. This figure is interpreted to suggest that S_3 may have been misidentified during regional mapping, and likely anastomoses with S_2.

Photo 17. Well-developed crenulation cleavage strikes 223° and dips moderately to the northeast, with crenulation cleavage oriented parallel to the pen (approximately 10 cm in length) in the jasper-hematite iron formation, Leitch Mine, Highway 580.

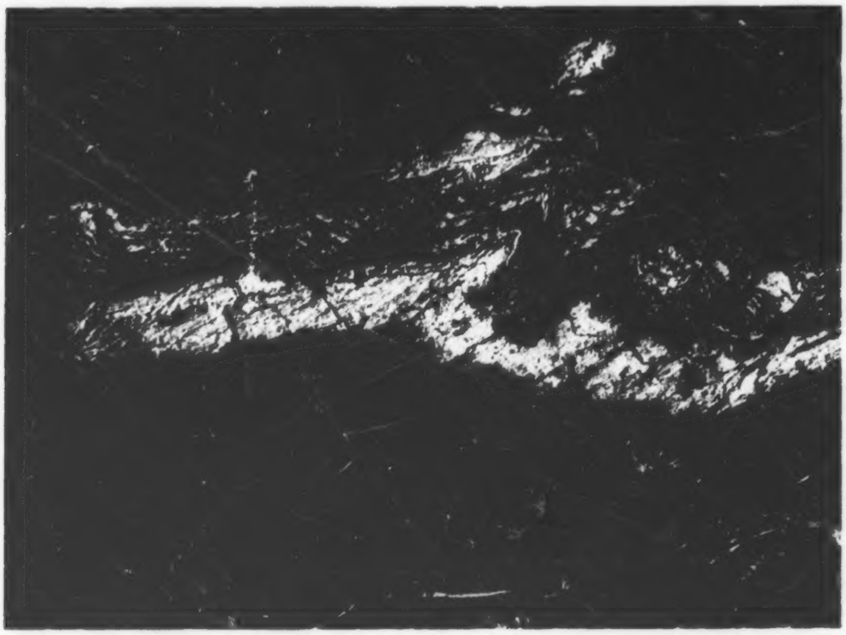

Photo 18. Well-developed S_3 spaced cleavage strikes 221° and dips moderately to the northeast with the S_3 cleavage oriented parallel to the pen (approximately 10 cm in length); jasper-hematite iron formation, Leitch Mine, Highway 580.

F_2 folds, on the scale of centimetres to less than 250 m, are well developed within the banded iron formations in the area of the Leitch Mine and in feldspathic wackes at Undersill Lake. They are upright isoclinal folds that trend approximately 260 to 275° and plunge moderately to the west, with fold axes that are generally axial planar to the S_2 regional foliation. Small-scale examples of F_2 folds within iron formations are exposed in the trenches near the Leitch Mine (Photo 19). Large-scale F_2 folds have been inferred from reversals in younging directions within stratigraphically continuous bands of metasedimentary rocks. The F_2 folds are also inferred from dip direction reversals within a succession of largely north-facing, steeply dipping wackes in the Undersill Lake area. Only a representative number of fold traces have been represented on the maps (*see* Preliminary Maps P.3512, P.3513 and P.3514), as there is likely a more complex fold history present at this location. This is further supported by the presence of sheath folds in the exploration trenches near the Long Lac Superior West property (*see* Figure 4). The axial trace of the F_2 folds appears to have the same orientation as the trace of the contact between the SSB and the CVB. This suggests that the F_2 folding event occurred after or during the juxtaposition of the 2 subbelts, and is interpreted to be due to subsequent rotation of earlier noncylindrical folds during intense shearing related to the Standingstone fault.

The F_3 folds were observed in rare outcrops of iron formation south of the Leitch Mine (*see* Photo 19). They occur as centimetre-scale tight to isoclinal folds and as centimetre-scale crenulation cleavages. The folds trend 225 to 240°, plunge moderately to the west, and contain fold axes that are axial planar to the S_3 cleavage (*see* Photo 19).

Photo 19. F_2 fold, with fold axis axial planar to S_2 cleavage with a refolded F_3 axis oriented in the direction of the pen (approximately 10 cm in length), in jasper-hematite banded iron formation adjacent to the Leitch Mine, Highway 580.

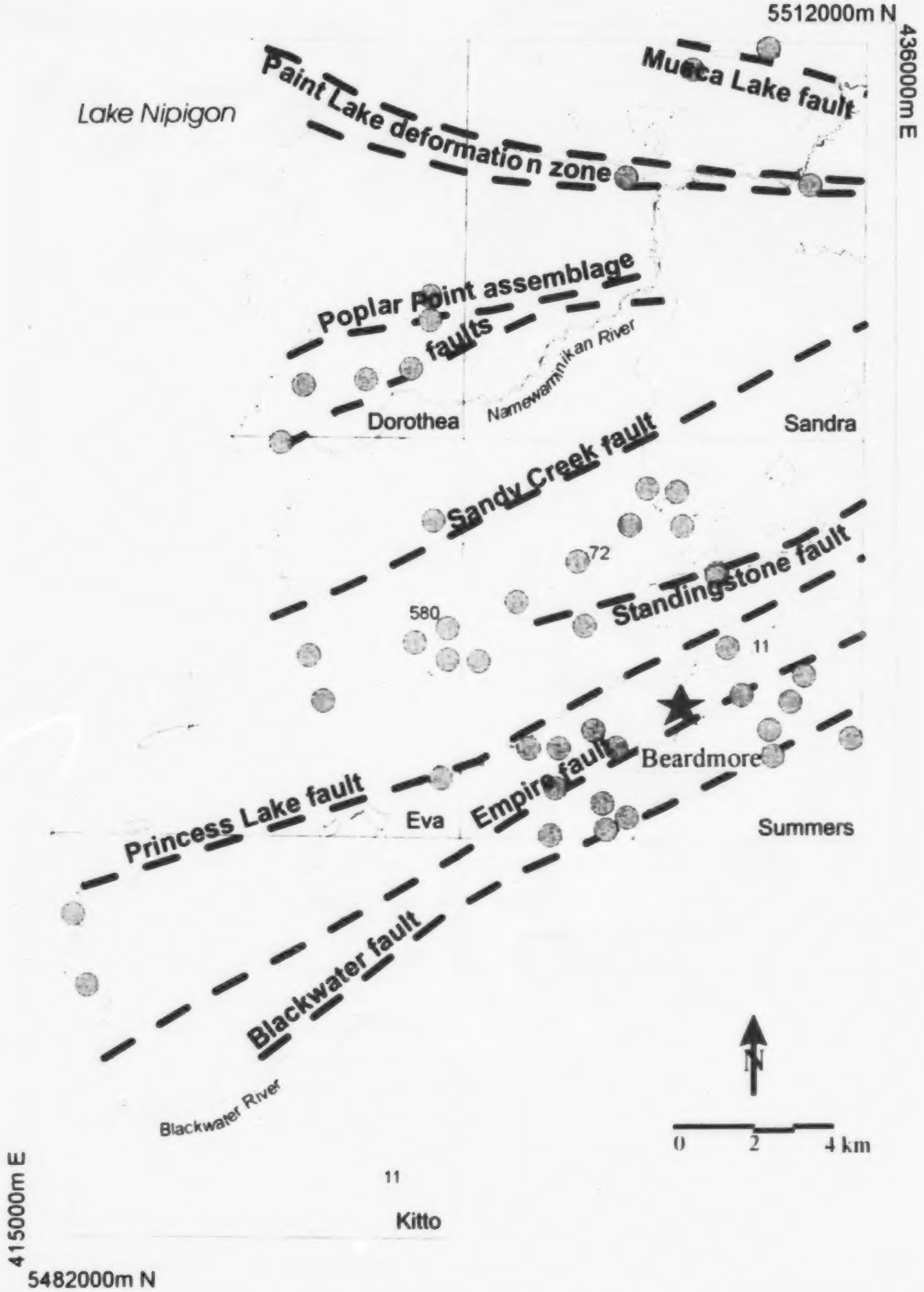
5512000m N
436000m E
Lake Nipigon
Paint Lake deformation zone
Mucca Lake fault
Poplar Point assemblage faults
Namewaminikan River
Dorothea
Sandra
Sandy Creek fault
72
Standingstone fault
580
11
Beardmore
Princess Lake fault
Empire fault
Eva
Summers
Blackwater fault
Blackwater River
N
0
2
4 km
11
Kitto
415000m E
5482000m N

Figure 11. Geographic sketch map showing location of major faults in the Beardmore–Geraldton Belt with respect to historical gold showings.

FAULTING

Faulting in the Beardmore portion of the Beardmore–Geraldton Belt may be subdivided into 2 discrete groups: north-trending faults, and east-trending fault systems or deformation zones. The age relationship between the 2 structural systems is not known, and both were probably active at multiple times. Interpretation of the position of these faults in areas of poor outcrop coverage was aided by the use of side-scan radar composite, satellite imagery, and airborne electromagnetic and magnetic survey data (Gupta 1991; OGS 1998).

North-Striking Faults

Multiple north-striking faults are interpreted to occur throughout the map area. Airborne geophysical data delineates periodic breaks in the regionally continuous banded iron formation that correspond well with the trend of the diabase dikes. The preferred interpretation is that discrete north-striking faults displaced and repeated strata within the iron formation, though an alternate interpretation is that the repetition is a result of folding. These discrete structures were later utilized as magma conduits during emplacement of the diabase dike swarm. Limited field structures including north-striking joints and veins support this interpretation.

Regional Deformation Zones

A number of regionally significant east-striking fault systems, or deformation zones, are present in the Beardmore area. These faults are generally delineated in the field by highly carbonatized and silicified rocks, and by intense shear fabrics. These zones are generally associated, but not necessarily coincident, with the subbelt boundaries.

BLACKWATER RIVER FAULT

The Blackwater River fault (Carter 1983, 1987; Williams 1987a, 1987b; Shanks 1990, 1993) is an expression of the boundary between the metasedimentary and metavolcanic rocks of the Wabigoon Subprovince and the metasedimentary rocks of the Quetico Subprovince (Figure 11). East of Beardmore, in McComber and Vincent townships, the fault trends approximately 075° and is coincident with the trend of the Blackwater River (Carter 1987). The fault can be delineated by the trend of aeromagnetic contours and is associated in the field with intense shearing (Carter 1987) and patchy carbonate alteration (Williams 1989). In the Beardmore area, the fault is not well exposed due to the presence of a large sand plain located in the middle of Kitto Township and the posttectonic intrusion of the Nipigon sills. In the few locations where the fault is exposed, rocks generally display an increase in strain, such as intense to extreme flattening of pillows within the metavolcanic rocks (upward of 1:20 elongation ratio) and development of a strong to intense cleavage within metasedimentary rocks. A graphitic shear is reported at the base of the falls on the Blackwater River, in Kitto Township (R. Coté, Prospector, personal communication, 2001), and is probably an expression of the fault. Immediately north of the Blackwater River fault, Shanks (1993) observed a series of subvertical, nonpenetrative planar surfaces, which he interpreted to be either slip surfaces or C-planes.

EMPIRE FAULT AND PRINCESS LAKE FAULT

Historically, the Empire fault was first recognized by Benedict and Titcomb (1947) in the underground workings of the Northern Empire Mine, and was interpreted to separate rocks of the SSB from the SVB (Benedict and Titcomb 1947; Shanks 1990, 1993). The fault dips steeply to the south within the mine workings and is slightly shallower than the average dip of the overturned metavolcanic flows. The fault is marked by a thin fault gouge of black graphite bordered by a few feet of sheared rock (Benedict and Titcomb 1947). Previous interpretations (Benedict and Titcomb 1947; Shanks 1993) placed the Empire fault adjacent to the metavolcanic–metasedimentary contact in western Eva Township and through the Princess Chain of Lakes in eastern Eva and Summers townships. Shanks (1993) interpreted kinematic indictors observed along the Empire fault to suggest a south-side up sense of motion.

A reinterpretation of the area has resulted in separation of the original Empire fault into 2 distinct faults, the Empire fault and the Princess Lake fault (*see* Figure 11). In eastern Summers Township, the Empire fault trends approximately 060° northeast and extends along the metavolcanic–metasedimentary contact in the area of the Northern Empire Mine. Further west, the fault bends to the south and passes obliquely through the SVB, striking toward Lion Bay. The Princess Lake fault extends parallel to the trend of the Princess Chain of Lakes, striking about 060° northeast through the southern edge of the SSB. This fault is evident in the area around the Princess Chain of Lakes where an increase in deformation occurs within the metavolcanic and metasedimentary rocks. The western extension of the fault may be associated with the occurrence of graphite in the metavolcanic rocks in western Kitto Township, immediately south of the metasedimentary–metavolcanic contact.

STANDINGSTONE FAULT

The Standingstone fault (Standingstone Lake – Watson Lake fault: Bruce and Laird 1937; Mackasey 1975, 1976; Lawson 1986; Shanks 1993) is the west extension of the Oxaline Lake – Watson Lake fault (Williams 1986, 1987a, 1987b, 1989) and is part of the ductile-brittle shear system on which the Leitch and Sand River mines are situated (*see* Figure 11). It has been interpreted to be a normal, south-side down fault (Carter 1987) that has experienced multiphase deformation from dip-slip to dextral strike-slip (Williams 1987a). The Standingstone fault trends about 075° northeast, and is clearly visible on side-scan radar composite photos and in aeromagnetic data. It is topographically expressed by a swampy valley that includes Standingstone Lake and its associated tributaries. The fault is manifested by the development of numerous small, northeast-striking carbonate shear zones. Rocks adjacent to the fault display a strong to intense penetrative cleavage that is generally developed counterclockwise to the regional bedding. The majority of the strain has been accommodated by banded iron formation. C–S fabrics in conjunction with numerous outcrop-scale Z-folds, are interpreted to indicate dextral strike-slip displacement.

SANDY CREEK – SANDRA LAKE FAULT

The Sandy Creek – Sandra Lake fault (Sandy Creek: Shanks 1993; Sandra Lake: Mackasey 1975) trends approximately 060° northeast (*see* Figure 11). Surface expressions of the fault include numerous discontinuous shear zones, with associated carbonate and chloritic alteration. This shearing and alteration is well exposed along the new "million dollar" logging road, located west of Eva Lake. No sense of displacement has been determined on this fault.

POPLAR POINT ASSEMBLAGE FAULTS

Bedding directions in the Poplar Point assemblage are discordant with the regional trends in the Beardmore–Geraldton Belt, and a pair of bounding faults have been interpreted to separate this assemblage from the adjacent units (*see* Figure 11). The position of the southern fault is not evident in the field and is shown to be coincident with the assemblage boundary (*see* Preliminary Maps P.3513 and P.3514). The northern fault is clearly seen on the side-scan radar composite and on aeromagnetic maps as a linear anomaly trending approximately 75 to 80° northeast through Dorothea and Sandra townships. In the field, a small outcrop on the north side of a beaver pond, south of the Tyson occurrences, displays an intense east- to northeast-striking fabric that may be an expression of this fault. It is associated with intense carbonatization and weak to moderate ankerite and calcite-flooding. The interpreted location of this fault may also explain the location of the gabbroic intrusion hosting the Tyson occurrence and the lack of a western extension to the northern metasedimentary subbelt.

PAINT LAKE FAULT

The Paint Lake fault, first termed the Devil's Walk – Paint Lake fault by Tyson (1945), marks the boundary between the Onaman–Tashota terrane to the north, and the Beardmore–Geraldton Belt to the south. The fault, delineated by topographic lineaments in Sandra and Dorothea townships (MacKasey 1975), is expressed as an intense zone of ductile deformation that appears to be bounded by 2 distinct subparallel linear faults (*see* Figure 11). The Paint Lake fault is well exposed along the shore of Lake Nipigon, north of Devil's Walk, in northwest Dorothea Township. Rocks are highly strained (Photo 20), as evidenced by the absence of primary volcanic features, such as pillows, and by the development of a strong to intense mylonitic fabric nearly parallel, or slightly counterclockwise to the fault zone.

The fault is interpreted to be an east-striking transcurrent fault that has experienced repeated periods of movement, including dextral and north-side up senses of motion (Mackasey 1975; Reilly and Williams 1986, 1987; Reilly 1988; DeWolfe 2001). Mackasey (1975), on the basis of an offset of a porphyritic diabase dike in Irwin Township, estimated the Paint Lake fault to have experienced up to 800 m of displacement.

MUSCA LAKE FAULT

The Musca Lake fault, striking approximately 105° southeast, occurs adjacent to Musca Lake in northeastern Dorothea Township. This is compiled data from earlier work, and the reader is referred to Mackasey (1975) for further information.

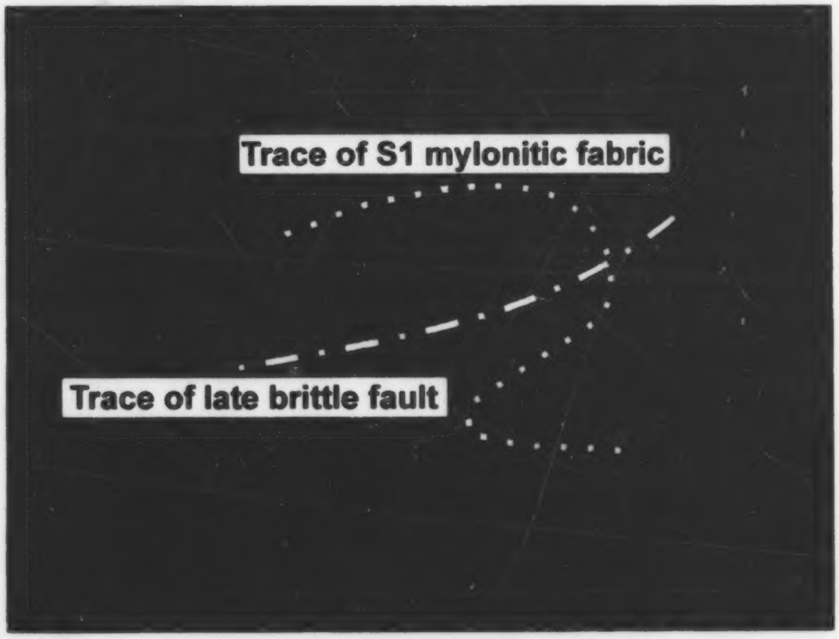

Photo 20. Mylonitic shear zone, defining the Paint Lake deformation zone, strikes 268° and dips steeply to the north in a felsic to intermediate metavolcanic rock of the Onaman–Tashota terrane. Pencil is approximately 10 cm in length.

Alteration and Metamorphism

ALTERATION

Alteration in the metavolcanic and metasedimentary rocks is generally weak to moderate, with intense alteration limited to zones that are tens of metres thick. Alteration is best developed in the mafic metavolcanic rocks and is often associated with shearing along the subbelt contacts with the development of strong to intense carbonatization and chloritization. Intense silicification is associated with the originally more permeable volcaniclastic metavolcanic units in the CVB east of Eva Lake and in the SVB adjacent to Lake Nipigon. Minor to moderate epidote and hematite alteration was observed throughout the Beardmore–Geraldton Belt, and is generally associated with local late fractures in the metavolcanic and metasedimentary rocks. Serpentine veins are common in the peridotite intrusion, and epidote and quartz-epidote veins occur in the Proterozoic diabase. Widespread axinite occurs in mafic metavolcanic rocks, generally near the contact with metasedimentary rocks and diorite-gabbro intrusive rocks.

Carbonatization is commonly a combination of calcite and ankerite and ranges from disseminated grains in the metasedimentary rocks to a weak to intense pervasive alteration in the metavolcanic rocks. Strong to intense carbonatization is generally associated with sheared or highly fractured areas, including both regional and local faulting, where it is pervasively flooded along the foliation planes and results in a light brown to yellow weathering. It is the characteristic alteration observed along the Blackwater, Standingstone and Sandy Creek fault systems, and along the limbs of the Z-folds north and south of the 72 Road (*see* Figures 5 and 11). A good example of intense carbonatization is exposed in sheared rocks associated with the Sandy Creek fault exposed along the "million dollar road", northwest of Eva Lake. Moderate to pervasive carbonate flooding occurs in the massive felsic flow and amygduloidal intermediate massive to pillowed flows north of the Sandy Creek fault. Moderate to strongly flooded and disseminated carbonatization also occurs locally within the intermediate metavolcanic rocks of the Poplar Point assemblage (PPA) in the NVB. The carbonatization of the metavolcanics rocks in the PPA appears to be associated with shearing related to the faults bounding the assemblage.

Various degrees of silicate alteration is observed in a number of areas and appears to be the most common in originally porous metavolcanic units. Moderate to intense flooded silicification occurs within the CVB in massive flows and along pillow selvages within pillowed flows, with good exposures east of Eva Lake. Weak to moderate silicification occurs as patches in both pillow cores and selvages in the SVB along the shore of Lake Nipigon in southwestern Kitto Township. The originally porous volcaniclastic metavolcanic rocks are silicified in different amounts, with an strongly silicified example in the PPA displaying quartz stringers in a silicified hyaloclastite matrix (*see* Photo 3). Alteration rinds on the fragments of some intermediate tuff breccias of the western portion of the PPA may also be a result of differential silicification. This silicification is commonly associated with a chloritization and/or carbonatization of the breccia matrix.

Weak to moderate pervasive chlorite alteration is observed in mafic metavolcanic units of the SVB and Bish Bay assemblage (BBA), and the matrix of volcaniclastic rocks in the CVB and PPA. The chloritization is pervasive, disseminated as 1.0 cm chlorite porphyroblasts in massive and pillowed mafic flows, and occurs along fractures within all metavolcanic rock units. The 0.3 to 1.0 cm wide fractures are generally subparallel to shear zones and locally displays weak to intense alteration. Within the BBA, moderate to intense chlorite alteration is observed within pillow selvages and in the matrix of a tectonic breccia. Intense chlorite alteration is associated with granodiorite dikes, and is intense in the matrix of a tuff breccia associated with trace sulphide mineralization located to the east of the basalt horizon in the PPA (*see* Figure 5). Similar intense chloritization forms a matrix to brecciated pillowed flows adjacent to some of the granodiorite dikes in the mafic metavolcanic horizon of the PPA (Photo 21). Although there are chill margins to the dikes indicating a post-volcanic intrusive event, this chlorite alteration may be the result of the granodiorite dikes intruding into a still wet relatively unconsolidated volcanic pile. A weak chloritization following fractures occurs in some intermediate flows west of the mafic metavolcanic rocks of the PPA (*see* Photo 9). This chlorite alteration may be following the aligned vesicles produced by flow lamination in the flow. In a nearby location, the chlorite alteration partially replaces fragments in a tuff breccia apparently following a later structure crosscutting stratigraphy (Photo 22). Total, or near total, replacement of interpillow hyaloclastite is common, with good examples observed along the shore of Lake Nipigon in the CVB. With the exception of the chloritized hyaloclastite, intense chlorite alteration is interpreted to be the result of hydrothermal activity and is associated with late fractures, shears and dike emplacement as well as high original porosity.

Weak to moderate hematite alteration occurs in the mafic metavolcanic rocks of the SVB and the BBA, and in the intermediate metavolcanic rocks of the CVB. It is commonly found as a weakly pervasive alteration in massive flows, and in pillow selvages. More intense hematization occurs as specular hematite in 1 to 3 cm wide veins and fracture-fillings within the mafic metavolcanic rocks north of Eva Lake (*see* Figure 4).

Alteration of the Proterozoic diabase is generally observed in joints and fractures. Commonly, the alteration is near the top of the sill, but is also observed in fractures in the middle of the sill, with good exposures occurring in the Warneford quarry in Kitto Township (*see* Figure 3). The 0.3 to 1 cm (up to 10 cm) wide joints contain very coarse-grained to pegmatitic subhedral hornblende, hornblende-albite, hornblende-pink feldspar and rare magnetite. Irregular pods of coarse-grained hornblende-feldspar and magnetite are observed in the upper portion of the sill. Continuous to discontinuous bleached alteration rims up to 5 cm wide commonly border the aplite dikelets exposed in the Warneford quarry (*see* Photo 13). Rare pectolite and wollastonite are observed in diabase along the pipeline in southeastern Kitto Township and near the lakeshore in southwestern Kitto Township suggesting fluid interaction between the diabase and calcareous metasedimentary rocks of the Sibley Group.

Moderate to intense, 0.3 to 1.0 cm wide epidote and quartz-epidote fractures occur within both Archean diabase dikes and gabbroic intrusions, and weak to moderate epidote and quartz-epidote alteration is common in the mafic metavolcanic rocks of the PPA. In the diabase, the alteration generally forms 2 to 8 m wide zones of moderate to intense alteration subparallel to the dike contacts. These zones have the same intensity and width in both the metasedimentary and metavolcanic rocks in the southern portion of the belt, but are generally not well exposed in the northern areas. The diabase also contains pods of epidote and quartz-epidote alteration up to 5 cm in diameter. The pillowed flows of the PPA have open-space drainage cavities that have been partial to totally filled with epidote or epidote-quartz.

Serpentine occurs in the Proterozoic pyroxene peridotite intrusion and in the Archean gabbro-peridotite intrusion located in the BBA (*see* Figure 6). In the Proterozoic peridotite, the serpentine alteration is observed along the shore of Lake Nipigon, imparting a blocky or brickwork appearance to the outcrop. This texture was also described by Sutcliffe (1991) as being relatively common in the ultramafic intrusions of the Lake Nipigon region. Serpentine occurs as 0.3 to 1.0 cm wide fracture fillings and is locally associated with antigorite. In some fractures, extreme weathering causes a central fracture-filling of serpentine with subparallel bands of medium-grained magnetite. The Archean peridotite in the BBA contains serpentine that occurs as acicular crystals up to 10 cm long and forms masses within fractures up to 5 cm wide. The best exposed north-striking serpentine vein is located on the shore of Lake Nipigon. The texture of this serpentinite is interpreted to indicate formation in extensional fractures during a late hydration alteration, possibly related to a retrograde metamorphism.

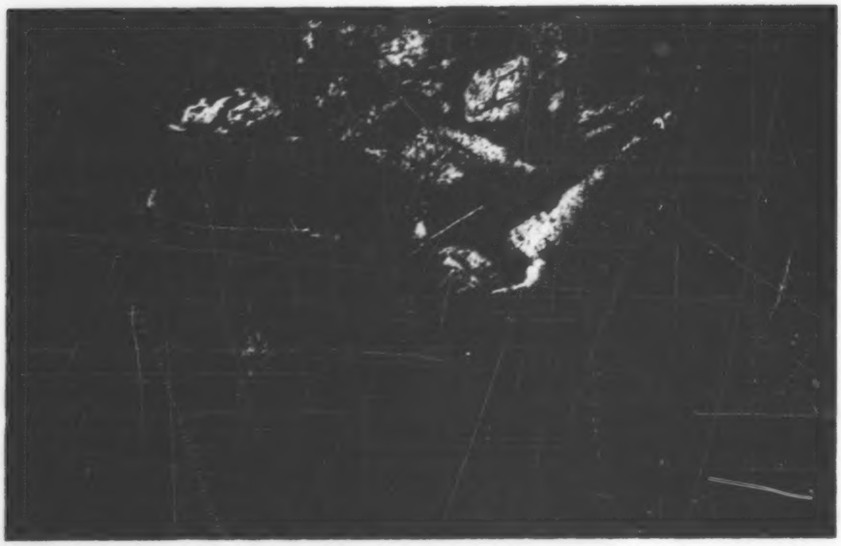

Photo 21. Intense chlorite alteration of the matrix in a brecciated pillowed basalt flow with fragments of chilled granodiorite, adjacent to granodiorite dike in the Poplar Point assemblage, northern metavolcanic subbelt.

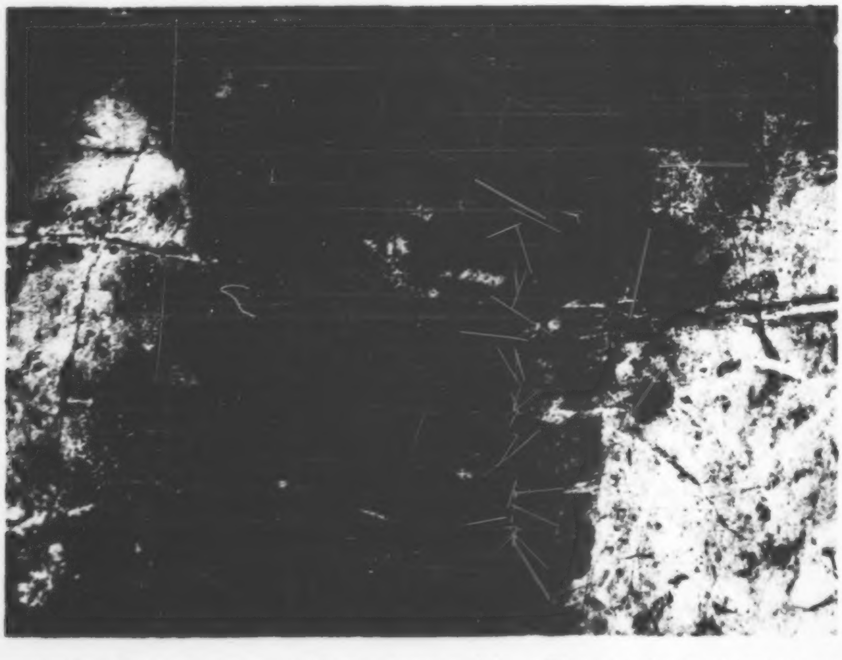

Photo 22. Intense silicification along a crosscutting fracture in a monolithic tuff breccia of the Poplar Point assemblage, northern metavolcanic subbelt.

Axinite

Axinite occurs in quartz-calcite veins hosted by mafic and intermediate metavolcanic rocks intruded by gabbro or diorite sills. Axinite is most abundant in 2 widely separated locations in west-central Dorothea Township and in northwest Summers Township, with an occurrence consisting of a single vein observed in Kitto Township not discussed here (Figure 12). The axinite has a pale to dark purple colour on fresh surfaces and a massive to bladed habit. In both locations in Dorothea and Summers townships, the axinite weathers a very pale purple to purplish white that in poorly exposed bush locations could be easily misidentified as feldspar in quartz-feldspar veins. Identification of axinite during the current mapping was possible due to the excellent exposure provided by a 1999 forest fire. The host rocks for the veins are usually intensely carbonatized metavolcanic rocks recognizable by a medium brown weathered surface. Petrological examinations and X-ray diffraction analyses identified the axinite to be of the magnesioaxinite variety in all 3 locations. It is distinguished by its high positive relief, low birefringence and inclined extinction. Axinite-bearing veins are up to 10 cm wide and consist of quartz, with minor epidote, and calcite-filling void spaces produced by weathering. The veins are associated with west- to southwest-trending extensional fracture systems, and occur in both vertical and subhorizontal orientations.

In Dorothea Township, the axinite-bearing veins are best exposed along the shore of Lake Nipigon, hosted by basaltic and pillowed flows and a gabbro-peridotite intrusion north of Bish Bay (*see* Figure 12). The axinite is medium to dark purple forming masses of tabular crystals upward of 1 cm in length with a generally random orientation. Massive, light green epidote and chlorite form septa up to 1 cm thick within the veins and as alteration selvages up to 1.5 cm thick along the veins. Scattered occurrences are hosted by basaltic flows and gabbro-peridotite intrusions for up to 3 km to the east of the lake. There is no indication that the veining diminishes toward the east, rather identification is limited by available outcrops.

In Summers Township, the veins are commonly hosted by andesitic flows and pillowed flows intruded by diorite sills, close to the contact with the metasedimentary rocks in the area of the fold nose (*see* Figure 12). The axinite is generally pale purple to lilac with fibrous crystals oriented 90° to the vein walls intergrown with actinolite, chlorite and/or clinozoesite, and riebeckite. Textures may be interpreted as either intergrowths of the axinite with other silicates or as replacement of the axinite by the amphiboles within extensional fractures. Exposures were observed to the limit of the current mapping, with the decrease in vein intensity attributed to decreasing bedrock exposure outside of the burn. A series of 3 holes drilled by Duncanex Resources in 1972 intersected numerous quartz, calcite, fluorite veins in the mafic metavolcanic rocks (Thompson 1972), which is interpreted to indicate that the axinite observed along the 72 Road continues for an unknown distance along the northeastern structural trend.

MINERAL CHEMISTRY AND GENESIS

Axinite is a group of borosilicate minerals with the general formula $X_2YAl_2BSi_4O_{15}(OH)$ that includes 4 end-members that are all calcium dominant at the *X*-site. Three of the end-members are named for their most abundant cations at the *Y*-site: magnesioaxinite ($Y = Mg$), ferroaxinite ($Y = Fe^{2+}$), and manganaxinite ($Y = Mn^{2+}$), and the fourth, tinzentite, is manganese rich ($X = CaMn$, $Y = Mn$; Sanero and Gottardi 1968; Lumpkin and Ribbe 1979; Grew 1996) and has also been referred to as mangansevcringite (Kurshakova 1968). Axinite was named for the axe-like crystal form commonly developed by the mineral, although it also may be platy, tabular, or wedge shaped. Axinite typically is a lilac-brown, but may also be yellow, orange-red, pale purple, yellowish green or colourless, with a hardness of between 6.5 and 7. For comparison, tourmaline, $(Na,Ca)(Mg,Li,Al,Fe^{2+})_3Al_6(B0_3)_3Si_6O_{18}$, in which boron bonds to 3 oxygens compared to axinite which bonds to 4 oxygens, may form blue, yellow, pink, red, black, and

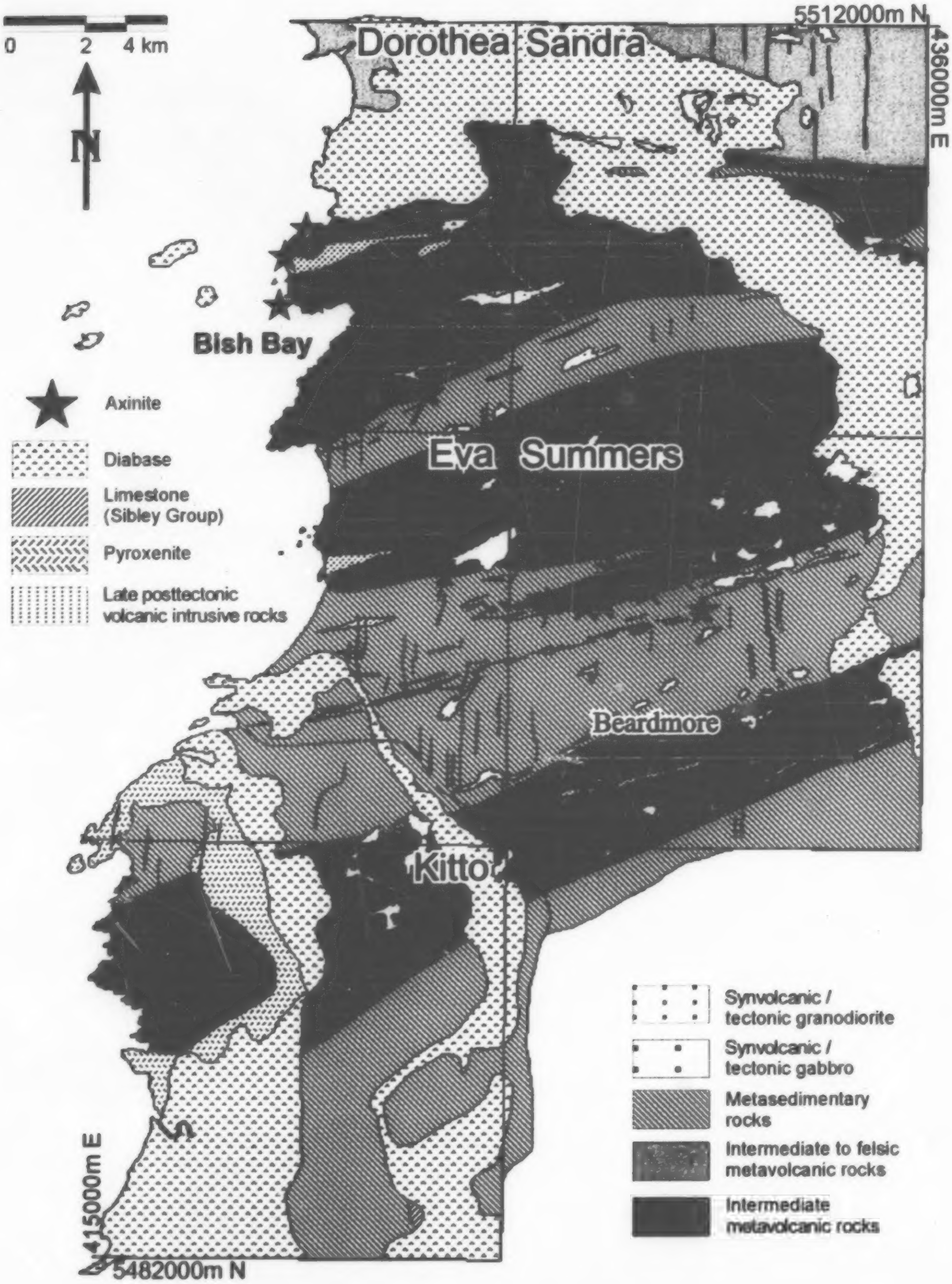
5512000m N
436000m E
Dorothea
Sandra
0
2
4 km
N
Bish Bay
Axinite
Diabase
Limestone (Sibley Group)
Pyroxenite
Late posttectonic volcanic intrusive rocks
Eva
Summers
Beardmore
Kitto
Synvolcanic / tectonic granodiorite
Synvolcanic / tectonic gabbro
Metasedimentary rocks
Intermediate to felsic metavolcanic rocks
Intermediate metavolcanic rocks
415000m E
5482000m N

Figure 12. Location of axinite occurrences in the map area.

green, or colourless prismatic crystals. Axinite is a relatively uncommon mineral that is often not recognized in the field, which results in this mineral being considered to be relatively rare.

There is a lack of understanding for the conditions of formation for axinite. Axinite occurs in a variety of environments, with one of the best known being altered calcareous sediments or basic igneous rocks that have experienced calc-silicate alteration, followed by metamorphism (Deer, Howie and Zussman 1986). Five modes of occurrence were proposed by Ozaki (1972): manganese ore deposits, pegmatites, contact and metasomatic ore deposits, regionally metamorphosed rocks, and veins in igneous and sedimentary rocks. Common features to these modes of occurrence seem to be nearby sources for boron, and Grew (1996) suggested that compositional variation of axinite may be greater than just these 5 modes. Grew (1996) also noted that "veins in igneous and sedimentary rocks" covers a variety of occurrences, including pegmatites, granitic plutons, diabase, and regionally metamorphosed rocks. Some occurrences, such as those hosted by arenaceous sediments in the Kyzyl–Espe polymetallic ore deposit in central Kazakhstan (Getling 1965), fit the altered and metamorphosed calcareous metasediment environment proposed by Deer, Howie and Zussman (1986). However, axinite is also common in and/or adjacent to intrusions including diabase in Silbach, Westphalia (Vallance 1966) and in the Norwegian Caledonides, where axinite is interpreted to occur instead of epidote due to boron-rich basic gabbroic and greenstone host rocks (Carstens 1965). Axinite is suggested to be an alternative mineral phase to tourmaline in aluminum-poor, calcium-rich paragenesis, with tourmaline replacing axinite in more aluminous compositions of South Island, New Zealand, based on the proposed reaction

Fe-axinite + chlorite + quartz → schörl/dravite + clinozoesite/epidote + actinolite + water

(Pringle and Kawachi 1980). This reaction may be complicated in higher regional-grade metamorphic environments with the assemblage *tourmaline-epidote-garnet* restricting axinite to boron-rich rocks (Robinson 1983), due to the occurrence of *tourmaline-epidote-quartz-calcite-garnet* selvages present between axinite-rich veins and tourmaline-bearing amphibolite host rock. These selvages are interpreted to be related to temperature rather than compositional controls. Experimental work by Nekrasov and Kashirtseva (1975) suggests an upper limit of 525°C for crystallization of axinite, although it most commonly forms at temperatures ranging from 300 to 350°C. In contrast, the crystallization temperature of tourmaline has a wide range of pressure–temperature combinations and may form in temperatures upward of 865°C (Grew 1996). However, the temperature of formation for axinite and tourmaline overlaps with the temperatures of auriferous fluids responsible for deposition of gold in a number of gold deposits (Robert 1996).

DISCUSSION

The controls on the formation of axinite in the Beardmore area are unclear. The composition of the axinite, associated vein minerals, host rock alteration, and host rock metamorphism are constant for both occurrences suggesting that temperature was not a major factor in controlling the formation of axinite in this area. However, the composition of the host rocks is different between the Dorothea and Summers townships occurrences. The Dorothea Township axinite veins are hosted by tholeiitic basalt flows and synvolcanic gabbro-peridotite sills of the NVB with lithogeochemical similarities to mid-ocean ridge basalt (*see* "Geochemistry"). The gabbro-peridotite sills are possible sources for the magnesium in the axinite, but a source for the boron is not obvious. Host rocks in Summers Township are calc-alkaline flows of the CVB intruded by calc-alkaline diorite sills interpreted to be posttectonic. These diorite sills have lower MgO contents than the gabbro-peridotite and are less probable sources for the magnesium in the axinite. The Summers Township occurrences are located along the contact with the metasedimentary rocks of the SSB that may have acted as a source for boron. The SSB metasedimentary rocks are cut by the Standingstone Lake fault, a major regional northeast-trending structure that may be a splay of the Paint Lake

Table 2. Axinite locations with associated mine and commodity type.

Location	Mine Name	Commodity	Type	Composition	Host Rock Lithology	Host Rock Age	Accessory Minerals [1]	Reference
Hedley Basin, British Columbia	Nickel Plate	Au, Ag, Cu, Zn, Co, Pb, Ni, Mo, Bi, As	skarn	?	metavolcanic and metasedimentary rocks	Paleozoic to Jurassic	scp, cal, qtz, ep, chl, czo, prh, or	Ray and Dawson (1994); Goldcliff Resource Corporation (2002)
Chibougamau, Quebec	Cooke	Au, Cu, Ag	?	ferroaxinite	metavolcanic and metasedimentary rocks	Archean	cal, qtz, kfs, tur, amp, act	Dubé and Guha (1993)
Cadillac, Quebec	McWatters	Au	vein-type	?	metasedimentary (Timiskaming) metavolcanic rocks	Archean	tur, ep, qtz	Jébrak et al. (1991); Morin et al. (1993)
Porcupine, Ontario	Paymaster, Goldhawk, Hollinger	Au	vein-type	?	metasedimentary (Timiskaming) metavolcanic rocks	Archean	czo, she, ab, hem, ttn, ep, ser, chl, tur	Sabina (2000); Hurst (1935)
Snow Lake, Manitoba	New Britannia (Nor Acme)	Au	?	?	volcano-sedimentary supracrustal sequences intruded by ultramafic and mafic intrusions	Aphebian	qtz, st, hbl, tr, ep, tur, chl, cal, srp, gp, czo, fel	Sabina (1987); TVX Normandy (2002)
Chihuahua, Mexico	Frisco	Au, Ag, Pb, Zn, Co	skarn	?	calcareous shale	Cretaceous (?)	qtz, fl, cal, hd, grt, ep, amp	Zamudio (1986); Koch (1956)
Luina, Tasmania	Mount Cleveland	Sn	?	?	calcareous mud and/or pelitic limestone	Middle to Upper Cambrian	cst, qtz, dol, sd, cal, tur, fl, chl	Jackson (1985); Hall (1990)
Cobalt District, Ontario	Christopher Columbus	Ag, Co, Ni, Cu	silver-cobalt vein	?	metasediment and Nipissing diabase	Huronian	cal, qtz, ep, td, agn, cob	Sabina (2000)
Gowganda, Elk Lake, Ontario	Castle, Morrison, Terra Nova	Ag, Co	silver-cobalt vein	?	metasediment and Nipissing diabase	Huronian	grt, str, ep, spc, hem, mar, cal, fel	Sabina (2000)
Mt. Logan, NWT–Yukon border	CanTung	W, Co	skarn	?	marble, chert	?	px, grt, act, ep, ttn, tur, atg, qtz, cal	Sabina (1992)
Timiskaming, Ontario	Lawson	Ag, Co, Cu, Ni	silver-cobalt vein	ferroaxinite	metasediment and Nipissing diabase	Huronian	qtz, cal, ep	Sabina (2000); Satterly (1977)
El Hamman, Central Morocco	El Hamman	Fl, Sn	skarn	manganaxinite, ferroaxinite	sedimentary rocks intruded by calc-alkaline granite	Silurian to late Carboniferous	da, cal, qtz, ep, she, grt, px	Sonnet and Verkaeren (1989)
Barca de Alva-Escalhao region, northeastern Portugal	Riba de Alva	W	skarn	ferroaxinite	metasedimentary rocks intruded by granite	Cambrian	czo, she, fel, cal, lab, ap, scp	Gasper and Inverno (2000)
Hidalgo, Mexico	Zimapan district	Pb, Zn, Ag, Cu, W, Mo, Au, Fe	skarn	?	calcareous metasedimentary and metavolcanic rocks intruded by calc-alkaline intrusive rocks	Cretaceous	adr, wo, she	Yta et al. (1996)
Dal'negorsk, Primorye region, Russia	Ftoroy Sovietskiy	B, Zn, Pb	skarn	?	limestone with chert and interbedded sandstone and/or argillite, intruded by granite	Triassic	da, qtz, cal, hd, px, wo, di, grt, ep, amp, fl, qtz	Wood et al. (1997); Wood (1996a, 1996b)
Rainy Lake – Thunder Bay, Ontario	Kaministikwai River occurrence	n/a	n/a	?	metavolcanic rocks	?	czo, chl, qtz, pct	Sabina (1991)
Cloyne, Ontario		?	?	ferroaxinite	metavolcanic rocks	?	qtz, cal, tur, ep, hbl, ilm, py	Robinson (1983); Grew (1996)

[1] For abbreviations, *see* Appendix 7.

fault to the north. Faulting may explain the lack of metasedimentary rocks in Dorothea Township, as the Bish Bay fault is interpreted to separate the Bish Bay and Poplar Point assemblages of the NVB. As a northeast-trending splay of the Paint Lake fault, the Bish Bay fault may have thrust a segment of the NSB beneath the NVB, thus, providing a source of boron for the formation of axinite in Dorothea Township.

Two of the occurrences appear to be hosted by north-trending diabase dikes intruding gabbro to diorite sills. One is an isolated occurrence of axinite located in southern Dorothea Township along the southern contact between the Poplar Point assemblage and the CSB, and the other is along the northern edge of the occurrences in Summers Township. In both occurrences, the axinite occurs within a diabase dike adjacent to a diorite sill. Axinite is associated with diabase intrusions in the Pechanga district (Serdyuchenko and Makarov 1971). Proterozoic diabase sills of the Beardmore area intrude the calcareous sedimentary rocks of the Sibley Group, which could have been a potential source for calcium in the axinite. However, Sibley Group sedimentary rocks are observed in only 1 location in the extreme southeast portion of the study area, approximately 15 km from the nearest axinite occurrence. The diabase sills are also probably unrelated to the axinite, as axinite was not observed in any of the numerous alteration fracture fillings. Both occurrences are associated with diorite sills interpreted to be posttectonic in age, which includes a sill located along the Bish Bay fault. This diorite sill along the fault is associated with the Tyson properties, containing weak to moderate gold mineralization in brecciated galena-pyrite quartz vein along the northern contact and molybdenum-pyrite quartz veins along the southern contact (Mackasey 1975; Bruce and Laird 1937). Both sets of veins are hosted by feldspar-porphyritic massive flows immediately adjacent to the dioritic intrusion. Although no axinite was observed within the intrusion or within the flows bounding the intrusion, the mineralization is an indication of the circulation of a hydrothermal mineralizing fluid.

The Summers Township axinite occurrences are located northeast of the Leitch and Sand River gold mines along the dominant regional structural trend. The Leitch and Sand River gold mines produced 847 690 ounces of gold at an average grade of 0.92 ounce gold per ton (Mason and White 1986), with most of the production from the Leitch Mine No. 2 and Sand River Mine No. 1 veins. These veins are actually different oreshoots on the same quartz vein, located in dilatant zones along a foliation parallel shear. The vein displays a crackseal texture with septa of sericitic and carbonatized wall rocks. The veins contain carbonate, sericite ± chlorite with minor amounts of pyrite, arsenopyrite, chalcopyrite ± pyrrhotite, ± tetrahedrite and rare scheelite. The shear is hosted by wacke and argillite of the SSB near the nose of a fold in the SSB–CVB contact, and close to the interpreted termination or splaying in a regional-scale fault, the Standingstone fault. Although there is no axinite in the veins, and no pervasive carbonatization of the host rocks common in the axinite occurrences, there is the potential that the same hydrothermal fluid may have been responsible for the auriferous veins and the axinite-hosting veins.

Axinite is reported in a number of Archean lode gold deposits, either intimately associated with the gold or simply within the same vein system (Table 2). Axinite, formed at the Cooke Mine, Chibougamau area, is interpreted to be a product of boron-rich hydrothermal fluids circulating through shear zones and fractures, and leeching volcanic and sedimentary rocks (Dubé and Guha 1993). In the McWatters Mine, Cadillac area, early tourmaline is formed by replacement of axinite, as evidenced by its partial epigenization in tourmaline (schörl and/or dravite) + epidote + quartz (Bardoux et al. 1990). In the Porcupine area, axinite is reported from the Paymaster, Hollinger, Goldhawk and Gold Island gold mines in quartz-calcite veins hosted by metavolcanic rocks and porphyries (Sabina 2000). Axinite is also reported as a minor mineral in a number of the silver deposits of the Cobalt and Gowganda areas (Sabina 2000). These diverse occurrences of axinite are interpreted to indicate that, like tourmaline, axinite may be a useful indicator of gold mineralization. However, similar to tourmaline, axinite is not exclusive to gold deposits, but rather defines a set of physical conditions that resulted in the formation of gold mineralization. The common features to these axinite occurrences are the co-existence of metavolcanic and metasedimentary rocks, possibly Timiskiming type, spatially associated with a major regional structure.

Regionally, axinite is not found on the western side of Lake Nipigon, and tourmaline is the dominant borosilicate mineral. As with the axinite in the Beardmore–Geraldton Belt, the tourmaline ± quartz veins are hosted by mafic metavolcanic rocks along the southern side of the Lac des Iles intrusive complex, north of the Max Creek fault (Hart and MacDonald 2000). A belt of clastic metasedimentary rocks is located to the south of the fault, but the correlation of these rocks with the 3 metasedimentary subbelts of the Beardmore–Geraldton Belt is unclear. There are a number of gold occurrences in quartz veins in the mafic metavolcanic rocks of the Lac des Iles intrusive complex and associated with iron formations in the metasedimentary rocks to the south. The reason for the occurrence of tourmaline rather than axinite is not obvious, but may be related to the lack of dioritic intrusions, difference in temperature and hydrothermal fluid type or conditions.

Axinite is also present in the metavolcanic rocks of the Shebandowan greenstone belt, to the south of the Quetico Subprovince located in an outcrop along the east side of the Kaministikiquia River along Highway 102 (Sabina 1991). The 1 to 10 cm wide quartz-chlorite-clinozoesite-calcite-axinite veins are hosted by intensely carbonatized mafic metavolcanic rocks. The axinite is massive, mauve to greyish violet and irregular in thickness along the vein length. As in the Beardmore area, the axinite weathers to a very pale purplish white to purplish grey hindering identification. This occurrence is also proximal to Timiskiming-type metasedimentary rocks and a major regional structure. There are also a number of gold occurrences in the area. Mafic metavolcanic rocks vary from tholeiitic to calc-alkaline intermediate and felsic rocks (Brown 1995). The field characteristics of this axinite occurrence are indistinguishable from these of the Beardmore area.

CONCLUSIONS

Axinite-bearing veins in the Beardmore area are hosted by metavolcanic rocks intruded by gabbro or diorite sills. The control on axinite formation is interpreted to be the calc-alkaline dioritic intrusions, intense carbonatization of the host metavolcanic rocks, and proximity to the contact with metasedimentary rocks, possibly Timiskiming type, and major regional structures and/or faults. Gold mineralization in the area is not directly related to the axinite-bearing veins, but is interpreted to occur along the same vein system, though further work is required to discover the relative timing of the axinite and gold mineralization. Similar controls appear to be present in a number of other axinite occurrences in the Superior Province (e.g., Chibougamau, Cadillac, Porcupine, Kaministikaquia) although most of these occurrences are associated with gold mineralization (e.g., Dubé and Guha 1993; Bardoux et al. 1990; Sabina 2000). Axinite, like tourmaline, is interpreted to be a useful indicator of gold mineralization. However, similar to tourmaline, axinite is not exclusive to gold deposits, but rather defines a set of physical conditions that favour the transport and deposition of gold. Nonetheless, the authors suggest that it may be an influencing factor, and encourage field and exploration geologists to pay special attention to axinite-rich regions.

METAMORPHISM

The metavolcanic and metasedimentary rocks of the Beardmore–Geraldton Belt (BGB) display little variation in mineral assemblages indicating an overall regional lower to middle greenschist-grade metamorphism. Mineral assemblages in the mafic and felsic intrusive rocks indicate that these rocks have undergone the same regional-grade metamorphism as the metavolcanic and metasedimentary rocks, indicating intrusion before the peak of regional metamorphism. Metasedimentary rocks of the Quetico Subprovince contain mineral assemblages indicative of an upper greenschist-facies metamorphism, which is a slightly higher metamorphic grade than the BGB. Proterozoic ultramafic and mafic intrusive rocks have not undergone metamorphism, distinguishing these rocks from the older rock types in the area.

The majority of Archean metavolcanic and metasedimentary rocks of the Beardmore–Geraldton Belt exhibit lower to middle greenschist-facies metamorphism. Metasedimentary rocks typically contain a mineral assemblage of quartz-albite-sericite ± epidote, indicative of lower to middle greenschist-facies metamorphism (Ehlers and Blatt 1982). The one exception occurs approximately 100 m south of the volcanic inlier along the lakeshore in northwestern Kitto Township, where anomalous amounts of biotite (>5%) are present. This is comparable to the mineral assemblage observed in the Quetico Subprovince metasedimentary rocks. This high biotite content is interpreted to be due to contact metamorphism during the intrusion of the adjacent ultramafic body.

Metavolcanic rocks in the BGB commonly contain albite-chlorite-actinolite ± biotite, indicative of lower to middle greenschist-facies metamorphism (Ehlers and Blatt 1982). Within metavolcanic rocks, igneous hornblende is commonly replaced by biotite and actinolite. Biotite may also occur as laths aligned with the fabric of the rock, some of which display partially replacement to chlorite. This may be interpreted to suggest retrograde metamorphism during development of the S_2 foliation.

Synvolcanic mafic to ultramafic intrusive rocks contain a mineral assemblage of albite-chlorite-actinolite ± biotite, which is indicative of middle greenschist-facies metamorphism (Ehlers and Blatt 1982), and which is similar to the metamorphic grade of the supracrustal units. Synvolcanic intermediate to felsic intrusive rocks contain sericite replacing feldspar phenocrysts indicative of lower to middle greenschist-facies metamorphism (Ehlers and Blatt 1982). Posttectonic mafic intrusive rocks contain a mineral assemblage of quartz-albite-sericite ± actinolite mineral assemblage, which is similarly indicative of middle greenschist-facies metamorphism (Ehlers and Blatt 1982). The common lower to middle greenschist-facies metamorphic grade for all rocks of the BGB is interpreted to indicate that the peak of regional metamorphism occurred after the latest stages of deformation.

The metasedimentary rocks of the Quetico Subprovince are generally more deformed and contain mineral assemblages indicative of a slightly higher greenschist-facies metamorphism than the BGB (Williams 1991). These rocks contain abundant medium- to coarse-grained, subhedral biotite with albite and muscovite, characteristic of an extended period of middle to upper greenschist-facies metamorphism (Ehlers and Blatt 1982). Locally, biotite displays weak to moderate replacement by chlorite.

The peridotite intrusion contains minor chlorite replacing biotite, biotite replacing hornblende, and serpentine, magnetite, and chlorite replacing olivine. The chlorite after biotite and serpentine-magnetite-chlorite after olivine may also represent a alteration during cooling. The majority of olivine and ferromagnesian crystals are fresh, supporting the interpretation that hydrothermal alteration rather than metamorphism affected these rocks. Serpentine-magnetite forms zoned haloes along vertical fractures, and appear to be an alteration product resulting from weathering of the peridotite. Similar, but less extensive, alteration along horizontal fractures and narrow vertical fractures results in the brickwork texture noted by Sutcliffe (1991). Replacement of hornblende by biotite is problematic, as hornblende is the only ferromagnesian mineral replaced. One interpretation may be that as the peridotite cooled, hornblende was replaced by biotite as the last igneous phase to crystallize in a hot, hydrous magma.

Diabase dikes display different metamorphism in a south to north pattern across the map area. The southern dikes appear to be metamorphosed to a lower greenschist grade, with plagioclase extensively replaced by sericite and the pyroxenes replaced by actinolite. The northern dikes display a similar mineral assemblage indicating a similar grade of lower greenschist-facies metamorphism, but replacement is not as extensive, which is interpreted to indicate a shorter period of time under greenschist-facies metamorphic conditions. Proterozoic diabase sills are relatively unmetamorphosed with most changes in mineralogy related to alteration.

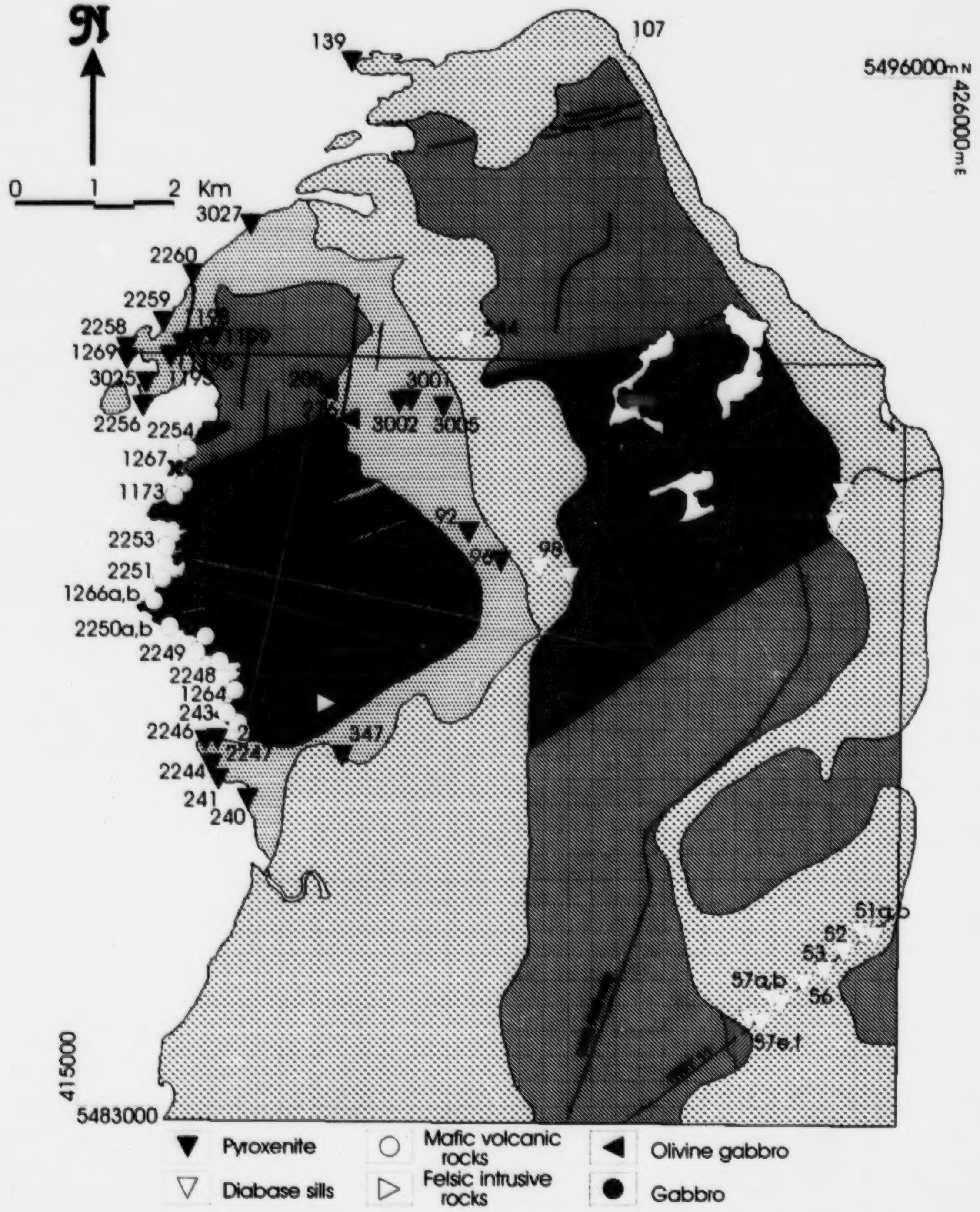

N
0
1
2 Km
139
107
5496000m N
426000m E
3027
2260
2259
2258
1269
3025
2256
2254
1267
1173
2253
2251
1266a,b
2250a,b
2249
2248
1264
243
2246
2247
2244
241
240
347
3001
3002
3005
92
98
51a,b
52
53
57a,b
56
57e,f
415000
5483000
Pyroxenite
Diabase sills
Mafic volcanic rocks
Felsic intrusive rocks
Olivine gabbro
Gabbro

Figure 13. Location of geochemical samples within Kitto Township and from the ultramafic to mafic intrusions in Eva and Kitto townships. Station numbers are listed on the figure. For analytical results, *see* Appendix 2. For geology legend, *see* Figure 6.

F2

Geochemistry

A total of 91 representative samples of metavolcanic, metasedimentary, and intrusive rocks were collected from the Beardmore–Geraldton Belt to be analyzed for whole rock major, trace, and rare earth element abundances. The majority of samples are from Proterozoic ultramafic intrusive rocks and diabase analyzed to aid in the identification of igneous petrogenetic processes, particularly along 2 stratigraphic sections through a sill in eastern Kitto Township and 2 traverses across the ultramafic intrusion in western Kitto Township (Figure 13). A lesser number of metavolcanic rocks were analyzed to help establish geochemical stratigraphic trends in the volcanic subbelts (Figures 13 and 14), with north-striking traverses positioned to complement the data made available by K.Y. Tomlinson (Tomlinson 1996).

Analytical work was completed at the Geoscience Laboratories of the Ministry of Northern Development and Mines, in Sudbury, Ontario (Appendix 1). The major element and select trace element analyses were completed by X-ray fluorescence using fused glass disks and press powder pellets, respectively. Carbon dioxide and sulphur were analyzed by infrared spectroscopy. The rare earth elements (REE) and other trace elements (tantalum, thorium, uranium and niobium) were analyzed by inductively coupled plasma mass spectrometry (ICP–MS) from a closed beaker digestion. Other trace elements and base metals were analyzed by inductively coupled plasma atomic emission spectroscopy (ICP–AES). All samples were analyzed for precious metals by ICP–AES, with a select number of diabase and ultramafic intrusive samples analyzed for platinum group elements (PGE) by nickel fire assay –ICP–MS (NFA–ICP–MS). The data from Tomlinson (1996) were also analyzed at the Geoscience Laboratories using a similar combination of XRF fused glass disks for major elements and press powder pellets for select trace elements, and the remaining trace and rare earth elements by ICP–MS.

MAFIC METAVOLCANIC ROCKS

A total of 22 samples of the mafic metavolcanic rocks were collected during the current mapping program (Appendix 2). The majority of these samples were collected along a north-trending traverse across the SVB, located along the shore of Lake Nipigon (*see* Figures 13 and 14). The results of these analyses were compared to the lithogeochemical results of detailed sampling along Highway 11 completed by Tomlinson (1996). The current SVB samples selected for analyses were from the least altered and metamorphosed massive and/or pillowed flows. A number of samples from along the southern margin of the CVB have geochemical characteristics similar to the other mafic metavolcanic rocks (Tomlinson 1996), although this unit is not distinguishable in the field. As previous detailed sampling had been completed on the best available outcrops, the lithogeochemistry completed by Tomlinson (1996) for the NVB were used in this report (*see* Figure 14). Two samples of the mafic metavolcanic horizon in the Poplar Point assemblage (PPA) of the NVB were also analyzed.

The mafic metavolcanic rocks are predominantly basalt with minor andesite regardless of the subbelt (*see* Figure 14). For the samples collected during this project, SiO_2 abundances range from 45.8 to 54.9 weight %, TiO_2 from 0.6 to 2.5 weight %, MgO from 5.3 to 10.7 weight %, and Mg-number from 0.27 to 0.63 (*see* Appendix 2). The basaltic rocks have analytical trends of high Ti/Zr and low Zr/Y and $(La/Yb)_N$ ratios that are generally characteristic of tholeiitic basalt (e.g., Pearce 1982; Figures 15 and 16). The basaltic rocks have a negative slope toward thorium with a lack of niobium and tantalum anomalies on mantle-normalized extended element diagrams (Figure 17), and $(La/Yb)_N$ ratios that are usually at or less than 1.0. The steep negative slope of sample 2250 on the extended element diagram (*see* Figure 17) would appear to be the result of alteration. Carbonate has been identified as a complexing agent capable of transporting the light rare earth elements (LREE; Lottermoser 1992). However, there is no evidence

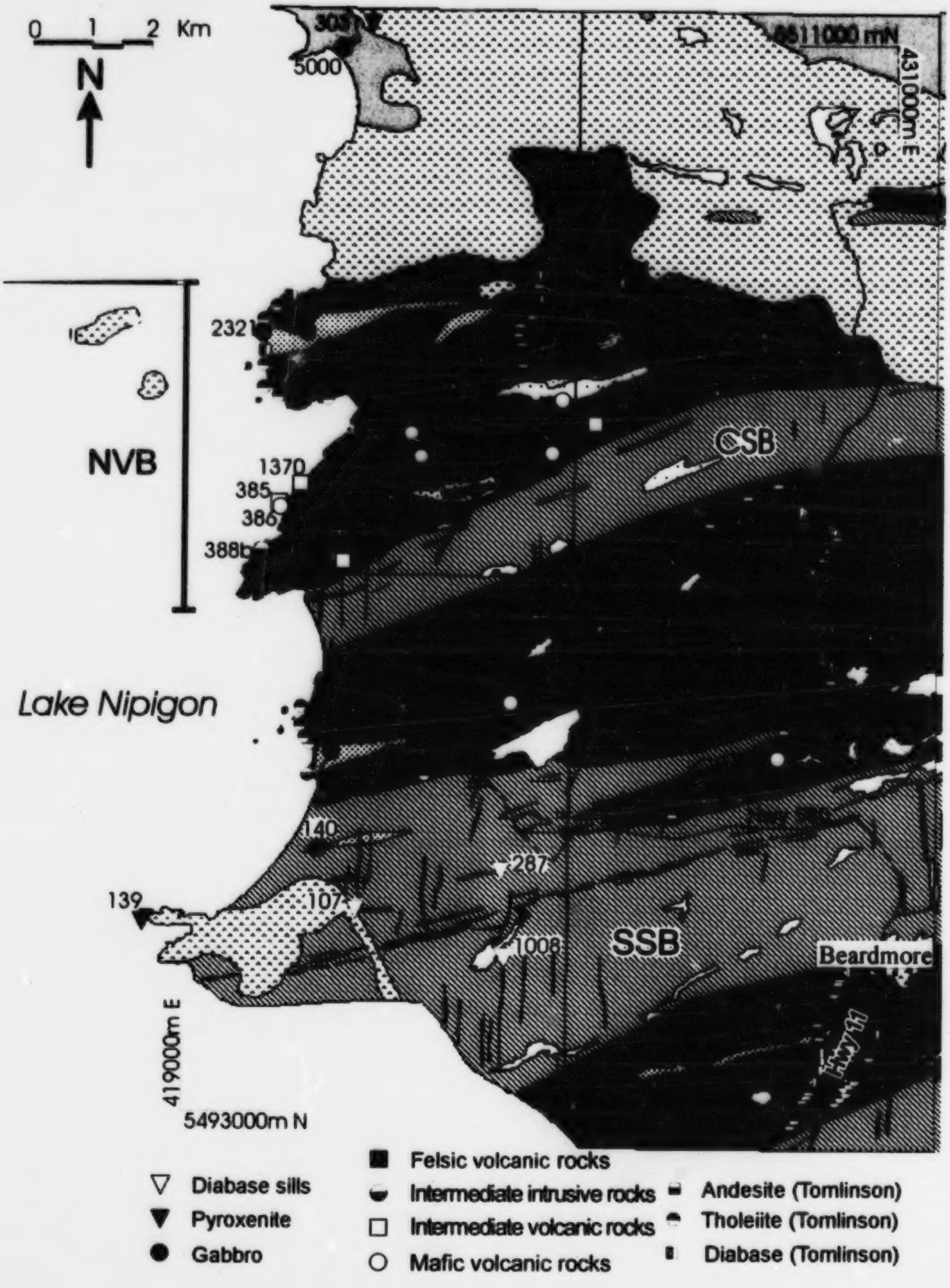
0 1 2 Km
N
303
5000
5511000 mN
431000m E
232
NVB
1370
385
386
388b
CSB
Lake Nipigon
140
287
139
107
1008
SSB
Beardmore
Hwy 11
419000m E
5493000m N
▽ Diabase sills
▼ Pyroxenite
● Gabbro
■ Felsic volcanic rocks
Intermediate intrusive rocks
☐ Intermediate volcanic rocks
○ Mafic volcanic rocks
Andesite (Tomlinson)
Tholeiite (Tomlinson)
Diabase (Tomlinson)

Figure 14. Location of lithogeochemical samples within Eva, Dorothea, and parts of Summers and Sandra townships collected during this mapping program, with additional unlabelled samples (*from* Tomlinson 1996). Station numbers are listed on the figure. For analytical results, *see* Appendix 2. For geology legend, *see* Figure 6.

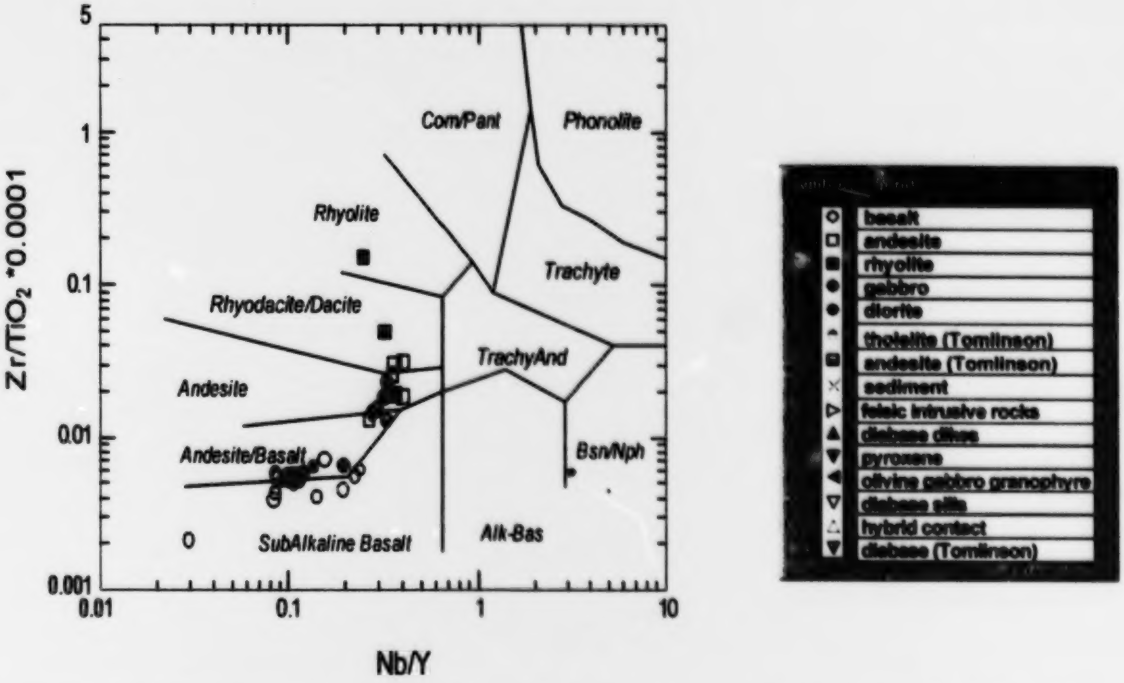

Figure 15. Nb/Y versus Zr/TiO_2 rock classification diagram with the mafic, intermediate and felsic metavolcanic rocks and associated synvolcanic and posttectonic intrusive rocks (*after* Floyd and Winchester 1978). Abbreviations used in diagram: Alk, alkaline; And, andesite; Bas, basalt; Bsn, basanite; Com, comendite; Nph, nephelinolite; Pant, pantellerite.

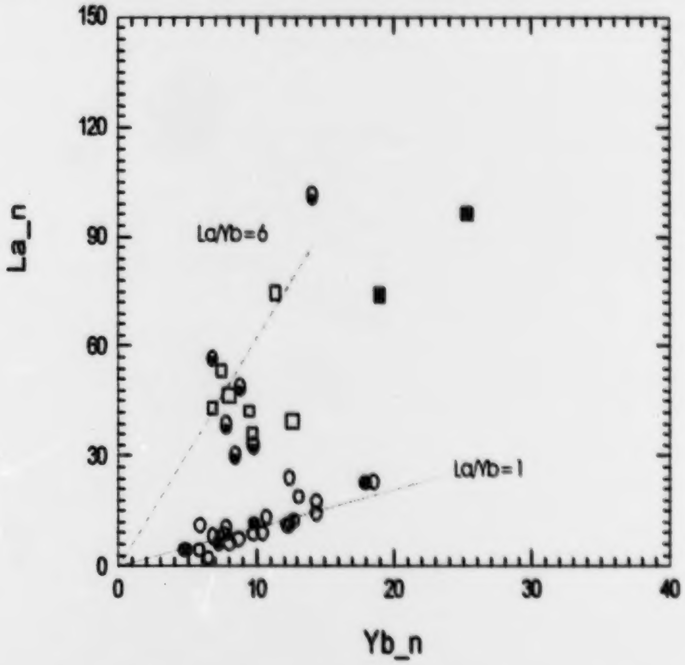

Figure 16. Ytterbium versus lanthanum chondrite-normalized diagram of the mafic, intermediate and felsic metavolcanic rocks and associated synvolcanic and posttectonic mafic intrusive rocks; normalized using the chondrite values of Nakamura (1974). Legend for symbols, *see* Figure 15.

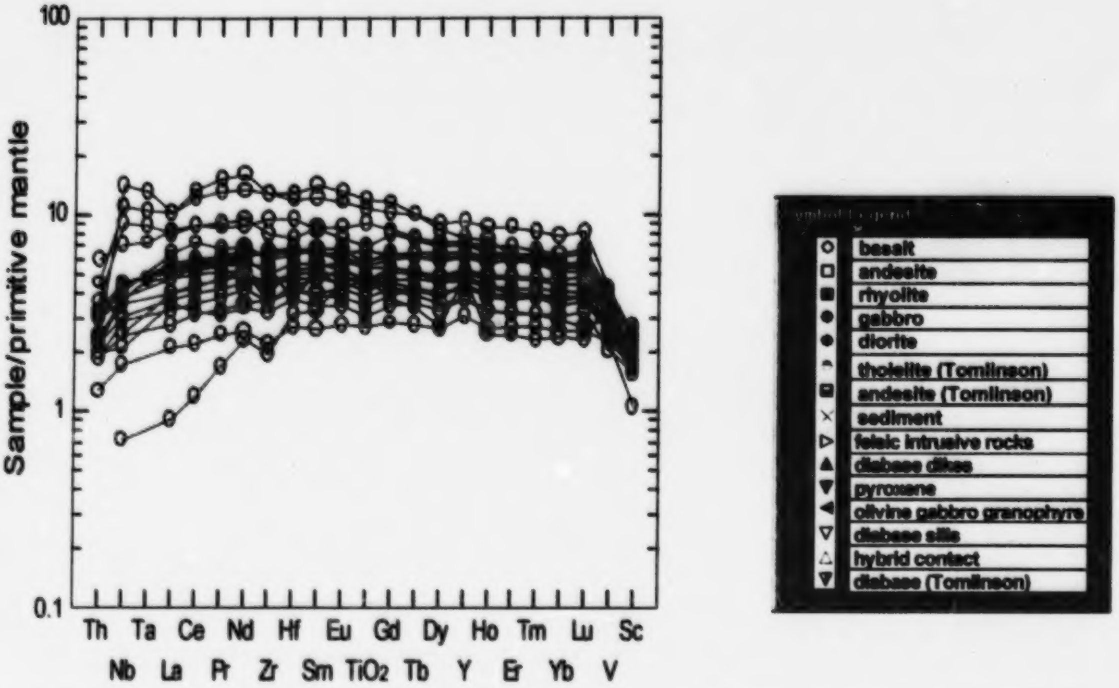

Figure 17. Mantle-normalized extended element diagram of the mafic metavolcanic rocks (*after* Kerrich and Wyman 1997).

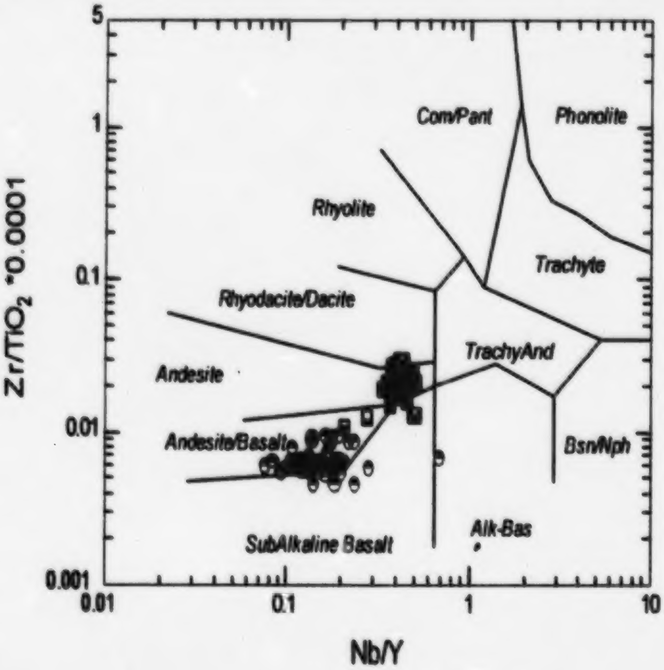

Figure 18. Nb/Y versus Zr/TiO_2 rock classification diagram with the mafic and intermediate metavolcanic rocks from Tomlinson (1996) (*after* Floyd and Winchester 1978). Legend for symbols, *see* Figure 17. For abbreviations, see Figure 15.

that this sample is highly carbonatized. Sample 1268 has a positive niobium anomaly on the extended element diagram, and also has the highest TiO_2, P_2O_5, and rare earth element contents of any of the basaltic rocks (*see* Figure 17). This combination of geochemical characteristics for sample 1268 is comparable to the high iron-titanium basalt or icelandite present in some of the volcanic assemblages of the Abitibi (e.g., Hart 1984; Binney and Barrie 1990; *see* Appendix 2), representing a fractionated tholeiite magma. However, other than sample 1268, there is little variation in the geochemistry along the traverse across the SVB. The 3 samples from the PPA are usually indistinguishable from the other basaltic rocks (*see* Appendix 2; *see* Figures 15 and 16). Sample 388 does have a higher $(La/Yb)_n$ and Zr/Y ratios and TiO_2 and niobium values than most of the basaltic rocks, and has some similarities to the CVB basaltic rocks of Tomlinson (1996) discussed below. This mixture of characteristics for sample 388 may be primary, but could also be related to an original volcaniclastic or pyroclastic origin, common to the CVB, concentrating heavy mineral and effecting the abundances of the high field-strength elements.

The mafic metavolcanic rocks from Tomlinson (1996) that are classified as basalt (Figure 18) have the tholeiitic geochemical characteristics of high Ti/Zr and low Zr/Y, $(La/Yb)_n$, and Th/Yb ratios (Figures 19, 20 and 21). These rocks are from the Highway 11 SVB traverse, scattered samples in the CVB traverses, and 2 samples in the NVB shoreline traverse. The element ranges reported by Tomlinson (1996) are greater than those for basaltic rock samples collected during the Phoenix Project, and more of the samples were andesitic in composition (*see* Figure 18). The Phoenix Project samples have a more restricted range for some elements, such as Al_2O_3 (12.11 to 17.13 wt %), Cr (200 to 478 ppm), and V (188 to 369 ppm), but generally have elemental ratios similar to Tomlinson (1996). A subset of samples within the NVB was characterized by Tomlinson (1996) as having lower Ti/Zr ratios than the majority of basaltic rocks. However, only sample 96KYT-303, which is part of the NVB shoreline traverse, is located in the current map area (*see* Figure 14). This sample also has higher Th/Yb ratios (*see* Figure 21) and negative tantalum and niobium anomalies on an extended element diagram. There are 3 samples, scattered through the SVB and NVB traverses, that have higher $(La/Yb)_n$, but varied Th/Yb ratios that are

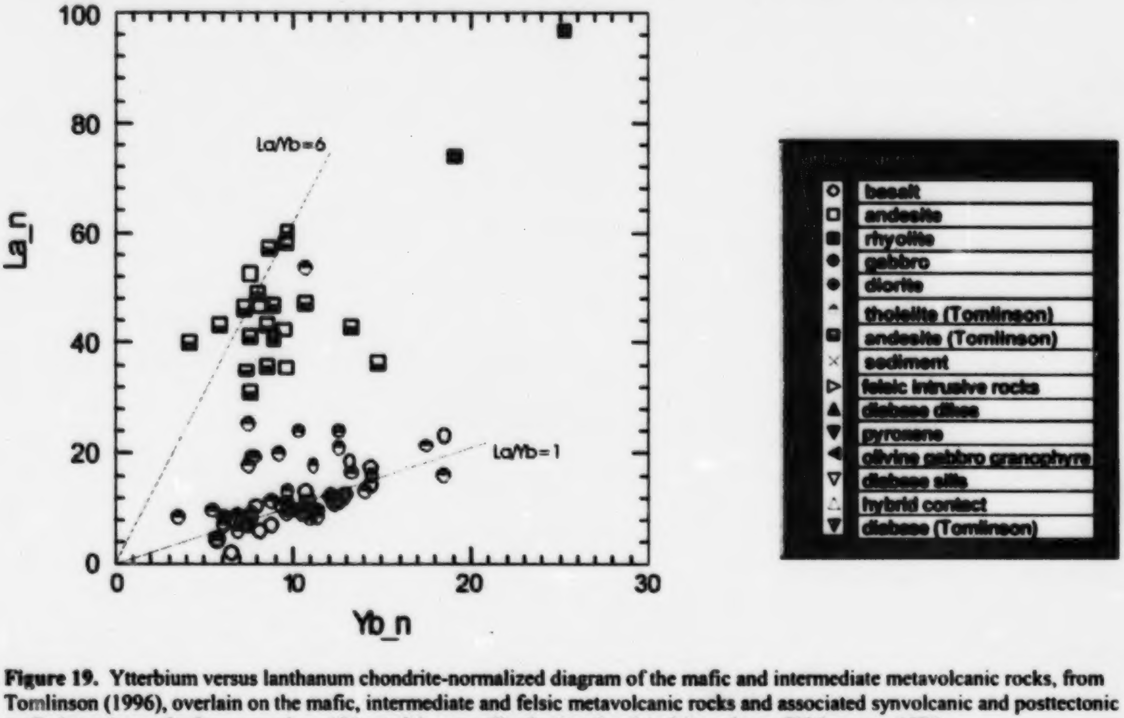

Figure 19. Ytterbium versus lanthanum chondrite-normalized diagram of the mafic and intermediate metavolcanic rocks, from Tomlinson (1996), overlain on the mafic, intermediate and felsic metavolcanic rocks and associated synvolcanic and posttectonic mafic intrusive rocks for comparison (this study); normalized using the chondrite values of Nakamura (1974).

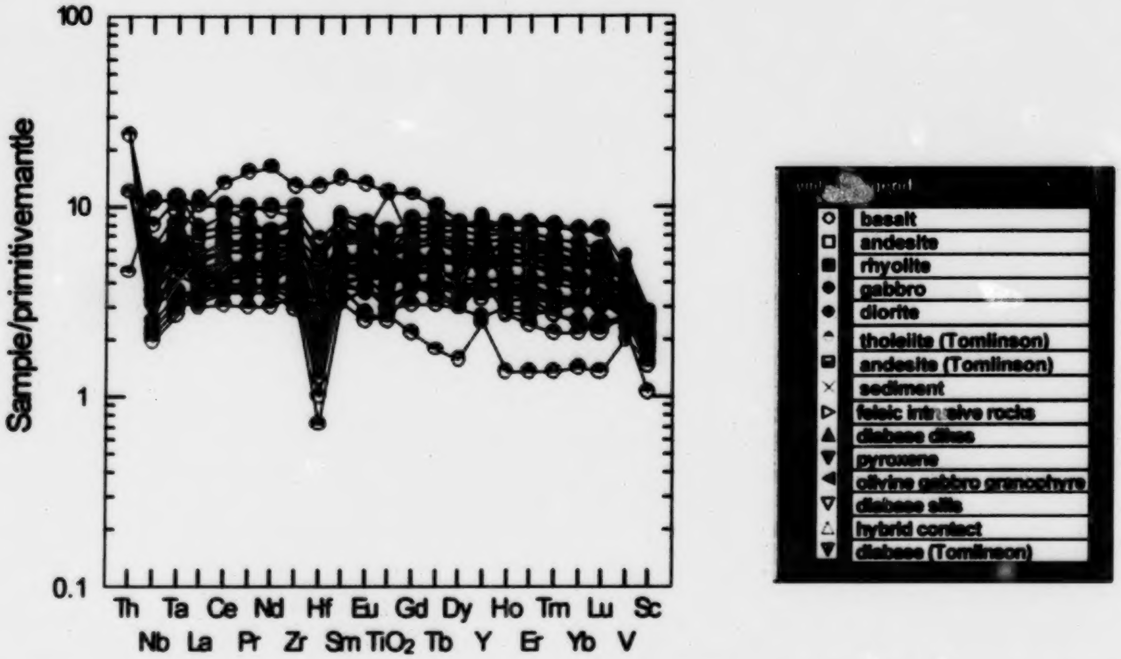

Figure 20. Mantle-normalized extended element diagram of the mafic metavolcanic rocks from Tomlinson (1996) (*after* Kerrich and Wyman 1997).

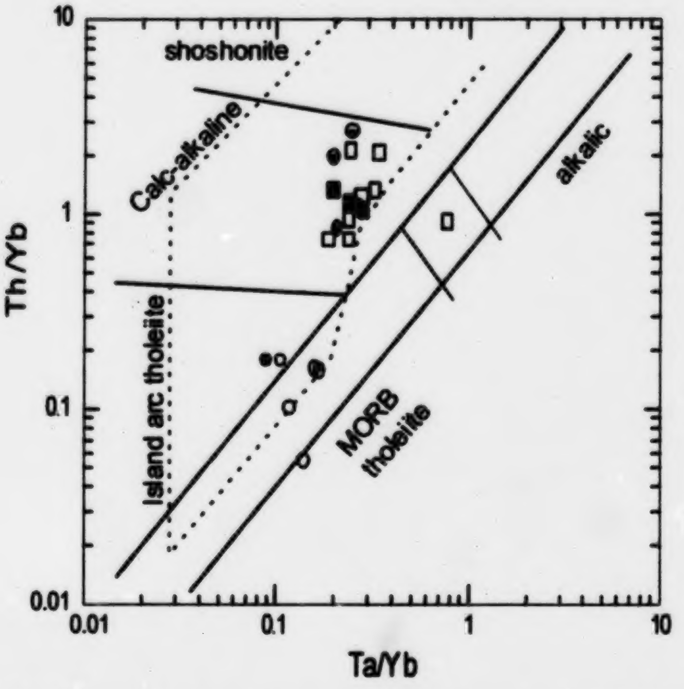

Figure 21. Ta/Yb versus Th/Yb tectonic discrimination diagram of the mafic, intermediate and felsic metavolcanic rocks, the associated synvolcanic and the posttectonic mafic intrusive rocks (*after* Pearce 1982). Legend for symbols, *see* Figure 20. Abbreviation: MORB, mid-ocean ridge basalt.

similar to this subset. Sample 96KYT-353 is part of the Highway 11 SVB traverse, and samples 96KYT-303 and 96KYT-304 are part of the NVB shoreline traverse (*see* Figures 13, 14 and 19). These geochemical differences are probably primary igneous characteristics as these samples are not significantly altered.

A number of samples from the CVB traverse have tholeiitic geochemical characteristics similar to the basalt, in contrast to the more calc-alkaline geochemistry of most of the metavolcanic rocks of the CVB. These samples are located along the southern margin of the subbelt, with 96KYT-308 located west of Eva Lake and 96KYT-55 and 96KYT-57 located along the 72 Road (*see* Figure 14). All 3 samples have depleted distinctive heavy REE (HREE) abundances that Tomlinson (1996) suggested was the result of residual garnet during the original partial melting event that formed these rocks (*see* Figure 19). Alternatively, sample 96KYT-308 has a high loss on ignition (LOI) value and is located close to the strong carbonate alteration associated with the trace of the Sandy Creek fault.

Analytical trends of decreasing magnesium, nickel and chromium and increasing iron, manganese, titanium, scandium and vanadium with increasing zirconium were implied by Tomlinson (1996) to be the result of olivine ± chromite fractionation and a lack of clinopyroxene or magnetite fractionation respectively (*see* Appendix 2). The weak decrease in Al_2O_3 with increasing zirconium indicates that some plagioclase fractionation occurred. The varied nature of the europium anomalies was interpreted to indicate either that plagioclase was only a moderately important fractionating mineral (*see* Figure 17).

Most of the tholeiitic basalt samples have the characteristics of mid-ocean ridge basalt (MORB), with $(La/Yb)_n$ ratios equal to or less than 1, negative slopes toward thorium, and no tantalum or nkiobium anomalies on extended element diagrams (*see* Figures 17 and 20; e.g., Sun and McDonough 1989). These samples also plot within the MORB field on many of the tectonic discrimination diagrams (e.g., Figures 21 and 22). The scandium depletion displayed by these rocks was also noted to be common for MORB and was interpreted by Hofmann (1988) to be the result of residual clinopyroxene during the partial-melting event that formed the MORB.

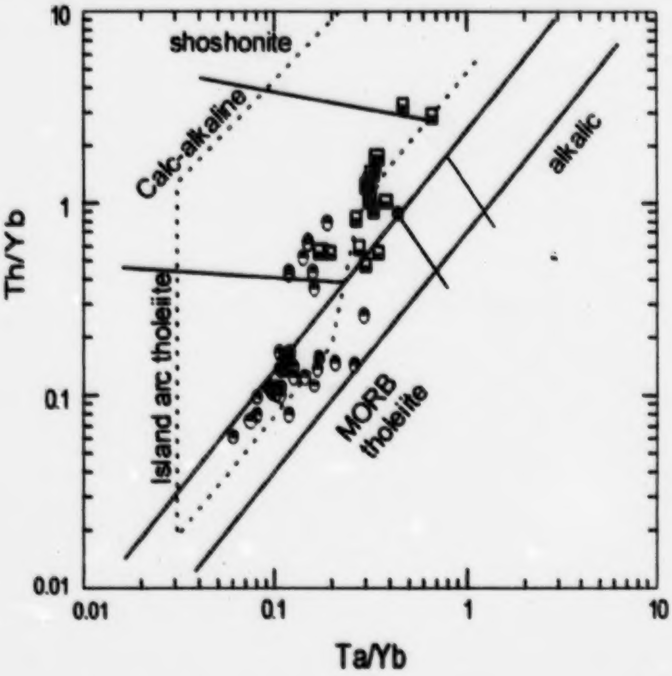

Figure 22. Ta/Yb versus Th/Yb tectonic discrimination diagram of the mafic and intermediate metavolcanic rocks from Tomlinson (1996) (*after* Pearce 1982). Legend for symbols, *see* Figure 20. Abbreviation: MORB, mid-ocean ridge basalt.

The subset of samples within the tholeiitic basalt field has many of the same MORB-like characteristics of the other basalt, but Th/Yb ratios and negative tantalum and niobium anomalies on extended element diagrams (e.g., *see* Figures 21 and 22) are characteristic of subduction-related volcanic rocks. This mixture of geochemical characteristics led Tomlinson (1996) to suggest that these rocks formed in a back-arc basin, similar to the Lau Basin, where there are volcanic rocks with both arc and/or MORB geochemical characteristics.

INTERMEDIATE TO MAFIC METAVOLCANIC ROCKS

The intermediate metavolcanic rocks are generally confined to the CVB and the Poplar Point assemblage (PPA) of the NVB, and were distinguished in the field by their colour index and the common presence of feldspar phenocrysts. Volcaniclastic units, tuffs, lapilli tuffs, and tuff breccias are much more common than in the tholeiitic basaltic rocks of the SVB and the Bish Bay assemblage (BBA) of the NVB, resulting in a limited availability of units suitable for whole rock geochemical sampling. A total of 9 samples were collected during the Phoenix Project, mainly to fill in gaps in the detailed sampling completed by Tomlinson (1996) along the 72 Road and by O'Brien (1985) along the shore of Lake Nipigon. The field classification correlates relatively well with the lithogeochemical classification of the samples, with the exception of minor inconsistent overlaps with the tholeiitic basalt.

Most of the intermediate metavolcanic samples from the Phoenix Project were from a traverse along the shore of Lake Nipigon (*see* Figure 14), and these rocks are predominantly andesite with minor basalt. For the samples collected during this project, SiO_2 abundances range from 59.1 to 68.9 weight %, TiO_2 from 0.57 to 0.88 weight %, MgO from 1.24 to 3.67 weight %, Zr from 165 to 179 ppm and La from 11.62 to 17.28 ppm (*see* Appendix 2). The andesitic rocks have analytical trends of low Ti/Zr, and high Zr/Y and $(La/Yb)_n$ ratios that are generally characteristic of calc-alkaline andesite and basalt (*see* Figures 15 and 16). These samples also have positive slopes toward thorium with prominent negative niobium and tantalum anomalies on a mantle-normalized extended element diagram (Figure 23), and $(La/Yb)_n$ ratios between 3.6 and 6.9.

The intermediate metavolcanic rocks sampled by Tomlinson (1996) and O'Brien (1985) were used to characterize the lithogeochemistry of the CVB (*see* Figure 14 for locations). These rocks are predominantly andesite (*see* Figure 18), and also have low Ti/Zr and high Zr/Y and $(La/Yb)_n$ ratios characteristic of calc-alkaline andesite and basalt (*see* Figures 19 and 20; e.g., Pearce 1982). The element ranges of Tomlinson (1996) generally overlap with those of andesite from the Phoenix Project (*see* Figure 18), with the exception of a small subgroup displaying more basaltic characteristics. This subgroup of basalt generally falls in the transitional range between the calc-alkaline andesite and tholeiitic basalt (*see* Figures 19 and 20). However, the Th/Yb and $(La/Yb)_n$ ratios are more calc-alkaline than tholeiitic (Figure 24). Sample 96KYT-98 is located along the southern side of the BBA, and samples 96KYT-72 and 96KYT-73 are located in the middle of the CVB. These last 2 samples are situated close to the interpreted trace of the Sandy Creek fault. In general, andesite is distinguished by higher Th/Yb ratios than the basalt (*see* Figure 22), and negative tantalum and niobium anomalies on an extended element diagram (*see* Figure 24).

Inter-element ratios in the andesite of the CVB are usually ambiguous, and it is generally difficult to determine if there are fractionation trends (Tomlinson 1996). The greater amount of scatter may be the result of alteration and/or the fragmental nature of many of the rock units in the CVB. Tomlinson (1996) subdivided the andesite into 3 subgroups based on La/Yb_n ratios of 8.3, 6.3, and 5.0. However, ignoring the outliers, the andesitic rocks have weak analytical trends of decreasing magnesium and chromium and weakly increasing iron, titanium, scandium and vanadium with increasing zirconium, that may be interpreted to be the result of olivine and clinopyroxene or magnetite fractionation, respectively (*see*

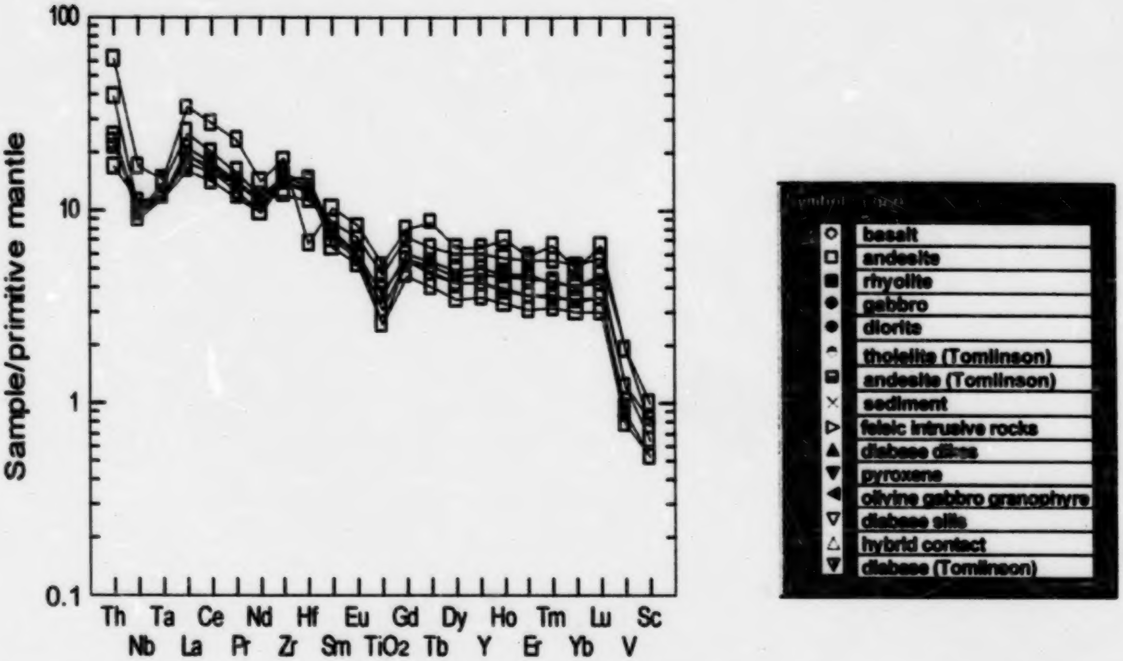

Figure 23. Mantle-normalized extended element diagram of the intermediate metavolcanic rocks (*after* Kerrich and Wyman 1997).

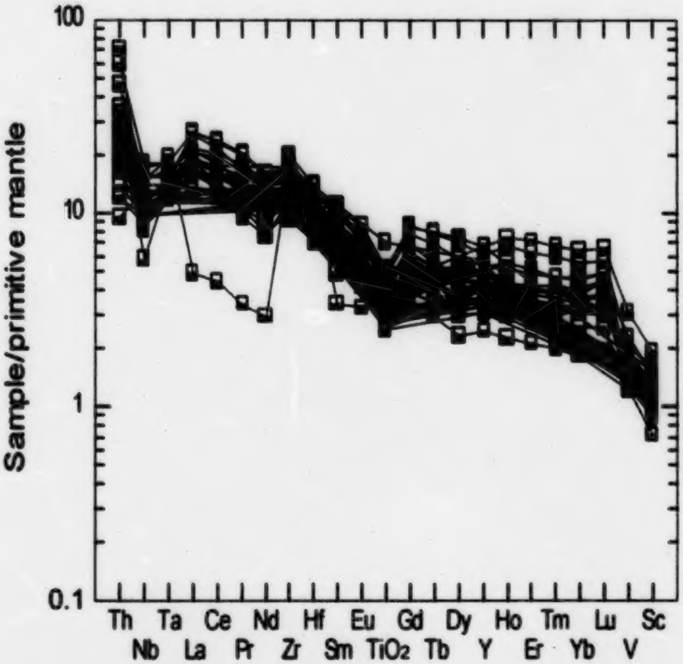

Figure 24. Mantle-normalized extended element diagram of the intermediate metavolcanic rocks from Tomlinson (1996) (*after* Kerrich and Wyman 1997). Legend for symbols, *see* Figure 23.

Appendix 2). Although there is a lack of europium anomalies, the weak decrease in Al_2O_3 with increasing zirconium indicates that some plagioclase fractionation has occurred.

Most of the andesitic rocks have the characteristics of calc-alkaline island-arc basalt, with $(La/Yb)_n$ and Th/Yb ratios greater than 1, and negative tantalum or niobium anomalies on extended element diagrams (*see* Figures 23 and 24; e.g., Sun and McDonough 1989). The andesite also plots within the island-arc field on most tectonic discrimination diagrams (e.g., *see* Figure 22). The subgroup of andesite is more similar to mid-ocean ridge basalt (e.g., *see* Figure 19), but with the Th/Yb ratios and negative tantalum and niobium anomalies (*see* Figures 21 and 22) characteristic of subduction related volcanic rocks. This subgroup is interpreted to indicate formation in a back-arc basin tectonic environment. The location of this subgroup within the CVB along the Sandy Creek fault is interpreted to indicate that the fault is a stratigraphic break rather than just a late deformation zone (*see* Figure 14).

INTERMEDIATE TO FELSIC METAVOLCANIC ROCKS

Two samples of felsic metavolcanic rocks were collected, one from the Poplar Point assemblage and the other from north of Eva Lake, in the CVB (*see* Figure 14; *see* Appendix 2). Classification of these samples as extrusive or subvolcanic feeder dikes was difficult, and these arguments are presented above (*see* "General Geology: Felsic Metavolcanic Rocks").

Sample 229 was collected from a feldspar-quartz porphyritic dike with peperitic textures that intruded a heterolithic intermediate tuff of the PPA of the NVB (*see* Figure 14). This sample is relatively unaltered, with a SiO_2 content of 72.69 weight %, K_2O of 2.57 weight %, and Na_2O of 3.51 weight % suggesting that it is a rhyolite (*see* Appendix 2). However, a TiO_2 value of 0.73 weight % places this sample in the dacite field, as shown in Figure 15. Sample 229 has a $(La/Yb)_n$ ratio of 3.85 and a Zr/Y ratio of 7.39, which, with moderately high yttrium and ytterbium values, places this sample in the range of the FII felsic metavolcanic rocks (Figure 25; Lesher et al. 1986). This classification can be indicative of a potential to host VMS mineralization, although a larger number of samples would be required to properly characterize this unit. The sample has a positive slope toward thorium, and negative tantalum and niobium anomalies on an extended element diagram (Figure 26). Although normalized to mantle values, the felsic chemistry of this sample indicates that it should be normalized to continental crust with the appropriate element order (Hofmann 1988; Figure 27). Additional material was also collected from this site and submitted for geochronology (*see* "Geochronology").

A sample of the fine- to very fine-grained massive flow located to the north of Eva Lake was collected for geochemical analyses (*see* Figure 14; *see*Appendix 2). Sample 225 has a SiO_2 content of 73.82 weight %, K_2O of 1.35 weight %, Na_2O of 4.78 weight %, and a TiO_2 value of 0.20 weight % that places this sample in the rhyolite field, as shown in Figure 15. This sample has a $(La/Yb)_n$ ratio of 3.79 and a Zr/Y ratio of 4.73 that, with moderately high yttrium and ytterbium values, also places this sample in the range of the FII felsic metavolcanic rocks (Lesher et al. 1986; *see* Figure 25). This classification can be indicative of a potential to host VMS mineralization, although a larger number of samples would be required to properly characterize these rocks. This sample is shown on a mantle-normalized diagram (*see* Figure 26), but, with sample 229, it should be normalized to continental crust with an appropriate element order (*see* Figure 27). Additional material was also collected from this site and submitted for geochronology (*see* "Geochronology").

Both of the felsic metavolcanic rock samples plot within the active continental margin and within-plate volcanic zone ranges on a modified Th/Yb–Ta/Yb diagram, as proposed by Gorton and Schandl (2000; Figure 28) and/or the destructive plate margin field on the Th–Ta–Hf/3 diagram of Wood (1980). The samarium and TiO_2 anomalies on a continental crust normalized diagram may be the result of an error in the normalizing factors (*see* Figure 27). This geochemistry is compatible with an arc environment, which is not incompatible with the interpretation for the associated intermediate metavolcanic rocks.

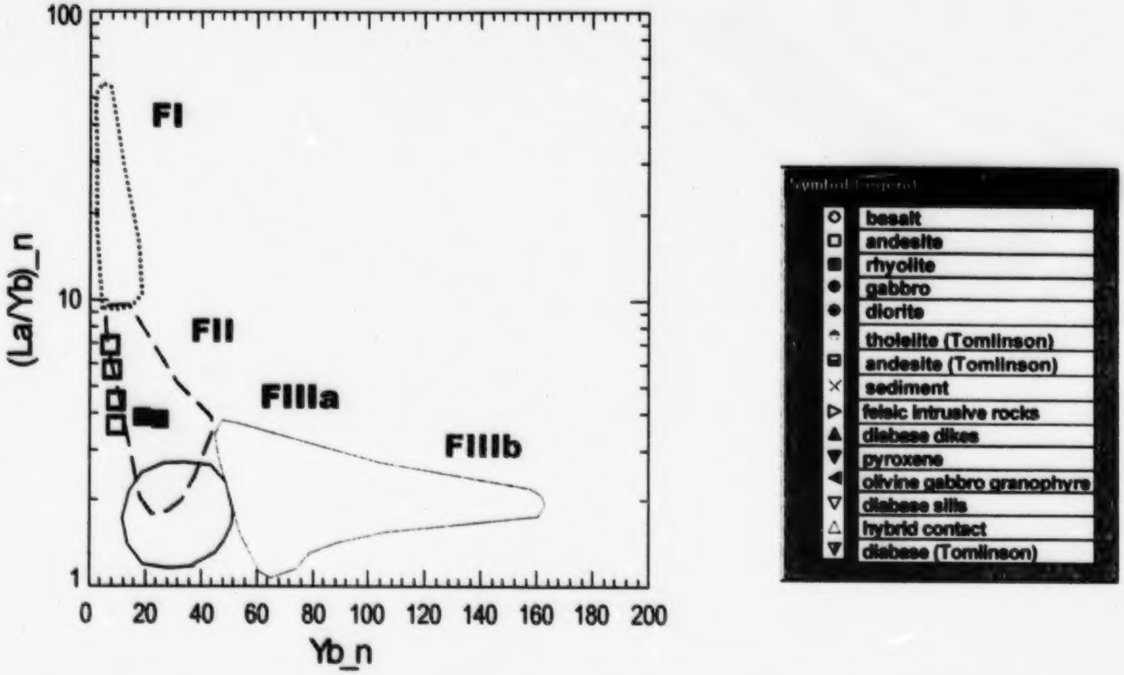

Figure 25. Ytterbium versus La/Yb chondrite-normalized diagram with fields for felsic volcanic rocks, from Lesher et al. (1986), normalized using the chondrite values of Nakamura (1974).

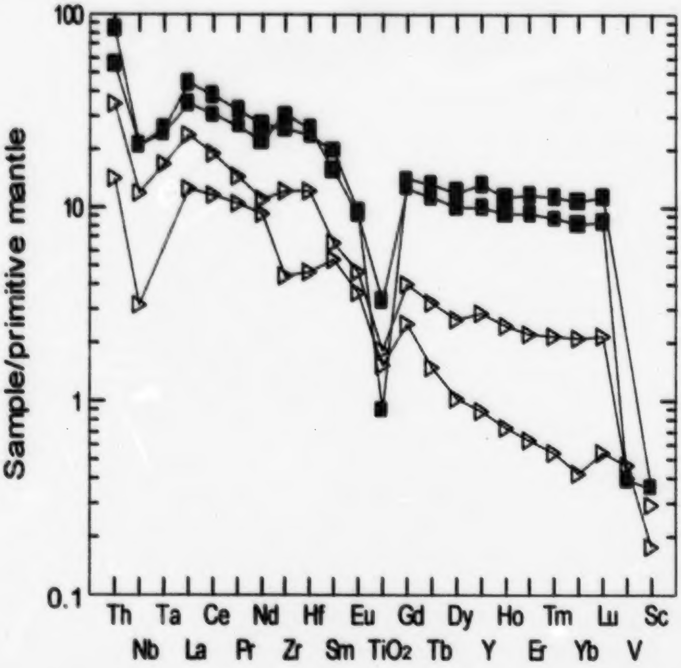

Figure 26. Mantle-normalized extended element diagram of the felsic metavolcanic rocks and felsic intrusive rocks (*after* Kerrich and Wyman 1997). Legend for symbols, *see* Figure 25.

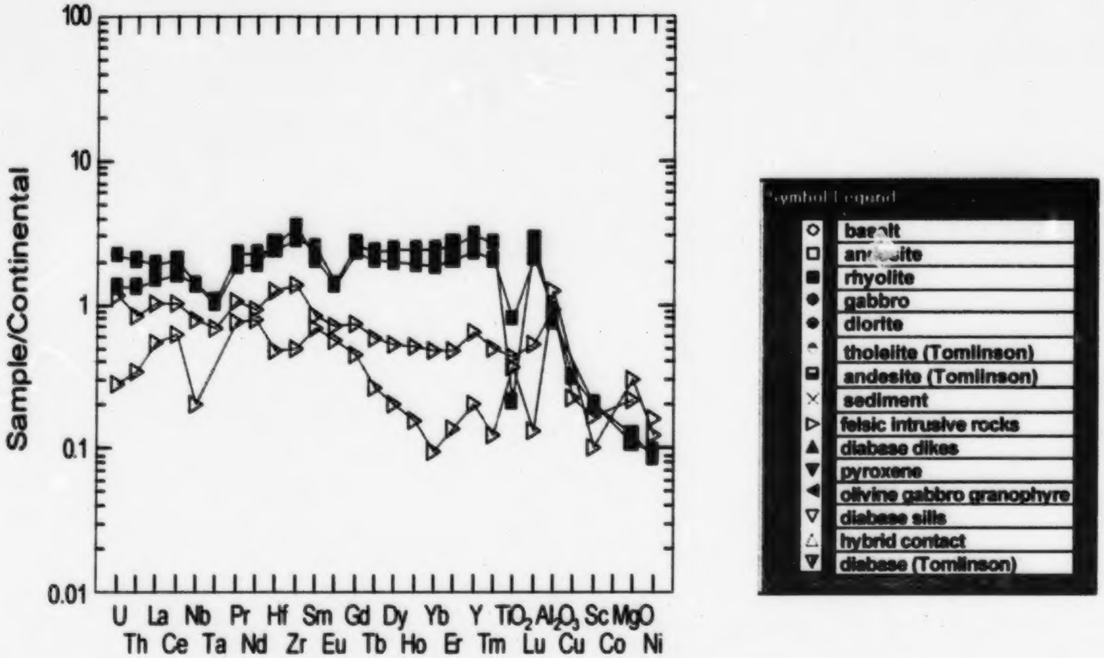

Figure 27. Continental-crust normalized extended element diagram of the felsic metavolcanic rocks and felsic intrusive rocks (*after* Hofmann 1988).

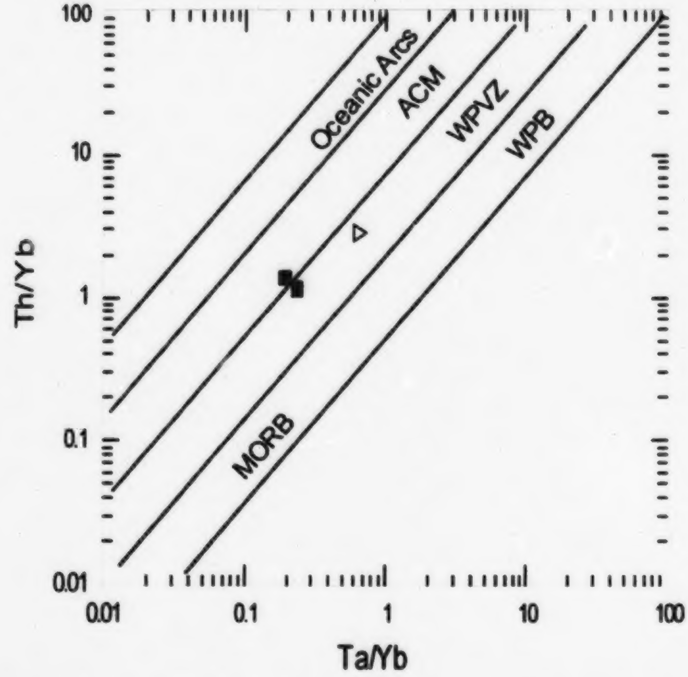

Figure 28. Ta/Yb versus Th/Yb tectonic discrimination diagram of the felsic metavolcanic rocks and felsic intrusive rocks (*after* Gorton and Schandl 2000). Abbreviations: ACM, active continental margin; MORB, mid-ocean ridge basalt; WPB, within-plate basalt; WPVZ, within-plate volcanic zone. Legend for symbols, *see* Figure 27.

SYNVOLCANIC MAFIC INTRUSIVE ROCKS

The mafic intrusive rocks have elemental abundances and ratios that generally reflect the composition of the metavolcanic rocks that they intrude (*see* Appendix 2). These massive, medium-grained intrusive rocks are located in the SVB and the Bish Bay assemblage (BBA) of the NVB (*see* Figures 13 and 14). A sample located on the southern edge of the CVB has a geochemical characteristic comparable to these intrusive rocks rather than the posttectonic mafic intrusive rocks of the rest of the CVB (*see* "Geochemistry: Posttectonic Mafic Intrusive Rocks").

Mafic intrusive rocks are geochemically similar regardless of the subbelt in which they are located, and are similar to the mafic metavolcanic rocks that they intrude (*see* Figures 13 and 14). These rocks were referred to as gabbro in the field, have SiO_2 contents of 49.18 to 50.62 weight %, TiO_2 of 0.63 to 0.83 weight %, Fe_2O_3 of 10.70 to 13.42 weight %, MgO of 6.53 to 8.35 weight %, and Mg-numbers of 0.55, and, thus, the analytical results are in agreement with this terminology. The gabbroic rocks have high Ti/Zr, and low Zr/Y and $(La/Yb)_n$ ratios that are characteristic of tholeiitic rocks and are comparable to the basalt which they intrude (*see* Figures 15 and 16). A negative slope toward thorium and a lack of niobium or tantalum anomalies on a mantle-normalized extended element diagram overlap with the values for the basaltic rocks (Figure 29). This overlap is interpreted to indicate that the same petrogenetic processes formed the 2 rock types, but the similarities also mean that the geochemistry will not aid in differentiating coarse-grained gabbroic textured flows from subvolcanic gabbroic intrusions.

The gabbro intrusion in the BBA (*see* Figure 14) appears to be a composite body, with a mafic southern phase and an ultramafic northern phase. The ultramafic phase has been classified as a peridotite with analyses of TiO_2 of 0.49 weight %, Al_2O_3 of 7.94 weight %, and MgO of 25.61 weight %, with a Mg number of 0.76 (*see* Appendix 2). The peridotite has lower elemental abundances, but Ti/Zr, Zr/Y, and

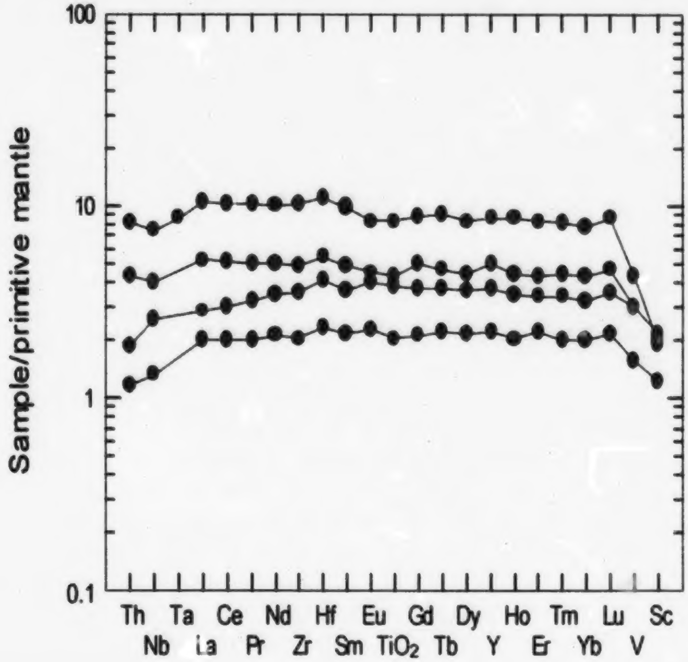

Figure 29. Mantle-normalized extended element diagram of the synvolcanic to syntectonic mafic intrusive rocks (*after* Kerrich and Wyman 1997). Legend for symbols, *see* Figure 27.

$(La/Yb)_n$ ratios that are comparable to the tholeiitic southern gabbroic phase, a sample of which was analyzed by Tomlinson (1996; *see* Figures 15 and 16). These similarities have been interpreted to indicate that the peridotite is a primitive phase of the larger gabbro intrusion.

Sample 444 is from a small body located along the southern edge of the CVB, mapped as a posttectonic gabbro in the field, but has a geochemistry with more in common with the tholeiitic gabbro of the SVB and NVB (*see* Figure 15). This sample is more fractionated than the other gabbroic rocks, with a SiO_2 analysis of 52.86 weight %, TiO_2 of 1.87 weight %, MgO of 3.46 weight %, and a Mg number of 0.26 (*see* Appendix 2). The Ti/Zr and Zr/Y ratios are comparable to the other gabbroic rocks, but this gabbro has a slightly higher $(La/Yb)_n$ ratio and flat slopes with weak negative niobium and tantalum anomalies on an extended element diagram that differs slightly with the other tholeiitic gabbro (*see* Figure 29). Sample 444 is interpreted to be unrelated to the subset of tholeiitic basalt located along the southern margin of the CVB in the same general area.

Analytical trends of decreasing magnesium, nickel and chromium and decreasing iron, titanium, scandium and vanadium with increasing zirconium are interpreted to indicate the fractionation of olivine ± chromite, and lack of clinopyroxene or magnetite, respectively (*see* Appendix 2). There are a few exceptions, such as peridotite sample 2321, that lacks the magnesium, nickel and chromium depletions indicative of olivine fractionation, and a gabbro, sample 444, that is depleted in scandium, suggesting clinopyroxene fractionation (*see* Figure 29). The depletion of Al_2O_3 in most of the gabbroic rocks with increasing zirconium is indicative of moderate fractionation of plagioclase, but the very weak to nonexistent europium anomalies suggest that plagioclase was not a major fractionating mineral phase. As described above, the gabbroic rocks display many of the geochemical characteristics of the basaltic rocks, with fractionation trends that are generally tholeiitic in nature.

The gabbroic rocks have the tholeiitic characteristics common to MORB, with $(La/Yb)_n$ and Th/Yb ratios less than 1, and no tantalum or niobium anomalies on extended element diagrams (*see* Figure 29; e.g., Sun and McDonough 1989). These samples plot within the MORB field on tectonic discrimination diagrams (e.g., *see* Figure 21), and are interpreted to indicate formation by similar petrogenetic process as the basalt. Sample 444 is also tholeiitic, but has a mixture of geochemical characteristics that are transitional between a MORB and an arc environment (*see* Figure 21). This transition is compatible with the proposed back-arc environment for the CVB, with sample 444 located along the southern margin, which is similar to a MORB environment.

SYNVOLCANIC INTERMEDIATE TO FELSIC INTRUSIVE ROCKS

A number of intermediate to felsic dikes intrude the metavolcanic rocks of the BGB, and a sample of a feldspar porphyritic dike in the SVB and a massive medium-grained granodiorite in the Poplar Point assemblage (PPA) were analyzed (*see* Figures 13 and 14; *see* Appendix 2). These samples are geochemically distinctive, and have few similarities to the metavolcanic rocks of the BGB.

The feldspar porphyritic rock, sample 267, intrudes the basalt of the SVB (*see* Figure 13) and has a SiO_2 analysis of 58.86 weight %, TiO_2 of 0.35 weight %, Na_2O of 3.85 weight %, and K_2O of 3.85 weight % (*see* Appendix 2). Although classified as a granodiorite in the field, this unit has a geochemistry that is more dioritic in composition. This diorite has Zr/Y and $(La/Yb)_n$ ratios that are much more elevated than the posttectonic diorite, and also higher than the dike samples in the Poplar Point assemblage. The steep slope and negative niobium and tantalum anomalies for this sample, on an extended element diagram (*see* Figure 26), are similar to those present in alkalic rocks, and the sample generally plots within the arc or alkalic range on tectonic discrimination diagrams (e.g., *see* Figure 28). The sample is interpreted to be either an early intrusive associated with the posttectonic intrusive rocks or, due to its alkalic nature, possibly part of a magmatic event related to the initial rifting during formation of the Nipigon Plate.

The felsic dike sampled in the PPA (*see* Figure 14) is massive fine to medium grained with a SiO_2 analysis of 69.10 weight %, TiO_2 of 0.41 weight %, Na_2O of 4.05 weight %, and K_2O of 2.01 weight %, indicating that it is granodoritic in composition (*see* Appendix 2). The granodiorite, sample 387, has Zr/Y and $(La/Yb)_n$ ratios that are higher than the andesite and posttectonic diorite, but not as high as the alkalic diorite dike. This sample has a steep slope toward thorium and negative niobium and tantalum anomalies on an extended element diagram (*see* Figure 26). The sample generally plots within the island-arc fields on tectonic discrimination diagrams, but in the within-plate volcanic zone toward the alkalic end of the range on a modified Th/Yb–Ta/Yb diagram (*see* Figure 28). Two separate phases of felsic dikes within the PPA were noted in the field, but contact relations between the two phases were not observed so that it was unclear if they were separate intrusive events. Sample 387 is geochemically distinct from the felsic metavolcanic feeder dike, which supports an interpretation of 2 intrusive events (e.g., *see* Figures 26 and 27). The more alkalic nature of the second, generally structurally controlled set of dikes, is interpreted to indicate that these dikes are not related to the volcanic event that formed the PPA.

POSTTECTONIC MAFIC INTRUSIVE ROCKS

A number of posttectonic mafic intrusions are located in the metasedimentary and metavolcanic rocks along the contact between the SSB and the CVB (*see* Figures 6 and 14). A sample from the diorite that hosts the Tyson gold and molybdenum showings, located along the northern boundary of the PPA, and a diorite located along the southern contact of the PPA were also analyzed as part of this group of rocks. These rocks form an internally consistent lithogeochemical group that is similar to the metavolcanic rocks of the CVB (*see* Appendix 2). The rocks are massive, fine- to medium-grained gabbro to diorite.

These mafic intrusive rocks are geochemically similar to the intermediate metavolcanic rocks of the CVB, with SiO_2 analyses ranging from 52.46 to 62.50 weight %, TiO_2 from 0.68 to 0.83 weight %, Fe_2O_3 from 6.42 to 10.60 weight %, MgO from 3.36 to 5.99 weight %, and Mg-numbers from 0.46 to 0.54 (*see* Appendix 2). The rocks have been classified as diorite, in part due to field characteristics, and also due to a more andesitic geochemical composition (e.g., *see* Figure 15). The diorite has lower Ti/Zr and higher Zr/Y and $(La/Yb)_n$ ratios that are similar to the andesite of the CVB, and generally characteristic of calc-alkaline rocks (*see* Figures 15 and 16). Two of the three subgroups proposed by Tomlinson (1996) for the andesite, based on $(La/Yb)_n$ ratios of 6.3 and 5.0, appear to be present in the diorite (*see* Figure 16). The dioritic rocks with the highest ratios intrude, or are close to the contact with, the metasedimentary rocks. Positive slopes toward thorium and moderately negative niobium or tantalum anomalies on a mantle-normalized extended element diagram overlap with the values for the andesite (Figure 30), but are quite different than the negative slopes of the gabbro and basalt. The 2 dioritic intrusions in the metasedimentary rocks have higher Th/Yb ratios that may be a result of the assimilation of metasedimentary rocks (Figure 31). The overlap between the diorite and andesite is interpreted to indicate that these 2 rock types formed by similar petrogenetic processes (e.g., *see* Figure 16), but the intrusion of diorite into both metavolcanic rocks and metasedimentary rocks indicate that some of these intrusions are younger.

The inter-element ratios for the diorite are ambiguous, as they were for the andesite, and it is generally difficult to determine the fractionation trends (*see* Appendix 2). The scatter is not as great as that observed in the andesite, and weak analytical trends of decreasing magnesium, nickel, chromium, titanium, scandium and vanadium with increasing zirconium are interpreted to indicate the fractionation of olivine ± chromite, clinopyroxene and magnetite. There is a general lack of europium anomalies, but a weak depletion of Al_2O_3 with increasing zirconium is indicative of a small degree of plagioclase fractionation. The diorite displays many of the geochemical characteristics of the andesite, with fractionation trends that are generally calc-alkaline in nature.

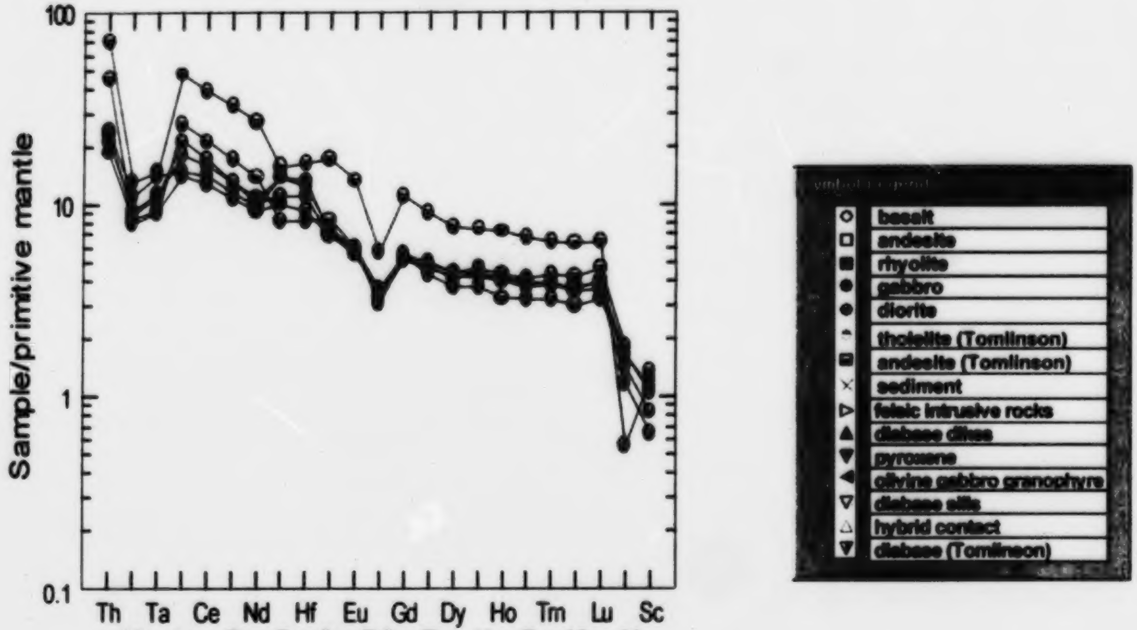

Figure 30. Mantle-normalized extended element diagram of the posttectonic mafic intrusive rocks (*after* Kerrich and Wyman 1997).

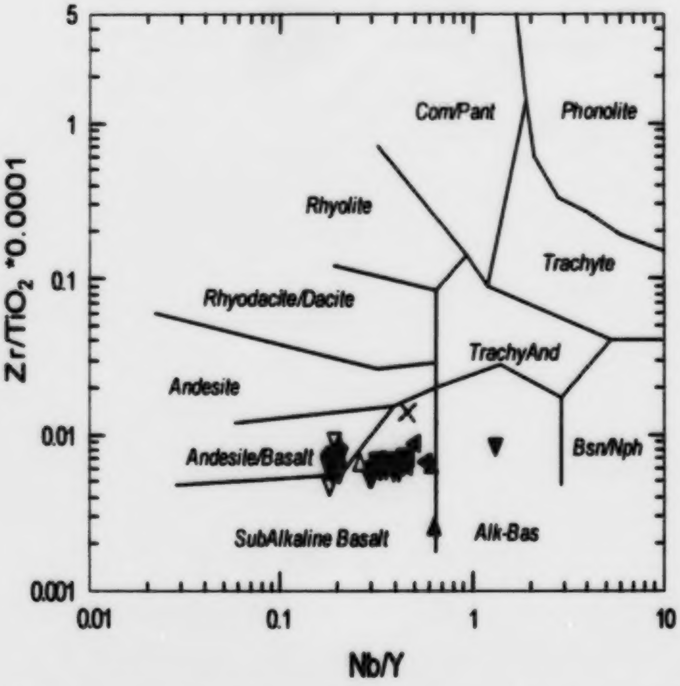

Figure 31. Nb/Y versus Zr/TiO_2 rock classification diagram with the Proterozoic diabase dikes, peridotite, olivine gabbro, and diabase sills (*after* Floyd and Winchester 1978). Legend for symbols, *see* Figure 30. For abbreviations, see Figure 15.

The calc-alkaline characteristics of the diorite, with $(La/Yb)_n$ and Th/Yb ratios greater than 1 and negative tantalum or niobium anomalies on extended element diagrams (*see* Figure 30; e.g., Sun and McDonough 1989), are similar to those of the andesite. These samples plot within the island-arc fields on tectonic discrimination diagrams (e.g., *see* Figure 21), and are interpreted to indicate formation by a similar petrogenetic process as the andesite. The higher $(La/Yb)_n$ and Th/Yb ratios in the diorite intruding or adjacent to the metasedimentary rocks may be the result of assimilation of metasedimentary material (e.g., *see* Figure 30). Contact relationships appear to indicate that these intrusive rocks are younger than the andesite, which is interpreted to indicate that, although the diorite formed in a similar arc environment, they were probably intruded after the tectonic event that resulted in the current subbelt configuration.

PROTEROZOIC MAFIC INTRUSIVE ROCKS

A total of 20 samples of the diabase sills and 18 samples of the ultramafic intrusion were collected during the current mapping program (*see* Appendix 2). Most of the diabase samples are concentrated in 2 rough stratigraphic sections through a sill, completed along Highway 11 and in a ballast quarry next to the CNR line (*see* Figure 13). The remaining samples are scattered through Kitto Township and the western portion of Dorothea Township. The ultramafic samples were collected along 3 traverses across the intrusion, with the remaining samples collected from a number of scattered locations (*see* Figures 13 and 14). Four samples of the north-striking diabase dikes were analyzed for comparison with the Proterozoic diabase sills. These dikes may represent a mixture of older Paleoproterozoic Marathon dike swarm and Mesoproterozoic dikes connected to the diabase sills.

Diabase Dikes

A total of 4 samples of diabase dikes were analyzed for comparison to the diabase sills, and to each other, in an attempt to determine if there is more than 1 generation of dikes in the map area. Three of the samples are from dikes that intrude the metasedimentary rocks, with 2 of the samples (107 and 1008) from the area around Undersill Lake, and the third, sample 1199, immediately adjacent to the ultramafic intrusion in western Kitto Township (*see* Figure 13). The fourth sample (sample 408) is located along the CSB–NVB contact, and is in contact with a posttectonic diorite intrusion. The first 2 samples resemble medium-grained examples of the synvolcanic gabbroic rocks in the field. The third sample is fine to very fine grained and was interpreted to form part of the chill contact of the ultramafic intrusion. The fourth is medium grained and is relatively unmetamorphosed, resembling the diabase that forms the sills. The diabase dikes are equivalent to subalkaline basalt, although 2 of the samples plot near the division between subalkaline and alkaline affinities (*see* Figure 31). Although this classification diagram is not intended for use with intrusive rocks, it is useful for comparing the different lithologies. Silica abundances range from 43.8 to 50.64 weight %, TiO_2 from 1.48 to 3.84 weight %, MgO from 5.78 to 6.39 weight %, and Mg-number from 0.37 to 0.47, which generally overlap with the basalt (*see* Appendix 2). The diabase dikes have analytical trends of low Zr/Y and moderate Ti/Zr and $(La/Yb)_n$ ratios that are more characteristic of tholeiitic rocks than calc-alkaline rocks (Figures 31 and 32). However, the Zr/Y and $(La/Yb)_n$ ratios are slightly higher than the basalts and the diabase sills. Two of the dikes, samples 107 and 408, have Th/Yb ratios greater than one with weak negative niobium and tantalum anomalies on mantle-normalized extended element diagrams (Figure 33), that are similar to the calc-alkaline andesite and diorite of the CVB. Sample 1008 and 1199 have Th/Yb ratios at or less than 1 and lack the negative tantalum and niobium anomalies. Sample 1008 also has the high TiO_2 and the positive vanadium anomaly, indicated on the extended element diagram (*see* Figure 33), which is probably associated with a higher magnetite content (*see* Appendix 2). A number of diabase dikes (dolerite) samples were collected and

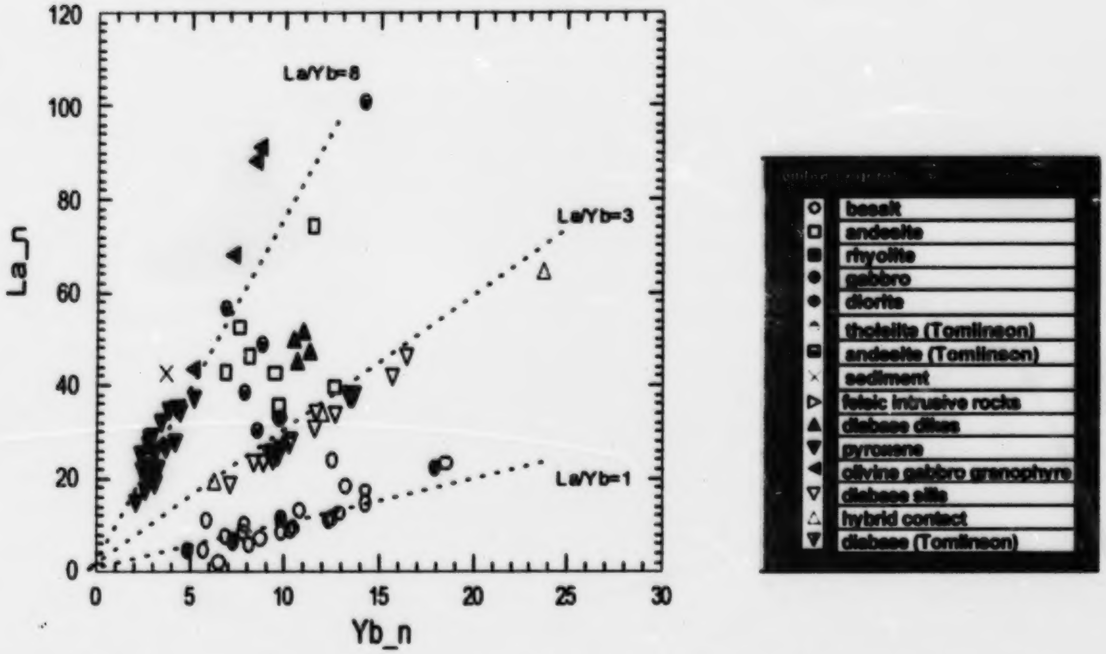

Figure 32. Ytterbium versus lanthanum chondrite-normalized diagram of the Proterozoic diabase dikes, peridotite, olivine gabbro, and diabase sills, overlain on the mafic, intermediate and felsic metavolcanic rocks and associated synvolcanic and posttectonic mafic intrusive rocks for comparison; normalized using the chondrite values of Nakamura (1974).

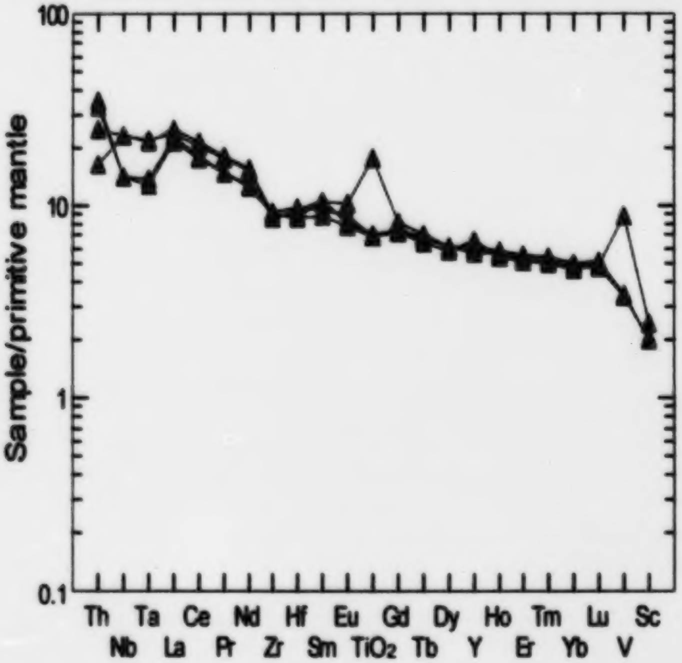

Figure 33. Mantle-normalized extended element diagram of the diabase dike rocks (*after* Kerrich and Wyman 1997). Legend for symbols, *see* Figure 32.

analyzed for major element abundances by Tomlinson (1996). Unfortunately, most of these samples were not analyzed for REE, which is the best means of geochemically separating the diabase dikes from the diabase sills. The Nb/Zr ratios indicate that most of the samples collected by Tomlinson (1996) are from the diabase sills or possibly dikes related to sills (Figure 34). The Nb/Zr ratios also highlight the difference between the 2 groups of dikes represented by samples 107 and 408 and samples 1008 and 1199.

Analytical trends of increasing iron, manganese, titanium, scandium and vanadium and decreasing magnesium, nickel and chromium with increasing zirconium are interpreted to be the result of a lack of magnetite or significant clinopyroxene fractionation and olivine ± chromite fractionation, respectively (*see*Appendix 2). The lack of europium anomalies on a chondrite-normalized REE diagram may suggest that plagioclase was not a major fractionating mineral, however there are insufficient samples to verify this interpretation. The dikes follow analytical trends of decreasing Al_2O_3 with increasing SiO_2, increasing CaO with increasing MgO, and increasing Na_2O with near constant Al_2O_3 (Figures 35, 36 and 37). These trends were attributed by Sutcliffe (1987) to be the result of the crystallization of olivine and plagioclase ± clinopyroxene. The diabase dikes and diabase sills define trends on some diagrams that may be a result of the assimilation of crustal material by an original magma composition represented by the sill (e.g., Figure 38). However, similar trends are present for all elements and are not consistent with the field relationships.

The diabase dikes have some of the trace element characteristics of MORB on tectonic discrimination diagrams (e.g., Figure 39), but are generally located on the boundary between the MORB and calc-alkaline island-arc basalt. The $(La/Yb)_n$ ratios are approximately equal to 5 (*see* Figure 32), with the positive slopes toward thorium and negative niobium and tantalum anomalies on extended element diagrams in accord with an island-arc basalt or arc-tholeiite model (e.g., Sun and McDonough 1989; e.g., *see* Figure 33). The differences in element abundances and ratios indicate that the diabase dikes are unrelated to the diabase sills and the Archean metavolcanic rocks of the BGB.

Ultramafic Intrusive Rocks

The 3 partial traverses across the peridotite located in western Kitto Townships were completed during this project (*see* Figure 13). The 2 traverses close to the shore of Lake Nipigon started within the intrusion and ended near the inner contact. The eastern traverse began in the diabase sill to the east and ended in the olivine granophyre located along the SVB–SSB contact. The peridotite samples are equivalent to subalkaline basalt (*see* Figure 28), or could be classified as komatiite based on the total alkali-silica (TAS) classification (*see* "Rock Type" in Appendix 3). Although these samples could be classified as komatiite or meimechite, which are low $Na_2O + K_2O$ "picritic" compositions using the TAS classification, these rocks are not volcanic in origin and this classification is not used elsewhere in this report. The terminology applicable to plutonic rocks results in these rocks being classified as pyroxene peridotite and subdivided into wehrlite and lherzolite based on the mineralogy (LeMaitre et al. 1989; *see* "Geochemistry: Ultramafic Intrusive Rocks").

PERIDOTITE

The analyses of peridotite show SiO_2 abundances that range from 41.17 to 47.56 weight %, TiO_2 from 0.56 to 1.28 weight %, Al_2O_3 of 2.82 to 7.26 weight %, MgO from 18.25 to 33.46 weight %, and Mg-number of 0.71 to 0.80 indicative of rocks that are much less evolved than any other rock type in the map area (*see* Appendixes 2 and 3). High Ti/Zr, Zr/Y and $(La/Yb)_n$ ratios for the peridotite are interpreted to be the result of depletion of the HREE and elements such as yttrium, scandium and vanadium rather than an enrichment in the high field-strength element (HFSE) common to alkalic rocks (*see* Figures 31 and 32).

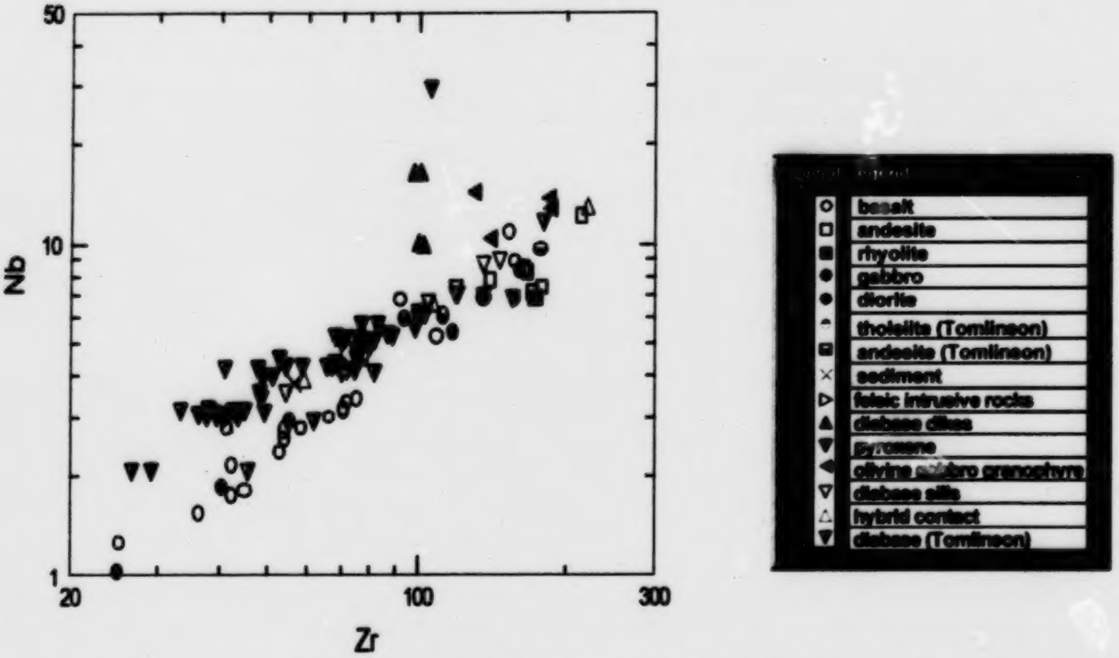

Figure 34. Log zirconium versus log niobium diagram of the Proterozoic diabase dikes, peridotite, olivine gabbro, and diabase sills (this study), with the diabase (dolerite) samples (Tomlinson 1996) overlain on the mafic, intermediate and felsic metavolcanic rocks and associated synvolcanic and posttectonic mafic intrusive rocks (this study) for comparison.

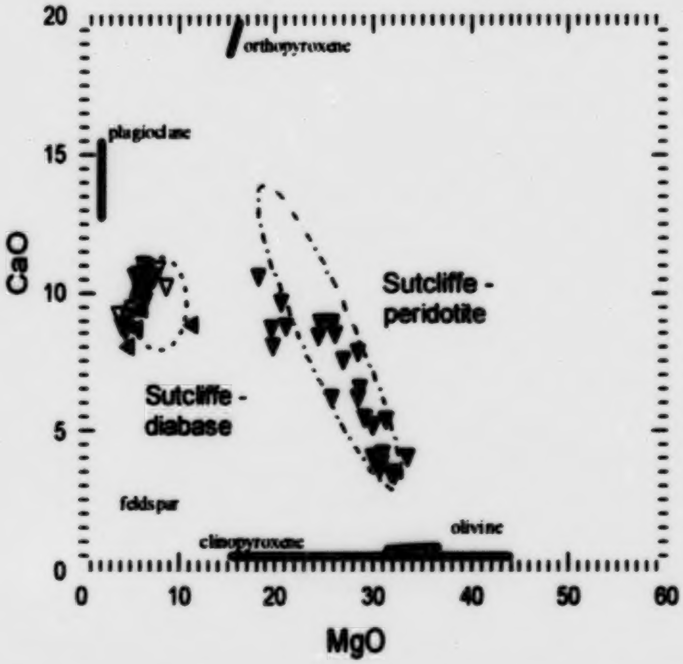

Figure 35. MgO versus CaO (in weight %) of the Proterozoic diabase dikes, peridotite, olivine gabbro, and diabase sills with ideal mineral chemistries, from Deer, Howie and Zussman (1966) and the fields for diabase and peridotite, from Sutcliffe (1986), (*after* Sutcliffe 1987). Legend for symbols, *see* Figure 34.

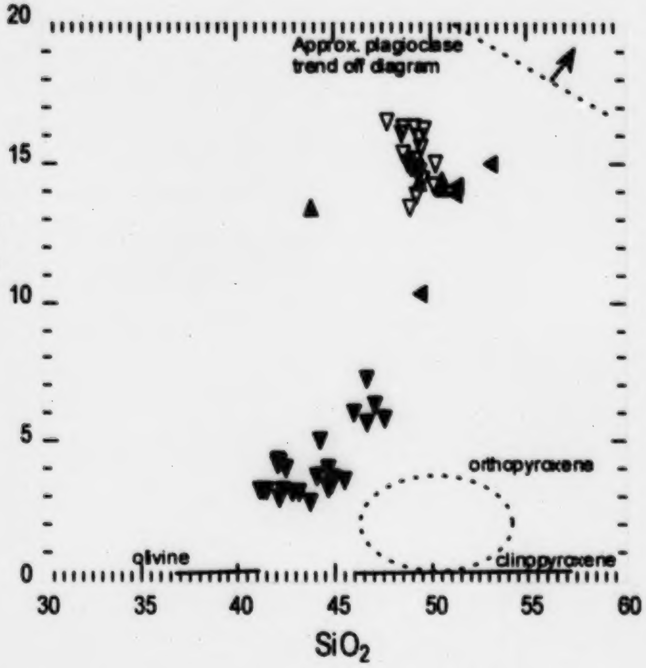

Figure 36. SiO_2 versus Al_2O_3 (in weight %) of the Proterozoic diabase dikes, peridotite, olivine gabbro, and diabase sills with the ideal mineral chemistries, from Deer, Howie and Zussman (1966), (*after* Sutcliffe 1987). Note that the plagioclase compositions plot off the diagram in the direction indicated by the arrow, along the trend shown by the line in the upper right of the figure. Legend for symbols, *see* Figure 34.

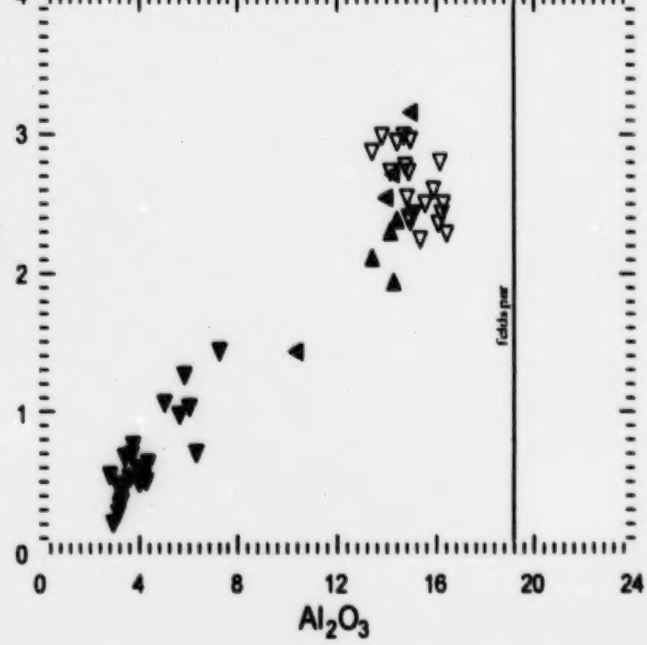

Figure 37. Al_2O_3 versus Na_2O (in weight %) of the Proterozoic diabase dikes, peridotite, olivine gabbro, and diabase sills with the ideal mineral chemistries, from Deer, Howie and Zussman (1966), (*after* Sutcliffe 1987). Legend for symbols, *see* Figure 34.

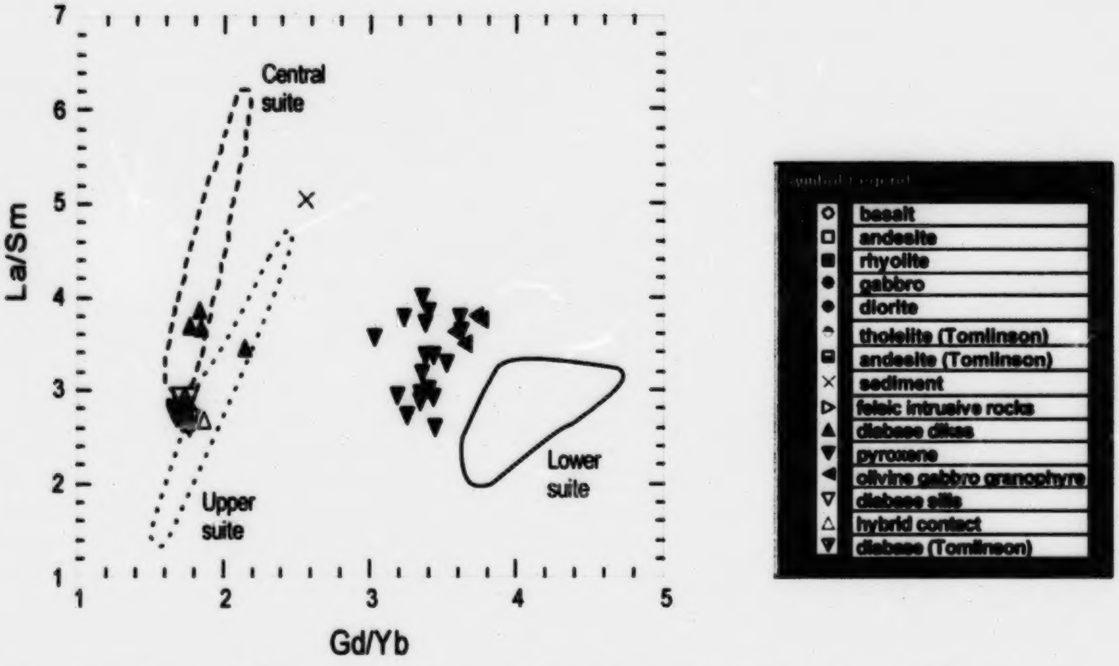

Figure 38. Gd/Yb versus La/Sm diagram of the Proterozoic diabase dikes, peridotite, olivine gabbro, and diabase sills, and a feldspathic wacke of the southern metasedimentary belt (this study) with the fields for the Lower, Central and Upper suite basalts of the Osler Group, from Lightfoot, Sutcliffe and Doherty (1991).

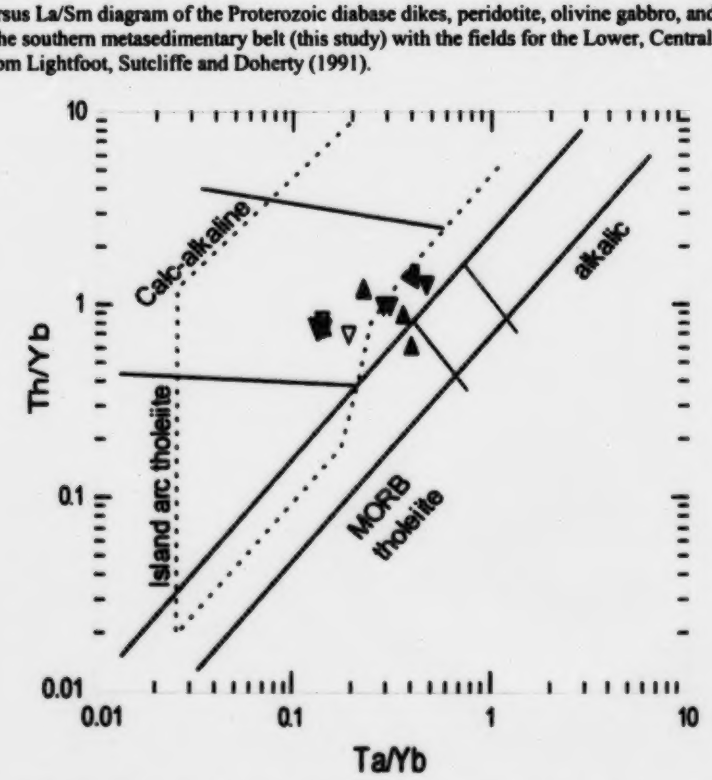

Figure 39. Ta/Yb versus Th/Yb tectonic discrimination diagram of the Proterozoic diabase dikes, peridotite, olivine gabbro, and diabase sills (*after* Pearce 1982). Legend for symbols, *see* Figure 38. Abbreviation: MORB, mid-ocean ridge basalt.

These higher ratios result in positive slopes with weak negative of niobium and tantalum anomalies on mantle-normalized extended element diagrams (Figure 40). Sutcliffe (1986) collected 7 samples collected from the intrusion and have been incorporated into this study. The element abundances and ratios for these samples are generally indistinguishable from the analyses completed during this project, with the exception of some of the HFSE, and these differences are attributed to analytical techniques. The single exception is sample 82RHS-0116, which has lower trace element abundance (e.g., *see* Figure 31).

The petrographic textures were interpreted to indicate that the peridotite is olivine cumulate, and, as such, would be unlikely to represent a primary magmatic composition. The peridotite is composed of primarily olivine-clinopyroxene with lesser orthopyroxene, which is evident from the trend shown in Figure 35. The restricted range for the peridotite in the Na_2O–Al_2O_3 and Al_2O_3–SiO_2 diagrams is indicative of plagioclase being relatively unimportant fractionating mineral, in contrast to the diabase sills (*see* Figures 36 and 37). However, the variation in the Sr/Yb ratios, with little variation in the Gd/Yb ratios, suggests that some plagioclase fractionation did occur (*see* Discussion *in* Lightfoot, Sutcliffe and Doherty 1991). The lack of variation for the peridotite samples on a La/Sm–Gd/Yb diagram indicates that there was probably very little contamination, and that fractional crystallization was a more important magmatic process (*see* Figure 38). Trends for the peridotite on Th/Yb–Th and Th/Yb–Yb diagrams support this interpretation and, as suggested by Lightfoot, Sutcliffe and Doherty (1991), may be the result of garnet fractionation. The moderately high $(La/Yb)_n$ ratios are consistent with the extraction of garnet or pyroxene producing depletion in the HREE. A chill margin was not observed in the map area, and the only peridotite chill composition available is from a dike sample by Sutcliffe (1987). The chill composition from Sutcliffe (1987) has some of the characteristics of the diabase, and may represent the magma composition extracted from the original liquid. Unfortunately, trace element and REE data are not available for the chill sample and the MgO content of the chill sample appears to be too low to represent a parental composition for the Kitto Township peridotite. Crustal contamination was proposed

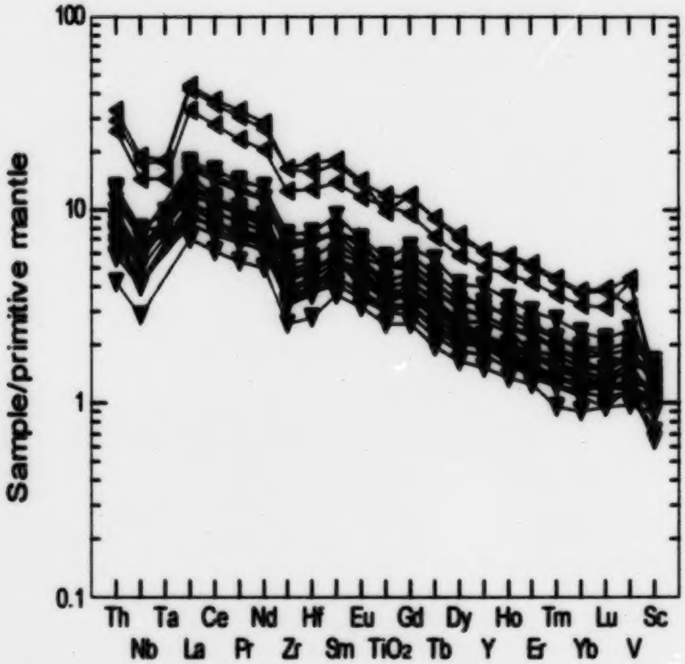

Figure 40. Mantle-normalized extended element diagram of the peridotite and olivine gabbro (*after* Kerrich and Wyman 1997). Legend for symbols, *see* Figure 38.

by Sutcliffe (1987) as one possible explanation for the high K_2O, P_2O_5, and TiO_2 in the peridotite, although this is not evident in the trace element data from the Kitto Township samples. The best approximation of the parental liquid was proposed to be a relatively iron-rich parental magma, enriched in incompatible elements, compared to the diabase source liquid (Sutcliffe 1991).

Comparison of the Kitto Township peridotite with the peridotite intrusions to the south of Lake Nipigon (e.g., Disreali, Leckie–Seagull; Sutcliffe 1986) is difficult due to a lack of trace element and REE analyses. The major element abundances are similar to the Kitto Township peridotite, and result in analytical trends comparable to those discussed below (e.g., *see* Figure 35). There are zirconium and yttrium analyses for a sample from Fox Mountain and Disreali Lake and, on a Zr–Y diagram (Figure 41), these samples plot with much higher yttrium than the Kitto Township peridotite. The yttrium values are probably suspect, as the Kitto Township peridotite analyses by Sutcliffe (1986) also plot with high yttrium values and also do not compare to the analyses from this project. Data filed for assessment credits on the Hele Township peridotite contain REE and trace element data with which to compare the Kitto Township samples (Cunnison and Pyke 2001). The Hele peridotite and olivine gabbro samples have borderline subalkaline basalt compositions similar to the Kitto Township peridotite and fall within the field of the basalt of the Lower Suite of the Osler Group on a La/Sm–Gd–Yb diagram (Figure 42). The analytical trends for the Hele Township samples are comparable to the Kitto Township peridotite and olivine gabbro on an extended element diagram, although shifted to slightly higher concentrations (Figure 43). The main difference between the Hele Township peridotite and the Disreali and Seagull peridotite analyses are slightly higher TiO_2 and $Na_2O + K_2O$ values. These major element differences may be the result of a change in composition progressing toward the south or a separate magma source, but additional work is required to assess the significance of these differences.

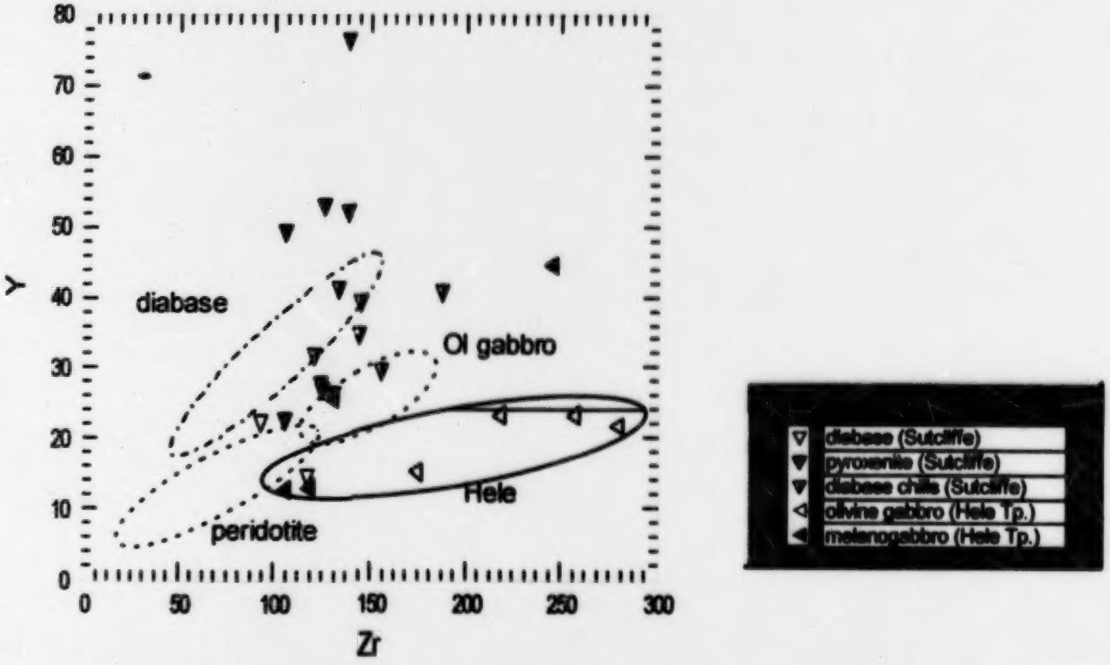

Figure 41. Zirconium versus yttrium diagram of the peridotites from Disreali, Seagull and Fox Mountain and the diabase samples, from Sutcliffe (1986), the samples for the Hele Township melanogabbro and olivine gabbro, from Cunnison and Pyke (2001), and the fields for the Kitto Township diabase, peridotite and olivine gabbro (this study, denoted by dashed lines).

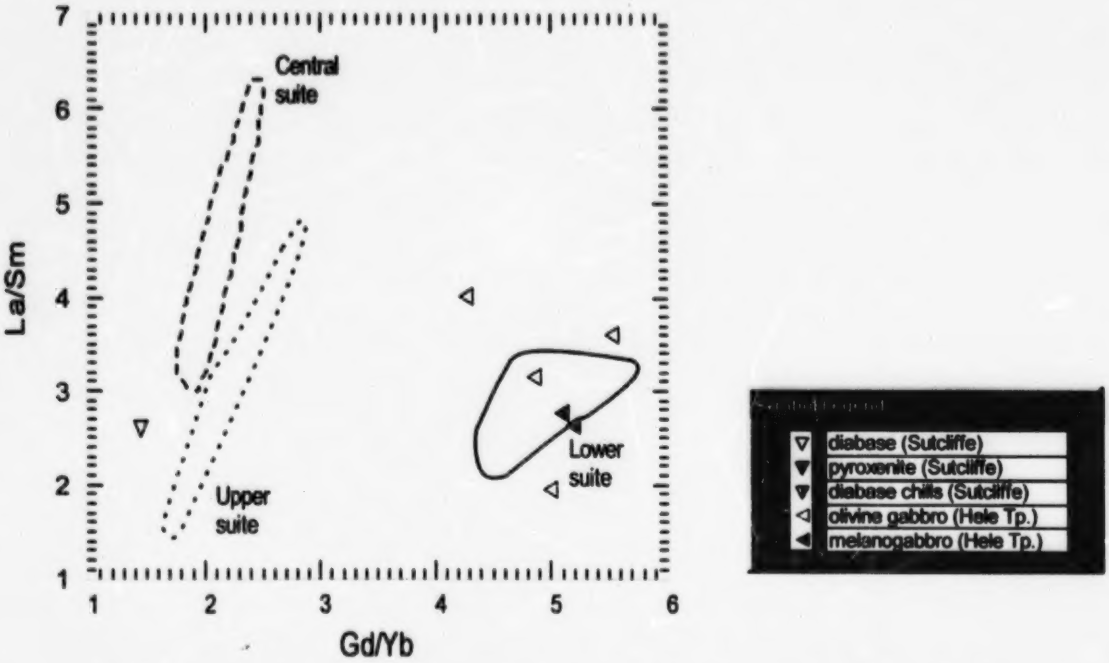

Figure 42. Gd/Yb versus La/Sm diagram of the diabase and Hele Township melanogabbro and olivine gabbro, from Cunnison and Pyke (2001), and the fields for the Lower, Central and Upper suite basalts of the Osler Group, from Lightfoot, Sutcliffe and Doherty (1991).

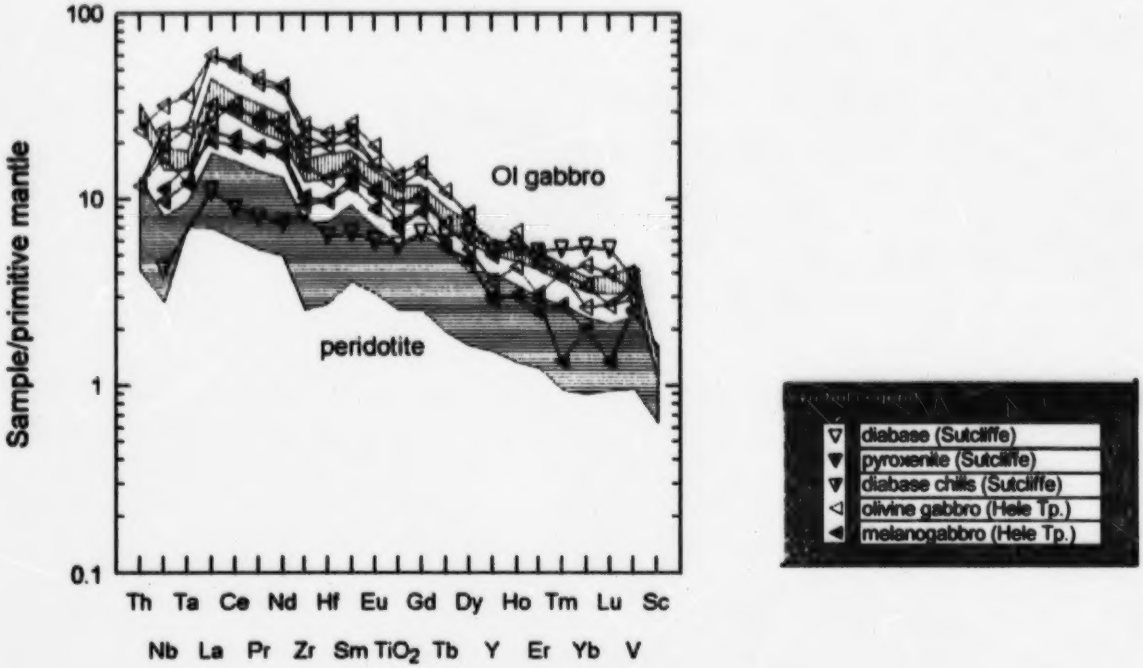

Figure 43. Mantle-normalized extended element diagram of the Hele Township melanogabbro and olivine gabbro with the fields for the Kitto Township peridotite and olivine gabbro (*after* Kerrich and Wyman 1997).

OLIVINE GABBRO

Three samples of the olivine gabbro were analyzed for comparison to the diabase and peridotite samples, and these samples form part of the eastern traverse across the peridotite (*see* Figure 13). The olivine gabbro is equivalent to subalkaline basalt (*see* Figure 31), and would be classified as subalkaline basalt or alkalic basalt based on TAS classification (*see* Appendix 3). These rocks have SiO_2 analyses ranging from 49.41 to 53.10 weight %, TiO_2 from 1.92 to 2.63 weight %, Al_2O_3 of 10.31 to 14.95 weight %, MgO from 4.74 to 11.13 weight %, and Mg-number of 0.39 to 0.58, which are similar to the diabase and tholeiitic basalt (*see*Appendixes 2 and 3). This geochemical similarity is reflected in the field, where olivine gabbro is nearly indistinguishable texturally and mineralogically from the diabase sills. High Zr/Y and $(La/Yb)_n$ ratios for the olivine gabbro are comparable to the peridotite, and are geochemically distinctive compared to the diabase sills and the other units in the map area (e.g., *see* Figure 32). The HFSE and REE abundances in the olivine gabbro are higher than the peridotite, with weak negative of niobium and tantalum anomalies on a mantle-normalized extended element diagram (*see* Figure 40).

The similarities in elemental ratios, but higher abundances for the olivine gabbro compared to the peridotite is interpreted to indicate that the gabbro is the fractionated portion of the intrusions. This interpretation is complicated by the assimilation textures observed along the contact between the gabbro and the country rocks. A single feldspathic wacke, the dominant lithology in the SSB, was analyzed for comparison with the gabbro and diabase (e.g., *see* Figures 32 and 38). The position of the wacke sample on these diagrams is interpreted to indicate that the geochemistry of the gabbro is not primarily the result of the assimilation of the metasedimentary rocks. The olivine gabbro samples plot along a trend similar to that defined by Lightfoot, Sutcliffe and Doherty (1991) based on the removal of fractional crystallization of 60% plagioclase, 30% augite, and 10% olivine (Figure 44). Assuming that crystallization is the dominant process, in Figure 44, the initial liquid composition would be located

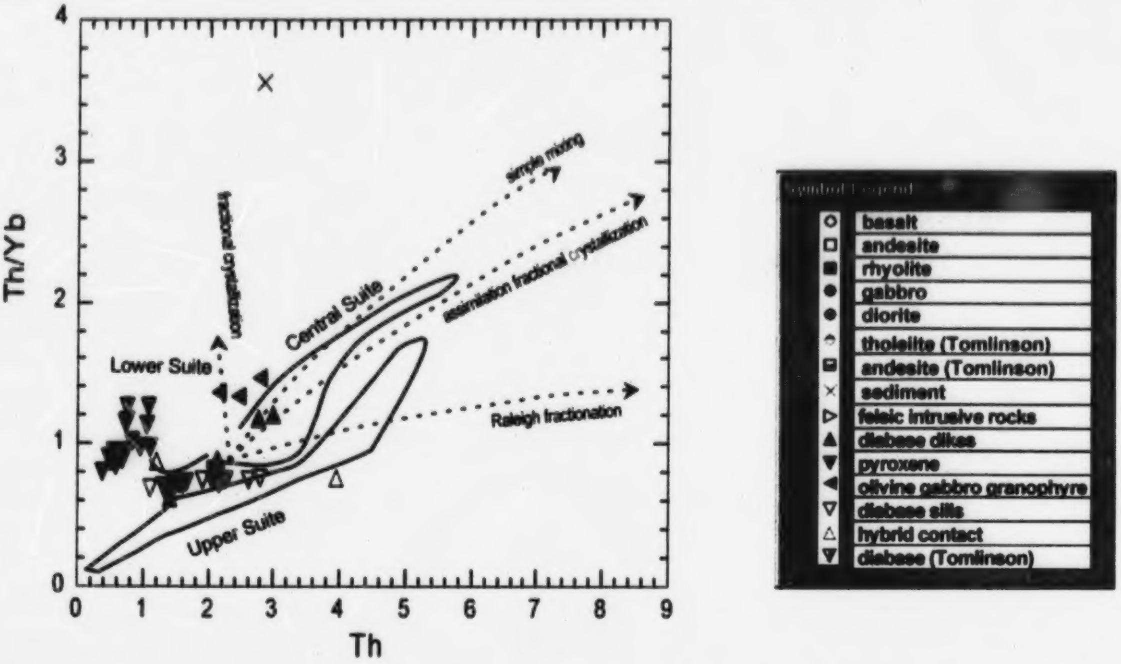

Figure 44. Thorium versus Th/Yb diagram with the Proterozoic diabase dikes, peridotite, olivine gabbro, and diabase sills, and a feldspathic wacke of the southern metasedimentary belt (this study) with the fields for the Lower, Central and Upper suite basalts of the Osler Group and trends for igneous processes, from Lightfoot, Sutcliffe and Doherty (1991).

between the olivine gabbro and peridotite. This assumption would explain the position of the olivine gabbro with the diabase sills on the Al_2O_3–SiO_2 and Na_2O–Al_2O_3 diagrams (*see* Figures 34 and 35), and agree with the variation in the Sr/Yb ratios indicating plagioclase fractionation observed in the peridotite. However, the position of the olivine gabbro with the diabase on the CaO–MgO diagram is difficult to explain by the fractionation of these minerals alone (*see* Figure 35).

A series of diagrams of analyses versus approximate stratigraphic height were plotted to determine if variations in element concentrations could be related to fractional crystallization. The stratigraphic sections through the peridotite are plotted with the samples toward to the outside of the crescent at the bottom, or assuming that the intrusion tops toward the olivine gabbro (Figures 45, 46 and 47; *see* Figure 13 for locations). The sections have slight increases in SiO_2 and TiO_2 values, and decreases in MgO through the peridotite and into the olivine gabbro (*see* Figure 45). A reversal in the analytical trends may occur in the inner samples of the peridotite, but the sample density is not sufficient to fully assess this reversal. The variety of trends in the western section may be due, in part, to a mixing of samples from more than one traverse to construct the stratigraphic section (*see* Figure 13). The element trends in the sections are comparable to the trends resulting from igneous fractionation. An estimate of a parental magma from the stratigraphic section is a magma with approximately 13 weight % MgO, 48 weight % SiO_2, and 1.5 weight % TiO_2. There is no significant variation in the La/Sm or Th/Nb ratios between the peridotite and olivine gabbro as would be expected if the olivine gabbro had assimilated a significant volumes of crustal material (*see* Figures 45 and 46). The significance of the fluctuations observed in some samples, beyond the apparent igneous trend, is not known, but appears to be restricted to the La/Sm ratio (e.g., sample 3002 in Figure 45). A greater sample density is required to properly evaluate these fluctuations and assess the validity of the interpreted igneous fractionation trend. However, the peridotite is interpreted to be an intrusive formed by a single pulse of magma with a base toward the outer edge of the crescent, that underwent fractional crystallization resulting in the formation of the olivine gabbro toward the top.

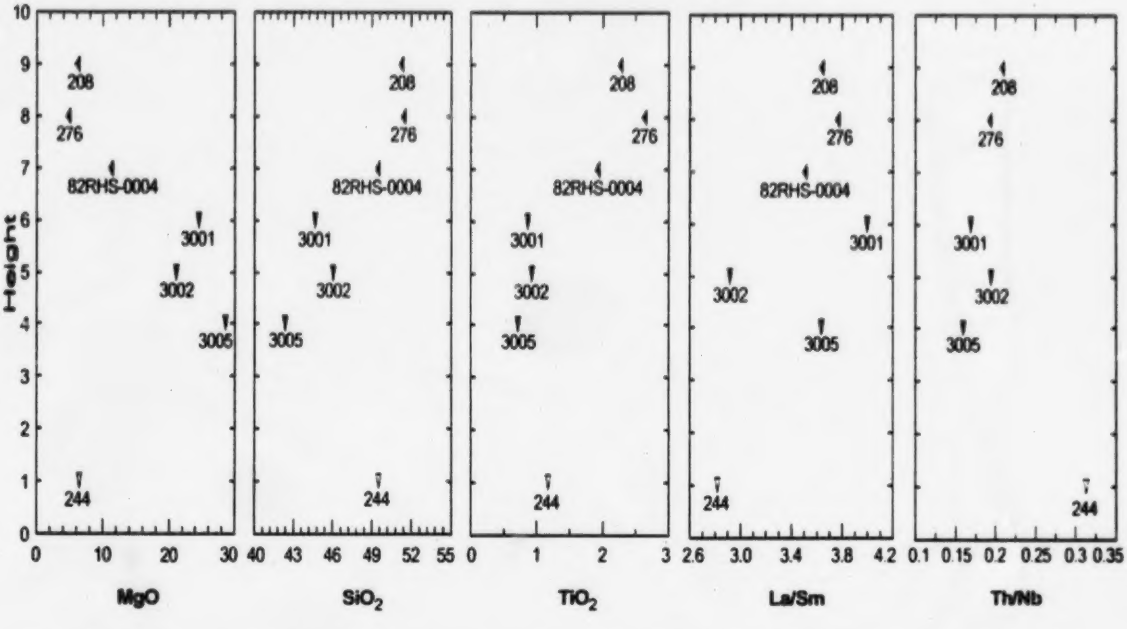

Figure 45. MgO, SiO_2, TiO_2, La/Sm, and Th/Nb versus approximate stratigraphic height for the eastern stratigraphic section through the peridotite and olivine gabbro. Legend for symbols, *see* Figure 44.

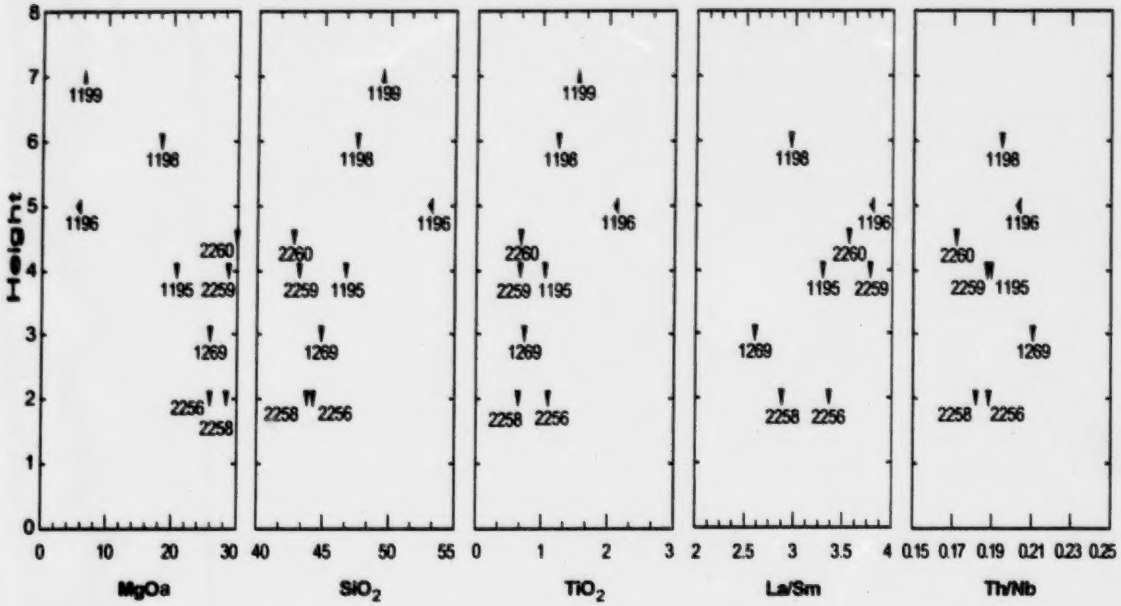

Figure 46. MgO, SiO_2, TiO_2, La/Sm, and Th/Nb versus approximate stratigraphic height for the western stratigraphic section through the peridotite and olivine gabbro. Legend for symbols, *see* Figure 44.

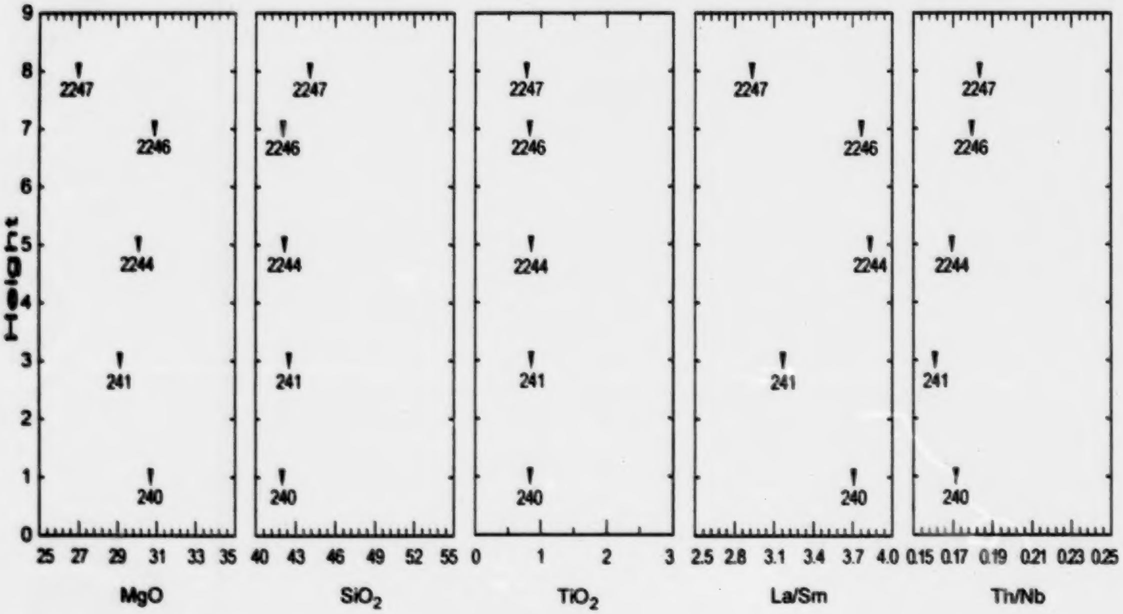

Figure 47. MgO, SiO_2, TiO_2, La/Sm, and Th/Nb versus approximate stratigraphic height for the southern stratigraphic section through the peridotite. Legend for symbols, *see* Figure 44.

Interpretation of a tectonic environment for the peridotite is not possible using the standard tectonic discrimination diagrams as the diagrams were developed for noncumulate rocks. The peridotite is comparable to basalt of the Lower Suite of the Osler Group (Sutcliffe 1987; Lightfoot, Sutcliffe and Doherty 1991), but these rocks are cumulate and are not directly comparable to a volcanic rock (*see* Figure 38). These rocks have higher La/Sm and Gd/Yb ratios than the diabase and are interpreted to be unrelated to the diabase sills, as was proposed by Sutcliffe (1987). Assuming that fractional crystallization is the primary igneous process, then the variation in the peridotite was used to estimate an initial magma composition. Based on the geochemical variation in the stratigraphic sections (*see* Figures 45, 46 and 47), the eruptive equivalents of the peridotite would be basalt similar in composition to the olivine gabbro and the Lower Suite of the Osler Group (*see* Figure 38). However, there are a large number of factors and the exact resultant volcanic composition is not known. There is no calc-alkaline, higher $(La/Yb)_n$ ratio basalt of appropriate age in the Lake Nipigon area that would correspond to the olivine gabbro compositions. A high degree of partial melt of an enriched upper mantle source material, possibly the plume component of a mantle diapir, was proposed for the formation of the Lower Suite volcanic rocks (Lightfoot, Sutcliffe and Doherty 1991) and is a good first approximation for the mechanism forming the peridotite.

Mafic Intrusive Rocks

DIABASE SILLS

The diabase sills define a relatively geochemically cohesive group that have the characteristics of subalkaline basalts, with analytical trends that indicate of a lack of magnetite crystallization (*see* Figures 31 and 32). The sills have SiO_2 values that range from 47.76 to 50.25 weight %, TiO_2 from 0.67 to 2.46 weight %, MgO from 3.90 to 8.71 weight %, and Mg-number from 0.31 to 0.63 that generally overlap with the diabase dikes and Archean basalts (*see* Appendix 2). Although, the diabase samples commonly contain olivine in thin section, the samples are generally quartz normative (*see* Appendix 3). The sills have analytical trends of low Zr/Y and moderate Ti/Zr and $(La/Yb)_n$ ratios that are more characteristic of tholeiitic rocks than calc-alkaline rocks (*see* Figures 31 and 32). However, the Zr/Y and $(La/Yb)_n$ ratios are slightly higher than the basalts, with positive slopes toward thorium with weak negative niobium and tantalum anomalies on mantle-normalized extended element diagrams (Figure 48). Although there are some similarities with both the tholeiitic basalt and calc-alkaline andesite, the diabase sills compositions most consistently overlap with some of the tholeiitic basalt subsets of the CVB.

The 2 approximate stratigraphic sections through a sill are from a series of rockcuts along Highway 11 and in a quarry situated on the same sill in eastern Kitto Township (Figures 49 and 50; *see* Figure 13 for sample locations). In the highway section, a chill contact was not observed and the diabase varies from a medium-grained base through a very coarse-grained core to a medium-grained upper portion. The variation in MgO, SiO_2, and Mg-numbers are interpreted to be the result of the fractionation of 2 separate magmas with the break between the magmas occurring around sample 56, which is also from approximately the middle of the traverse (*see* Figure 49). Samples 53, 57a, and 57b have high TiO_2 and Fe_2O_3 values indicative of a higher magnetite content, but samples 51b and 53 are magnetite porphyritic in outcrop (*see* Figure 49). Sample 57b has granophyric textures in thin section and is one of the more evolved diabase samples in this section, and is interpreted to be located toward the top of the lower pulse of magma. Although the contacts were not observed, the La/Sm ratios may provide an indication of assimilation of crustal material, but there is little variation in the ratios suggesting that assimilation was not a major process (*see* Figure 49). The quarry section is a composite, or two-part, section through the same sill as the highway traverse (*see* Figure 13). The 3 stratigraphically lower samples were collected from the CNR rockcut and include a basal chill margin; the 3 stratigraphically higher samples are from the CNR ballast quarry approximately 450 m to the south. The lower 3 samples were collected across approximately 2 m starting at the chill margin. These samples display little variation in MgO, SiO_2, TiO_2, or Mg-number, and are roughly comparable to the higher MgO samples in the highway section (*see* Figure 50). There is a break in the section between the lower and upper portions interpreted to indicate 2 separate magmas, as in the highway section. The La/Sm ratios of the lower samples are slightly higher than the other samples in either of the sections and may be the result of assimilation of country rock. However, unless another lithology was originally present, the underlying rocks are tholeiitic basalt of the SVB, which, if assimilated, would not have changed the La/Sm ratios of the diabase. The lack of variation in the Th/Nb ratios suggests that these lower 3 samples did not assimilate crustal material, or at least crustal material with higher thorium than the diabase. These stratigraphic sections indicate that the sills do not represent a single cooling unit, and were formed by multiple pulses of magma, as was also noted by Sutcliffe (1987) in the other Proterozoic sills of the Lake Nipigon area.

The diabase sills samples from this project are quite similar geochemically to the diabase samples collected from the Lake Nipigon area by Sutcliffe (1986). A chill sample from the Kopka cone sheet, northwest of Lake Nipigon, and a chill sample from Vint Bay have trends on an extended element diagram comparable to the Phoenix Project diabase samples (Figure 51). The major element abundances are similar to the Phoenix Project diabase, and result in trends comparable to those discussed below (e.g., *see* Figure 35). The minor differences between the samples from this project and those analyzed by Sutcliffe (1986, 1987) may be a result of differences in analytical techniques. The diabase chill samples, collected from different areas by Sutcliffe (1986), are geochemically distinct (e.g., *see* Figure 51). The difference in the chill compositions may reflect differences in magma composition across the Lake Nipigon area, possibly related to the sills being formed by multiple pulses of magma rather than the fractionation of a single pulse.

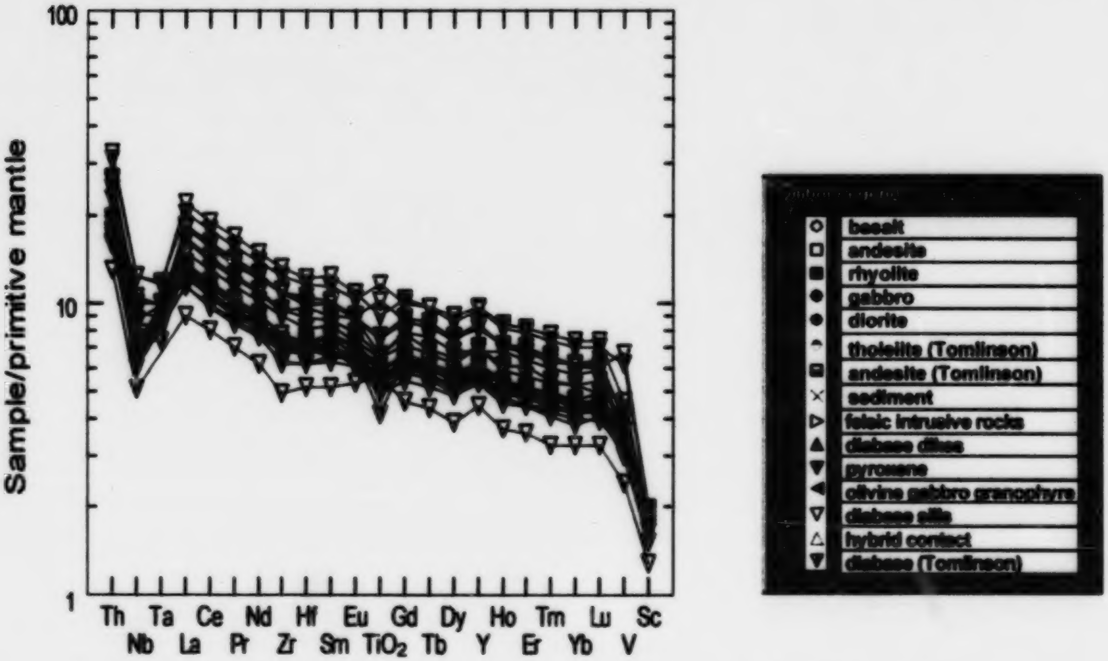

Figure 48. Mantle-normalized extended element diagram of the diabase sills (*after* Kerrich and Wyman 1997).

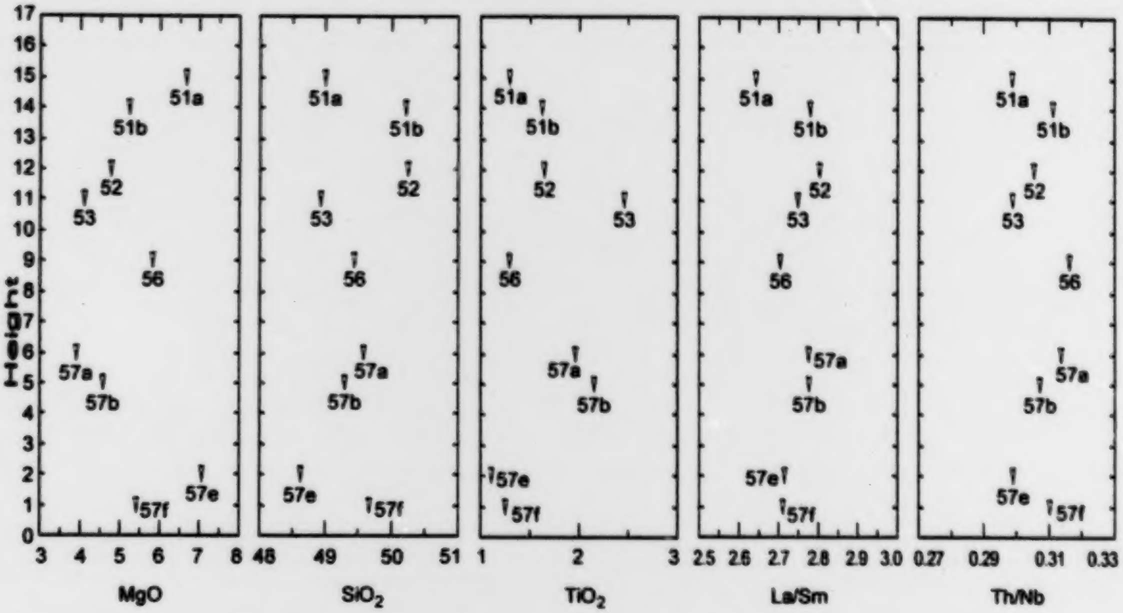

Figure 49. MgO, SiO$_2$, TiO$_2$, La/Sm, and Th/Nb versus approximate stratigraphic height for the highway stratigraphic section through the diabase sill. Legend for symbols, *see* Figure 48.

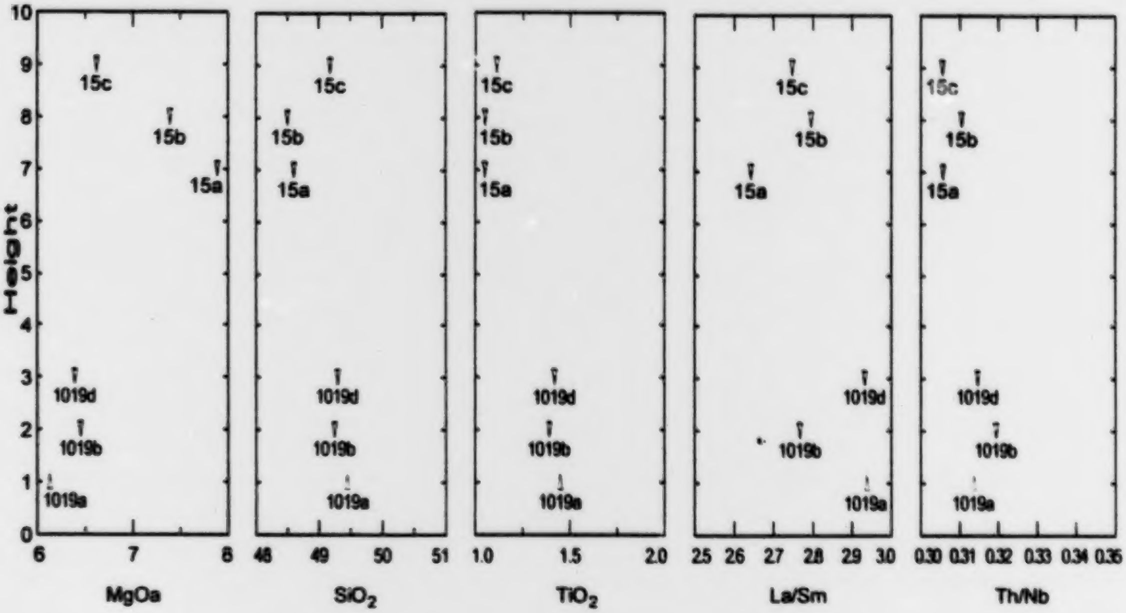

Figure 50. MgO, SiO$_2$, TiO$_2$, La/Sm, and Th/Nb versus approximate stratigraphic height for the quarry stratigraphic section through the diabase sill. Legend for symbols, *see* Figure 48.

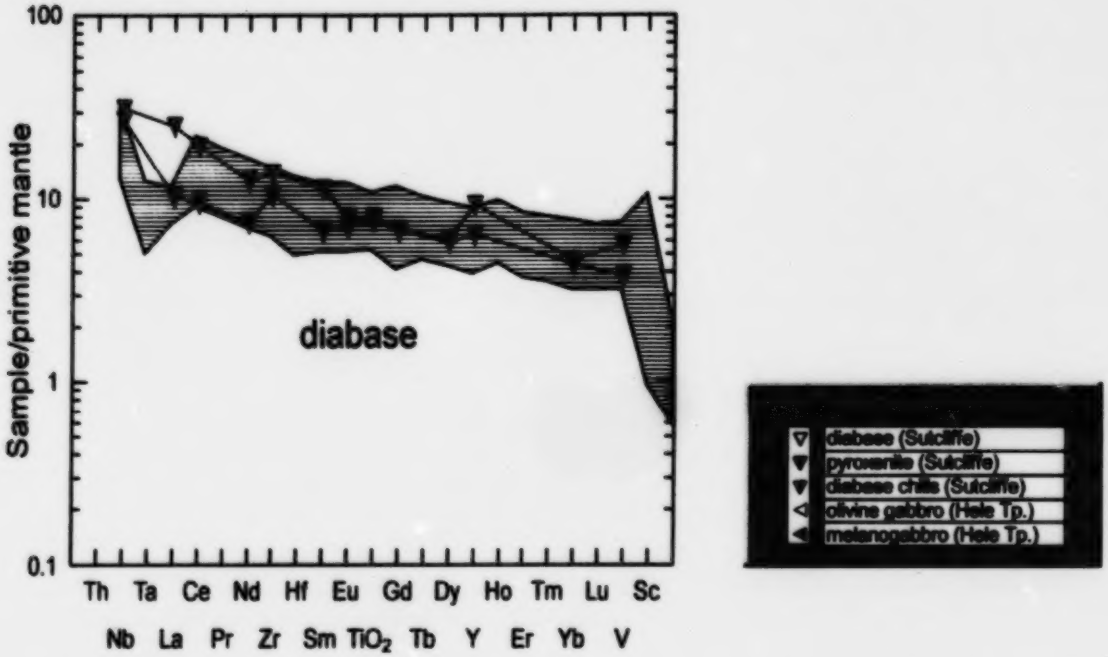

Figure 51. Mantle-normalized extended element diagram of the diabase sills chill samples from Sutcliffe (1986) (*after* Kerrich and Wyman 1997).

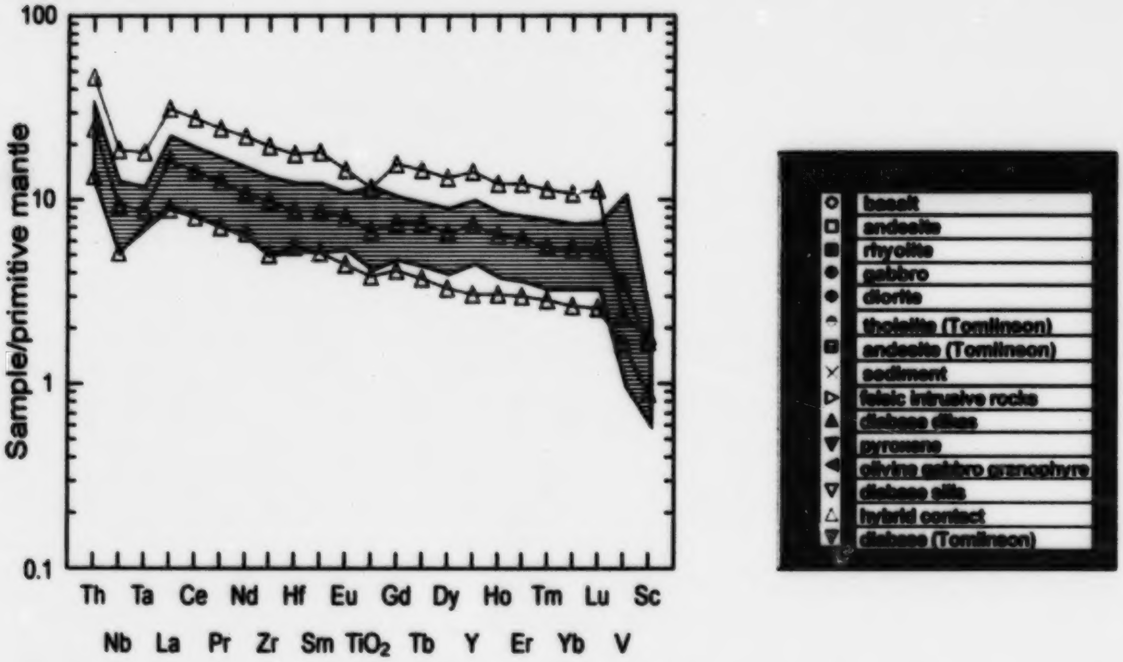

Figure 52. Mantle-normalized extended element diagram of the diabase sills chill samples from Sutcliffe (1986) (*after* Kerrich and Wyman 1997).

Two samples of chill diabase and a sample of fine-grained diabase with flow foliation textures were collected in the map area. These samples have elemental ratios that are generally comparable to the other diabase (e.g., *see* Figure 32), but the elemental abundances range from the lowest to the highest of all of the diabase samples (e.g., Figure 52). The chill sample forming part of the quarry stratigraphic section (*see* Figure 49: sample 1019a) has elemental abundances that are generally indistinguishable from the other diabase samples (e.g., *see* Figure 32). The other chill sample, sample 347, is from along the southern contact of the peridotite (*see* Figure 13). This sample is very fine grained, and was originally mapped as a peridotite. This sample has a Zr/Y ratio and MgO content comparable to the peridotite, but has a $(La/Yb)_n$ ratio comparable to the diabase (e.g., *see* Figure 32), and is interpreted to be a hybrid diabase that has assimilated a minor amount of peridotite resulting in the mixture of geochemical characteristics. A mineralized sample collected from the same locations contains trace to 1%, very fine-grained, disseminated sulphide and has anomalous platinum group elements (*see* "Mineralization"). Sample 139 is flow foliated with aligned fine-grained plagioclase laths, and is from near the lower contact of a sill intruding the metasedimentary rocks of the SSB (*see* Figure 13). This sample has high elemental abundances that could be interpreted to be the result of extreme fractional crystallization (e.g., *see* Figure 32). Alternatively, assimilation of crustal material is possible, but is considered to be less likely or a minor process as this sample has element ratios comparable to the other diabase samples (e.g., *see* Figure 32). The variations in the chill sample compositions for this project, and the previous work by Sutcliffe (1986, 1987) is interpreted to be a result of a combination of minor variations in the compositions of the different pulses of magma, and assimilation of minor amounts of country rock. This would mean that a chill sample is only applicable as an indication of the parental melt compositions for the igneous modelling purposes of the samples collected in the same portion of a the same sill and, therefore, formed from the same pulse of magma.

The parental magma for the diabase sills was interpreted, by Sutcliffe (1987), to be a fractionated liquid due to the low Mg-numbers common to the diabase. The element trends observed in the samples from this project follow analytical trends of decreasing Al_2O_3 with increasing SiO_2, increasing CaO with increasing MgO, and increasing Na_2O with near constant Al_2O_3 (*see* Figures 35, 36 and 37). These trends were attributed by Sutcliffe (1987) to be the result of the crystallization of olivine and plagioclase ± clinopyroxene. The fractionation of these minerals, with the addition of magnetite, would explain the geochemical variation observed in the stratigraphic sections. The scandium depletion on the extended element diagram (*see* Figure 48) is interpreted be the result of clinopyroxene being a residual mineral during the partial-melting event that formed these rocks (e.g., Hofmann 1988).

The trace element abundances of the diabase sills display a mixture of MORB and calc-alkaline basalt characteristics on tectonic discrimination diagrams (e.g., *see* Figure 39). The $(La/Yb)_n$ ratios are greater than 1, with positive slopes toward thorium and negative niobium and tantalum anomalies on extended element diagrams indicative of island-arc basalt or arc tholeiite (e.g., Pearce 1982; Sun and McDonough 1989; e.g., *see* Figure 48). The diabase sills are similar geochemically to the basalt flows of the Upper Suite of the Osler Group located to the south (*see* Figure 38), as was noted by Sutcliffe (1987). There is the possibility that the sills represent a part of the magma feeder system that erupted the volcanic rocks to the south. Alternatively, these sills may have been part of a feeder system for overlying flows that have been subsequently eroded, exposing the sills.

Geochronology

Samples collected from a massive felsic flow from the CVB and a feldspar-quartz porphyritic felsic feeder dike from the PPA during the 2001 field mapping season were submitted for U/Pb zircon age determinations (Figure 53). The samples are described in greater detail above (*see* "General Geology: Intermediate to Felsic Metavolcanic Rocks"). The flow is a pink massive aphanitic rock with minor carbonate alteration and trace, disseminated sulphide. Thin section analysis indicates that the rock consists of a fine-grained quartz and feldspar matrix with a few rare feldspar phenocrysts and clusters of feldspar phenocrysts that are moderately to well sericitized. The synvolcanic dike is grey, massive and quartz-feldspar porphyritic with peperitic textures along the contact with the tuff breccia. In thin section, this rock consists of coarse-grained phenocrysts of plagioclase and subrounded quartz in fine-grained quartz, plagioclase and sericite altered groundmass. Approximately 2% of the plagioclase phenocrysts tend to be broken and have chlorite alteration along the edges. The quartz grains have conchoidal fractures and discrete reaction rims.

The sample from the flow, 225, yielded a relatively abundant population of small, colourless to light yellow, euhedral to subhedral zircon prisms ranging from greater than 3:1 euhedral broken long prisms to 2:1 subhedral prisms typically with cracks and fluid inclusions. Four fractions were analyzed. Two of these are concordant and provide a weighted ^{207}Pb/^{206}Pb age of 2724.9 ± 1.1 Ma (Figure 54 (upper)). The remaining analyses are up to 2.9% discordant, and one of these has a large uncertainty in U/Pb age due to imprecise ^{238}U/^{235}U data. The four analyses define a discordia line with upper and lower intercept ages of 2724.6 ± 1.1 Ma and 42 +195/–180 Ma, respectively, suggesting recent lead loss (*see* Figure 54). Due to the concordance of fractions Z2 and Z4, the weighted mean ^{207}Pb/^{206}Pb age of these fractions is preferred. This is interpreted as the primary crystallization age of the volcanic unit (J. Ketchum, Royal Ontario Museum, written communication, 2002).

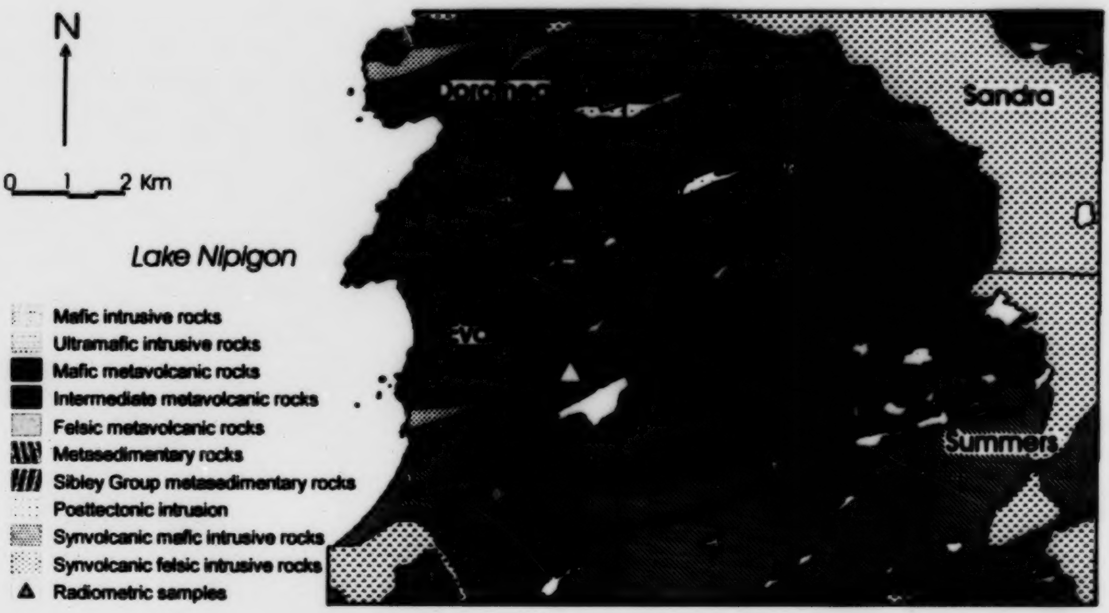
N
0 1 2 Km
Lake Nipigon
Sandra
Summers
Mafic intrusive rocks
Ultramafic intrusive rocks
Mafic metavolcanic rocks
Intermediate metavolcanic rocks
Felsic metavolcanic rocks
Metasedimentary rocks
Sibley Group metasedimentary rocks
Posttectonic intrusion
Synvolcanic mafic intrusive rocks
Synvolcanic felsic intrusive rocks
▲ Radiometric samples

Figure 53. Location map of samples collected for radiometric age determinations.

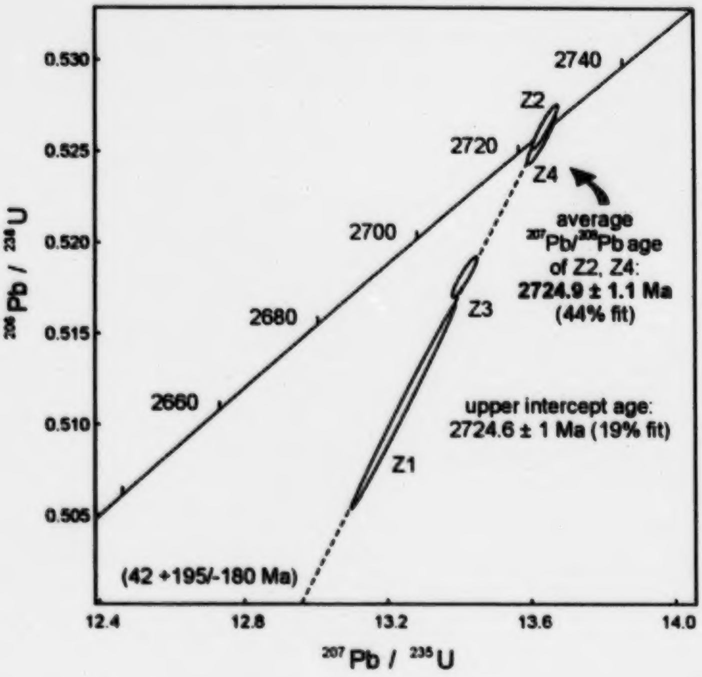

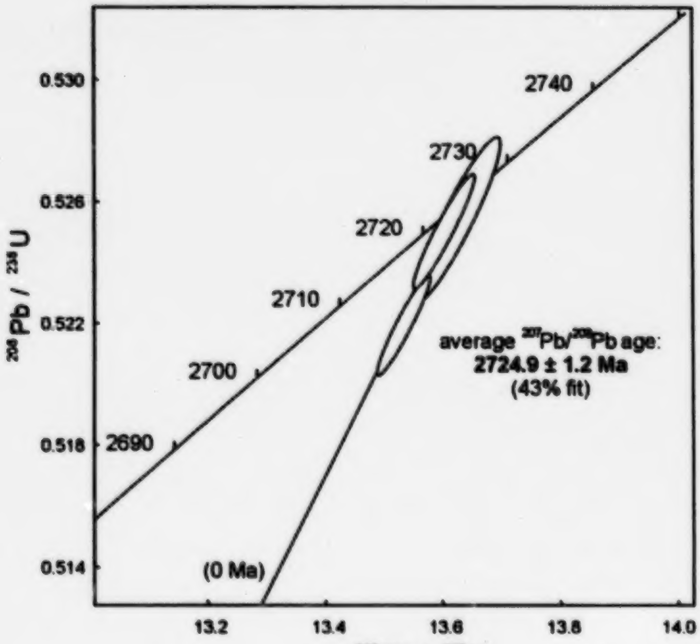

Figure 54. ^{207}Pb/^{235}U versus ^{206}Pb/^{238}U isochrons for sample 225 (upper) and for sample 229 (lower).

The felsic dike, sample 229, yielded abundant colourless, small to large, subhedral to anhedral, equant to 2:1 zircon prisms, many with cracks and inclusions. There is no obvious evidence of inherited grains or cores, and a single zircon population appears likely. Grains selected for abrasion and analysis were larger subhedral 2:1 prisms and prism fragments that, although of the best quality available, contained cracks and fluid inclusions. Three fractions were analyzed. Two of the analyses are concordant within uncertainty; the third is 0.8% discordant. The analyzed fractions are clearly all the same age and provide a weighted mean $^{207}Pb/^{206}Pb$ age of 2724.9±1.2 Ma (Figure 54 (lower)). This is interpreted as the primary age of the felsic dike (J. Ketchum, Royal Ontario Museum, written communication, 2002).

The felsic dike is likely to be a feldspar-quartz porphyritic feeder dike that intruded a wet, unconsolidated tuff breccia of the Poplar Point assemblage. If this interpretation is correct, then the age of the dike should closely approximate the eruption age. If not, then 2725 Ma must be interpreted as a minimum age for the tuff breccia.

A number of lithologies relevant to the Proterozoic igneous activity from around Lake Nipigon and the northern part of Lake Superior have radiometric age determinations. Two samples from diabase sills from different parts of Lake Nipigon have ages of 1108.8 +4/–2 Ma, and these sills are interpreted to be related to the Nipigon diabase sills on the east side of Lake Nipigon (Davis and Sutcliffe 1985). The sills intrude Sibley Group sedimentary rocks that have an Rb/Sr age of 1340±33 Ma (Wanless and Loveridge 1978). A quartz-feldspar porphyritic rhyolite near the base of the Osler Group has an age of 1107 +4/–2 Ma (Davis and Sutcliffe 1985) and a rhyolite flow near the top of the Osler Group has an age of 1097±3.7 Ma (Davis and Sutcliffe 1985).

A number of detrital ages for the southern, central and northern metasedimentary subbelts (SSB, CSB and NSB) and Max Creek conglomerate west of Lake Nipigon were supplied by D.W. Davis (Jack Satterly Laboratory, Royal Ontario Museum, personal communication, 2002). A conglomerate from the CSB gave the widest range of U/Pb detrital zircon ages with a maximum of 2922 Ma and a minimum of 2696±2 Ma. A conglomerate sample from the NSB had a maximum U/Pb detrital zircon age of 2890 Ma and a minimum of 2710±3 Ma, while a sandstone from the SSB gave a range of 2828 Ma to 2703±4 Ma. These results imply that sedimentation must have extended to younger then 2696 Ma and that a stable platform available for erosion of rocks at least 2922 Ma old had been exposed in the area. These ages are comparable to age determinations from the west side of Lake Nipigon, where the Max Creek conglomerate gave detrital zircon ages from 2927 Ma to 2696±1 Ma. A U/Pb detrital zircon age as young as 2687 Ma was reported by Percival and Sullivan (1988).

Economic Geology

Mineralization within the Beardmore–Geraldton Belt is generally associated with foliation-parallel carbonatized, brittle-ductile shear zones quartz-carbonate veining. Locally in the southern metavolcanic subbelt (SVB), mineralization is often associated with banded iron formations. Mineralization in the remainder of the map area is minor and generally restricted to disseminated pyrite and minor pyrrhotite and chalcopyrite within both metavolcanic and metasedimentary rocks associated with intrusive rocks. Past prospecting in the area has led to the development of 3 major gold mines, the Leitch, the Sand River and the Northern Empire mines, and numerous occurrences, including 1 historic molybdenum-gold showing (*see* Figure 5: Tyson property) and 1 new gold showing (*see* Figure 4: Coté–Archie Lake property). Sampling during this mapping program discovered a new platinum group element occurrence associated with the peridotite intrusion in southern Kitto Township (*see* Figure 3).

GOLD

Gold production in the Beardmore area totalled greater than one million ounces, with the Leitch gold mine producing 847 690 ounces of gold at a grade of 0.92 ounce of gold per ton, the Sand River gold mine producing 50 065 ounces gold at a grade of 0.32 ounce of gold per ton, and the Northern Empire Mine producing 149 493 ounces gold at a grade of 0.35 ounce of gold per ton (Mason and White 1986; *see* Figures 4 and 5 for locations). Gold mineralization in these mines and the showings in the map area is generally associated with brittle-ductile quartz-carbonate veins. The Leitch and Sand River gold mines are crackseal-textured quartz veins with varied amounts of pyrite, arsenopyrite, chalcopyrite and tetrahedrite, and septa of sericitic and carbonatized wall rocks. The veins are hosted by dilatant zones in a foliation-parallel orientation within the metasedimentary rocks of the southern metasedimentary subbelt (SSB), and these structures have been interpreted by Shanks (1993) to be related to shearing either along the limbs of the regional Z-fold or a transpression zone related to the SSB–CVB contact. The Northern Empire Mine is hosted by a series of *en échelon* quartz veins containing differing amounts of pyrite, arsenopyrite, pyrrhotite and chalcopyrite hosted by carbonatized, sheared metavolcanic rocks and interflow iron formation of the SVB near the Empire fault and the SVB–SSB contact. The quartz veining occurs in brittle features of the deformed iron formation. Gold mineralization occurs in other brittlely deformed interflow iron formations of the SVB, hosted by early quartz stringers containing arsenopyrite, pyrite, pyrrhotite and chalcopyrite.

The quartz veins present within metavolcanic and metasedimentary rocks throughout the belt generally consist of foliation-parallel fracture fillings, extensional arrays, or veinlet fillings. The veins sampled during this project range from less than a centimetre to a few tens of centimetres in width and, locally, can by traced along strike for up to 20 m. These veins contain varied amounts of carbonate (ankerite and calcite), chlorite, and/or black tourmaline with sulphide mineral contents that vary from trace to 1% fine-grained disseminated pyrite. Wall-rock alteration is not common or consists of a weak carbonate and chlorite alteration, and the chloritic shear that bounds some veins contain 5 to 10%, fine- to medium-grained, disseminated cubic pyrite. Few of the veins that were sampled during this project contained arsenopyrite, with the exception of known gold showings, such as the veins north of the Sand River Mine, the Buffalo–Beardmore occurrence and the Archie Lake gold occurrence in Summers Township (*see* Figure 4). With the exception of previously discovered gold occurrences (*see* "Mineral Occurrences"), all the vein samples collected during this project yielded less than 1 g/t gold (Appendix 4).

Intensely carbonate-altered and variably sheared mafic and intermediate metavolcanic rocks in the central metavolcanic subbelt (CVB) and Poplar Point assemblage (PPA) are generally associated with faulting. Multiple zones of intense shearing, 6 to 8 m wide, oriented subparallel to the Sandy Creek fault occur in the area north and east of Eva Lake (*see* Figure 4). These shear zones are intensely carbonatized, with a mixture of calcite and ankerite, and contain fine, less than 0.5 cm wide veinlets of foliation-parallel quartz or carbonate. Locally, the shear zones contain greater than 5% disseminated sulphide minerals. The Archie Lake is quartz hosted, but occurs in moderately carbonatized and sheared andesite of the CVB. Along the southern side of the PPA, a zone of moderate to intense carbonate alteration is weakly sheared. Quartz veining and sulphide mineralization is uncommon (*see* Figure 5). With the exception of previously discovered gold occurrences (*see* "Mineral Occurrences"), all gold values were less than 1 g/t for veins and wall rock sampled during this project (*see* Appendix 4).

Quartz veins within the diabase intrusions and associated dikes generally consist of very weak to weak fracture fillings. They range in size from 0.3 to 3 cm in width, and are rarely traceable for more then a couple of metres. Most are associated with epidote, hornblende-albite and chlorite veins, and generally do not contain sulphide minerals. No samples were assayed from this material.

SULPHIDE MINERALIZATION

Base Metals

No significant amounts of base metal sulphide mineralization were observed in the BGB, although numerous small occurrences are present throughout all 3 of the metavolcanic subbelts. Notable locations are within the mafic metavolcanic rocks (SVB) along the lakeshore in Kitto Township (Figure 55), the intermediate metavolcanic rocks (CVB) along both Highway 580 and the 72 Road (Figure 56), and the intermediate metavolcanic rocks (NVB) of the Poplar Point assemblage (Figure 57).

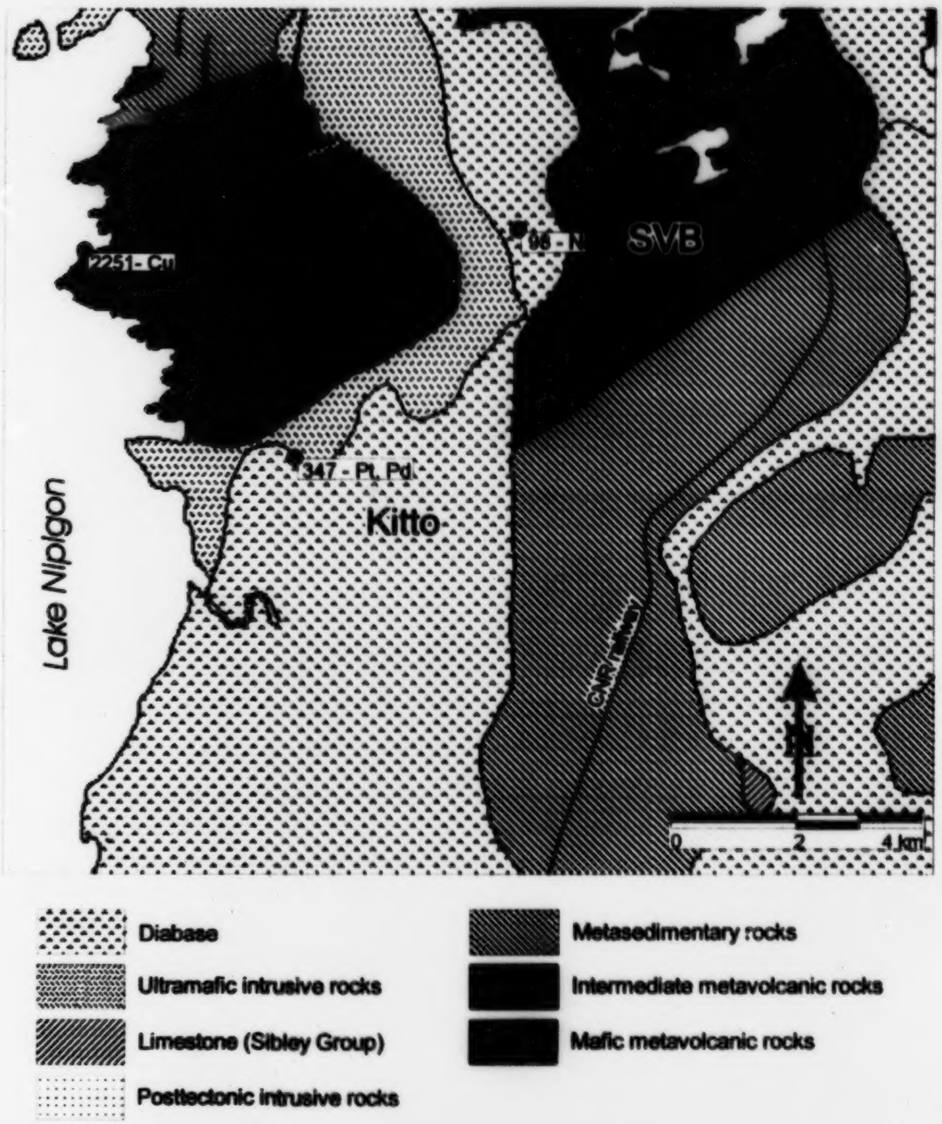
2251 - Cu
98 - N
SVB
347 - Pt, Pd
Kitto
Lake Nipigon
CNR railway
0
2
4 km
Diabase
Ultramafic intrusive rocks
Limestone (Sibley Group)
Posttectonic intrusive rocks
Metasedimentary rocks
Intermediate metavolcanic rocks
Mafic metavolcanic rocks

Figure 55. Locations of significant base metal results discovered in Kitto Township. Numbers refer to field sample numbers; *see* Appendix 5 for analytical data collected for the samples.

SOUTHERN METAVOLCANIC SUBBELT

Significant sulphide mineralization is rare in the SVB, and is commonly associated with shear zones and brittle fracturing of the interflow iron formations. The shear zones and brittlely fractured iron formations may contain quartz veinlets and stringers, with varied amounts of pyrite, pyrrhotite and, in rare cases, arsenopyrite. This style of quartz veining is commonly associated with gold mineralization.

Base metal sulphide mineralization was observed in 2 shears within the SVB. Intense gossan staining was observed in a shear zone within mafic metavolcanic rocks along the railroad, south of Beardmore (*see* Figure 56: sample 1440). The 10 to 30 cm wide shear zone contains disseminated pyrite, and trends subparallel to the regional cleavage in the area. Analyses of samples from the shear zone returned values of 559 ppm Zn and 365 ppm Cu, with no detectable precious metals (*see* Appendix 4). A shear zone occurs along the shore of Lake Nipigon in Kitto Township, approximately 1 km north of the Goodman showing, and contains trace to very weak carbonate alteration (*see* Figure 55: sample 2251). The shear zone hosts 2 to 3% disseminated pyrite, is approximately 30 cm wide, and analyses of a sample returned a value of 754 ppm Cu, with no detectable precious metals (*see* Appendix 4).

CENTRAL METAVOLCANIC SUBBELT

Numerous small carbonate shear zones, with varied quantities of sulphide minerals, are present throughout the central metavolcanic belt (CVB), although only 1 sample yielded anomalous results. Along the 72 Road, sulphide minerals are present in a carbonatized shear zone, which is approximately 2 m wide and trends subparallel to the regional cleavage in the area (*see* Figure 56: sample 1383). The shear contains 5 to 10% fine-grained pyrite with minor chalcopyrite. The best analyses, from a

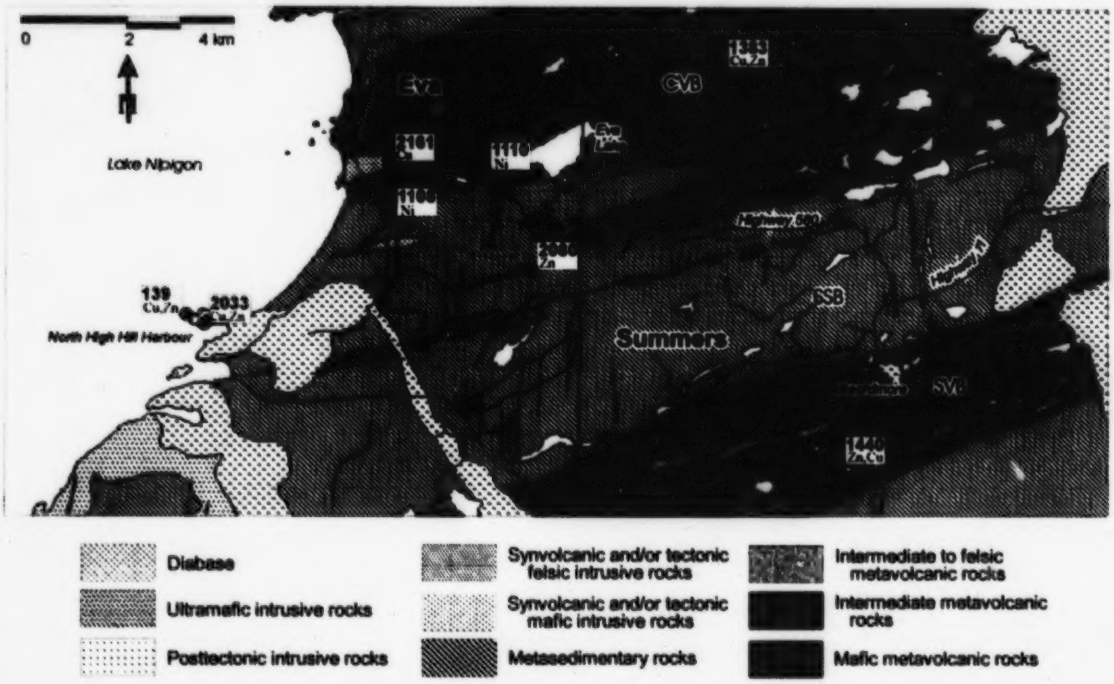

0
2
4 km
N
Lake Nipigon
Eva
CVB
1383
Cu,Zn
2161
Cu
1110
Ni
Eva Lake
1166
Ni
2080
Zn
Highway 580
Highway 11
SSB
139
Cu,Zn
2033
Cu,Zn
North High Hill Harbour
Summers
Beardmore
SVB
1440
Zn,Cu
Diabase
Ultramafic intrusive rocks
Posttectonic intrusive rocks
Synvolcanic and/or tectonic felsic intrusive rocks
Synvolcanic and/or tectonic mafic intrusive rocks
Metasedimentary rocks
Intermediate to felsic metavolcanic rocks
Intermediate metavolcanic rocks
Mafic metavolcanic rocks

Figure 56. Locations of significant base metal results discovered in Eva and Summers townships. Numbers refer to field sample numbers; *see* Appendix 5 for analytical data collected for the samples.

previously sampled trench, were 2069 ppm Cu with 286 ppm Zn, and no detectable precious metals (Appendix 5). This mineralization is located along the interpreted strike of the Sandy Creek fault, and could represent a remobilization of synvolcanic mineralization.

Anomalous nickel values were obtained from 2 locations in the andesite, along the north side of the CVB–SSB contact north of Highway 580. Sample 1108 (*see* Figure 56) contains disseminated chalcopyrite, and weak to moderate, foliation-parallel, quartz and epidote veins averaging 1 to 3 cm in width with fine- to medium-grained chlorite. Sample 1108 was analyzed and returned a value of 217 ppm Ni, with no detectable precious metals (*see* Appendix 5). Approximately 1 km east of sample 1108, sample 1110 contains disseminated sulphide minerals occurring in both a quartz vein and its host intermediate to mafic metavolcanic rock (*see* Figure 56). The previously trenched quartz vein is 0.3 to 1.0 cm wide and occurs as open-space fillings. An analysis of a sample collected from the vein did not contain any notable analytical values. The host rock contained a moderate amount of carbonate alteration and a weak to moderate amount of sulphide minerals. An analysis of a sample collected from the previously sampled trench returned a value of 358 ppm Ni, with no detectable precious metals (*see* Appendix 5: samples 1110a, 1110b).

Two intrusion-associated malachite-chalcopyrite-bearing quartz veins occur within the CVB (*see* Figure 56: sample 2161). The first vein is approximately 10 to 30 cm wide and occurs in weak fracture fillings within metavolcanic rocks near a diorite intrusion. It contains 3 to 5% disseminated chalcopyrite, 7 to 10% malachite, and 10 to 15% xenoliths of intermediate to mafic metavolcanic rock, which have been moderately to intensely altered to hematite and chlorite. The best assay from the vein returned a value of 5102 ppm Cu, with no precious metals detected (*see* Appendix 4). A second malachite showing occurs approximately 1 km east of Eva Lake (*see* Figure 56). At this location, a pyrite-chalcopyrite-malachite-bearing fracture occurs in metavolcanic rocks adjacent to a gabbroic intrusion. The host rock displays moderate siliceous alteration, plus weak to moderate hematite and epidote alteration. No sample was collected at this location.

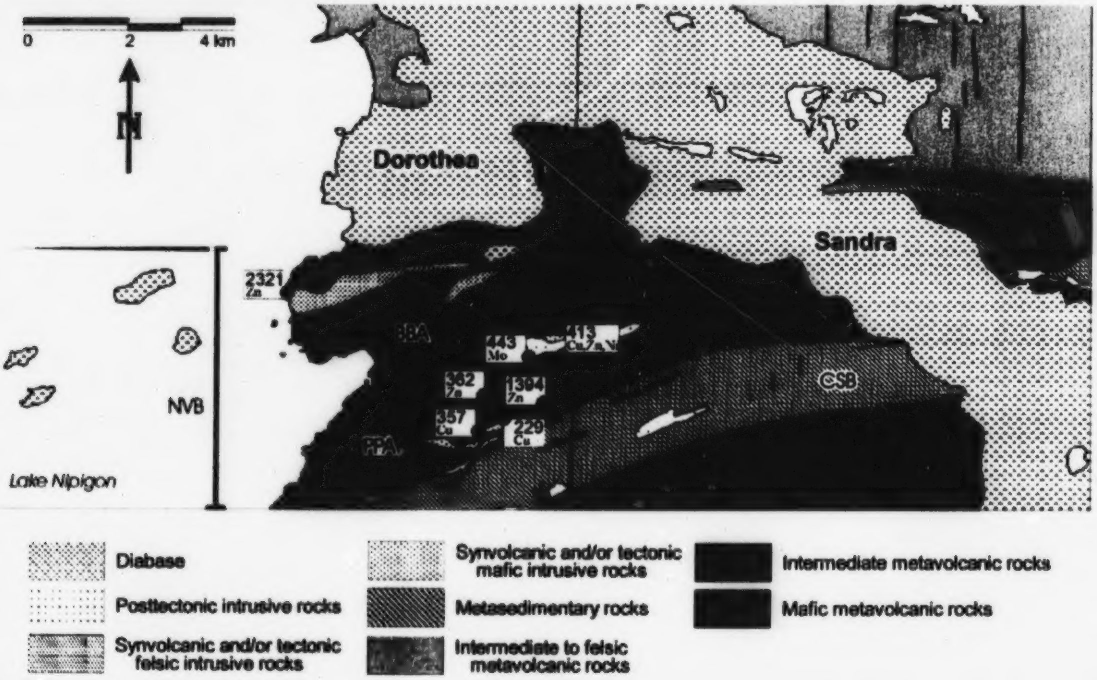
0
2
4 km
N
Dorothea
Sandra
2321
Zn
BBA
443
Mo
413
Cu,Zn,V
362
Zn
1304
Zn
357
Cu
229
Cu
CSB
PPA
NVB
Lake Nipigon
Diabase
Posttectonic intrusive rocks
Synvolcanic and/or tectonic felsic intrusive rocks
Synvolcanic and/or tectonic mafic intrusive rocks
Metasedimentary rocks
Intermediate to felsic metavolcanic rocks
Intermediate metavolcanic rocks
Mafic metavolcanic rocks

Figure 57. Locations of significant base metal results discovered in Dorothea and Sandra townships. Numbers refer to field sample numbers; *see* Appendix 5 for analytical data collected for the samples.

Sulphide mineralization in the CVB is closely association with structures or the posttectonic diorite suggesting a genetic connection between the mineralization and intrusions. The lack of significant synvolcanic sulphide mineralization is in distinct contrast to the PPA.

NORTHERN METAVOLCANIC SUBBELT

Significant accumulations of sulphide mineralization are rare in the basalts of NVB, and only a single anomalous assay was returned from samples collected in mafic metavolcanic rocks of the Bish Bay assemblage in the NVB (*see* Figure 57). Weak, fracture-filled pyrite is present in a quartz vein hosted by lapilli tuff, and is adjacent to the gabbro-peridotite intrusion. A quartz vein less than 0.3 cm wide crosscuts the regional cleavage, and an analysis returned values of 445 ppm Zn and 193 ppm Cu, with no detectable precious metals (*see* Figure 57: sample 2321; *see* Appendix 4: sample 2321b). A sample of the peridotite from the same outcrop contained anomalous values of 645 ppm Ni and 3007 ppm Cr, respectively (*see* Figure 57: sample 2321; Appendix 6, sample 2321c; Appendix 2, sample 2321a, respectively).

The intermediate to mafic metavolcanic rocks from the Poplar Point assemblage (PPA) within the NVB contain a number of sulphide occurrences. Sulphide mineralization consisting of pyrite and pyrrhotite with minor chalcopyrite occurs as interpillow pods and vesicle fillings in mafic metavolcanic flows and as patches in the matrix of tuff breccias. The tuff breccias with sulphide patches generally have an intensely chloritized matrix and are closely associated with peperitic textured, subvolcanic felsic feeder dikes, and are located immediately to the east of the mafic metavolcanic horizon (*see* Figure 6). Only one sample of a patch composed of approximately 10% disseminated subhedral pyrite had an anomalous analysis, which returned a value of 344 ppm Zn, with no detectable precious metals (*see* Figure 57: sample 362; *see* Appendix 5: sample 362). No other samples collected from this style of mineralization had anomalous base metal contents (*see* Appendix 5).

The felsic dikes intruding the intermediate metavolcanic rocks of the PPA are associated with several anomalous base metal showings. Immediately north of the Dorothea Gold property, a pyrite-malachite-pyrrhotite quartz vein occurs as fracture fillings within quartz-feldspar porphyry. The 3 to 10 cm wide vein contains approximately 5% patchy to disseminated pyrite and pyrrhotite and trace epidote and chlorite alteration. The best analysis contained 4554 ppm Cu, with trace amounts of gold (*see* Figure 57: sample 229; *see* Appendix 4: sample 229c). Several hundred metres west of the Dorothea Gold property, 3 to 5% disseminated pyrite occurs in a fine- to medium-grained feldspar porphyry. The rock displays very weak to weak chlorite, ankerite and albite alteration associated with less than 0.3 cm wide irregular quartz fracture fillings, and was analyzed at 1366 ppm Cu, with no detectable precious metals (*see* Figure 57: sample 357; *see* Appendix 4: sample 357).

Anomalous showings within the PPA are also associated with sheared metavolcanic rocks. A sheared lapilli tuff containing tabular quartz fragments, and approximately 5% very coarse-grained and disseminated pyrite was analyzed at 28 708 ppm Cu (2.8%), 1105 ppm Zn and 349 ppm Ni, with no detectable precious metals (*see* Figure 57: sample 413; *see* Appendix 5: sample 413). A second shear zone to the south, 1 to 3 m wide, displays moderate to strong carbonate and hematite alteration and contains 2 to 3% fine-grained arsenopyrite. The shear is hosted within intermediate metavolcanic rocks, and trends subparallel to the regional cleavage in the area. A sample collected from a previously sampled trench, was analyzed at 1123 ppm Zn, with no detectable precious metals (*see* Figure 57: sample 1394; *see* Appendix 4: sample 1394).

The 3 modes of sulphide mineralization in the PPA is interpreted to be a result of 2 different mechanisms. The close association between sulphide mineralization and felsic intrusive rocks in the PPA suggests a genetic connection between the mineralization and intrusive rocks, possibly to the intrusion of the posttectonic diorite or to S-type granite. However, sulphide mineralization, occurring as vesicle fillings and in interpillow spaces, have been observed in the footwall zones of some VMS deposits (e.g., Ansil mine; H.L. Gibson, Laurentian University, personal communication, 2000). The sulphide patches in the chloritized tuff breccias associated with synvolcanic felsic feeder dikes are interpreted to be related to the same early VMS hydrothermal system. The FII-type geochemistry of the synvolcanic felsic dikes with peperitic contacts is consistent with a high potential for volcanogenic massive sulphide mineralization in the PPA.

SOUTHERN METASEDIMENTARY SUBBELT

Sulphide mineralization in this subbelt is generally rare, occurring as trace, disseminated, fine-grained pyrite. Moderate pyrite occurs in feldspathic wacke of the southern metasedimentary subbelt next to a diabase dike, along the road to the Sand River Mine (*see* Figure 56: sample 2080). Disseminated pyrite occurs in feldspathic wacke in the approximately 10 to 30 cm wide zone along the contact with the dike, and this sample was analyzed at 795 ppm Zn, with no detectable precious metals (*see* Appendix 5: sample 2080).

PROTEROZOIC ULTRAMAFIC AND MAFIC INTRUSIVE ROCKS

Trace pyrite sulphidization occurs within the diabase near the base of a sill located along the north shore of North High Hill Harbour (*see* Figure 4). The diabase contains medium-grained flow-foliated plagioclase crystals in a fine-grained groundmass, with localized patches of coarse-grained, pink feldspar. Two samples, 2033 and 139, located approximately 400 m apart, yielded anomalous copper and zinc values of 663 ppm Cu and 190 ppm Zn, and 647 ppm Cu and 200 ppm Zn, respectively (*see* Appendix 6: samples 2033 and 139, respectively). As discussed above, the geochemistry for sample 139 is more fractionated than most of the diabase samples in the map area, which was interpreted to be a result of either a higher degree of fractionation or the assimilation of crustal material (*see* "Geochemistry"). The high zinc values in these 2 samples would favour the assimilation of crustal material as zinc is not commonly concentrated in mafic intrusive rocks.

Nickel–Copper

Only 2 anomalous nickel values were returned from sampling of the diabase sills and peridotite. These values are interpreted to be associated with the assimilation of peridotite rather than magmatic sulphide mineralization within the diabase sill. However, there is a possibility that the Proterozoic intrusive rocks may have been a source for nickel and copper in base metal sulphide mineralization that is currently not exposed. Testing to determine if these rocks have been associated with the formation of nickel-copper sulphide mineralization involves an examination of the geochemistry and a number of assumptions to determine if there has been nickel depletion of the magma as a result of crustal contamination or fractional crystallization (e.g., Naldrett et al. 1984; Lightfoot, Keays and Doherty 2001). The potential for nickel-copper sulphide mineralization in the Proterozoic lithologies of the map area is considered to be low. However, the tests for this style of mineralization are not conclusive, and additional sampling of chill contacts, detailed geophysics and prospecting are required to fully evaluate the Proterozoic rocks.

A high potential for nickel-copper sulphide mineralization is usually associated with evidence of the assimilation of crustal material by the magma providing sulphur or decreasing the solubility of nickel and copper in the magma (e.g., Lightfoot et al. 1997). The test for crustal contamination for the peridotite, olivine gabbro and diabase samples are discussed above (*see* "Geochemistry") and there is little evidence for crustal assimilation. This interpretation is based on the lack of geochemical variation that can be best explained by fractional crystallization rather than the addition of material of crustal composition (e.g., *see*

Figures 38 and 45). However, there is field evidence for assimilation observed along the olivine gabbro with the SSB metasedimentary rocks, and the diabase with Quetico Subprovince metasedimentary rocks (*see* Photo 14). An additional check for contamination is through a La/Sm–SiO_2 diagram (Figure 58), which indicates a near constant La/Sm ratio and SiO_2 content within each lithology, consistent with a lack of crustal contamination. Crustal contamination should have resulted in an increase in SiO_2 values and the La/Sm ratio, although Naldrett and Lightfoot (1993) indicates that this type of test for crustal contamination is not conclusive.

DIABASE SILLS

The test for nickel depletion, and depletion in the other chalcophile elements, is best completed using magnesium as an indicator of fractionation in either MgO–Ni (Naldrett et al. 1984) or Ni/MgO–Mg# (molar Mg/(Mg+Fe) (Naldrett and Lightfoot 1993). The diabase has low nickel content, but also has low MgO values and falls within the range of fractionated mafic magmas on a MgO–Ni diagram hindering an accurate interpretation (Figure 59). A variation on this plot (MgO–log Ni), presented by Lightfoot, Keays, and Doherty (2001) is restricted to the lower MgO values (Figure 60) and the diabase values follow the trend of the within-plate basalts, indicating the diabase is not depleted in nickel. Examination of the relationship between copper and MgO indicates that copper in the diabase gradually increases with decreasing MgO, and the diabase chill sample plots in the centre of the diabase field (Figure 61). This trend is interpreted to be an igneous fractionation trend, and suggests that copper was not depleted by a sulphide mineral phase (e.g., Lightfoot et al. 1997). These sills resemble the Upper Suite basalts of the Osler Group (e.g., *see* Figure 38) and Lightfoot, Sutcliffe and Doherty (1991) indicated that the upper portions of the Central and Upper Suites were depleted in nickel. It was interpreted that, due to the similarity in geochemistry between the basalts and the diabase sills, the sills may contain excess nickel. A lack of nickel enrichment may indicate that these sills are not directly related to the Osler Group basalts. Alternatively, the rocks directly overlying the nickel-sulphide mineralization may not be directly related to the mineralization and, therefore, are not depleted in nickel compared to MgO as observed in many komatiitic nickel-copper sulphide deposits (e.g., Lesher and Stone 1996). Recognition of depletion or enrichment is further complicated by the construction of the sills by multiple pulses of magma that may have followed separate fractional crystallization trends seen in Figures 62 and 63. There is a possibility nickel-sulphide mineralization may be present at the base of some sills, and this mineralization may only be located using detailed geophysical surveys and prospecting.

There are 3 anomalous samples, samples 139, 347 and 98, on the MgO–Ni (*see* Figure 59) and MgO–Cu (*see* Figure 61) diagrams. As discussed above, sample 139 also has anomalous zinc values, which are interpreted to relate to the assimilation of the underlying country rock. Sample 347 is located along the contact between the diabase and the peridotite (*see* Figure 13), and contains trace to 1% fine-grained disseminated sulphide mineralization, which is reflected in the anomalous nickel and copper values. This sample has a mixture of geochemical characteristics that have been interpreted to be the result the assimilation of a minor amount of peridotite (*see* "Geochemistry"). Sample 98 was not as geochemically distinctive as sample 347, but has a higher than average MgO (*see* Figure 59; *see* Appendixes 2, 3 and 6: sample 98). This sample is located in a similar stratigraphic position in the sill, near the contact with the peridotite (*see* Figure 13), and the anomalous nickel value may also be a result of the assimilation of a very limited amount of peridotite or a more primitive diabase phase enriched in nickel. The peridotite tops to the inside of the crescent, and these anomalous diabase samples may have interacted with the lower contact of the intrusion assimilating peridotite enriched in platinum group elements (*see* Figure 13). It is possible that the best mineralization may be present along the base of the intrusion, similar to the drill results from the Seagull intrusion, where the best mineralization is located along the basal contact (East–West Resources Corporation 2000). The basal contact of the peridotite and the adjacent diabase are probably the areas with the best potential to host nickel-copper or PGE mineralization in the map area.

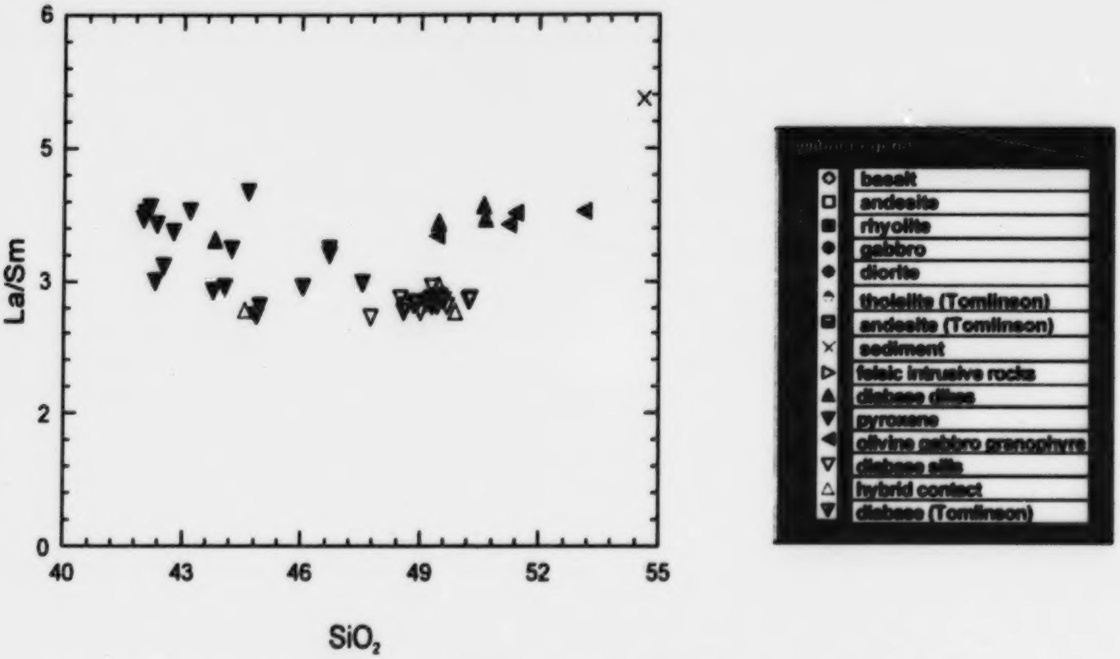

Figure 58. SiO_2 versus La/Sm diagram with the Proterozoic diabase dikes, peridotite, olivine gabbro, and diabase sills, and a feldspathic wacke of the southern metasedimentary subbelt (*after* Lightfoot, Sutcliffe and Doherty 1991).

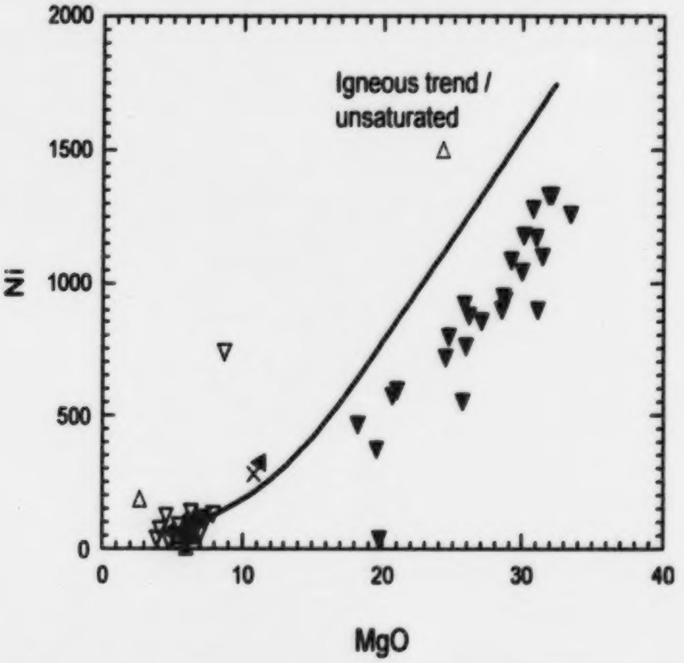

Figure 59. MgO versus nickel diagram for the Proterozoic diabase dikes, peridotite, olivine gabbro, and diabase sills, and a feldspathic wacke of the southern metasedimentary subbelt with the igneous fractionation trend for an idealized sulphur-unsaturated magma from Naldrett et al. (1984). Legend for symbols, *see* Figure 58.

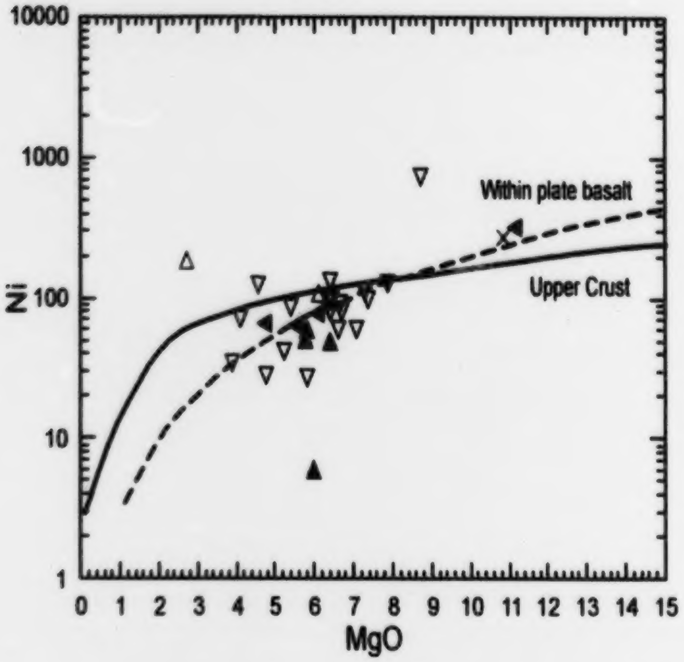

Figure 60. MgO versus log nickel diagram with the Proterozoic diabase dikes, olivine gabbro, and diabase sills, and a feldspathic wacke of the southern metasedimentary subbelt with the trends for sulphur-unsaturated within-plate basalt and upper crust from Lightfoot, Keays and Doherty (2001). Legend for symbols, *see* Figure 58.

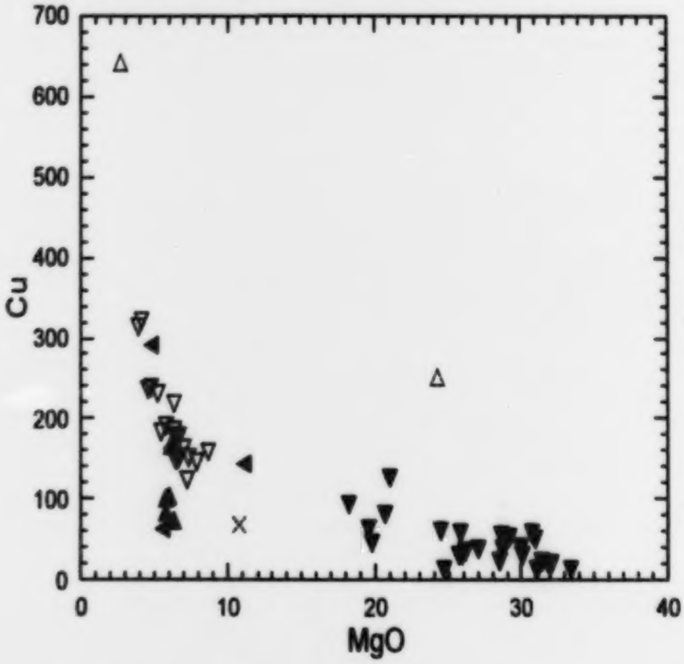

Figure 61. MgO versus copper diagram with the Proterozoic diabase dikes, peridotite, olivine gabbro, and diabase sills, and a feldspathic wacke of the southern metasedimentary subbelt (*after* Lightfoot et al. 1997). Legend for symbols, *see* Figure 58.

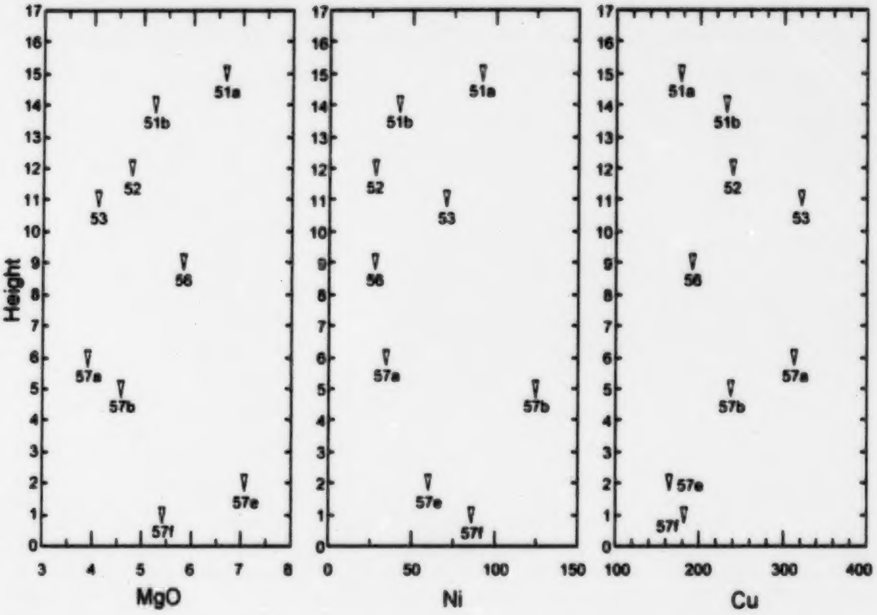

Figure 62. MgO, nickel and copper versus approximate stratigraphic height for the highway stratigraphic section through the diabase sill. Legend for symbols, *see* Figure 58.

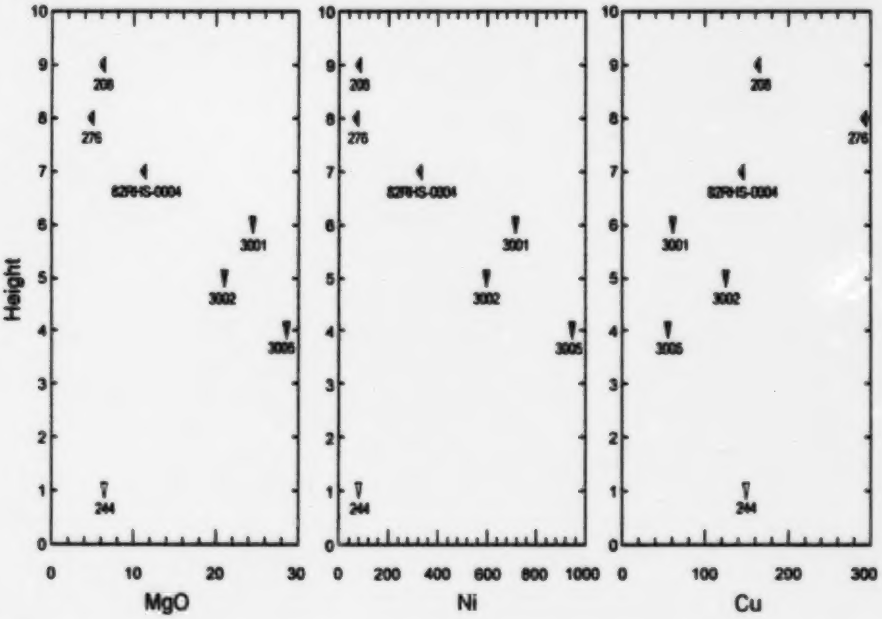

Figure 63. MgO, nickel and copper versus approximate stratigraphic height for the eastern stratigraphic section through the peridotite and olivine gabbro. Legend for symbols, *see* Figure 58.

PERIDOTITE – OLIVINE GABBRO

The peridotite samples plot below the igneous fractionation trend on a MgO-Ni diagram, possibly as a result of nickel depletion in a sulphide mineral phase (*see* Figure 59). However, a basic assumption for this diagram is that the rocks approximate a liquid composition and the peridotite is a cumulate. These samples appear to fall on a trend subparallel to the ideal fractionation trend with decreasing MgO values. This trend for the peridotite is interpreted to be an igneous fractionation trend starting at approximately 200 ppm Ni and 13 weight % MgO producing a high MgO cumulate and a lower MgO fractionate approximating the olivine gabbro or diabase (*see* "Geochemistry"). The trend subparallel to but lower in nickel than the ideal may be interpreted to indicate that the parental magma was slightly depleted in nickel. However, the olivine gabbro plots along the same trend as the diabase, along the within-plate basalt trend, shown in Figure 60, indicating that the parental magma was probably not depleted in nickel. Although there is field evidence of assimilation of crustal material, there is no clear geochemical evidence of crustal contamination (e.g., *see* Figure 58) and the peridotite is interpreted to have a low potential for nickel-copper sulphide mineralization.

The peridotite samples appear to follow an igneous fractionation trend of increasing copper with decreasing MgO (*see* Figure 61), and is consistent with the trend observed for nickel. The olivine gabbro samples follow the same enrichment trend, consist with an interpretion of enrichment due to continued fractional crystallization (*see* Figure 61). The exception is sample 1196, which plots with the diabase dikes, as seen in Figure 61. Stratigraphic variation of copper, nickel and MgO in the intrusion (e.g., Figure 63) are interpreted to be a result of the fractionation of a single pulse of magma and are not indicative of a potential for copper mineralization.

MOLYBDENUM

Two molybdenum-bearing quartz veins are hosted by lapilli tuff in the NVB, northern Dorothea Township. The shear-parallel veins are 10 to 30 cm in width and display weak to moderate carbonate alteration and very weak hematite alteration. Alteration minerals associated with molybdenum include sericite, ankerite and calcite. The molybdenum generally occurs as large irregular patches, up to 2 cm in diameter, in quartz veins and can comprise up to 15% of the vein material. An assay of the molybdenite-bearing quartz vein returned a value of 3839 ppm Mo (*see* Appendix 5: sample 443; *see* Figure 57: sample 443). A more detailed description of the vein is given by Mackasey (1975).

MAGNETITE

Magnetite is hosted by chemical metasedimentary rocks that occur as interflow sediments in the metavolcanic subbelts and as sedimentary horizons in the metasedimentary subbelts. Interflow metasediments, consisting of magnetite-chert iron formations, are present in the CVB and the SVB (*see* Figure 6). Within the CVB, iron formations occur as brecciated magnetite-chert units and magnetite-chert-bearing pyroclastic rocks. Exposures of either unit are rare and interpretation of the mode of formation is hindered since adjacent rock types are poorly exposed and are difficult to correlate using the regional airborne magnetic survey (OGS 1998). There are approximately 5 stratigraphically stacked formations in the SVB composed of units up to 2 m thick consisting of thinly bedded magnetite and chert. These iron formations are of interest where crosscutting quartz veins in shears result in minor sulphidization, the formation of arsenopyrite and the deposition of gold.

Magnetite is concentrated in the clastic-magnetite-argillite iron formations occurring as multiple horizons within the SSB, south of the Standingstone fault (*see* Figures 6 and 11). These iron formations are regionally continuous and can be traced east to the Geraldton area. The magnetite-dominated iron formations consist of 0.05 to 0.3 m (may be up to 1 m) thick magnetite beds intercalated with 0.1 to 0.2 m thick argillite and rare siltstone beds forming units up to 25 m thick. A similar, but shorter strike length, clastic iron formation is located in the CSB close to the contact with the metavolcanic rocks of the PPA. These iron formations were explored for their potential as sources of iron ore in the early 1900s (Mason and White 1986).

Magnetite also occurs as coarse-grained crystals in both the diabase and peridotite intrusions, and as isolated quartz-magnetite fracture fillings within feldspathic wacke, mafic metavolcanic and gabbroic rocks. The shear-parallel quartz veins are between 1.0 to 10 cm in width, and often contain minor pyrite.

HEMATITE

Hematite occurs in abundance within jasper-hematite banded iron formations located in the SSB, along the contact with the CVB, north of the Standingstone fault (*see* Figure 6 and 11). The units range from 10 cm to over 3 m in thickness, and comprise 0.5 to 1.0 cm jasper beds intercalated with 0.3 to 2.0 cm specular hematite beds and 0.5 to 4 cm mudstone beds. These iron formations were explored along with the clastic iron formations for their potential as sources of iron ore in the early 1900s (Mason and White 1986).

Hematite is also present as an alteration product within magnetite-chert iron formations and within clastic-magnetite-argillite iron formations, where the hematite alteration is so intense that it could be misidentified in the field as jasper horizons. Specular hematite occurs sporadically in fractures with quartz in the mafic metavolcanic rocks of all 3 volcanic subbelts and, locally, in quartz fractures in the intermediate to felsic metavolcanic rocks near Eva Lake.

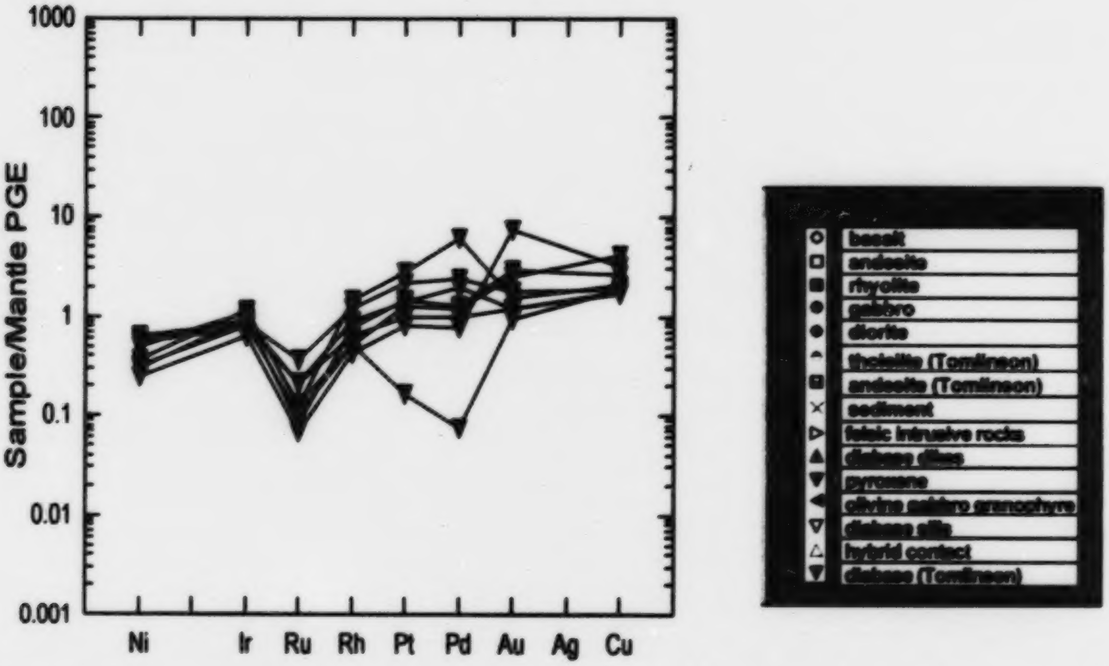

Figure 64. Metal mantle-normalized element diagram for the peridotite, using the normalizing factors of McDonough and Sun (1995) (*after* Barnes et al. 1987).

PLATINUM GROUP ELEMENTS

A crescent-shaped Proterozoic peridotite intrusion, overlain by diabase, occurs in Eva and Kitto townships (*see* Figures 6 and 13). Sulphide mineralization is not common in either the peridotite or diabase, although trace to very weak amounts of disseminated pyrite and chalcopyrite was observed in a few locations. There is 1 sample, 347, in the diabase sill immediately adjacent to the peridotite, with anomalous platinum and palladium values, which contains trace to 1% sulphide mineralization and is also anomalous in nickel (*see* Figure 55; *see* "Sulphide Mineralization: Nickel-Copper"; *see* Appendix 6: sample 347A). This sample location has been designated the "Phoenix occurrence" and is discussed in "Mineral Occurrences: Platinum Group Element Mineralization: Phoenix Occurrence". There are a number of interflow chert-magnetite iron formations with minor sulphide mineralization in the adjacent metavolcanic rocks that are a potential sulphur source for the formation of PGE mineralization in the peridotite.

Mantle-normalized metal diagrams provide an indication of the rock type and an indication if the rock has been depleted in PGE (e.g., Figure 64). The peridotite samples appear to have patterns similar to those commonly observed in komatiites and high-MgO basalt by Barnes et al. (1987; *see* Figure 64). These abundances indicate that the PGE values in the peridotite are relatively unfractionated compared to mantle values. The anomalously high palladium value is from sample 3001 (*see* Appendix 6) and the anomalously high gold is from sample 1198 (*see* Appendix 6), and both samples are located toward the inner upper side of the peridotite (*see* Figure 13). The low platinum and palladium values occur in sample 3005, also located toward the outer side or base of the peridotite, stratigraphically below sample 3001 (*see* Figures 13 and 63). The depletions in sample 3005 may be the result of a depletion in PGE indicating a concentration elsewhere in the peridotite, although there is the possibility of an analytical error. Only 2 olivine gabbro samples were analyzed and, although hosting highly varied PGE contents, these samples are generally slightly depleted in PGE compared to the peridotite (Figure 65). The diabase

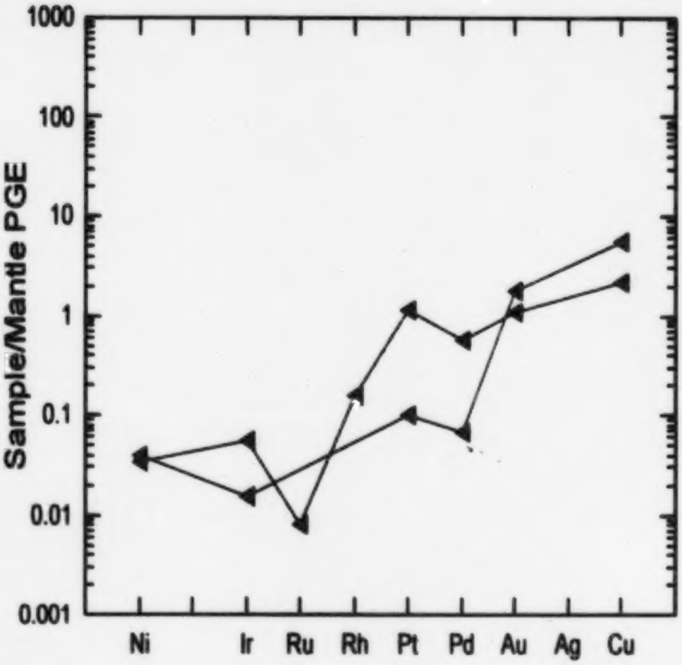

Figure 65. Metal mantle-normalized element diagram for the olivine gabbro, using the normalizing factors of McDonough and Sun (1995) (*after* Barnes et al. 1987). Legend for symbols, *see* Figure 64.

sills have PGE contents that result in patterns resembling flood basalts or ocean floor basalts (Figure 66). The diabase sills have platinum and palladium concentrations greater than mantle values, and so have not been depleted in platinum group elements. The diabase is probably not a source for PGE mineralization.

The PGE ratio diagrams may also be used to examine the possibly igneous processes and magmatic affinity of the host rocks (e.g., Figure 67). On a Ni/Cu–Pd/Ir diagram, the peridotite samples plot in the layered intrusion field of Barnes et al. (1987), trending toward a point that was an approximation of the olivine cumulate in some komatiite flows (*see* Figure 67). The trend from the peridotite to the olivine gabbro is along the trend predicted to be controlled by the fractionation of olivine, consistent with the cumulate nature of the peridotite. The diabase samples plot within the flood basalt field on the Ni/Cu–Pd/Ir diagram (*see* Figure 67), consistent with a more evolved composition of the mantle-normalized metal diagram (*see* Figure 66). The peridotite samples plot toward the olivine cumulate composition on the Cu/Ir– Ni/Pd diagram, out of the range of the compositional fields presented by Barnes et al. (1987; Figure 68). The olivine gabbro samples plot within or near the field defined by PGE reefs, or along a trend indicative of chromite fractionation from a parental peridotite composition (*see* Figure 68). The diabase samples plot below the range shown by Barnes et al. (1987) with a lower Ni/Pd ratio than the olivine gabbro, potentially in the range of the PGE reefs.

Barnes et al. (1993) proposed that the Cu/Pd ratios are useful guides for PGE exploration, as the Cu/Pd ratio is an indicator of the original PGE content of the magma (Figure 69). The peridotite and olivine gabbro plot with Cu/Pd ratios less than mantle values and palladium values slightly greater than mantle values (*see* Figure 69). These values are interpreted to indicate that the parental magma was not depleted in PGE, and the peridotite has the potential to host PGE mineralization if a crustal sulphur source was available. Unfortunately, the parental magma composition of the peridotite is not known, and more detailed igneous modelling to test the interpretation is not possible.

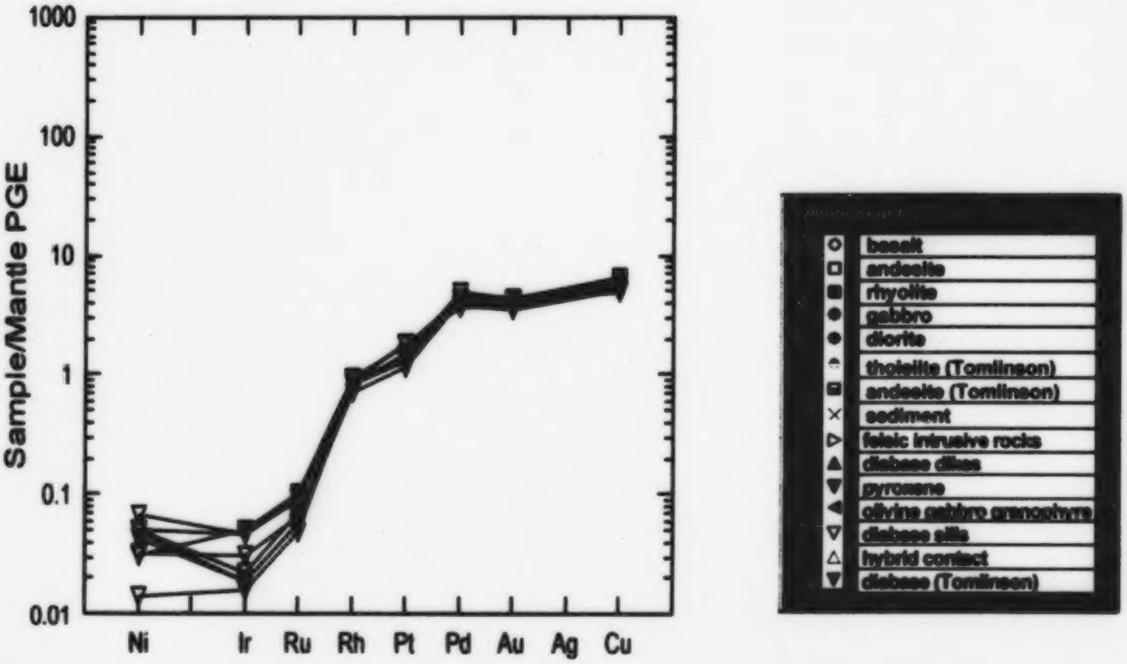

Figure 66. Metal mantle-normalized element diagram for the diabase sills, using the normalizing factors of McDonough and Sun (1995) (*after* Barnes et al. 1987).

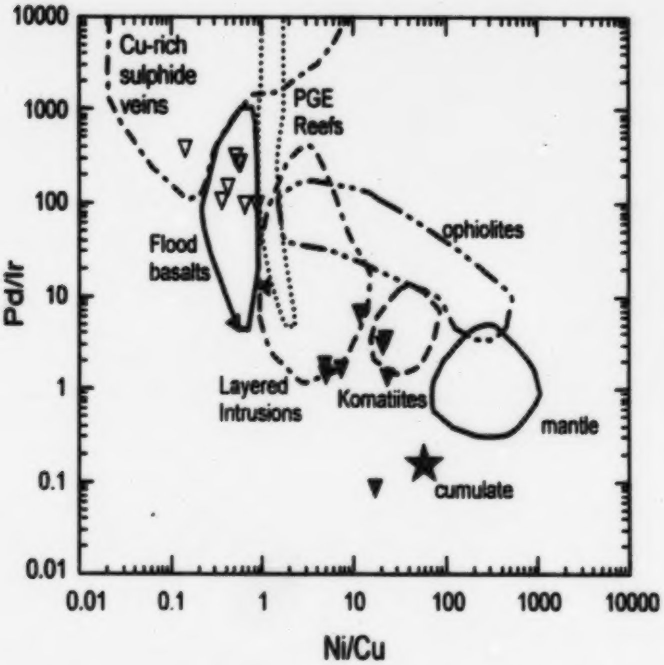

Figure 67. Log Ni/Cu versus log Pd/Ir diagram with the Proterozoic diabase dikes, olivine gabbro, and diabase sills (this study) with the fields for layered intrusions and flood basalts and an olivine cumulate from a komatiite flow from Barnes et al. (1987). Legend for symbols, *see* Figure 66.

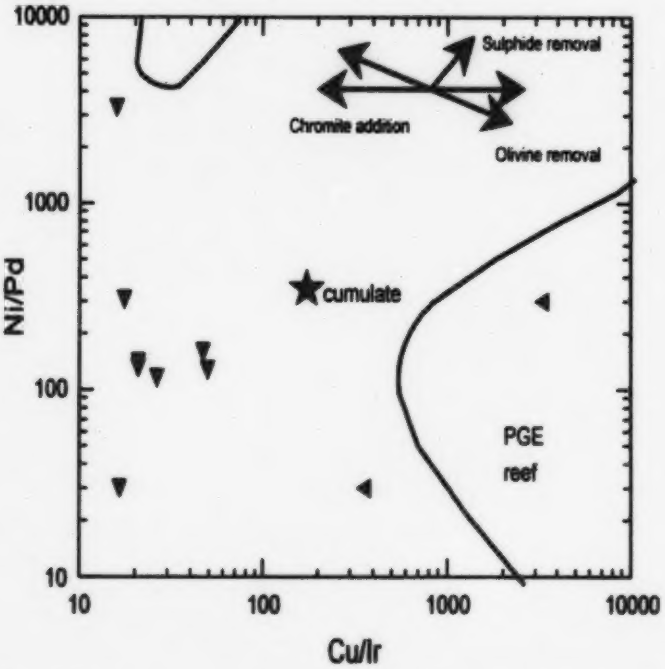

Figure 68. Log Cu/Ir versus log Ni/Pd diagram with the Proterozoic diabase dikes, olivine gabbro, and diabase sills (this study) with the fields for platinum group element (PGE) reef deposits and an olivine cumulate from a komatiite flow from Barnes et al. (1987). Legend for symbols, *see* Figure 66.

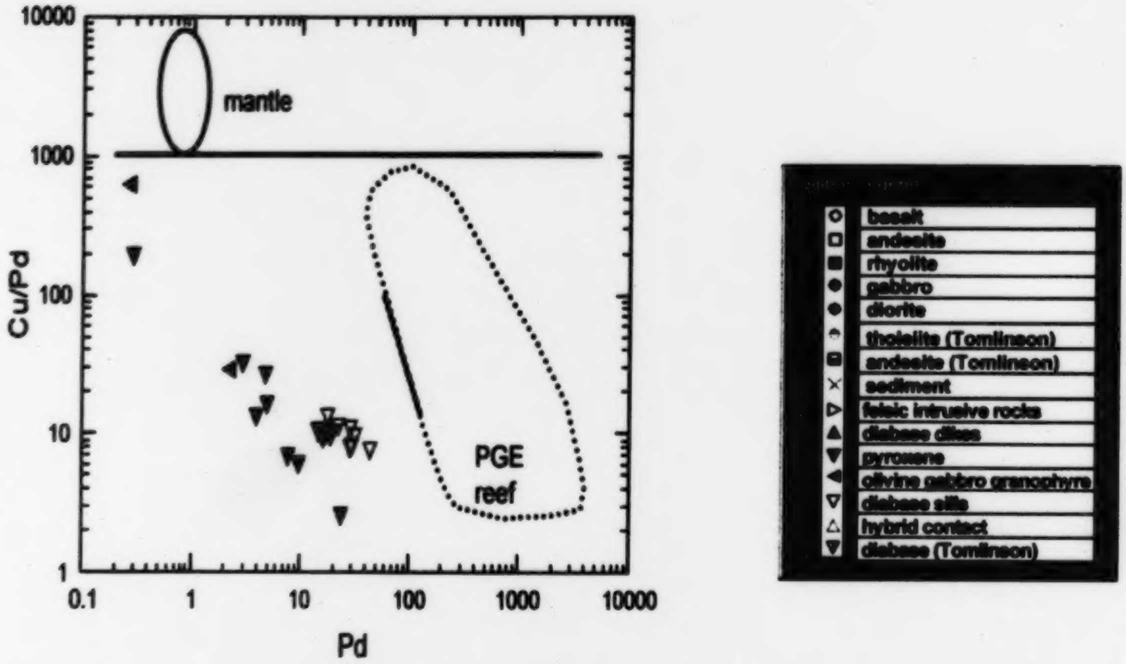

Figure 69. Log palladium versus log Cu/Pd diagram with the Proterozoic diabase dikes, olivine gabbro, and diabase sills (this study) with the fields for platinum group element (PGE) reef deposits and mantle from Barnes et al. (1987).

Mineral Occurrences

Exploration and prospecting in the Beardmore area was initially conducted mainly for iron ore in the early 1900s, but expanded to gold in 1925 (Mason and White 1986). The area has been extensively explored for gold and, to a lesser extent, for base metals resulting in the discovery of a number of mineral occurrences (Table 3, *see* back pocket), as well as the past-producing Northern Empire, Leitch and Sand River mines (*see* Figures 3, 4 and 5). A wide variety of techniques have been applied to exploration in the area (Table 4, *see* back pocket), including the extensive use of diamond drilling (Figure 70; OGS, 2002). Information on the lithologic units, mineralization and alteration for the occurrences is listed in Table 5 (*see* back pocket). Only the occurrences that have been worked on since the last geological reports of Mackasey (1975) and Shanks (1993) or were visited by the authors are described in detail below. Occurrences without recent work are listed in Table 6. Exploration in the Beardmore area has recently expanded to included platinum group elements, specifically in the ultramafic intrusion in Eva and Kitto townships.

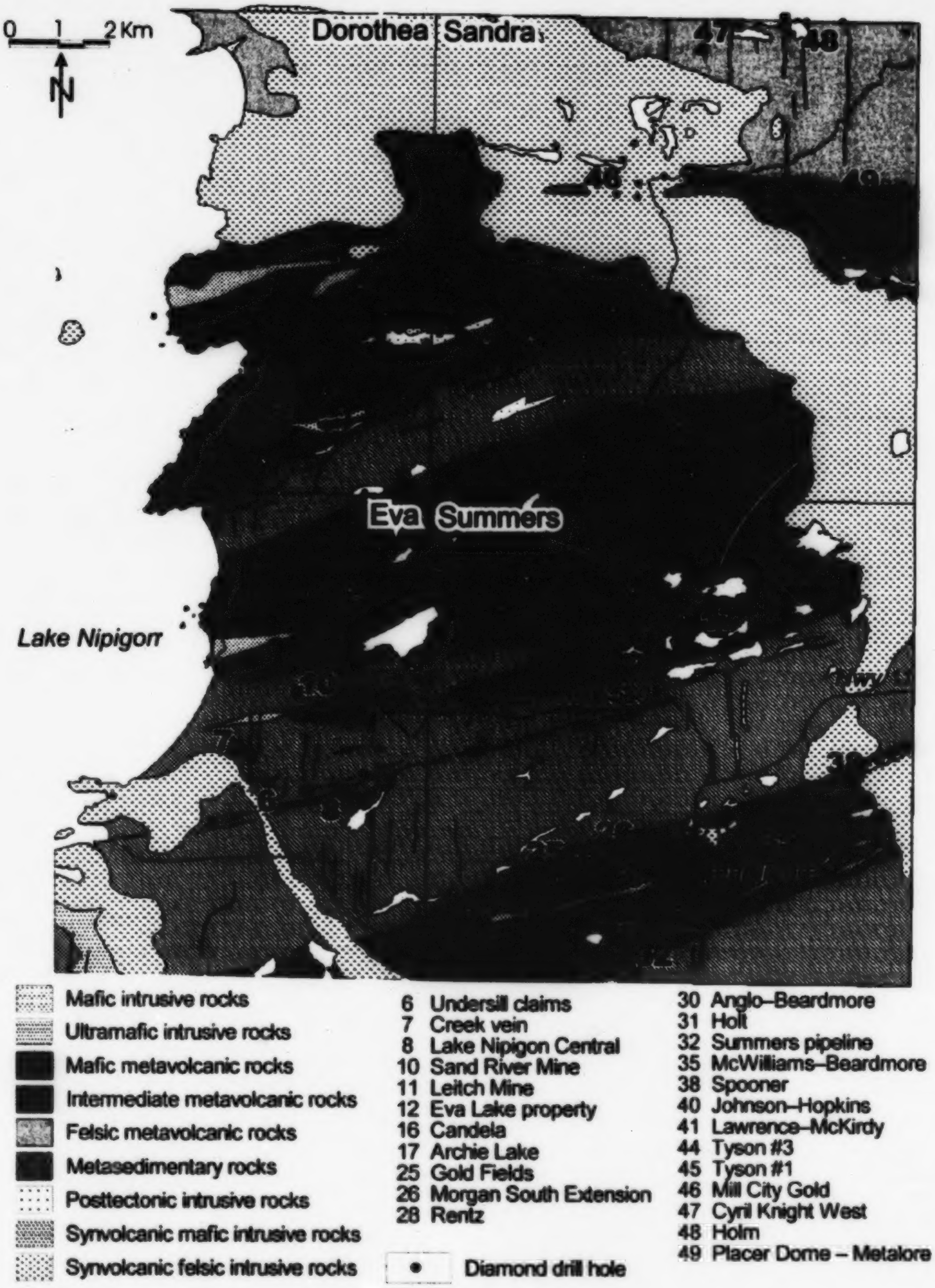
0 1 2 Km
N
Dorothea
Sandra
Eva
Summers
Lake Nipigon
46
47
48
49
Mafic intrusive rocks
Ultramafic intrusive rocks
Mafic metavolcanic rocks
Intermediate metavolcanic rocks
Felsic metavolcanic rocks
Metasedimentary rocks
Posttectonic intrusive rocks
Synvolcanic mafic intrusive rocks
Synvolcanic felsic intrusive rocks
Diamond drill hole
6 Undersill claims
7 Creek vein
8 Lake Nipigon Central
10 Sand River Mine
11 Leitch Mine
12 Eva Lake property
16 Candela
17 Archie Lake
25 Gold Fields
26 Morgan South Extension
28 Rentz
30 Anglo–Beardmore
31 Holt
32 Summers pipeline
35 McWilliams–Beardmore
38 Spooner
40 Johnson–Hopkins
41 Lawrence–McKirdy
44 Tyson #3
45 Tyson #1
46 Mill City Gold
47 Cyril Knight West
48 Holm
49 Placer Dome – Metalore

Figure 70. Location of diamond-drill holes and associated properties in Eva, Summers, Dorothea and Sandra townships, Beardmore area.

Table 6. Mineral occurrences with no recent work.

Map Number [1]	Deposit Name (year) [2]	Township	Commodity	References
8	Lake Nipigon Central (1984)	Eva	Fe	Shanks (1993)
9	Murphy Claims (1937)	Eva	Au	Waring (1937)
13	Montmorr (1937)	Eva	Au	Teare (1937)
18	Ardmore (1991)	Summers	Au	OGS (2000)
19	Long Lac Superior 2 (1934)	Summers	Au	Ferguson, Groen and Haynes (1971)
20	Empire Contact (1936)	Summers	Au	Ferguson, Groen and Haynes (1971)
21	Long Lac Superior West (1934)	Summers	Au	Speed and Craig (1992)
22	Wilport (1935)	Summers	Au	Ferguson, Groen and Haynes (1971)
23	Undersill Lake Property (1984)	Summers	Au	Mason and White (1986); Clemmer (1984)
27	Canadian Beardmore (1991)	Summers	Au	OGS (2000)
34	Hac–Craig (1983)	Summers	Au	OGS (2000)
35	McWilliams–Beardmore (1936)	Summers	Au	Mason and White (1986)
36	Banner (1991)	Summers	Au	OGS (2000)
37	Pauline Lake (1983)	Summers	Au	OGS (2000)
38	Spooner, F. (1925)	Summers	Au	Mason and White (1986); Scime (1989)
39	Northern Empire Mine (1932)	Summers	Au, Ag	Mason and White (1986)
42	Craig, C.L. (1969)	Dorothea	Au	OGS (2000)
45	Tyson #1 (1963)	Dorothea	Au, Mo	Mason and White (1986)
47	Cyril Knight West (1982)	Sandra	Au	Ferguson, Groen and Haynes (1971)

[1] "Map Number" refers to the property number on Preliminary Maps P.3513 and P.3514 (*see* back pocket).

[2] "Year" is approximate year of first recorded use.

GOLD

Exploration for gold in the Beardmore area has been on-going since the 1930s, but most of the major discoveries had been made by the end of that decade. The Beardmore gold camp was started in 1925 with the discovery of an auriferous quartz-carbonate vein east of Beardmore by T.G. Powers and P. Silam (Mason and White 1986), which led to the development of the Northern Empire Mine in 1934. The other 2 major gold producers in the Beardmore area are the Sand River Mine, and the Leitch Mine, both discovered by R. Cryderman, in 1934 and 1935, respectively (Mason and White 1986). Together, the 3 mines produced greater than one million ounces of gold, with the Leitch gold mine producing 847 690 ounces at a grade of 0.92 ounce gold per ton, the Sand River gold mine producing 50 065 ounces at a grade of 0.32 ounce gold per ton, and the Northern Empire Mine producing 149 493 ounces at a grade of 0.35 ounce gold per ton (Mason and White 1986; Table 7, *see* back pocket).

The majority of the prospecting has been concentrated in the supracrustal rocks of Summers, Eva, Dorothea and Sandra townships (*see* Figures 4 and 5), with no historical records of previous prospecting in Kitto Township until the recent discovery of gold and copper by H.K. Goodman in 1997 on the shore of Lake Nipigon (*see* Figure 3). The gold occurrences of the Beardmore area are listed by the geological subbelt in which they occur.

Southern Metavolcanic Subbelt

The gold deposits of the southern metavolcanic subbelt (SVB) are hosted by quartz and quartz-carbonate veins in shear zones, and sulphidized iron formation cut by shears. Properties in Kitto Township are restricted to the Speke Point showings, on the shore of Lake Nipigon (*see* Figure 3). The numerous showings to the east in Summers Township include the sulphidized iron formation hosted Morgan, Rentz, Holt and Summers Pipeline properties, and the quartz and quartz-carbonate vein hosted Gold Fields, the Morgan South, and the Buffalo–Beardmore properties (*see* Figure 3).

SPEKE POINT SOUTH

This showing consists of moderately sheared massive flows of mafic metavolcanic rocks located on the east shore of Lake Nipigon in Kitto Township, approximately 1 km north of Lion Bay (*see* Figure 3: property 3; *see* Preliminary Map P.3512: property 3). D.C. Goodman, H.K. Goodman and H.G. Goodman initially worked the showing under an OPAP (Ontario Prospectors Assistance Program) grant (D.C. Goodman 1997; H.K. Goodman 1997), which consisted of establishing a 10 mile flagged and blazed grid, conducting a beep mat survey, and a prospecting survey (*see* Table 4). Areas of beep mat response were stripped, blasted and grab samples were collected wherever mineralization, deformation or quartz veins occurred. In total, 40 samples were taken from the property. The beep mat survey outlined a zone, 100 feet wide, of highly sheared mafic metavolcanic rocks that is mineralized and displays iron carbonate and chlorite alteration (*see* Table 5). Numerous east-striking graphite-rich rust zones occur within this 100-feet wide zone, and contain areas of deformation and folding with the development of several crackseal quartz veins. The mineralized zones dip roughly 25° north and contain up to 5% pyrite and chalcopyrite. Crackseal quartz veins generally contain pyrite and chalcopyrite and have hematitic alteration. The best assays from this showing are 0.103 g/t Au from a rusty quartz vein with minor chlorite alteration and pyrite, and 0.617 g/t Au from a highly sheared metavolcanic rock with hematite staining and minor pyrite.

Current exposures consist of spherulitic and pillowed mafic metavolcanic flows displaying weak carbonate alteration along fractures and moderate shear-parallel hematitic alteration. The rocks also contain shear-parallel quartz veins ranging from 1 to 3 cm in width. Moderate amounts of pyrite and graphite are present within the shear zones and quartz veins. An analysis from a sample collected from a graphitic shear with 1 to 2% fine-grained pyrite and pyrrhotite yielded 228 ppm Cu (*see* Appendix 5).

SPEKE POINT CENTRAL

The Speke Point Central occurrence is located on the east shore of Lake Nipigon approximately 1.5 km north of the Speke Point South property (*see* Figure 3: property 2; *see* Preliminary Map P.3512: property 2) and has experienced the same work history as the Speke Point South (*see* Table 4). The showing is a 25-feet wide, 50-feet long zone of banded cherty magnetic iron formation and foliation-parallel quartz veins, containing zones of very fine disseminated pyrite and lesser chalcopyrite (D.C. Goodman 1997; H.K. Goodman 1997). The best gold assay obtained from this showing is 16.217 g/t Au from a narrow, pyritic, rusty quartz veinlet hosted in highly sheared mafic metavolcanic rocks. The showing also yielded some anomalous copper analyses, including 734 ppm Cu from a highly sheared mafic metavolcanic with 2 to 3% fine disseminated pyrite and 112 ppm Cu from a recrystallized, cherty, magnetite iron formation with minor pyrite, chalcopyrite and malachite staining.

Current exposure consists of vesicular, pillowed, mafic metavolcanic flows, chert-magnetite iron formation and pillow fragment breccia. Moderate to strong open-space and fracture-filling quartz tourmaline veins are present throughout the pillowed flows, and are associated with moderate hematite alteration. Pyrite and graphite occur in wall-rock fragments associated with a 10 to 30 cm wide quartz vein that crosscuts the iron formation. An analysis of a sample collected from the quartz vein yielded 280 ppm Cu and 161 ppm Zn (*see* Appendix 5).

SPEKE POINT NORTH

The Speke Point North occurrence is located on the shore of Lake Nipigon (*see* Figure 3: property 1; *see* Preliminary Map P.3512: property 2), approximately 300 m north of the Speke Point Central property in Kitto Township. The showing consists of a 100-feet wide zone of sheared mafic metavolcanic flows containing disseminated pyrite and chalcopyrite with silicification, chloritization, sericitization and iron carbonate alteration as well as a 6-feet wide magnetite iron formation. A rusty quartz vein, 10 inches wide occurs adjacent to the iron formation (D.C. Goodman 1997; H.K. Goodman 1997). The quartz vein and wall rocks are abundantly mineralized with pyrite and chalcopyrite, and contain quartz veins and stringers that occur along seams up to 3 feet wide. The zone contains a pillow breccia with highly silicified pillow fragments and pillows (*see* Table 5). The breccia contains up to 3% very finely disseminated pyrite and chalcopyrite with increasing sulphide mineralization in the fragmental sections. H.G. Goodman collected 35 samples from this showing in 1997, with the best gold assays reported as 1.509 g/t Au and 1.440 g/t Au from sheared, altered mafic metavolcanic rocks, rusty recrystallized quartz veins and magnetite iron formation. An analysis of 420 ppm Cu was obtained from a rusty sheared metavolcanic rock containing abundant pyrite and chalcopyrite mineralization adjacent to the pillow breccia.

A recent visit to the occurrence showed massive and pillowed flows and pillow fragment breccia as well as chert-magnetite iron formation. Shear-parallel quartz veins with pyrite, magnetite and carbonate alteration are also present. A grab sample from a quartz-vein crosscutting iron formation analyzed at 133 ppm Cu (*see* Appendix 5).

C.J. MORGAN

The C.J. Morgan occurrence is located south of the Princess Chain of Lakes (*see* Figure 3: property 5; *see* Preliminary Map P.3513: property 24), near the contact of the metasedimentary rocks of the SSB and the metavolcanic rocks of the NVB, approximately 3 km west of Beardmore. The metasedimentary rocks are located north of the Empire fault. The property consists of several bands of iron formation, that are 1 to 2 m wide and several metres long, with a few small gabbro intrusions (*see* Table 5). Initial work on the property was completed in the early 1940s and visible gold was reported from a major gossan zone that contained a 0.5 m wide quartz-carbonate vein that returned assay values of 1, 2 and 8 ounces of gold per tonne (Bent 1989b). In 1989, a joint venture between Golden Dragon Resources and Glen Auden Resources initiated reconnaissance geological mapping and sampling at the Morgan showing with the exception of stripped areas that were mapped at a scale of 1:500 and channel sampled (*see* Table 4). A VLF–EM ground geophysical survey was conducted over the entire property, which confirmed the presence of significant sulphide mineralization associated with at least one major structure interpreted to be the Empire fault.

The mineralized zone of sulphide and/or oxide iron formation hosted in sheared mafic metavolcanic rocks extends 85 m west and pinches out from 5 to 0.3 m wide. The iron formation is altered with a 0.8 m wide zone of massive sulphide mineralization consisting of 60% arsenopyrite and 40% pyrrhotite with an associated 5 m wide halo of strong iron-carbonate alteration. Present within this hydrothermal alteration zone are narrow, discontinuous, quartz veinlets in extensional fractures and quartz stringers, which host up to 5% disseminated cubic pyrite along their margins and within the host rocks. The host rocks to the south of the mineralized zone consists of strongly foliated, carbonatized and chloritized mafic pillowed flows. To the north are massive mafic pillowed flows with strong carbonate alteration. Of 19 grab samples collected from the property, the highest value returned was 5900 ppb Au. One quartz-carbonate vein sample was analyzed at 1700 ppb Au (Bent 1989b).

GOLD FIELDS

The Gold Fields property is located in southwestern Summers Township, east of the town of Beardmore, near the contact of the metasedimentary rocks of the SSB and the metavolcanic rocks of the SVB (*see* Figure 3: property 6; *see* Preliminary Map P.3513: property 25). In 1981, Gold Fields Mining Ltd. conducted 47.36 miles of line cutting, ground geophysical magnetometer and VLF–EM surveys and diamond-drilled 4 holes in 1982 (Knox 1981; *see* Table 4). In 1989, Golden Dragon Resources Ltd. and Glen Auden Resources Inc. conducted reconnaissance-scale mapping and sampling, mechanical stripping and a ground geophysical VLF–EM survey. The areas of mechanical stripping were mapped at a scale of 1:500 and channel sampled.

The showing consists of a quartz-carbonate vein exposed approximately 700 m east of the C.J. Morgan occurrence and hosted by foliated and strongly chloritized mafic metavolcanic rocks. The quartz-carbonate vein is approximately 20 cm wide and undulates along strike. Narrow discontinuous quartz-carbonate veinlets with 1 to 3% arsenopyrite and pyrite crystals are present in the host rock. Light green sericitization and iron staining is present along fractures and hosts up to 3% fine-grained disseminated crystals and stringers of arsenopyrite and pyrite along vein margins. Four channel samples of the vein material returned a value of 0.45 g/t Au. A grab sample from the reconnaissance mapping returned an assay of 10 g/t Au, and a channel sample of the wall rock assayed 1.7 g/t Au (Bent 1989b).

The 4 diamond drill holes, totalling 484.7 m, were drilled in a stratigraphic north to south section across the property (Bald 1982; *see* Preliminary Map P.3513). The holes intersected chloritized and carbonatized massive mafic flows and interflow chert-magnetite iron formations (OGS 2002). A number of quartz and quartz-carbonate veins containing varied amounts of pyrite, pyrrhotite and arsenopyrite were recorded, but no assays were reported. All 4 holes intersected graphitic shears that may represent faulting subparallel to the Princess and Empire faults. A fifth 122 m deep hole was drilled to the northeast in the metasedimentary rocks of the SSB (*see* Preliminary Map P.3513).

A recent property visit documented fine- to medium-grained massive mafic flows, pillowed flows, fine-grained tuff and fine- to medium-grained gabbro. The massive flows contains weak to moderate foliation-parallel and fracture-controlled boudinaged quartz veins that are 0.3 to 10 cm in width. Epidote and carbonate alteration are present as well as weak disseminated arsenopyrite. Two samples collected from the property returned the following analytical results:

Sample Number	Assay (ounce Au per ton)	Rock Type	Mineralization
5076	0.03	Fine to medium-grained gabbro	Disseminated arsenopyrite
5078	n.d	Mafic metavolcanic	Fine-grained sulphide

Base metal analyses from the property are reported in Appendix 5.

MORGAN SOUTH EXTENSION

The Morgan South extension is located 1.5 km west of Beardmore in the SVB, on a major tectonic break known as the Empire fault (*see* Figure 3: property 7; *see* Preliminary Map P.3513: property 26). The fault transects the property from the southwest to the northeast corner, separating the metavolcanic rocks to the south from the metasedimentary rocks to the north. Three main areas of the property were power stripped, blasted and sampled (*see* Table 4).

The showing consists of a quartz vein and quartz lens system hosted in moderately sheared, altered, and silicified mafic pillowed metavolcanic flows (*see* Table 5). The quartz veins and lenses are crackseal type, blue-grey and contain abundant arsenopyrite, pyrite and lesser chalcopyrite. The sulphide minerals are disseminated throughout the quartz, but there is some concentration along the lithologic contacts. The contact is highly sheared and sulphide mineralization and silicification extends for approximately 1 foot on either side of the contact. Chloritization and sericitization is found throughout the mineralized zone as well as in wall-rock seams within the quartz veins. Of the 30 grab samples collected by H.G. Goodman, 6 of the samples returned values that were higher than 1 g/t Au. The best assay results reported were 4.18 g/t Au from a dark grey quartz vein with up to 5% arsenopyrite, pyrite and chalcopyrite and 5.25 g/t Au from a white quartz vein with darker blue quartz containing 3 to 4% arsenopyrite-rich seams and abundant pyrite (Fekete 1992; H.G. Goodman, Jr. 1994; H.G. Goodman 1997).

RENTZ

The Rentz showing is located in southwestern Summers Township (*see* Figure 3: property 8; *see* Preliminary Map P.3513: property 28), approximately 1 km west of the town of Beardmore. The area is underlain by fine- to medium-grained massive and pillowed mafic metavolcanic rocks of the SVB and 2 units of banded iron formation (*see* Table 5). In 1989, Golden Dragon Resources and Glen Auden Resources conducted reconnaissance-scale mapping and sampling, mechanical stripping and a ground geophysical VLF–EM survey (*see* Table 4). The areas of mechanical stripping were mapped at a scale of 1:500 and channel sampled, and 2 areas were exposed by power stripping north and south of the Swamp Lake shear zone (Bent 1989b). To the north, the banded iron formation units are strongly oxidized and carbonatized with alternating bands of magnetite-rich material and jasper, and the area is approximately 1.5 m wide and 125 m long. Flat-lying, milky-white, fractured, quartz-carbonate veins, approximately 0.25 m wide, transect the banded iron formation. Some veins host arsenopyrite, sphalerite and pyrite along vein margins and other veins are without any trace of sulphide minerals. South of the shear zone, a 35 m wide zone of strongly sheared and hydrothermally altered pillowed and moderately carbonatized metavolcanic rocks with minor discontinuous quartz-carbonate stringers is exposed for 35 m along strike. The shear zone displays small-scale kink-folding, chloritization and limonite staining. Seven grab samples of sulphidized iron formation and host basalt were collected for analysis, and the highest assay value was 1.2 g/t Au. Six grab samples of quartz-carbonate vein and/or wall-rock material were collected, but yielded only low gold values.

A single 79.3 m hole drilled by Gold Fields in 1982 is located to the east of the Rentz occurrence (Bald 1982; *see* Preliminary Map P.3513). The hole intersected chloritized massive mafic flows and tuffs with occasional quartz-carbonate veins (OGS 2002). These veins may contain up to 3% arsenopyrite, but no assays have been reported.

Current exposure consists of massive and pillowed mafic metavolcanic rocks, chert-magnetite iron formation and 1 to 3 cm wide, fracture-filling quartz veins with tourmaline. Two samples were collected from partially filled trenches along the recent logging roads with the following analytical results:

Sample Number	Assay (ounce of Au per ton)	Rock Type	Mineralization
5092	n.d.	Quartz vein with tourmaline and carbonate alteration	Disseminated chalcopyrite and pyrite
5093	0.31	Iron formation	Fine-grained sulphide
5093	0.009	Quartz vein	Sulphide

Base metal analyses from the property are reported in Appendix 5.

BUFFALO–BEARDMORE

The Buffalo–Beardmore property is located in southern Summers Township (*see* Figure 3: property 10; *see* Preliminary Map P.3513: property 29), south of the Anglo–Beardmore showing. For a description of previous work on this property, refer to Speed and Craig (1992). Recent work on this property has included the Anglo–Beardmore occurrence in a single larger property, and is described with that occurrence.

Current exposure consists of mafic massive and pillowed flows, lapilli tuff and chert-magnetite iron formation. These units host weak to moderate fracture-controlled quartz veins, from 0.3 to 100 cm wide. Mineralization is present in the form of weakly to intensely disseminated to flooded pyrite, chalcopyrite and pyrrhotite. Analyses of grab samples from this location gave the following assays:

Sample Number	Assay (ounce Au per ton)	Rock Type	Mineralization
5058	n.d.	Massive flow, carbonate alteration	Massive sulphide
5061	n.d.	Quartz vein	Disseminated sulphide
5064	0.03	Massive flow	Gossan type

Base metal analyses from the property are reported in Appendix 5.

ANGLO–BEARDMORE

The Anglo–Beardmore property is located in southern Summers Township (*see* Figure 3: property 13; *see* Preliminary Map P.3513: property 30). For a description of past work on this property, refer to Speed and Craig (1992).

A total of 283 reverse-circulation holes were drilled on the occurrence by Legion Resource in 1987 (Sproule 1987; OGS 2002). No gold assays were reported, but a number of anomalous arsenic values were recorded with a high of 571 ppm As. A series of 23 diamond drill holes, totalling 3085 m, were drilled by A. Lafontaine in 1996 and 1997 on a number of targets on or around the Anglo–Beardmore and Buffalo–Beardmore occurrences (Goettel 1998; *see* Preliminary Map P.3513). Twelve holes had been completed in the area of the trenching and were sampled during this mapping project (*see* "Buffalo–Beardmore"). These holes intersected chloritized and carbonatized massive mafic flows and chert-magnetite iron formation, cut by quartz and quartz-carbonate veins. The iron formations are sulphidized with pyrite, pyrrhotite, chalcopyrite, and up to 40% arsenopyrite. The best assay reported was 3.16 g/t Au over 1.16 m in hole LA-96-12. Two holes, drilled approximately 500 m along strike to the west of the trenching, intersected up to 1.64 g/t Au over 0.49 m in a quartz vein with 5% arsenopyrite.

Current exposure consists of mafic massive and pillowed mafic flows and medium-grained gabbro. Moderate, pervasive carbonate alteration is present in all the rock types. Weak to intense mineralization in the form of disseminated pyrite is present in the mafic metavolcanic rocks. A sample from the massive flow unit assayed 0.08 ounce gold per ton and 158 ppm Cu (*see* Appendix 5).

HOLT

The Holt property is located in southern Summers Township near Warneford Creek (*see* Figure 3: property 11; *see* Preliminary Map P.3513: property 314), and is underlain by mafic metavolcanic rocks of the SVB. The showing consists of chert-magnetite iron formation hosted by mafic massive flows (*see* Table 5). Previous work consisted of stripping and collecting grab samples (Holt 1995; *see* Table 4). The following assay values were reported: 2.057, 2.5 and 5.5 g/t Au and 1.0, 1.1 and 1.4% Cu and 260.6 ppm Zn.

SUMMERS PIPELINE

The Summers Pipeline occurrence is located in southern Summers Township, and was previously named the Mathe showing (*see* Figure 3: property 12; *see* Preliminary Map P.3513: property 32). It is underlain by mafic metavolcanic rocks of the SVB. For a description of work up to 1988, refer to Speed and Craig (1992, p.247). In 1996, work consisted of prospecting, drilling, blasting and sampling (*see* Table 4). Prospecting was conducted to resample the Mathe showing and during this period, a new zone, the Summers Pipeline showing, was discovered. It consists of mineralized banded iron formation that is 11 to 12 feet wide where it is most strongly mineralized and contains a 1-foot wide quartz vein with arsenopyrite in the fractures (*see* Table 5).

Grab samples from the old showing assayed 2.057, 2.949 and 4.046 g/t Au from sugary quartz with sulphide seams, banded iron formation with 5% sulphide minerals, and quartz with 50% sulphide minerals, respectively. Grab samples from the new showing assayed 88.115, 17.417, 1.920 and 3.343 g/t Au from samples containing 90% arsenopyrite with quartz and pyrite, iron formation with 25% fine disseminated sulphide minerals, sugary iron formation with 10% disseminated sulphide minerals, and quartz with arsenopyrite, pyrite and pyrrhotite, respectively.

A single 80 m deep diamond drill hole intersected carbonatized massive mafic flows and interflow chert-magnetite iron formation (Thorsteinson 1984; OGS 2002). The best assay was 0.69 g/t Au over 0.3 m in a quartz vein hosted by iron formation.

Southern Metasedimentary Subbelt

The mineral occurrences, prospects and mines in the SSB are generally vein-type deposits, for example, the Leitch Mine and the Sand River Mine with crackseal-type quartz veins and the Northern Empire Mine with an *en échelon* quartz vein system. A number of showings are associated with a band of clastic-magnetite-argillite iron formation that crosses the SSB (e.g., Murphy, Undersill claims, and Long Lac Superior).

UNDERSILL CLAIMS

The Undersill claims are located in central Eva Township and extend to the west of Undersill Lake (*see* Figure 4: property 2; *see* Preliminary Map P.3513: property 6). In 1989, Mingold Resources conducted an exploration program consisting of 13.12 miles of contract line cutting, ground geophysical VLF–EM and magnetometer surveys at 400-foot spacing, till and rock lithogeochemical sampling, semidetailed geological mapping, and diamond drilling (Richardson 1988; Nelson 1989). Although no previous recorded work history exists in the assessment files prior to 1989, trenches and blasted pits were discovered on the property during the Mingold exploration program (*see* Table 4). East-northeast-striking interbedded argillite, siltstone and sandstone underlie the property, and foliation-parallel bedding strikes 080° with steep to vertical dips (*see* Table 5). Overall, the metasedimentary rocks contain trace to 2% disseminated, fine- to medium-grained pyrite and minor nonmineralized white quartz veins. A relatively thin band of chert-magnetite iron formation is interbedded with the clastic metasedimentary rocks and is 30.5 to 91.4 m thick, trends 080° and dips subvertically. Generally, the iron formation consists of finely laminated magnetite (75%) and chert ± jasper (25%), and is moderately deformed except near line 60 west where the iron formation is offset 90 m by a north-northeast-striking fault. In the fault zone, the beds are contorted, folded, kinked to ripped, boudinaged and broken (Nelson 1989). The iron formation and white quartz veins along and near the contact between the iron formation and the clastic metasedimentary rocks lack mineralization. The iron formation appears to feather out to the east and is overlain by Proterozoic diabase to the west. A massive north-northeast-striking gabbro dike, that is moderately magnetic and 61 m thick, intrudes the metasedimentary rocks in the northwest corner of the property, south of the Creek vein, and contains minor pyrite and arsenopyrite mineralization. A subhorizontal to gently west-dipping Proterozoic diabase sill overlies the metasedimentary rocks west of the gabbro dike. The best assay from the property was 3.0 g/t Au in a grab sample of the gabbro dike, which contains minor pyrite and arsenopyrite mineralization.

The diamond-drilling program consisted of 6 drill holes, totalling 656.1 m, that tested 2 target areas (Nelson 1989; *see* Preliminary Map P.3513; OGS 2002). Hole UND-1 was drilled in an approximate west direction and intersected a diabase and quartz gabbro containing grey to white quartz veins that host mineralization. Hole UND-2 is located northeast of UND-1 and intersected clastic metasedimentary rocks, diabase and gabbro. Further to the northeast, UND-3 intersected clastic metasedimentary rocks with minor disseminated pyrite and occasional quartz veining. The best assay was hosted by quartz veining in a sericite- and chlorite-altered shear zone. Holes UND-4, UND-4a and UND-5 were drilled approximately 500 m to the east of the first 3 holes and intersected clastic metasedimentary rocks and iron formation containing quartz and quartz-carbonate veins and stringers with trace to 1% disseminated pyrite. The best assay in UND-5 is associated with a blue-grey quartz vein in sheared metasedimentary rocks, and the best assay results from the drill holes are shown below:

Drill Hole Number	Assay (g/t Au over length)	Rock Type	Mineralization
UND-1	2.596 / 0.21 m	Quartz vein	1% pyrite
UND-3	1.125 / 0.76 m	Metasedimentary rocks	Trace pyrite
UND-5	1.644 / 0.15 m	Quartz vein	

CREEK VEIN

The Creek vein occurrence is located in central Eva Township (*see* Figure 4: property 1; *see* Preliminary Map P.3513: property 7) near the contact between the diabase and the metasedimentary rocks. The vein was drilled in 1935 by Sand River Gold Mines Company Ltd., but was considered too low grade at the time. The area was dormant until 1979 when Elcamber (Camel) Resources Ltd. acquired the property. They initiated a program that included collection and review of all available data, relocation, geological mapping, trenching, sampling and a ground geophysical magnetic survey (Tough and Gledhill 1979; *see* Table 4). In 1987 to 1988, Cryderman Gold established an exploration grid, conducted ground geophysical magnetic and VLF–EM surveys, completed some power stripping and some geological mapping and conducted diamond drilling (Rennick 1988). Gold values were present across widths from less than 1 foot to greater than 11 feet, along a minimum strike length of 700 feet. A section of the zone, 400 feet wide, averaged 0.189 ounce gold per ton across an average width of 6.125 feet. The results indicate that the Creek vein represents a complex system of auriferous, pyritic, quartz-carbonate shear zones within the diorite dike, possibly extending beyond the limits of the dike (Rennick 1988).

A series of 33 diamond drill holes, totalling 3962 m, were completed in the area of the Creek vein (Rennick 1988; OGS 2002). These holes intersected metasedimentary rocks of the SSB intruded by a diorite, probably similar to the posttectonic diorite exposed to the north, and crosscut by a north-trending diabase dike. The metasedimentary rocks are chloritized and sericitized and cut by quartz and quartz-carbonate veins with up to 10% pyrite, minor chalcopyrite, magnetite and arsenopyrite, and occasional coarse grains of visible gold. The best assays were from veins hosted by the brecciated margin phase of the diorite, with a high assay of 5.59 g Au/t over 4.02 m, but most intersections were approximately 0.5 m in width.

SAND RIVER MINE

The Sand River Mine is a past-producing gold mine from the early Beardmore gold camp (*see* Figure 4: property 5; *see* Preliminary Map P.3513: property 10). It is located in eastern Eva Township, southwest of the Leitch Mine. For past descriptions of the property, refer to Mason and White (1986). A series of 10 diamond drillLholes, totalling 612 m, were completed in the area of the Sand River vein by Cryderman Gold (Rennick 1988; OGS 2002). The holes intersected sericitized, chloritized and carbonatized metasedimentary rocks of the SSB cut by quartz and quartz-carbonate veins. The veins contain up to 6% pyrite with the best assay returned of 15.26 g/t Au over 0.27 m.

During the 2001 Phoenix Bedrock Mapping Project, 2 grab samples were collected from a quartz vein located north of the Sand River shaft, along the south side of the swamp containing the tailings from the Leitch Mine (*see* Figure 4). The quartz vein contains minor chlorite along fractures and up to 1% fine-grained disseminated arsenopyrite. The vein is bounded by sheared, chlorite and iron carbonate altered wacke up to 2 cm wide. Assays of the vein and wall-rock shear returned values of 0.04 and 0.01 ounce of gold per ton, respectively (*see* Appendix 4).

A composite longitudinal section of the Sand River Mine and Leitch Mine vein system was constructed based on the information contained in Ferguson (1967a, 1967b) (Figures 71, 72 and 73, *see* back pocket). These figures indicate that the Sand River Mine vein is part of the same northwest-dipping quartz vein that also hosted the Leitch Mine No. 2 vein. Gold mineralization is concentrated in west-plunging oreshoots (*see* Figure 71) of limited strike extent, but that have good down plunge continuity (*see* Figure 72). These figures indicate that the Sand River Mine vein has the potential to be as extensive below the diabase sill as the Leitch Mine No. 2 vein (*see* Figures 71, 72 and 73). The quartz veins located to the north of the Sand River Mine vein, sampled during this project, are similar to the Sand River Mine vein and have the potential to host similar mineralization with a similar vein geometry.

LEITCH MINE

The Leitch Mine is an important past-producer of gold in the Beardmore area (*see* Figure 4: property 6; *see* Preliminary Map P.3513: property 11). It is located in eastern Eva Township near the Summers Township boundary. For past descriptions of the property, refer to Mason and White (1986).

During the 2001 Phoenix Bedrock Mapping Project, a grab sample of a crackseal-textured quartz vein from the mine dump on the Leitch Mine property was sampled. The quartz vein assayed 1.75 ounces of gold per ton and 6934 ppm W (*see* Appendix 4).

A composite longitudinal section (*see* Figures 71, 72 and 73, *see* back pocket) was constructed from the longitudinal sections, surface and subsurface plans previously published by Ferguson (1967a, 1967b). There was conflicting information on these maps as the No. 3 vein is shown to strike north on the surface plan and northwest on the 900-foot level plan, and it was noted that No. 3 vein and the No. 1 vein merge at the 1800-foot level (Ferguson 1967a). This information was interpreted to indicate that this oreshoot had a twist, or change in plunge and strike direction down the length, and this convoluted shape is difficult to represent in a pseudo-three-dimensional drawing. As a result, the lower portion of the No. 3 vein in the longitudinal section looking 240° does not follow the trend of the other veins. The composite section is important for the following points:

- The Leitch Mine No. 2 vein and the Sand River Mine vein are the same vein, and represent separate ore shoots.
- The vein is foliation parallel and is at a low angle to the regional fold axis.
- The Leitch Mine No. 2 vein and the Sand River Mine vein are composed of multiple oreshoots that dip steeply to the north with steep west to northwest plunges.
- The dimensions and geometry of the oreshoots are controlled by a roughly west-striking and north-dipping structure.
- Mineralization continues for a short distance to the east past the change in strike.

Gold mineralization appears to be concentrated in a series of dilate zones in a single vein controlled by the intersection of 2 regional foliations. There is a potential for similar zones of dilatency to be present in other northeast-trending quartz veins in the SSB and CVB in the area of the fold in the SSB–CVB contact (*see* Figure 4). The structure controlling the veins in the Leitch Mine changes to the east near the contact between the SSB and the CVB, in the area of the No. 4 and No. 1 veins (*see* Figures 71 and 72). The No.1 vein appears to occupy the northwest-striking structure that controls the geometry of the oreshoots, but there is no indication in the literature that there were other auriferous veins in a similar orientation. The control on the orientation of the No. 4 vein is not clear, and further work is required to fully understand the important of the orientation of this vein.

Central Metavolcanic Subbelt

CALHET

The Calhet showing is located 350 m northwest of Minnow Lake in Summers Township (*see* Figure 4: property 15; *see* Preliminary Map P.3513: property 14). Previous work in the area consisted of surface stripping, removing of overburden and washing (*see* Table 4). The area is underlain by massive flows and green volcanic breccia containing weak to moderate carbonate and chlorite alteration (*see* Table 5). The volcanic breccia has a moderate shear fabric striking 080° and contains discoloured orange clasts that display a high degree of carbonate alteration. The contact between the breccia and the massive mafic flow is intensely sheared, intensely carbonatized and chloritized. The rocks are soft and fissile and contain *en échelon* quartz veins striking 110°, with narrow mineralized bands of pyrite with minor chalcopyrite and arsenopyrite. Twenty-five grab samples were taken from the area of the Calhet occurrence, of which 11 samples yielded anomalous gold values over 100 ppb Au and 3 significant values greater than 0.05 ounce of gold per ton. A grab sample collected from a grey to white banded quartz vein containing 2 to 3% disseminated pyrite and chalcopyrite assayed 0.107 ounce of gold per ton (Fekete 1992).

MINNOW LAKE

The Minnow Lake occurrence is located northeast of Minnow Lake in north-central Summers Township (*see* Figure 4: property 16; *see* Preliminary Map P.3513: property 15). The showing occurs in a 160 m wide zone of strong northeast-striking deformation with metasedimentary rocks bounded within mafic to intermediate metavolcanic rocks consisting of tuff and lapilli tuff (*see* Table 5). This zone is bordered to the north by lapilli tuff and to the south by pillowed and amygdaloidal and/or vesicular flows. Previous work on the property consisted of mechanical stripping and a beep mat survey (*see* Table 4). One mechanically stripped area revealed a wide mineralized zone of pyrite, magnetite and chalcopyrite. A sample collected from this zone is reported to have assayed 28 g/t Au (Lafontaine 1999).

CANDELA

The Candela occurrence is located in northwest Summers Township (*see* Figure 4: property 11; *see* Preliminary Map P.3513: property 16). Exploration work on the property consisted of diamond drilling from 1952 to 1954 by Candela Development Company (*see* Table 4). In 1987, Stratmin Resources conducted a magnetometer survey and geological mapping on an exploration grid (Lavoie 1987; Kilbourne 1987), which indicated that the property is underlain by light green aphanitic to fine-grained intermediate to mafic metavolcanic flows that generally trend 070° with vertical to subvertical dips (*see* Table 5). The flows generally contain amygdules filled with chlorite and/or quartz-carbonate that are up to 1 cm in size and are commonly foliated along cleavage planes. The foliation varies from very weak to intense with minor amounts of sericitization and carbonatization along cleavage planes. Minor tuffs contain white, angular to subangular quartzofeldspathic clasts and minor clasts of host rock that are commonly destroyed and altered by shearing. A breccia contains up to 30 cm angular bombs and metavolcanic clasts of intermediate to felsic composition surrounded by a fine-grained mafic volcanic matrix.

Two silicate-sulphide iron formations, striking approximately 070° with vertical dips, occur on the property. The northern iron formation was traced semi-continuously across the property, whereas the southern iron formation was only present in the eastern half of the claim group. The iron formations are composed of banded chert-magnetite hosting up to 3% pyrite, chert hosting 1 to 5% pyrite and chert-breccia consisting of chert and/or quartz nodules hosted within a siliceous tuffaceous matrix and commonly containing up to 30% coarse pyrite. Throughout the iron formations, pyrite occurs as fine-grained disseminations, aggregates and coarse discontinuous clots. High concentrations of massive pyrite appear in horizontal and vertical seams, ranging in width from 5 to 30 cm, and large massive clots of similar size. Quartz veins occur throughout the iron formations in 2 principal orientations: horizontal seams or fracture-fillings, and north-striking seams or fractures dipping vertically or at 45°. The veins generally do not contain sulphide mineralization and barren quartz veinlets transect pyrite aggregates indicating that the veins were emplaced after mineralization. Felsite sills or dikes, diabase dikes and gabbro intrusions also crop out on the property.

Sulphide mineralization was observed in 2 old trenches and is present as pyrite and magnetite in the iron formation. The trenches contain a series of quartz-carbonate veins that host abundant pyrite, chalcopyrite and malachite. The 5 to 15 cm wide veins are hosted in strongly schistose and sericitic mafic metavolcanic rocks and strike approximately 245°, with dips of 65° to the northwest. A fresh grab sample, collected from pyrite-chert iron formation containing 20% coarse pyrite and minor quartz carbonate, contained no significant assay results. A grab sample from a quartz-carbonate vein, containing chalcopyrite, malachite, pyrite and specularite, assayed 0.053 ounce of gold per ton and 2.26 ounces of silver per ton with 6.7% Cu and 4% Zn (*see* Appendixes 4 and 5).

Stratmin Resources completed a series of 8 diamond drill holes, totalling 1203 m, in the area around the Candela occurrence (Kilbourne 1987; OGS 2002). The holes intersected predominantly intermediate to mafic metavolcanic rocks with interflow chert-magnetic iron formation intersected in only 3 holes (SS8801, SS8805 and SS8806). Quartz and quartz-carbonate veins cut the metavolcanic rocks and contained varied amounts of sulphide mineralization. The best assay was 2.42 g/t Au over 1.46 m hosted by a quartz vein in a iron formation. Analyses of up to 1455 ppm Cu over 0.6 m were also returned from holes in the same area.

ARCHIE LAKE

The Archie Lake showing is located in north-central Summers Township below the western end of Archie Lake (*see* Figure 4: property 17; *see* Preliminary Map P.3513: property 17). Previous exploration work consisted of geological mapping, lithogeochemical sampling, trenching, ground geophysical magnetometer and VLF–EM surveys, airborne geophysical magnetometer survey, and diamond drilling (*see* Table 4). The property is located in the intermediate to mafic metavolcanic belt and hosted by sheared massive, pillowed and tuffaceous metavolcanic rocks. The area is associated with quartz veins, gabbro intrusions and diabase dikes. Quartz veins are associated with iron-carbonate alteration accompanied by epidote and tourmaline. Sulphide mineralization consists of pyrite, arsenopyrite and chalcopyrite.

Placer Dome completed a 5-hole diamond-drilling program, totalling 884 m, in the area around the Archie Lake occurrence (MacEachern 1989; OGS 2002). The holes intersected mafic metavolcanic rocks with varied feldspar phenocryst contents, an iron formation in one hole, and material described as metasedimentary rocks usually associated with fault zones. The lithologies are carbonatized and silicified with quartz veins and sulphide mineralization associated with the veins and as disseminations of up to 40% pyrite, chalcopyrite, and arsenopyrite. No assay results were reported.

COTÉ–ARCHIE LAKE

The Coté–Archie Lake showing is located in northern Summers Township approximately 1.5 km west of Archie Lake (*see* Figure 4: property 14; *see* Preliminary Map P.3513: property 33), and was discovered in 2001 by R. Coté, a local prospector. The property is underlain by massive mafic metavolcanic flows, and a fine-grained gabbro intrusion, that have been weakly to moderately iron carbonatized, and epidote and calcite altered. Epidote occurs as very small patches less then 0.3 cm in size. Mineralization consists of up to 10% fine-grained subhedral pyrite and 20% very fine-grained arsenopyrite in shear-parallel quartz veins that are 0.3 to 1 cm wide. Quartz veins contain sheared wall rock and wall-rock fragments along with massive to semi-massive blebs of sulphide minerals. Also present are north-striking magnetite-filled fractures less than 0.3 cm wide. The quartz veins are interpreted to be hosted by a shear subparallel to the Sandy Creek fault and the north limb of the regional Z-fold, in a dilatent zone associated with the nearby diorite intrusion. During a recent property visit in 2002, the authors sampled the property and obtained the following analytical values (*see* Appendix 4):

Sample Number	Assay (ounce of Au per ton)	Rock Type	Mineralization
444	n.d.	Massive, medium-grained gabbro	
444a	n.d.	Quartz stringer	Medium-grained euhedral arsenopyrite
444b	0.13	Quartz vein	Very fine-grained arsenopyrite and pyrite
444c	0.08	Quartz vein	Very fine grained arsenopyrite, fine-grained subhedral massive pyrite
444d	0.01	Mafic metavolcanic	Semi-massive needles of arsenopyrite

Northern Metavolcanic Subbelt

DOROTHEA GOLD PROPERTY

The Dorothea gold property is located in southeastern Dorothea Township (*see* Figure 5: property 4; *see* Preliminary Map P.3514: property 43), within intermediate to mafic metavolcanic rocks of the Poplar Point assemblage. In 1988, Glen Auden Resources conducted bedrock mapping, line cutting, ground geophysical induced polarization surveys and diamond drilling (*see* Table 4). In 1994, F. Houghton and P. Lassila shared ownership of 4 claims, and performed prospecting, power stripping and collected grab samples at several locations on the property (Lassila 1995, 1996, 1998). In 1996, additional prospecting, power stripping, bedrock mapping and ground geophysical magnetometer surveys were completed and 15 grab samples were collected for analysis. In May 1997, the property was optioned to Poplar Point Explorations, which completed line cutting, ground geophysical VLF–EM and magnetometer surveys, geological mapping, induced polarization surveys, prospecting, grab sampling and power stripping. A total of 24 grab samples were collected for analysis. The most recent work was completed in the spring of 1999, when prospecting was completed on the northern part of the property.

The Dorothea gold property consists of 2 mineralized zones with significant gold values. The first showing consists of carbonatized and sheared host rocks that contain quartz veins, pyrite, and arsenopyrite (*see* Table 5). Samples collected from these veins have assayed up to 0.174 ounce of gold per ton. The second showing returned values of 0.1, 0.22, 0.19 and 1.18 ounce of gold per ton from small quartz-calcite veins. The showings are hosted by well-fractured, fine-grained dacitic to rhyodacitic flows that have been moderately to intensely carbonatized and silicified to different degrees. The silicification is associated with quartz veining and minor pyrite in local minor to moderate shear zones. Five out of 15 grab samples, collected in 1996, were analyzed at between 5 and 444 ppb Au. Grab samples from various locations on the property returned assay values between 9 and 14 606 ppb Au with the highest values obtained from quartz-calcite veins with minor sulphide mineralization at the second showing. Grab samples, taken in 1997, were collected from quartz veins, iron carbonatized and silicified zones and pyritic zones. The following gold values were obtained from this sampling: 2.54 g/t Au from a pyritic quartz vein; 88.46 g/t Au and 1.47g/t Au from quartz-calcite veins; and 1.28 g/t Au from pyritic quartz-ankerite carbonatized breccia. Assay samples collected from trenches returned values of 1.28, 0.02, 0.69 and 0.19 g/t Au.

Current exposure consists of heterolithic, poorly sorted tuff breccia with angular to subangular clasts, fine- to medium-grained massive flow, quartz diorite, quartz feldspar porphyry and a 1 to 2 m wide coarse-grained gabbroic flow. Alteration consists of very weak fracture-filling epidote and intense, flooded chlorite. Extensional quartz, pyrite, malachite, 3 to 10 cm quartz veins are present along with moderate, disseminated fracture-filling pyrrhotite and pyrite. Results from assays (*see* Appendix 5) are shown below:

Sample Number	**Assay (ppm)**	**Rock Type**	**Mineralization**
229c	4554 Cu	Quartz vein	Disseminated pyrite
229b	2839 Cu	Quartz vein	Disseminated pyrite
229	126 Zn	Mafic metavolcanic	Disseminated to patchy pyrite and pyrrhotite
229	425 Cu	Mafic metavolcanic	Disseminated to patchy pyrite and pyrrhotite
369	332 Cu	Intermediate metavolcanic	Trace pyrite in fracture
369	151 Zn	Intermediate metavolcanic	Trace pyrite in fracture

Poplar Point Assemblage

JOHNSON–HOPKINS

In 1988, Glen Auden Resources completed a series of 6 diamond-drilled holes, totalling 891 m, in the same area as the drilling conducted by Hopkins (1959; OGS 2002; *see* Figure 5: property 2; *see* Preliminary Map P.3514: property 40). These drill holes intersected mafic to intermediate flows and breccias intruded by quartz diorite, feldspar and quartz-feldspar porphyry dikes. Rocks are sericitized and carbonatized and are cut by quartz and quartz-carbonate veins and stringers (Bent 1989a). Some diamond-drill sections contained trace to 1% fine-grained disseminated pyrite, and most assays were reported to be less than 500 ppb Au. The best assay was obtained from drill hole DDH-4, which returned 8.0 g/t Au and 8100 ppm As over a 0.6 m section containing a 12.7 cm wide quartz vein in a quartz diorite with trace pyrite. Hole DDH-3 intersected 2.3 g/t Au over 0.7 m in a strongly sericitized, altered quartz-feldspar porphyry cut by a 5 cm quartz-carbonate vein.

LAWRENCE–MCKIRDY

This showing is located in south-central Dorothea Township (*see* Figure 5: property 3; *see* Preliminary Map P.3514: property 41) to the east of the Johnson–Hopkins occurrence. The reader is referred to Bruce and Laird (1937) for an early description of this showing. In 1998, Glen Auden Resources conducted line cutting, a ground geophysical induced polarization survey and diamond drilling (*see* Table 4). In 1994, F. Houghton and P. Lassila stripped and assayed the old trenches. The original showing was described as a rusty shear zone, greater than 25 feet in length and 6 feet in width, hosted in mafic metavolcanic rocks. The shear zone hosts an intricate network of ankerite stringers with common calcite segregations. Along the hanging-wall side of the zone are irregular masses of quartz up to 6 inches in width. In the middle of the zone is a lens of siliceous vein material that is 6 to 12 inches in width and 20 feet in length and hosts arsenopyrite as well as pyrite and galena. A grab sample of this material yielded 0.08 ounce of gold per ton (Bruce and Laird 1937). Grab samples collected by Houghton and Lassila in 1994 returned assays between 0.1 and 0.2 ounce of gold per ton.

Two diamond drill holes completed by Glen Auden Resource in 1988 were located in the area of the Lawrence–McKirdy occurrence (Bent 19889a; OGS 2002; *see* Figure 5). These holes totalled 308 m and intersected carbonatized and silicified mafic flows and tuff breccias with up to 10% disseminated sulphides. The best intersection was 1.1 g/t Au over 0.91 m in a quartz vein with 10% arsenopyrite. In the same hole, a section of semi-massive pyrite and pyrrhotite was analyzed at 5950 ppm Cu.

Paint Lake Deformation Zone

PLACER DOME–METALORE

The Placer Dome–Metalore occurrence is located in eastern Sandra Township along the trace of the Paint Lake fault, within the metavolcanic rocks of the Onaman–Tashota terrane (*see* Figure 5: property 11; *see* Preliminary Map P.3514: property 49). A series of 4 diamond drill holes, totalling 984 m, intersected massive mafic flows and pillowed flows and metasedimentary rocks (Hunt 1989; OGS 2002). The flows are silicified to different degrees and are cut by quartz and quartz-carbonate veins with up to 10% pyrite and pyrrhotite, but no assays were reported. A number of graphitic argillite veins were intersected, and probably form part of the Paint Lake fault system.

HOLM

The Holm occurrence is located in northern Sandra Township on the west side of Pirum Lake (*see* Figure 5: property 10; *see* Preliminary Map P.3514: property 48). For work history prior to 1985, see Mackasey (1975) and Laird (1937). In 1985, Parquet Resources conducted line cutting, ground geophysical magnetometer and VLF–EM surveys, and diamond drilling (Pudifin 1987; *see* Table 4). The property is underlain by intermediate to felsic metavolcanic pyroclastic rocks and flows that form part of a belt located north of the Paint Lake fault and extending several miles east from Lake Nipigon. Pyroclastic rocks consist of tuff, tuff breccia and pyroclastic breccia. Commonly, the fragmental nature of these rocks can only be seen on clean, smooth weathered surfaces. Several zones of shearing and brecciation are mineralized with chalcopyrite and pyrite. The chalcopyrite mineralization was traced over a strike length of 525 feet by trenching and shallow diamond-drill holes. A series of quartz veins and disseminated chalcopyrite occur over widths of 50 to 150 feet. An average of 2.78% Cu was delineated in a zone 550 feet long, 2.67 feet wide and 80 feet deep within a quartz vein. A vein of chalcopyrite, pyrite and minor subrounded quartz fragments and chlorite and carbonate is located in one of the trenches. The vein is 7.5 to 10 cm wide by 15 m long and strikes 280°/70°. A channel sample from the trench was analyzed at 16.8% Cu, 0.09 ounce of gold per ton, and 3.55 ounces of silver per ton, with traces of cobalt, lead, molybdenum, nickel and zinc.

Parquet Resources completed a program of 6 diamond-drill holes, totalling 1535 m, that intersected carbonatized and silicified intermediate to felsic flows and tuffs, lapilli tuffs, and tuff breccias, diorites, and quartz and quartz-feldspar porphyritic dikes (Pudifin 1987; OGS 2002). These units are cut by quartz and quartz-carbonate veins and pyrite-pyrrhotite stringers are associated with the dikes. The best gold assay was 3.66 g/t Au over 0.91 m, and, in the same holes, semi-massive chalcopyrite was analyzed at 2.3% Cu over 0.10 m.

MILL CITY GOLD

The Mill City Gold occurrence is located in central Sandra Township along the trace of the Paint Lake fault, within the felsic to intermediate metavolcanic rocks of the Onaman–Tashota terrane (*see* Figure 5: property 8; *see* Preliminary Map P.3514: property 46). A series of 7 diamond-drill holes, totalling 2164 m, intersected intermediate flows and tuffs and clastic metasedimentary rocks that underlie a Proterozoic diabase sill (Paul 1988; OGS 2002). The rocks are cut by quartz and quartz-carbonate veins with brecciated zones and laminated veins of quartz-tremolite-epidote that have a description similar to the axinite-bearing quartz-chlorite veins exposed along the shore of Lake Nipigon. Up to 3% blebby to disseminated pyrite-pyrrhotite occurred in the metavolcanic rocks and sporadically in the veins. The best assay was 1.37 g/t Au over 1.43 m. A fault zone intersected in most holes is probably part of the Paint Lake fault system.

BASE METALS

The Leitch property was initially explored by numerous companies for iron deposits in the early 1900s. R. Cryderman discovered gold on the adjoining property, later to be known as the Sand River Mine, in 1934. Molybdenite was discovered in Dorothea Township in the 1950s and Lamble (1959) reported that the deposit contained a total of 7500 tons grading at least 1.5 % MoS_2 to a depth of 40 feet (Mackasey 1975).

Central Metavolcanic Subbelt

EVA LAKE PROPERTY

The Eva Lake property is located north of Eva Lake in northeastern Eva Township (*see* Figure 4: property 10; *see* Preliminary Map P.3513: property 12). The first recorded work on the property was in 1962, by Jensen, who conducted approximately 420 m of diamond drilling (*see* Table 4). This was followed by an extensive program of prospecting and sampling conducted by Meridian Mining from 1969 to 1971, which collected 230 representative samples at regular intervals across a 6000 m^2 area (Oja 1970). In 1991, under an OPAP (Ontario Prospectors Assistance Program) grant, H.G. Goodman, Jr. conducted power stripping, manual stripping, rock washing, prospecting, and sampling of various targets on the property (Goodman 1991). In 1995, A. Lafontaine performed prospecting, stripping, surface trenching and sampling and, in 1996, the prospecting area was extended, with mechanical stripping, bedrock trenching, and grab sampling also completed (Lafontaine and Lafontaine 1995a, 1995b, 1996). Subsequent prospecting was performed in 1997 (Lafontaine and Lafontaine 1997). The property consists of highly carbonatized and sheared feldspar porphyry that forms a topographic dome. It is locally siliceous and approximately 300 m in diameter. Thin section analysis indicates that the mineralization consists predominantly of fine-grained disseminated pyrite grains that are generally less then 5 mm in size with finer grained sphalerite, chalcopyrite and possibly argentite occurring within the pyrite grains. The mineralization is present in the carbonatized host rock as well as in black, mylonitic slip planes throughout the altered zone. A diabase dike, 100 feet wide striking approximately 010 to 020°, transects the central portion of the area.

In 1970, Meridian Mining obtained significant silver values from the main trench across a length of 50 feet. The silver assays were 8.76, 12.56, 17.6, 25.21 and 44 ounces of silver per ton. Twenty-four samples from outside the main trench returned assay values that ranged from trace amounts to 1.27 ounces of silver per ton with an average of 0.25 ounce of silver per ton. Significant assays from the 1991 exploration campaign include 100 ppm Cu and 280 ppm As from a white to rusty quartz vein containing coarse disseminated pyrite, 140 ppm As from a brecciated iron formation with quartz-pyrite replacement in bands of coarse crystals (50%), and 460 ppm As and 210 ppm Cu from a green quartz brecciated rock containing coarse-grained pyrite.

A. Lafontaine uncovered a disseminated to massive sulphide body in a trench, 5 m wide, 250 m long and 1 m deep, located in mafic to intermediate metavolcanic rocks. Mineralization consists of chalcopyrite, pyrite and sphalerite and significant assays include 0.013 g/t Au from a carbonatized, silicified porphyry and 813 ppm Ag from a mafic intrusive rock containing pyrite. Other significant assays for this showing are 305.145 g/t Ag and 0.053 g/t Au from a highly carbonatized gabbro, 500.2 ppm Cu and 103.6 ppm Zn from a carbonatized, silicified feldspar porphyry, and 2100 ppm Cu from a metavolcanic rock with no recognizable mineralization. An assay sample collected in 1997 from a well-mineralized shear zone yielded 1174 g/t Au and 15.77 g/t Ag.

On a recent visit to the property, the authors identified the exposed rock as a silicified massive mafic metavolcanic flow. It was pink-white to light grey in colour due to weak to intense carbonatization, and sericitization. A sample was taken for whole rock analysis and for geochronology (*see* Appendix 2: sample 229).

Southern Metasedimentary Subbelt

PRINCESS PROPERTY

The Princess property is located in southeastern Eva Township (*see* Figure 4: property 3; *see* Preliminary Map P.3513: property 5), south of Princess Lake and 3.2 km west of the Northern Empire Mine. Although it is underlain by metasedimentary rocks of the SSB, the property is situated just north of the contact between the metasedimentary rocks and the mafic metavolcanic rocks of the SVB. The showing consists of parallel quartz veins with pyrite-arsenopyrite hosted in shear zones and some iron formation (*see* Table 5). Previous work, consisting of prospecting to locate old trenches, hand mucking, blasting and minor stripping in areas of thin overburden, discovered a large shear zone with considerable malachite and pyrite mineralization. Grab samples from a trench within this shear zone, containing pyrite, chalcopyrite and malachite, was analyzed at 523, 855 and 1098 ppm Cu with no precious metals detected (MacAdam 1992).

MOLYBDENUM

Northern Metavolcanic Subbelt

TYSON #3

This showing is located in eastern Dorothea Township in the NVB (*see* Figure 5: property 7; *see* Preliminary Map P.3514: property 44). For previous work descriptions, refer to Mason and White (1986).

Current exposure consists of weakly carbonatized and hematized lapilli-tuff with feldspar phenocrysts and quartz veins 10 to 30 cm wide with sericite, ankerite, calcite and molybdenite. Molybdenite occurs as irregular-shaped flakes, and compound flakes, up to 2 cm in diameter, disseminated through the quartz vein. An assay of 3839 ppm Mo was obtained from a sample of quartz vein collected from the waste rock pile adjacent to the trenches (*see* Appendix 5).

PLATINUM GROUP ELEMENTS

Phoenix Occurrence

The occurrence, located in west-central Kitto Township, is situated on the southern contact between the peridotite and diabase in a stream bed (*see* Figure 3: property 4; *see* Preliminary Map P.3512: property 4). This occurrence was discovered during the 2001 Phoenix Bedrock Mapping Project in the stream bed located along the contact. The host rock consists of a fine-grained, dark green diabase containing trace to 1% pyrrhotite and pyrite, initially mapped as peridotite. Geochemically, an unmineralized sample from the sample location is similar to the diabase with some characteristics indicative of the assimilation of a minor amount of peridotite (*see* "Geochemistry"). Diabase in a nearby overlying outcrop has small, 0.3 to 1.0 cm wide, hornblende-albite fracture fillings that are common in the diabase near the contacts of the sills. A grab sample of the sulphide mineralized diabase returned 282 ppb Pd and 157 ppb Pt (*see* Appendix 6: sample 347a).

Recommendations For Mineral Exploration

GOLD MINERALIZATION

Axinite is a borosilicate mineral that, similar to tourmaline, is associated with gold mineralization in a number of areas in the Superior Province (e.g., Chibougamau, Cadillac, Porcupine, Kaministikaquia). However, as with tourmaline, axinite is not exclusive to gold deposits, but rather defines a set of physical conditions that favour the transport and deposition of gold. Nonetheless, the authors suggest that the axinite may be related to the gold mineralization, and encourage field and exploration geologists to pay special attention to axinite-rich regions (*see* Figure 12).

There is a potential for gold mineralization in the mafic and intermediate metavolcanic rocks adjacent to the subbelt and assemblage contacts. Past work has concentrated in the metasedimentary rocks in the area around the fold in the contact between the SSB–CVB. The potential for gold mineralization in the adjacent metavolcanic rocks is based on

- auriferous quartz-carbonate veins hosted by andesite flows in the adjacent CVB (e.g., Coté–Archie Lake occurrence)
- association with dilant zone created around a posttectonic diorite
- gold and molybdenite mineralization is also associated with a posttectonic diorite intrusion along the southern side of the BBA (e.g., Tyson occurrences)

There is a potential for gold mineralization, as well as copper and molybdenite mineralization in the metavolcanic rocks and associated posttectonic intrusions (*also see* “Base Metal and Gold Mineralization”).

There is the potential for additional gold mineralization in quartz veins hosted by structures subparallel to parallel to the Sand River Mine – Leitch Mine No. 2 vein. This vein is hosted by foliation-parallel brittle fractures with steep northwest dips and plunges of about 320°. Auriferous veins that are exposed along the south side of the swamp containing the Leitch Mine tailings are similar in appearance to the descriptions of the veins within the mines. The geometry of these veins is expected to be comparable to the Sand River Mine and Leitch Mine veins, which must be taken into consideration when drilling.

The southwest portion of the SVB in western Kitto Township has not been extensively explored, and not all of the older work in the area was recorded in the assessment files. This area has the potential to host gold mineralization similar to the iron-formation associated brittle-fracture-hosted quartz stringers of the Northern Empire Mine. The best areas for potential mineralization are in the iron formations along the northern boundary of the SSB.

VOLCANOGENIC MASSIVE SULPHIDE MINERALIZATION

Base Metals

The tuff breccia and andesite flows east of the basalt horizon in the Poplar Point assemblage have the potential to host volcanogenic massive sulphide base metal mineralization. This is based on

- an analysis of 344 ppm Zn in a sulphide patch in a tuff breccia (*see* Appendix 5)
- intense chloritization of the tuff breccia matrix
- synvolcanic felsic feeder dikes with peperitic contacts
- an FII-type geochemistry for the felsic dikes is commonly observed in felsic rocks with a high potential for volcanogenic massive sulphide mineralization

Although this area has been explored in the past, application of a northwest strike to the interpretation of the geological and geophysical data may present previously unrecognized targets for exploration.

BASE METALS AND GOLD MINERALIZATION

Co-incidence of structures related to faulting and the location of posttectonic diorite intrusions have the potential to host copper and/or molybdenum mineralization as well as gold mineralization. The area of best potential is along the northern boundary of the Poplar Point assemblage at the contact with the Bish Bay assemblage. This is based on the following observations:

- a pyrite-malachite-pyrrhotite quartz vein within quartz-feldspar porphyry contained 4554 ppm Cu (*see* Figure 57: sample 229)
- disseminated pyrite in a fine- to medium-grained feldspar porphyry was analyzed at 1366 ppm Cu (*see* Figure 57: sample 357)
- a sheared lapilli tuff containing 5% pyrite was analyzed at 28 708 ppm Cu (2.8%), 1105 ppm Zn and 349 ppm Ni (*see* Figure 57: sample 413)
- a sample of the Tyson No. 2 vein returned an analysis of 3839 ppm Mo
- gold mineralization occurs at the Tyson No. 1 vein
- axinite-bearing veins were observed in the basalts of the Bish Bay assemblage, to the west along the same structures

The potential for similar mineralization is possible along the CVB–SSB contact, based on

- the occurrence of multiple diorite sills
- locally intense carbonate alteration
- axinite-quartz-carbonate veins in the andesite
- the Archie Lake base metal occurrence associated with quartz veins, diorite intrusions and diabase dikes
- the Coté–Archie Lake gold showing in quartz pods is hosted by carbonatized andesite and intruded by diorite sills, which returned a best assay 0.31 ounce of gold per ton

PLATINUM GROUP ELEMENT MINERALIZATION

The basal contact of the peridotite and the adjacent diabase are the areas with a high potential to host PGE mineralization in the map area. This is based on the following observations:

- sulphide-mineralized diabase next to the basalt peridotite returned values of 282 ppb Pd and 157 ppb Pt
- Cu/Pd ratios are less than mantle values, but palladium values are slightly greater than mantle values, which are interpreted to indicate that the parental magma was not previously depleted in PGE, and is, therefore, a good source from which to concentrate PGE
- lower platinum and palladium values toward the base of the peridotite, possibly indicating an enrichment in PGE elsewhere in the peridotite
- minor sulphide mineralization in the adjacent metavolcanic rocks
- assimilation of metasedimentary rocks and hornfels of basalt and interflow iron formations, suggesting that some of the sulphur from the sulphide mineralization may have been assimilated

Random sampling of the diabase sills should also be performed. Depletion of PGE compared to the generally consistent concentration (e.g., *see* Figure 66) may be an indication of a PGE mineralizing event.

Appendix 1:

Analytical Methods and Detection Limits

Appendix 1. Analytical methods and detection limits.

Method	**Analytes**													
XRF:														
Major elements	SiO_2	TiO_2	Al_2O_3	Fe_2O_3	MnO	MgO	CaO	Na_2O	K_2O	P_2O_5	LOI			
units	*wt %*	*wt %*	*wt %*	*wt %*	*wt %*	*wt %*	*wt %*	*wt %*	*wt %*	*wt %*	*wt %*			
detection limits	*0.01*	*0.01*	*0.01*	*0.01*	*0.01*	*0.01*	*0.01*	*0.01*	*0.01*	*0.01*	*0.05*			
Trace elements	As	Nb	Y	Zr	Cr	Ni								
units	*ppm*	*ppm*	*ppm*	*ppm*	*ppm*	*ppm*								
detection limits	*2.000*	*2.000*	*1.000*	*3.000*	*4.000*	*2.000*								
IR Spectroscopy:														
	CO_2	S												
units	*wt %*	*wt %*												
detection limits	*0.03*	*0.01*												
ICP–MS:														
REE	La	Ce	Pr	Nd	Sm	Eu	Gd	Tb	Dy	Ho	Er	Tm	Yb	Lu
units	*ppm*	*ppm*	*ppm*	*ppm*	*ppm*	*ppm*	*ppm*	*ppm*	*ppm*	*ppm*	*ppm*	*ppm*	*ppm*	*ppm*
detection limits	*0.20*	*0.30*	*0.03*	*0.20*	*0.03*	*0.004*	*0.03*	*0.001*	*0.01*	*0.002*	*0.01*	*0.01*	*0.01*	*0.001*
Trace elements	Cs	Hf	Nb	Rb	Sr	Ta	Th	U						
units	*ppm*	*ppm*	*ppm*	*ppm*	*ppm*	*ppm*	*ppm*	*ppm*						
detection limits	*0.01*	*0.10*	*0.08*	*0.20*	*2.00*	*0.30*	*0.05*	*0.01*						
ICP–AES:														
	Be	Co	Cu	Mo	Sc	V	W	Zn						
units	*ppm*	*ppm*	*ppm*	*ppm*	*ppm*	*ppm*	*ppm*	*ppm*						
detection limits	*3.000*	*5.000*	*5.000*	*8.000*	*1.000*	*5.000*	*40.000*	*2.000*						
	Au	Pd	Pt	Sb										
units	*ppb*	*ppb*	*ppb*	*ppm*										
detection limits	*5.00*	*8.00*	*8.00*	*0.10*										
NFA–ICP–MS:														
	Ru	Rh	Pd	Ir	Pt	Au								
units	*ppb*	*ppb*	*ppb*	*ppb*	*ppb*	*ppb*								
detection limits	*0.13*	*0.08*	*0.11*	*0.04*	*0.14*	*0.73*								

Abbreviations:
ICP–AES, inductively coupled plasma atomic emission spectroscopy;
ICP–MS, inductively coupled plasma mass spectrometry;
IR, infrared;
NFA–ICP–MS, nickel fire assay – inductively coupled plasma – mass spectrometry;
XRF, X-ray fluorescence

Appendix 2:

Whole Rock Geochemical Analyses

Appendix 2. Whole rock geochemical analyses.

Field Number	**242**	**243**	**259**	**388**	**430**	**432**	**1171**	**1173**	**1264**
Lab Number	**01TRH038**	**01TRH037**	**01TRH044**	**01TRH075**	**01TRH082**	**01TRH083**	**01TRH046**	**01TRH045**	**01TRH036**
UTM East	416958	416812	417410	420265	422990	422813	416552	416140	416918
UTM North	5487794	5487918	5487839	5502452	5504031	5504423	5488890	5490670	5488202
Lithology	2	2	2	2	2	2	2	2	2
Symbol	○	○	○	○	○	○	○	○	○
SiO_2	47.44	47.23	46.14	46.74	49.77	50.27	52.98	52.29	45.41
TiO_2	1.27	0.96	0.89	2.55	1.16	1.00	1.49	1.06	0.82
Al_2O_3	14.43	16.19	15.42	12.62	15.08	14.35	15.05	14.96	14.43
Fe_2O_3	16.61	10.86	12.54	14.34	13.15	12.65	8.94	10.44	13.07
MnO	0.23	0.28	0.22	0.21	0.21	0.20	0.20	0.21	0.19
MgO	7.24	5.05	5.74	4.10	7.01	7.14	6.59	5.82	10.22
CaO	8.38	11.46	9.88	7.71	11.06	10.03	7.56	8.86	10.28
Na_2O	1.97	2.31	2.17	1.40	1.96	2.51	3.11	3.83	1.48
K_2O	0.10	0.12	0.06	0.61	0.17	0.26	0.28	0.16	0.07
P_2O_5	0.09	0.06	0.06	0.23	0.06	0.07	0.16	0.03	0.05
LOI	3.66	6.51	8.38	10.27	1.62	2.86	4.92	3.44	3.90
Total	101.43	101.02	101.51	100.80	101.26	101.34	101.27	101.09	99.91
Mg #	0.46	0.48	0.48	0.36	0.51	0.53	0.59	0.53	0.61
Rb	1.03	2.14	0.75	16.18	2.50	6.99	5.18	4.00	1.45
Sr	110.04	122.84	128.00	117.78	171.44	124.24	75.76	88.09	123.68
Cs	0.11	0.07	0.09	0.73	0.44	0.53	0.41	0.33	0.19
La	3.63	2.78	2.54	7.05	2.72	3.29	5.80	0.63	2.23
Ce	10.22	7.80	7.03	23.79	7.72	8.98	15.66	2.12	6.32
Pr	1.66	1.27	1.16	4.20	1.30	1.40	2.40	0.47	1.05
Nd	8.70	6.74	6.14	21.57	6.98	6.93	12.08	3.18	5.72
Sm	2.83	2.26	2.10	6.21	2.42	2.11	3.70	1.46	1.76
Eu	1.01	0.83	0.76	2.19	0.97	0.89	1.28	0.79	0.70
Gd	3.77	3.06	2.80	6.93	3.20	2.71	4.73	2.42	2.51
Tb	0.69	0.54	0.51	1.09	0.55	0.46	0.80	0.42	0.44
Dy	4.70	3.51	3.30	6.23	3.33	2.97	5.04	2.60	2.88
Ho	0.99	0.78	0.71	1.21	0.70	0.64	1.06	0.54	0.64
Er	2.90	2.27	2.00	2.98	1.92	1.84	3.00	1.51	1.89
Tm	0.43	0.34	0.31	0.42	0.29	0.28	0.45	0.23	0.29
Yb	2.70	2.18	2.02	2.50	1.70	1.72	2.80	1.42	1.86
Lu	0.43	0.33	0.30	0.38	0.27	0.27	0.42	0.20	0.28
As	2	5	9	14	n.d.	n.d.	2	18	7
Ta	n.d.	n.d.	n.d.	0.43	n.d.	n.d.	0.30	n.d.	n.d.
Nb	3.21	2.55	2.18	7.92	1.78	2.72	5.04	0.51	2.05
Nb*	n.d.	n.d.	n.d.	6	n.d.	n.d.	4	n.d.	n.d.
Hf	2.04	1.53	1.48	3.98	1.63	1.32	2.94	0.96	1.28
Zr	71.16	52.60	49.12	141.22	50.30	44.30	101.30	25.73	43.80
Zr*	70	51	49	143	45	41	106	22	41
Y	26.30	19.81	17.97	30.03	18.47	16.94	27.74	13.98	16.21
Y*	29	23	22	35	21	19	32	17	20
Th	0.27	0.21	0.19	0.39	0.39	0.20	0.50	n.d.	0.16
U	0.07	0.05	0.05	0.10	0.10	0.05	0.13	0.01	0.05
Cr	216	427	344	143	430	363	273	425	459
Ni	49	119	91	62	131	97	53	196	212
Ti/Zr	10.7	10.9	10.9	10.8	13.8	13.5	8.8	24.7	11.2
La/Yb_n	0.9	0.9	0.8	1.9	1.1	1.3	1.4	0.3	0.8
Zr/Y	2.7	2.7	2.7	4.7	2.7	2.6	3.7	1.8	2.7

Symbols as used in accompanying figures

Mg# cation Mg/(Fe+Mg)

* analyzed by XRF-trace

n.d. not detected

— not analyzed

Samples analyzed by ICP–MS, unless otherwise indicated

La/Yb n chondrite-normalized La: 0.329, Yb: 0.22; *from* Nakamura (1974)

Appendix 2. Continued

Field Number	**1266b**	**1268**	**2248**	**2249**	**2250**	**2250b**	**2251**	**2253**	**2254**
Lab Number	**01TRH057**	**01TRH028**	**01TRH035**	**01TRH034**	**01TRH033**	**01TRH058**	**01TRH031**	**01TRH029**	**01TRH030**
UTM East	415880	416265	416721	416426	416087	416087	415990	416046	416303
UTM North	5489335	5490833	5488568	5488693	5489018	5489018	5489617	5490035	5491282
Lithology	2	2	2	2	2	2	2	2	2
Symbol	○	○	○	○	○	○	○	○	○
SiO_2	49.72	50.70	45.53	48.18	47.25	47.64	44.22	50.00	46.18
TiO_2	0.74	2.35	1.00	1.19	0.59	0.98	1.98	1.42	1.25
Al_2O_3	12.08	14.98	16.05	15.48	15.00	14.39	14.16	14.47	14.92
Fe_2O_3	13.22	12.50	14.12	12.28	12.52	14.01	16.90	15.10	16.58
MnO	0.24	0.24	0.19	0.23	0.20	0.22	0.31	0.25	0.23
MgO	9.45	5.10	8.89	5.79	9.73	6.60	6.68	6.54	7.31
CaO	12.30	5.42	7.89	8.42	11.57	10.97	10.58	6.19	8.86
Na_2O	1.83	2.67	2.00	1.37	1.55	1.51	1.45	2.91	2.50
K_2O	0.10	0.26	0.31	1.17	0.19	0.24	0.11	0.09	0.13
P_2O_5	0.05	0.30	0.07	0.08	0.04	0.06	0.17	0.09	0.08
LOI	1.75	6.34	4.69	7.15	2.97	4.45	4.59	4.31	3.46
Total	101.48	100.88	100.73	101.33	101.62	101.08	101.16	101.37	101.50
Mg #	0.59	0.45	0.56	0.48	0.61	0.61	0.44	0.46	0.47
Rb	1.28	3.21	7.46	24.04	3.67	3.23	2.42	0.56	1.75
Sr	75.76	65.76	93.44	77.74	118.10	126.76	146.78	71.68	114.11
Cs	0.03	0.34	0.65	1.80	0.11	0.07	0.29	0.05	0.18
La	1.89	7.12	4.04	4.40	1.45	2.82	5.50	3.49	3.85
Ce	5.52	21.68	9.22	12.72	3.96	7.89	15.62	9.72	10.54
Pr	0.90	3.60	1.53	1.87	0.67	1.28	2.48	1.61	1.67
Nd	4.81	18.16	7.97	9.38	3.44	6.61	12.97	8.26	8.80
Sm	1.75	5.38	2.50	2.98	1.18	2.19	3.79	2.80	2.96
Eu	0.64	1.94	0.89	1.12	0.47	0.74	1.45	1.08	0.95
Gd	2.35	6.12	3.23	3.57	1.70	2.92	5.06	3.71	3.83
Tb	0.45	1.07	0.56	0.66	0.30	0.50	0.82	0.66	0.66
Dy	2.84	6.64	3.62	4.55	1.95	3.50	5.39	4.32	4.35
Ho	0.63	1.41	0.80	0.99	0.43	0.74	1.14	0.94	0.96
Er	1.78	4.11	2.33	2.98	1.28	2.24	3.31	2.86	2.78
Tm	0.28	0.60	0.35	0.46	0.20	0.33	0.49	0.42	0.43
Yb	1.80	3.87	2.28	2.98	1.25	2.21	3.05	2.65	2.77
Lu	0.29	0.61	0.36	0.48	0.19	0.35	0.50	0.40	0.42
As	n.d.	n.d.	n.d.	2	n.d.	n.d.	n.d.	n.d.	n.d.
Ta	n.d.	0.54	n.d.	n.d.	n.d.	n.d.	0.36	n.d.	n.d.
Nb	1.74	10.20	2.62	2.93	1.22	2.48	6.47	3.27	3.09
Nb*	n.d.	8	n.d.	2	n.d.	n.d.	6	2	2
Hf	1.27	3.68	1.74	1.94	0.84	1.55	2.37	2.08	2.01
Zr	41.94	135.64	60.29	66.43	27.29	54.82	87.01	68.86	69.56
Zr*	40	145	56	67	52	25	89	73	70
Y	16.36	35.62	21.52	25.09	10.97	20.58	29.57	23.15	24.18
Y*	17	42	24	28	23	14	33	28	28
Th	0.16	0.21	0.25	0.26	0.11	0.22	0.31	0.28	0.28
U	0.04	0.06	0.08	0.10	0.03	0.06	0.07	0.07	0.07
Cr	392	189	220	237	342	328	291	214	229
Ni	73	31	163	97	178	66	142	40	86
Ti/Zr	10.6	10.4	9.9	10.7	13.0	10.7	13.6	12.4	10.8
La/Yb_n	0.7	1.2	1.2	1.0	0.8	0.9	1.2	0.9	0.9
Zr/Y	2.6	3.8	2.8	2.6	2.5	2.7	2.9	3.0	2.9

Symbols as used in accompanying figures

Mg# cation Mg/(Fe+Mg)

* analyzed by XRF-trace

n.d. not detected

— not analyzed

Samples analyzed by ICP–MS, unless otherwise indicated

La/Yb n chondrite-normalized La: 0.329, Yb: 0.22; *from* Nakamura (1974)

Appendix 2. Continued

Field Number **Lab Number**	**202** **01TRH089**	**330** **01TRH069**	**368** **01TRH093**	**385** **01TRH072**	**386** **01TRH073**	**388b** **01TRH076**	**410** **01TRH080**	**1370** **01TRH086**	**225** **01TRH054**
UTM East	425210	425949	424453	420608	420610	420265	421716	420978	424517
UTM North	5504067	5504567	5504053	5503257	5503164	5502452	5502261	5503573	5499839
Lithology	3	3	3	3	3	3	3	3	4
Symbol	☐	☐	☐	☐	☐	☐	☐	☐	■
SiO_2	54.87	59.05	65.30	62.75	55.26	61.54	68.01	58.73	70.52
TiO_2	1.01	0.79	1.15	0.55	0.82	0.67	0.56	0.66	0.19
Al_2O_3	15.84	15.54	15.81	15.22	14.96	15.04	15.67	15.10	11.99
Fe_2O_3	9.34	7.76	5.63	5.74	8.05	6.08	4.15	7.65	3.75
MnO	0.17	0.09	0.06	0.10	0.13	0.11	0.06	0.10	0.08
MgO	2.49	3.51	0.97	1.96	2.00	1.82	1.22	3.21	0.66
CaO	5.71	4.06	2.52	4.22	7.32	3.64	3.23	4.80	2.46
Na_2O	2.81	4.23	4.34	3.82	3.51	2.93	4.28	4.16	4.57
K_2O	1.55	0.42	1.58	1.38	1.23	2.56	1.31	0.73	1.29
P_2O_5	0.16	0.17	0.17	0.14	0.19	0.13	0.12	0.15	0.03
LOI	7.14	5.77	2.67	4.91	7.59	6.30	2.10	5.84	4.56
Total	101.10	101.39	100.20	100.78	101.07	100.82	100.70	101.14	100.09
Mg #	0.35	0.47	0.26	0.40	0.33	0.37	0.37	0.45	0.26
Rb	51.97	13.24	67.20	43.27	36.26	39.23	35.05	14.00	28.93
Sr	105.25	97.72	152.22	117.92	93.60	100.38	202.88	149.14	74.09
Cs	1.26	1.66	2.50	1.49	1.00	1.62	1.68	> 5.00	1.01
La	12.10	13.22	23.76	13.50	10.86	14.37	17.04	11.85	30.28
Ce	27.91	29.50	50.02	28.26	24.93	31.19	35.06	14.14	67.78
Pr	3.80	3.82	6.39	3.41	3.23	3.90	4.29	10.04	8.76
Nd	15.90	15.06	19.28	13.07	13.29	15.35	16.16	85.03	36.13
Sm	3.86	3.40	4.58	2.83	3.15	3.29	3.43	> 30.00	8.57
Eu	1.23	0.99	1.43	0.89	0.96	1.01	1.00	> 5.00	1.58
Gd	4.31	3.56	4.76	2.68	3.30	3.26	3.32	> 30.00	8.53
Tb	0.69	0.58	0.92	0.43	0.55	0.50	0.52	> 5.00	1.41
Dy	4.35	3.59	4.76	2.55	3.35	3.10	3.10	37.99	8.83
Ho	0.93	0.76	1.15	0.54	0.74	0.63	0.64	> 10.00	1.85
Er	2.66	2.21	2.80	1.46	2.12	1.75	1.76	> 20.00	5.58
Tm	0.41	0.31	0.49	0.23	0.32	0.26	0.27	> 5.00	0.84
Yb	2.62	2.01	2.46	1.46	1.99	1.70	1.66	> 20.00	5.34
Lu	0.42	0.31	0.49	0.22	0.34	0.26	0.26	> 5.000	0.84
As	n.d.	2	n.d.	n.d.	3	12	12	7	3
Ta	0.49	0.49	0.60	0.48	0.48	0.48	0.56	15.56	1.06
Nb	7.31	7.87	11.84	6.44	7.90	6.93	6.98	6.52	15.01
Nb*	6	7	9	5	7	6	6	6	13
Hf	3.48	3.91	2.06	4.13	3.84	4.39	4.49	> 30.00	7.32
Zr	130.60	156.63	210.13	164.62	152.71	170.72	171.20	44.21	253.73
Zr*	132	159	210	166	154	169	168	167	284
Y	24.37	20.07	31.59	14.19	18.96	16.78	16.79	5.67	50.92
Y*	27	23	29	16	21	19	19	18	60
Th	1.92	1.85	5.20	1.92	1.43	2.06	3.35	18.22	7.05
U	0.55	0.51	1.42	0.52	0.39	0.55	1.01	16.78	2.01
Cr	95	143	24	90	168	118	157	173	37
Ni	31	37	n.d.	8	39	13	8	38	n.d.
Ti/Zr	4.6	3.0	3.3	2.0	3.2	2.4	2.0	8.9	0.4
La/Yb_n	3.1	4.4	6.5	6.2	3.6	5.7	6.9	0.4	3.8
Zr/Y	5.4	7.8	6.7	11.6	8.1	10.2	10.2	7.8	5.0

Symbols as used in accompanying figures

Mg# cation Mg/(Fe+Mg)

* analyzed by XRF-trace

n.d. not detected

— not analyzed

Samples analyzed by ICP–MS, unless otherwise indicated

La/Yb n chondrite-normalized La: 0.329, Yb: 0.22; *from* Nakamura (1974)

Appendix 2. Continued

Field Number	229	1267	444	1019a	1266a	2321a	4016	5000	267
Lab Number	01TRH063	01TRH027	01TRH084	01TRH010	01TRH032	01TRH087	01TRH090	01TRH064	01TRH047
UTM East	424326	416152	429578	424651	415880	420297	421043	421625	418080
UTM North	5503786	5491046	5499904	5490737	5489335	5506140	5506137	5510954	5488043
Lithology	4	6	7	7	7	7	7	7	8
Symbol	■	X	●	●	●	●	●	●	▷
SiO_2	70.54	52.39	51.96	49.80	48.74	40.19	51.37	47.08	55.62
TiO_2	0.71	0.39	1.84	1.46	0.82	0.45	1.16	0.94	0.33
Al_2O_3	14.12	14.78	13.16	14.80	14.68	7.36	13.67	15.55	20.05
Fe_2O_3	2.67	5.82	18.77	14.51	13.30	15.20	15.11	13.90	2.93
MnO	0.04	0.09	0.21	0.22	0.21	0.23	0.23	0.22	0.05
MgO	0.58	10.39	3.40	6.17	8.28	23.74	5.34	7.08	1.57
CaO	2.39	5.93	3.61	9.90	10.28	5.24	9.50	11.20	4.82
Na_2O	3.41	1.28	5.08	3.00	2.62	0.21	2.75	1.82	5.37
K_2O	2.50	4.56	0.09	0.69	0.12	0.06	0.08	0.05	3.64
P_2O_5	0.16	0.24	0.17	0.13	0.05	0.03	0.08	0.06	0.12
LOI	2.87	3.50	3.21	0.65	2.55	7.33	2.06	3.41	5.54
Total	100.00	99.39	101.50	101.35	101.66	100.07	101.34	101.31	100.03
Mg #	0.30	0.78	0.26	0.46	0.55	0.76	0.41	0.50	0.52
Rb	89.73	105.93	1.69	21.84	1.86	5.29	1.21	0.63	72.93
Sr	37.36	349.62	106.10	164.80	62.26	4.74	84.83	169.37	112.84
Cs	> 5.00	> 5.00	0.52	1.33	0.04	1.60	0.28	0.08	1.20
La	23.50	13.40	7.16	11.33	1.94	1.36	3.61	3.65	8.61
Ce	53.75	28.86	18.36	25.27	5.32	3.58	9.98	9.19	20.67
Pr	7.17	3.67	2.80	3.43	0.89	0.55	1.66	1.39	2.92
Nd	30.10	15.03	13.53	14.68	4.71	2.82	8.39	6.72	12.71
Sm	7.01	2.66	4.30	3.86	1.62	0.97	2.87	2.16	2.38
Eu	1.52	0.70	1.42	1.33	0.68	0.38	1.13	0.77	0.61
Gd	7.42	1.97	5.30	4.48	2.24	1.25	3.90	2.95	1.49
Tb	1.21	0.27	0.97	0.80	0.40	0.24	0.73	0.50	0.16
Dy	7.39	1.54	6.18	4.83	2.68	1.58	4.72	3.26	0.75
Ho	1.51	0.31	1.40	1.04	0.57	0.34	1.05	0.72	0.12
Er	4.48	0.82	4.07	2.92	1.63	1.05	3.15	2.08	0.30
Tm	0.65	0.13	0.61	0.41	0.25	0.15	0.48	0.33	0.04
Yb	4.08	0.77	3.89	2.65	1.60	1.00	3.13	2.13	0.21
Lu	0.63	0.12	0.64	0.40	0.26	0.16	0.49	0.34	0.04
As	8	n.d.	46	3	n.d.	n.d.	n.d.	4	n.d.
Ta	0.99	n.d.	0.35	0.36	n.d.	n.d.	n.d.	n.d.	n.d.
Nb	15.13	3.63	5.33	6.68	1.82	0.94	2.82	2.83	2.24
Nb*	12	2	4	5	n.d.	n.d.	n.d.	n.d.	n.d.
Hf	7.95	1.68	3.38	2.68	1.26	0.72	2.32	1.65	1.44
Zr	307.21	60.95	116.95	103.17	40.45	23.76	79.60	54.01	49.58
Zr*	340	54	116	108	42	23	68	54	49
Y	41.11	7.96	35.88	26.84	14.23	9.06	27.62	18.19	3.35
Y*	46	8	39	33	20	10	29	23	4
Th	4.63	2.72	0.69	2.09	0.16	0.10	0.35	0.37	1.19
U	1.19	0.78	0.18	0.70	0.04	0.04	0.10	0.10	0.26
Cr	48	1096	70	177	322	3007	71	311	50
Ni	n.d.	266	8	108	58	699	23	101	n.d.
Ti/Zr	1.4	3.8	9.4	8.5	12.2	11.4	8.7	10.4	4.0
La/Yb_n	3.9	11.6	1.2	2.9	0.8	0.9	0.8	1.1	27.4
Zr/Y	7.5	7.7	3.3	3.8	2.8	2.6	2.9	3.0	14.8

Symbols as used in accompanying figures

Mg# cation Mg/(Fe+Mg)

* analyzed by XRF-trace

n.d. not detected — not analyzed

Samples analyzed by ICP–MS, unless otherwise indicated

La/Yb n chondrite-normalized La: 0.329, Yb: 0.22; *from* Nakamura (1974)

Appendix 2. Continued

Field Number	**387**	**140**	**398**	**408b**	**413**	**2156**	**208**	**276**	**1196**
Lab Number	**01TRH074**	**01TRH067**	**01TRH077**	**01TRH079**	**01TRH081**	**01TRH068**	**01TRH049**	**01TRH048**	**01TRH051**
UTM East	420575	421285	429070	423647	425378	421515	418108	418374	416249
UTM North	5502710	5497392	5498910	5502907	5504961	5499047	5492022	5491669	5492644
Lithology	8	9	9	9	9	9	10g	10g	10g
Symbol	▷	◓	◓	◓	◓	◓	◀	◀	◀
SiO_2	66.37	50.68	61.62	58.22	53.75	55.82	51.18	51.08	53.24
TiO_2	0.39	0.70	0.67	1.24	0.69	0.74	2.26	2.61	2.12
Al_2O_3	14.87	17.84	16.32	14.21	16.15	16.98	13.90	14.13	14.99
Fe_2O_3	3.81	10.24	6.33	11.92	7.91	8.02	12.96	14.10	10.36
MnO	0.07	0.17	0.08	0.18	0.12	0.11	0.18	0.18	0.14
MgO	1.16	5.79	3.74	1.55	3.44	3.29	6.07	4.71	5.53
CaO	3.42	5.15	4.27	5.00	5.27	10.88	9.42	7.96	8.71
Na_2O	3.89	3.95	5.30	3.70	3.33	2.06	2.54	2.69	3.17
K_2O	1.93	1.86	0.12	2.49	1.04	0.03	1.17	1.69	1.71
P_2O_5	0.12	0.23	0.15	0.56	0.12	0.12	0.18	0.25	0.28
LOI	4.61	4.40	2.67	1.76	9.24	3.33	1.31	1.19	0.97
Total	100.65	101.00	101.26	100.83	101.07	101.39	101.17	100.59	101.23
Mg #	0.38	0.53	0.54	0.21	0.46	0.45	0.48	0.40	0.51
Rb	43.29	47.24	2.98	54.84	30.96	0.52	29.90	35.08	32.75
Sr	134.79	> 450.00	255.75	188.47	129.16	242.38	> 450.00	> 450.00	> 450.00
Cs	1.71	1.32	0.48	3.91	3.66	0.15	0.50	0.52	0.44
La	16.14	17.90	12.48	32.84	14.71	9.73	22.33	28.79	30.14
Ce	34.15	37.99	28.34	68.85	30.45	22.76	48.60	62.93	65.52
Pr	4.04	4.75	3.66	8.97	3.63	2.98	6.46	8.46	8.94
Nd	14.85	18.57	14.56	36.80	13.93	12.51	28.06	35.88	38.31
Sm	2.90	3.70	3.15	7.61	3.10	3.04	6.14	7.65	7.95
Eu	0.78	1.00	1.00	2.27	0.95	0.92	1.95	2.32	2.40
Gd	2.41	3.18	3.20	6.55	3.04	3.33	5.64	6.87	7.09
Tb	0.35	0.47	0.51	0.97	0.50	0.53	0.79	0.97	0.98
Dy	1.92	2.71	3.05	5.63	3.11	3.23	4.27	5.23	5.45
Ho	0.40	0.54	0.65	1.19	0.66	0.68	0.76	0.94	0.96
Er	1.05	1.55	1.80	3.23	1.86	1.91	2.00	2.39	2.55
Tm	0.16	0.24	0.28	0.48	0.29	0.28	0.27	0.32	0.33
Yb	1.04	1.47	1.73	3.08	1.80	1.85	1.58	1.83	1.90
Lu	0.16	0.24	0.27	0.48	0.30	0.29	0.23	0.28	0.29
As	11	30	n.d.	8	n.d.	6	n.d.	n.d.	n.d.
Ta	0.69	0.37	0.46	0.61	0.45	0.38	0.60	0.73	0.75
Nb	8.57	5.74	6.70	9.43	6.24	5.94	10.36	12.70	13.73
Nb*	7	4	6	7	5	4	8	10	10
Hf	3.72	2.51	4.16	5.05	3.43	2.88	4.00	4.88	5.42
Zr	141.76	99.37	158.87	179.69	129.05	112.93	152.28	184.88	216.17
Zr*	137	91	156	176	125	111	140	184	184
Y	11.00	14.95	17.26	29.58	16.89	18.53	20.39	24.09	25.54
Y*	13	17	20	34	19	20	23	28	28
Th	2.96	3.88	1.85	5.99	1.99	1.56	2.16	2.45	2.79
U	1.05	1.16	0.62	1.49	0.63	0.39	0.47	0.53	0.62
Cr	65	235	134	43	139	141	151	78	194
Ni	n.d.	45	34	n.d.	35	54	77	67	65
Ti/Zr	1.6	4.2	2.5	4.1	3.2	3.9	8.9	8.5	5.9
La/Yb_n	10.4	8.1	4.8	7.1	5.5	3.5	9.5	10.5	10.6
Zr/Y	12.9	6.6	9.2	6.1	7.6	6.1	7.5	7.7	8.5

Symbols as used in accompanying figures

Mg# cation Mg/(Fe+Mg)

* analyzed by XRF-trace

n.d. not detected

— not analyzed

Samples analyzed by ICP–MS, unless otherwise indicated

La/Yb n chondrite-normalized La: 0.329, Yb: 0.22; *from* Nakamura (1974)

Appendix 2. Continued

Field Number	**92**	**96**	**240**	**241**	**1195**	**1198**	**1269**	**2244**	**2246**
Lab Number	**01TRH021**	**01TRH020**	**01TRH043**	**01TRH042**	**01TRH050**	**01TRH052**	**01TRH026**	**01TRH041**	**01TRH040**
UTM East	419902	420313	417099	416727	416096	416438	415538	416643	416566
UTM North	5490217	5489848	5486830	5487103	5492500	5492698	5492452	5487270	5487575
Lithology	10	10	10	10	10	10	10	10	10
Symbol	▼	▼	▼	▼	▼	▼	▼	▼	▼
SiO_2	47.04	45.02	41.30	41.67	46.69	47.70	45.28	41.65	41.90
TiO_2	1.10	0.73	0.83	0.83	1.05	1.24	0.75	0.84	0.83
Al_2O_3	7.31	3.68	4.26	3.94	5.64	5.84	3.46	4.21	4.12
Fe_2O_3	15.03	14.97	16.76	16.43	14.51	14.60	15.16	17.05	16.86
MnO	0.19	0.20	0.22	0.22	0.22	0.20	0.20	0.21	0.21
MgO	19.92	25.78	30.18	28.56	20.66	18.30	26.12	29.69	30.78
CaO	8.11	8.84	3.54	5.32	9.64	10.58	8.94	4.00	3.78
Na_2O	1.44	0.69	0.62	0.48	0.97	1.26	0.69	0.49	0.59
K_2O	0.48	0.23	0.49	0.52	0.49	0.48	0.24	0.52	0.46
P_2O_5	0.12	0.06	0.09	0.08	0.10	0.12	0.06	0.09	0.09
LOI	0.18	0.24	1.64	1.63	0.74	0.48	0.21	1.12	0.57
Total	100.93	100.46	99.92	99.69	100.70	100.78	101.12	99.87	100.19
Mg #	0.72	0.77	0.78	0.78	0.74	0.71	0.77	0.78	0.78
Rb	12.02	5.62	12.22	13.05	11.72	11.80	5.17	13.68	10.88
Sr	302.28	142.42	194.76	158.72	225.42	248.55	137.55	170.48	180.27
Cs	0.32	0.13	0.29	0.27	0.38	0.26	0.11	0.28	0.29
La	11.55	6.28	9.18	8.26	11.25	12.26	6.23	9.31	8.97
Ce	26.31	15.06	20.05	19.26	25.23	28.46	15.02	19.97	19.76
Pr	3.58	2.13	2.60	2.62	3.44	3.95	2.16	2.60	2.60
Nd	15.42	9.43	11.17	11.68	15.46	17.99	9.85	11.06	11.46
Sm	3.44	2.32	2.48	2.61	3.42	4.14	2.39	2.43	2.38
Eu	1.08	0.74	0.83	0.70	1.15	1.20	0.70	0.68	0.79
Gd	3.16	2.18	2.09	2.24	3.42	3.83	2.33	2.18	2.16
Tb	0.45	0.32	0.30	0.33	0.50	0.59	0.34	0.30	0.30
Dy	2.47	1.80	1.64	1.84	2.71	3.06	1.94	1.66	1.66
Ho	0.45	0.31	0.28	0.32	0.49	0.57	0.33	0.30	0.30
Er	1.16	0.83	0.70	0.84	1.27	1.44	0.88	0.77	0.77
Tm	0.16	0.12	0.10	0.11	0.16	0.20	0.11	0.10	0.10
Yb	0.94	0.67	0.62	0.67	0.97	1.14	0.68	0.64	0.60
Lu	0.13	0.09	0.09	0.09	0.14	0.16	0.10	0.09	0.10
As	n.d.	n.d.	n.d.	n.d.	n.d.	n.d.	n.d.	n.d.	n.d.
Ta	n.d.	n.d.	n.d.	n.d.	0.30	0.33	n.d.	n.d.	n.d.
Nb	5.20	2.98	4.13	3.90	5.02	5.72	3.02	4.42	4.21
Nb*	4	2	3	3	4	5	3	3	4
Hf	2.14	1.20	1.56	1.46	2.08	2.34	1.38	1.53	1.63
Zr	81.67	46.37	57.82	54.97	73.45	88.33	48.59	56.04	60.65
Zr*	72	41	47	48	70	83	44	52	54
Y	11.47	8.19	7.44	8.08	12.12	14.66	8.24	7.37	7.69
Y*	15	10	10	10	14	18	10	10	10
Th	1.06	0.57	0.71	0.63	0.95	1.11	0.64	0.75	0.76
U	0.22	0.12	0.19	0.18	0.20	0.21	0.14	0.20	0.19
Cr	91	1641	3912	3235	1875	1789	2460	3230	3267
Ni	40	555	1252	1061	557	469	764	1158	1162
Ti/Zr	8.1	9.4	8.6	9.1	8.6	8.4	9.3	9.0	8.2
La/Yb_n	8.2	6.3	9.9	8.2	7.8	7.2	6.1	9.7	10.0
Zr/Y	7.1	5.7	7.8	6.8	6.1	6.0	5.9	7.6	7.9

Symbols as used in accompanying figures

Mg# cation Mg/(Fe+Mg)

* analyzed by XRF-trace

n.d. not detected

— not analyzed

Samples analyzed by ICP–MS, unless otherwise indicated

La/Yb n chondrite-normalized La: 0.329, Yb: 0.22; *from* Nakamura (1974)

Appendix 2. Continued

Field Number	**2247**	**2256**	**2258**	**2259**	**2260**	**3001**	**3002**	**3005**	**3025**
Lab Number	**01TRH039**	**01TRH025**	**01TRH024**	**01TRH023**	**01TRH022**	**01TRH060**	**01TRH061**	**01TRH059**	**01TRH055**
UTM East	416716	415749	415522	416010	416383	419157	419047	419575	415783
UTM North	5487585	5491843	5492590	5492901	5493528	5491909	5491882	5491815	5492140
Lithology	10	10	10	10	10	10	10	10	10
Symbol	▼	▼	▼	▼	▼	▼	▼	▼	▼
SiO_2	44.00	44.20	44.10	43.58	41.07	44.68	46.51	42.00	42.88
TiO_2	0.78	1.10	0.65	0.68	0.65	0.86	0.93	0.70	0.97
Al_2O_3	3.76	5.02	2.84	3.16	3.02	4.02	15.67	3.24	3.32
Fe_2O_3	15.48	15.88	15.61	16.93	16.79	16.43	—	17.87	16.26
MnO	0.20	0.20	0.20	0.22	0.22	0.23	0.21	0.23	0.21
MgO	26.94	25.85	28.66	28.96	28.72	24.46	21.25	28.33	29.12
CaO	7.55	6.15	7.91	6.58	4.93	8.39	8.83	6.09	5.00
Na_2O	0.76	1.06	0.55	0.48	0.27	0.59	1.05	0.42	0.44
K_2O	0.27	0.40	0.21	0.26	0.27	0.34	0.40	0.29	0.72
P_2O_5	0.07	0.11	0.06	0.06	0.07	0.08	0.08	0.08	0.12
LOI	0.46	0.60	0.23	0.27	4.78	0.72	0.15	1.05	0.93
Total	100.27	100.58	101.02	101.17	100.78	100.78	101.18	100.30	99.97
Mg #	0.78	0.76	0.78	0.77	0.77	0.75	0.73	0.76	—
Rb	6.13	8.95	4.67	6.11	6.79	7.98	9.08	6.92	17.31
Sr	157.57	204.83	146.27	112.83	45.35	154.01	247.26	151.03	113.40
Cs	0.14	0.37	0.11	0.18	0.31	0.32	0.22	0.22	0.42
La	7.20	11.35	5.77	7.40	6.56	10.52	8.78	7.11	13.08
Ce	17.19	25.85	13.32	15.20	14.16	20.41	20.25	15.76	28.56
Pr	2.36	3.44	1.85	2.00	1.89	2.72	2.86	2.06	3.78
Nd	10.50	15.24	8.42	8.87	8.17	11.83	12.59	9.18	15.88
Sm	2.46	3.38	2.01	1.96	1.84	2.63	3.01	1.96	3.38
Eu	0.75	0.96	0.61	0.64	0.58	0.91	0.93	0.63	0.91
Gd	2.30	2.92	1.92	1.93	1.69	2.52	2.78	1.91	3.08
Tb	0.34	0.41	0.27	0.27	0.24	0.37	0.41	0.26	0.42
Dy	1.83	2.28	1.55	1.51	1.36	1.95	2.27	1.46	2.29
Ho	0.33	0.40	0.29	0.27	0.25	0.38	0.40	0.27	0.41
Er	0.86	1.11	0.73	0.70	0.70	0.90	1.05	0.65	1.06
Tm	0.12	0.14	0.09	0.10	0.09	0.13	0.14	0.09	0.13
Yb	0.72	0.85	0.57	0.60	0.56	0.75	0.81	0.53	0.89
Lu	0.10	0.13	0.09	0.09	0.08	0.11	0.11	0.07	0.13
As	n.d.	n.d.	n.d.	n.d.	n.d.	n.d.	n.d.	n.d.	n.d.
Ta	n.d.	0.40	n.d.	n.d.	n.d.	n.d.	n.d.	n.d.	0.38
Nb	3.53	5.68	2.99	3.02	2.85	3.97	4.26	3.00	6.48
Nb*	2	4	2	3	3	3	4	2	5
Hf	1.51	2.11	1.23	1.37	1.16	1.45	1.75	1.11	2.48
Zr	54.60	76.88	42.55	47.96	40.71	52.28	65.02	41.90	92.90
Zr*	48	77	38	41	38	51	59	36	88
Y	8.70	10.18	6.67	6.66	6.25	9.27	10.91	7.01	10.72
Y*	10	13	9	9	8	12	13	10	13
Th	0.65	1.07	0.54	0.57	0.49	0.67	0.83	0.48	1.21
U	0.13	0.21	0.11	0.12	0.11	0.13	0.17	0.11	0.32
Cr	2402	2891	2568	2669	2603	2107	1930	2111	3050
Ni	853	921	902	944	995	716	604	939	1048
Ti/Zr	8.6	8.6	9.2	8.5	9.6	9.9	8.6	10.0	6.3
La/Yb_n	6.7	8.9	6.8	8.2	7.8	9.4	7.2	9.0	9.8
Zr/Y	6.3	7.6	6.4	7.2	6.5	5.6	6.0	6.0	8.7

Symbols as used in accompanying figures

Mg# cation Mg/(Fe+Mg)

* analyzed by XRF-trace

n.d. not detected

— not analyzed

Samples analyzed by ICP-MS, unless otherwise indicated

La/Yb n chondrite-normalized La: 0.329, Yb: 0.22; *from* Nakamura (1974)

Appendix 2. Continued

Field Number	**3027**	**15a**	**15b**	**15c**	**51a**	**51b**	**52**	**53**	**56**
Lab Number	**01TRH056**	**01TRH013**	**01TRH014**	**01TRH015**	**01TRH001**	**01TRH002**	**01TRH003**	**01TRH004**	**01TRH005**
UTM East	417107	424590	424590	424590	424944	424914	424794	424659	424307
UTM North	5494150	5490279	5490279	5490279	5485067	5485081	5484969	5484851	5484556
Lithology	10	12	12	12	12	12	12	12	12
Symbol	▼	▽	▽	▽	▽	▽	▽	▽	▽
SiO_2	42.14	49.34	49.13	50.06	49.72	50.63	50.64	49.44	50.09
TiO_2	0.56	1.07	1.06	1.13	1.31	1.63	1.65	2.49	1.31
Al_2O_3	3.20	15.60	16.30	16.58	15.09	14.28	15.10	13.53	16.11
Fe_2O_3	16.14	13.61	13.60	12.96	14.60	15.68	15.22	18.54	13.70
MnO	0.21	0.20	0.20	0.19	0.21	0.23	0.22	0.25	0.20
MgO	31.28	8.01	7.49	6.74	6.76	5.28	4.81	4.14	5.90
CaO	5.39	10.96	10.60	11.05	10.70	9.44	9.15	8.82	10.74
Na_2O	0.44	2.27	2.38	2.54	2.43	2.74	2.97	2.90	2.62
K_2O	0.22	0.39	0.45	0.44	0.53	0.75	0.86	0.77	0.53
P_2O_5	0.05	0.09	0.10	0.11	0.11	0.16	0.16	0.18	0.11
LOI	0.43	n.d.	0.19	0.09	0.27	0.53	0.58	0.45	0.18
Total	100.06	101.52	101.50	101.88	101.74	101.36	101.37	101.50	101.49
Mg #	0.79	0.54	0.52	0.51	0.48	0.40	0.39	0.31	0.46
Rb	5.32	10.77	12.43	12.26	14.94	23.71	25.26	22.87	14.40
Sr	126.75	159.51	164.69	168.68	157.25	165.74	179.00	168.83	173.91
Cs	0.27	0.38	0.64	0.58	0.90	1.16	0.63	0.91	0.55
La	4.80	7.73	7.73	8.53	8.26	12.30	12.60	13.88	9.07
Ce	10.85	17.36	17.15	19.26	18.91	27.48	28.39	31.38	20.34
Pr	1.48	2.39	2.34	2.61	2.56	3.71	3.86	4.26	2.82
Nd	6.75	10.44	10.31	11.38	11.41	16.32	16.93	18.84	12.06
Sm	1.60	2.92	2.77	3.10	3.13	4.43	4.50	5.05	3.35
Eu	0.52	1.07	1.01	1.10	1.08	1.46	1.49	1.71	1.20
Gd	1.52	3.42	3.21	3.66	3.73	5.13	5.29	5.92	3.81
Tb	0.21	0.59	0.55	0.65	0.64	0.89	0.92	1.03	0.67
Dy	1.21	3.63	3.54	3.89	4.00	5.45	5.56	6.34	4.12
Ho	0.22	0.77	0.74	0.81	0.84	1.18	1.18	1.33	0.88
Er	0.60	2.14	2.12	2.34	2.38	3.22	3.39	3.78	2.41
Tm	0.07	0.31	0.30	0.33	0.35	0.49	0.48	0.55	0.37
Yb	0.45	1.99	1.87	2.09	2.14	2.97	3.03	3.49	2.27
Lu	0.07	0.29	0.30	0.32	0.34	0.44	0.47	0.52	0.34
As	n.d.	n.d.	n.d.	n.d.	2	2	2	2	n.d.
Ta	n.d.	n.d.	n.d.	n.d.	0.41	0.41	0.40	0.48	n.d.
Nb	2.04	4.42	4.28	4.90	4.96	7.13	7.43	8.79	5.13
Nb*	n.d.	2	3	3	4	5	5	7	4
Hf	0.85	1.91	1.89	2.14	2.17	3.03	3.21	3.54	2.27
Zr	29.65	72.91	69.18	79.58	81.66	120.77	120.30	134.66	86.13
Zr*	29	69	70	78	81	120	120	137	83
Y	5.44	19.90	19.22	21.23	21.68	30.70	31.04	33.73	22.67
Y*	7	24	24	27	28	38	37	43	28
Th	0.36	1.35	1.33	1.50	1.48	2.22	2.27	2.63	1.62
U	0.08	0.40	0.39	0.45	0.45	0.65	0.68	0.78	0.48
Cr	3021	270	215	190	296	127	45	234	58
Ni	1090	130	100	62	93	42	28	71	28
Ti/Zr	11.3	8.8	9.2	8.5	9.6	8.1	8.2	11.1	9.1
La/Yb_n	7.1	2.6	2.8	2.7	2.6	2.8	2.8	2.7	2.7
Zr/Y	5.5	3.7	3.6	3.7	3.8	3.9	3.9	4.0	3.8

Symbols as used in accompanying figures

n.d. not detected

— not analyzed

Mg# cation Mg/(Fe+Mg)

Samples analyzed by ICP-MS, unless otherwise indicated

* analyzed by XRF-trace

La/Yb n chondrite-normalized La: 0.329, Yb: 0.22; *from* Nakamura (1974)

Appendix 2. Continued

Field Number	**57a**	**57b**	**57e**	**57f**	**98**	**100**	**244**	**287**	**373**
Lab Number	**01TRH006**	**01TRH007**	**01TRH008**	**01TRH009**	**01TRH019**	**01TRH018**	**01TRH062**	**01TRH065**	**01TRH071**
UTM East	423985	423920	423763	423695	420800	421185	419860	424385	418121
UTM North	5484302	5484276	5484125	5484097	5489780	5489652	5492669	5497047	5506292
Lithology	12	12	12	12	12	12	12	12	12
Symbol	▽	▽	▽	▽	▽	▽	▽	▽	▽
SiO_2	49.40	49.92	49.39	49.82	48.56	49.52	50.04	49.93	48.01
TiO_2	1.95	2.18	1.13	1.25	0.90	1.20	1.18	1.18	0.66
Al_2O_3	14.36	13.99	16.49	16.22	16.73	15.18	15.75	15.29	15.92
Fe_2O_3	16.77	17.51	13.60	13.38	13.38	14.21	13.30	13.83	9.53
MnO	0.23	0.23	0.19	0.20	0.19	0.21	0.20	0.21	0.11
MgO	3.89	4.63	7.18	5.44	8.86	7.38	6.48	6.80	8.11
CaO	9.18	8.72	10.55	10.59	10.33	10.69	11.07	11.02	12.33
Na_2O	2.93	3.02	2.46	2.81	2.32	2.39	2.52	2.46	3.59
K_2O	0.74	0.91	0.43	0.49	0.35	0.46	0.45	0.46	0.34
P_2O_5	0.19	0.15	0.10	0.11	0.08	0.11	0.10	0.10	0.03
LOI	0.11	0.19	n.d.	0.56	0.07	0.14	0.25	0.05	2.85
Total	99.75	101.45	101.55	100.87	101.75	101.49	101.34	101.33	101.50
Mg #	0.32	0.34	0.51	0.45	0.57	0.51	0.49	0.49	0.63
Rb	20.49	24.88	11.70	13.38	13.20	9.60	11.70	12.14	8.01
Sr	171.10	167.35	180.66	180.95	163.43	170.06	167.92	166.13	147.87
Cs	0.90	0.70	0.58	0.71	0.36	0.25	0.32	0.46	0.38
La	15.05	12.31	8.33	9.30	8.78	6.22	8.51	7.84	2.45
Ce	33.77	27.55	18.69	20.88	20.06	14.19	18.37	17.32	5.67
Pr	4.62	3.80	2.53	2.83	2.68	1.94	2.48	2.40	0.87
Nd	20.04	16.71	11.13	12.47	11.95	8.37	10.95	10.45	4.53
Sm	5.42	4.44	3.07	3.43	3.40	2.27	3.02	2.90	1.54
Eu	1.80	1.51	1.02	1.20	1.11	0.89	1.13	1.11	0.58
Gd	6.08	5.16	3.56	3.97	3.87	2.74	3.76	3.75	2.06
Tb	1.04	0.88	0.61	0.67	0.68	0.47	0.65	0.61	0.38
Dy	6.58	5.65	3.71	4.27	4.10	2.87	4.04	3.80	2.40
Ho	1.38	1.16	0.77	0.89	0.88	0.61	0.83	0.80	0.53
Er	3.88	3.24	2.12	2.46	2.46	1.71	2.36	2.28	1.53
Tm	0.57	0.46	0.32	0.36	0.36	0.24	0.35	0.33	0.23
Yb	3.61	3.03	2.06	2.28	2.19	1.59	2.15	2.10	1.50
Lu	0.55	0.45	0.31	0.36	0.33	0.24	0.33	0.34	0.24
As	n.d.	2	n.d.	n.d.	n.d.	n.d.	n.d.	n.d.	n.d.
Ta	0.47	0.41	n.d.	0.30	n.d.	n.d.	n.d.	n.d.	n.d.
Nb	8.83	7.12	4.82	5.34	5.20	3.61	4.59	4.56	1.50
Nb*	7	5	4	4	3	3	3	3	n.d.
Hf	3.72	3.08	2.05	2.23	2.22	1.58	2.34	2.13	1.14
Zr	141.84	113.90	79.28	85.54	83.08	58.47	81.16	74.80	39.38
Zr*	146	122	76	87	81	55	79	76	36
Y	35.64	30.03	20.59	22.72	22.63	15.70	21.59	21.20	13.18
Y*	44	38	26	28	27	20	25	24	17
Th	2.77	2.19	1.44	1.66	1.58	1.10	1.44	1.37	0.17
U	0.80	0.67	0.41	0.51	0.47	0.33	0.43	0.40	0.20
Cr	70	222	148	163	2672	218	175	180	307
Ni	34	126	61	86	751	115	82	83	180
Ti/Zr	8.2	11.5	8.5	8.8	6.5	12.3	8.7	9.5	10.0
La/Yb_n	2.8	2.7	2.7	2.7	2.7	2.6	2.6	2.5	1.1
Zr/Y	4.0	3.8	3.9	3.8	3.7	3.7	3.8	3.5	3.0

Symbols as used in accompanying figures

Mg# cation Mg/(Fe+Mg)

* analyzed by XRF-trace

n.d. not detected

— not analyzed

Samples analyzed by ICP-MS, unless otherwise indicated

La/Yb n chondrite-normalized La: 0.329, Yb: 0.22; *from* Nakamura (1974)

Appendix 2. Continued

Field Number **Lab Number**	**1019b** **01TRH011**	**1019d** **01TRH012**	**3031** **01TRH088**	**107** **01TRH016**	**408** **01TRH078**	**1008** **01TRH085**	**1199** **01TRH053**	**139** **01TRH017**	**347** **01TRH070**
UTM East	424651	424651	422140	421985	423647	424447	416639	418383	418295
UTM North	5490737	5490737	5511363	5496422	5502907	5495595	5492729	5496235	5487385
Lithology	12	12	12	12g	12g	12g	12g	12h	12h
Symbol	▽	▽	▽	▲	▲	▲	▲	△	△
SiO_2	49.73	49.68	49.78	50.96	50.80	43.37	49.54	50.24	42.28
TiO_2	1.40	1.43	1.42	1.49	1.50	3.80	1.54	2.54	0.83
Al_2O_3	15.01	14.95	14.88	14.24	14.42	13.25	14.34	12.18	6.43
Fe_2O_3	14.81	14.92	14.84	14.69	14.40	19.04	14.60	20.68	15.04
MnO	0.21	0.21	0.21	0.22	0.21	0.23	0.25	0.26	0.17
MgO	6.51	6.44	6.42	6.02	5.86	5.72	6.40	2.72	22.95
CaO	9.78	9.71	9.93	9.55	9.52	10.12	10.39	7.68	5.38
Na_2O	2.76	2.56	2.80	2.31	2.39	2.09	1.94	2.96	1.06
K_2O	0.62	0.72	0.57	1.05	1.08	1.20	1.02	1.12	0.62
P_2O_5	0.13	0.14	0.13	0.14	0.14	0.19	0.18	0.31	0.07
LOI	0.53	0.49	0.43	0.61	0.93	1.82	0.89	0.13	4.84
Total	101.50	101.26	101.42	101.28	101.24	100.83	101.08	100.82	99.67
Mg #	0.47	0.46	0.46	0.45	0.45	0.37	0.47	0.21	0.75
Rb	17.80	21.75	16.97	27.93	32.98	63.44	41.65	32.18	19.76
Sr	164.46	168.47	163.15	204.75	203.42	437.24	295.60	158.59	68.64
Cs	0.82	0.91	0.62	2.06	2.51	3.76	2.72	1.10	0.68
La	10.20	11.32	11.13	14.97	15.58	16.30	17.08	21.35	6.03
Ce	22.88	25.18	24.61	31.62	32.02	35.96	37.95	48.34	14.10
Pr	3.12	3.40	3.34	4.10	4.10	4.84	4.97	6.77	1.95
Nd	13.65	14.89	14.68	16.79	17.41	20.62	21.04	29.64	8.79
Sm	3.69	3.86	3.97	3.89	4.21	4.71	4.66	8.06	2.26
Eu	1.24	1.32	1.48	1.32	1.47	1.71	1.38	2.42	0.74
Gd	4.28	4.59	4.67	4.33	4.40	4.90	4.48	9.22	2.45
Tb	0.72	0.75	0.82	0.69	0.72	0.76	0.75	1.56	0.40
Dy	4.54	4.75	5.04	4.27	4.47	4.51	4.46	9.78	2.42
Ho	0.96	1.00	1.11	0.88	0.96	0.92	0.90	2.02	0.50
Er	2.69	2.89	3.07	2.49	2.68	2.45	2.57	5.81	1.43
Tm	0.39	0.40	0.44	0.37	0.40	0.37	0.38	0.84	0.21
Yb	2.57	2.58	2.81	2.36	2.49	2.28	2.42	5.25	1.31
Lu	0.36	0.40	0.43	0.35	0.38	0.36	0.37	0.84	0.19
As	2	n.d.	n.d.	53	n.d.	n.d.	4	n.d.	n.d.
Ta	0.34	0.36	0.40	0.53	0.56	0.90	0.88	0.75	n.d.
Nb	6.04	6.66	6.21	10.15	9.96	16.34	16.53	13.18	3.68
Nb*	4	6	4	9	9	15	14	11	n.d.
Hf	2.52	2.72	2.99	2.64	3.00	2.95	2.75	5.48	1.70
Zr	95.52	105.90	106.18	98.04	107.12	108.18	106.05	203.10	61.61
Zr*	101	106	104	101	103	97	101	221	56
Y	24.82	26.53	27.31	22.70	23.92	23.79	24.44	51.50	12.69
Y*	32	32	31	30	28	26	27	65	14
Th	1.93	2.10	2.08	2.78	3.00	1.40	2.14	3.98	1.15
U	0.60	0.64	0.61	0.36	0.43	0.31	0.44	1.21	0.37
Cr	170	290	213	47	202	105	167	224	1872
Ni	100	135	97	6	61	50	49	186	1418
Ti/Zr	8.8	8.1	8.0	9.1	8.4	21.1	8.7	7.5	8.1
La/Yb_n	2.7	2.9	2.6	4.2	4.2	4.8	4.7	2.7	3.1
Zr/Y	3.8	4.0	3.9	4.3	4.5	4.5	4.3	3.9	4.9

Symbols as used in accompanying figures

Mg# cation Mg/(Fe+Mg)

* analyzed by XRF-trace

n.d. not detected

— not analyzed

Samples analyzed by ICP–MS, unless otherwise indicated

La/Yb n chondrite-normalized La: 0.329, Yb: 0.22; *from* Nakamura (1974)

Appendix 3:

Normative Calculations

Appendix 3. Normative calculations.

Sample	**107**	**408**	**1008**	**1199**	**92**	**96**	**240**	**241**	**1195**	**1198**
Rock Type	diabase dike	diabase dike	diabase dike	diabase dike	peridotite	peridotite	peridotite	peridotite	peridotite	peridotite
TAS Class	bslt, subalk	bslt, subalk	tep, bsn	bslt, subalk	meim	kom	kom	kom	meim	meim
SiO_2	50.59	50.58	43.76	49.38	46.64	44.78	41.98	42.42	46.64	47.52
TiO_2	1.48	1.49	3.83	1.54	1.09	0.73	0.84	0.84	1.05	1.24
Al_2O_3	14.14	14.36	13.37	14.29	7.25	3.66	4.33	4.01	5.63	5.82
$Fe_2O_{3\,total}$	14.58	14.34	19.21	14.55	14.90	14.89	17.04	16.72	14.50	14.54
MnO	0.22	0.21	0.23	0.25	0.19	0.20	0.22	0.22	0.22	0.20
MgO	5.98	5.83	5.77	6.38	19.75	25.64	30.68	29.07	20.64	18.23
CaO	9.48	9.48	10.21	10.36	8.04	8.79	3.60	5.42	9.63	10.54
Na_2O	2.29	2.38	2.11	1.93	1.43	0.69	0.63	0.49	0.97	1.26
K_2O	1.04	1.08	1.21	1.02	0.48	0.23	0.50	0.53	0.49	0.48
P_2O_5	0.14	0.14	0.19	0.18	0.12	0.06	0.09	0.08	0.10	0.12
CO_2	0.06	0.12	0.09	0.13	0.12	0.31	0.10	0.18	0.14	0.08
LOI	0.61	0.93	1.82	0.89	0.18	0.24	1.64	1.63	0.74	0.48
H_2O^+	0.07	0.12	0.27	0.14	0.03	0.03	0.06	0.05	0.05	0.05
Total	101.28	101.24	100.83	101.08	100.93	100.46	99.92	99.69	100.70	100.78
SiO_2 adj	51.120	51.125	44.404	49.936	47.195	45.433	42.563	43.047	47.198	48.044
TiO_2 adj	1.495	1.506	3.886	1.557	1.103	0.741	0.852	0.852	1.062	1.254
Al_2O_3 adj	14.288	14.515	13.567	14.451	7.336	3.713	4.390	4.069	5.697	5.884
Fe_2O_3 adj	4.890	4.851	5.926	4.693	4.310	3.892	4.333	4.246	4.056	4.202
FeO adj	8.856	8.678	12.207	9.017	9.688	10.092	11.646	11.446	9.554	9.446
MnO adj	0.222	0.212	0.233	0.253	0.192	0.203	0.223	0.223	0.223	0.202
MgO adj	6.042	5.893	5.855	6.452	19.985	26.014	31.106	29.499	20.887	18.431
CaO adj	9.579	9.582	10.360	10.476	8.136	8.918	3.650	5.500	9.745	10.656
Na_2O adj	2.314	2.406	2.141	1.952	1.447	0.700	0.639	0.497	0.982	1.274
K_2O adj	1.051	1.092	1.228	1.031	0.486	0.233	0.507	0.538	0.496	0.485
P_2O_5 adj	0.141	0.142	0.193	0.182	0.121	0.061	0.091	0.081	0.101	0.121
Q	4.493	4.240	—	3.419	—	—	—	—	—	—
Or	6.213	6.451	7.261	6.094	2.870	1.370	2.974	3.157	2.919	2.857
Ab	19.550	20.309	18.063	16.475	12.218	5.884	5.358	4.170	8.263	10.729
An	25.456	25.516	23.710	27.552	12.062	6.259	7.546	7.221	9.618	8.861
Ne	—	—	—	—	—	—	—	—	—	—
C	—	—	—	—	—	—	—	—	—	—
En	10.685	10.472	12.592	11.615	17.435	23.565	6.188	12.137	24.273	27.598
Fs	6.275	6.094	8.622	6.644	3.897	4.565	1.157	2.356	5.184	6.317
Hy-Mg	10.074	9.788	3.329	10.646	14.513	10.036	10.313	9.285	13.678	12.746
Hy-Fe	6.786	6.534	2.615	6.985	3.721	2.230	2.212	2.068	3.351	3.347
Fo	—	—	3.768	—	18.976	30.414	44.569	40.602	18.785	14.122
Fa	—	—	3.261	—	5.362	7.448	10.536	9.966	5.073	4.087
Mt	7.079	7.016	8.566	6.786	6.235	5.605	6.227	6.104	5.848	6.064
He	—	—	—	—	—	—	—	—	—	—
Il	2.835	2.853	7.359	2.950	2.090	1.398	1.604	1.605	2.006	2.371
Ap	0.326	0.328	0.446	0.421	0.280	0.140	0.209	0.186	0.233	0.279
Z	0.020	0.021	0.020	0.020	0.014	0.008	0.010	0.010	0.014	0.017
Tn	—	—	—	—	—	—	—	—	—	—
Cc	0.136	0.272	0.204	0.295	0.273	0.701	0.226	0.406	0.317	0.181
Cm	0.070	0.104	0.182	0.098	0.053	0.376	0.871	0.726	0.438	0.423
Mg#	54.876	54.761	46.091	56.053	78.619	82.126	82.642	82.124	79.579	77.669
FeO_t/MgO	2.194	2.213	2.996	2.052	0.679	0.522	0.500	0.518	0.632	0.718
Salic	55.712	56.516	49.034	53.540	27.150	13.513	15.878	14.548	20.800	22.447
Femic	37.459	36.663	41.490	38.982	68.332	80.696	81.649	81.767	73.014	70.335
CI	55.564	54.964	56.972	60.066	78.816	94.537	72.690	80.510	90.346	91.445
DI	30.256	31.000	25.324	25.988	15.088	7.254	8.332	7.327	11.182	13.586
SI	26.096	25.711	21.402	27.876	55.644	63.556	64.494	63.815	58.060	54.468
AR	1.328	1.340	1.328	1.272	1.286	1.160	1.332	1.242	1.212	1.238

For abbreviations used in "Rock Type", *see* Appendix 7; for other abbreviations, notes and explanations, *see* end of Appendix 3.

Appendix 3. Continued

Sample	1269	2244	2246	2247	2256	2258	2259	2260	3001	3002
Rock Type	peridotite	peridotite	peridotite	peridotite	peridotite	peridotite	peridotite	peridotite	peridotite	peridotite
TAS Class	kom	kom	kom	kom	meim	kom	kom	kom	kom	kom
SiO_2	44.79	42.08	41.92	43.90	44.13	43.68	43.12	42.68	44.61	46.00
TiO_2	0.74	0.85	0.83	0.78	1.10	0.64	0.67	0.68	0.86	0.92
Al_2O_3	3.42	4.25	4.12	3.75	5.01	2.81	3.13	3.14	4.01	6.03
$Fe_2O_{3\,total}$	15.00	17.23	16.87	15.45	15.86	15.46	16.75	17.45	16.40	15.50
MnO	0.20	0.21	0.21	0.20	0.20	0.20	0.22	0.23	0.23	0.21
MgO	25.84	30.00	30.80	26.88	25.81	28.38	28.66	29.85	24.42	21.02
CaO	8.84	4.04	3.78	7.53	6.14	7.83	6.51	5.12	8.38	8.73
Na_2O	0.68	0.50	0.59	0.76	1.06	0.54	0.47	0.28	0.59	1.04
K_2O	0.24	0.53	0.46	0.27	0.40	0.21	0.26	0.28	0.34	0.40
P_2O_5	0.06	0.09	0.09	0.07	0.11	0.06	0.06	0.07	0.08	0.08
CO_2	0.18	0.23	0.33	0.41	0.17	0.18	0.16	0.23	0.10	0.07
LOI	0.21	1.12	0.57	0.46	0.60	0.23	0.27	4.78	0.72	0.15
H_2O^+	0.03	0.06	0.05	0.05	0.05	0.03	0.04	0.05	0.06	0.03
Total	101.12	99.87	100.19	100.27	100.58	101.02	101.17	100.78	100.78	101.18
SiO_2 adj	45.382	42.728	42.601	44.596	44.732	44.279	43.738	43.350	45.198	46.558
TiO_2 adj	0.750	0.863	0.843	0.792	1.115	0.649	0.680	0.691	0.871	0.931
Al_2O_3 adj	3.465	4.315	4.187	3.809	5.078	2.848	3.175	3.189	4.063	6.103
Fe_2O_3 adj	3.916	4.358	4.267	4.024	4.282	3.913	4.197	4.284	4.273	4.289
FeO adj	10.152	11.820	11.587	10.501	10.613	10.581	11.512	12.093	11.107	10.257
MnO adj	0.203	0.213	0.213	0.203	0.203	0.203	0.223	0.234	0.233	0.212
MgO adj	26.182	30.462	31.301	27.306	26.162	28.769	29.071	30.319	24.742	21.275
CaO adj	8.957	4.102	3.841	7.649	6.224	7.937	6.603	5.200	8.490	8.836
Na_2O adj	0.689	0.508	0.600	0.772	1.074	0.547	0.477	0.284	0.598	1.053
K_2O adj	0.243	0.538	0.467	0.274	0.405	0.213	0.264	0.284	0.344	0.405
P_2O_5 adj	0.061	0.091	0.091	0.071	0.112	0.061	0.061	0.071	0.081	0.081
Q	—	—	—	—	—	—	—	—	—	—
Or	1.428	3.156	2.736	1.607	2.378	1.252	1.551	1.668	2.025	2.385
Ab	5.790	4.260	5.026	6.473	9.018	4.596	4.008	2.384	5.032	8.866
An	5.605	7.834	7.280	6.063	7.779	4.653	5.701	6.535	7.345	10.678
Ne	—	—	—	—	—	—	—	—	—	—
C	—	—	—	—	—	—	—	—	—	—
En	24.686	6.892	6.020	19.049	14.094	22.055	16.837	11.326	21.786	20.764
Fs	4.758	1.342	1.119	3.645	2.703	4.131	3.417	2.336	4.858	4.798
Hy-Mg	8.869	12.298	11.633	9.426	11.018	7.274	10.305	15.415	11.923	13.156
Hy-Fe	1.961	2.747	2.481	2.069	2.424	1.563	2.399	3.648	3.050	3.487
Fo	31.153	41.830	43.978	34.432	33.013	37.595	37.690	38.018	27.514	20.988
Fa	7.591	10.298	10.336	8.330	8.007	8.903	9.671	9.916	7.757	6.131
Mt	5.639	6.262	6.125	5.782	6.161	5.633	6.042	6.162	6.161	6.188
He	—	—	—	—	—	—	—	—	—	—
Il	1.415	1.625	1.586	1.491	2.102	1.224	1.283	1.302	1.645	1.760
Ap	0.140	0.209	0.209	0.163	0.258	0.140	0.140	0.163	0.187	0.187
Z	0.009	0.011	0.011	0.010	0.015	0.008	0.008	0.008	0.010	0.012
Tn	—	—	—	—	—	—	—	—	—	—
Cc	0.407	0.519	0.744	0.924	0.384	0.407	0.361	0.519	0.226	0.159
Cm	0.548	0.717	0.717	0.537	0.645	0.566	0.586	0.598	0.480	0.441
Mg#	82.134	82.123	82.804	82.254	81.461	82.896	81.823	81.715	79.882	78.711
FeO_t/MgO	0.522	0.517	0.493	0.517	0.553	0.490	0.526	0.526	0.604	0.664
Salic	12.823	15.250	15.042	14.143	19.175	10.501	11.260	10.587	14.402	21.929
Femic	81.314	81.952	82.159	80.579	76.819	84.247	84.227	85.787	79.836	72.474
CI	96.222	73.148	72.395	88.190	78.914	94.919	86.931	79.786	90.208	85.674
DI	7.218	7.416	7.762	8.080	11.396	5.848	5.559	4.052	7.057	11.251
SI	63.576	63.880	64.910	63.684	61.506	65.350	63.863	64.148	60.252	57.070
AR	1.162	1.284	1.306	1.201	1.301	1.152	1.164	1.145	1.162	1.216

For abbreviations used in "Rock Type", *see* Appendix 7; for other abbreviations, notes and explanations, *see* end of Appendix 3.

Appendix 3. Continued

Sample	**3005**	**3027**	**208**	**276**	**1196**	**15a**	**15b**	**15c**	**51a**	**51b**
Rock Type	peridotite	peridotite	ol gb	ol gb	ol gb	diabase sill	diabase sill	diabase sill	diabase sill	diabase sill
TAS Class	kom	kom	bslt, subalk	bslt, subalk	bsad	bslt, subalk	bslt, subalk	bslt, subalk	bslt, subalk	bslt, subalk
SiO_2	42.28	42.23	51.22	51.36	53.10	48.57	48.46	49.15	48.97	50.17
TiO_2	0.70	0.56	2.26	2.62	2.11	1.05	1.05	1.11	1.29	1.62
Al_2O_3	3.26	3.21	13.91	14.21	14.95	15.36	16.08	16.28	14.86	14.15
$Fe_2O_{3\,total}$	17.99	16.17	12.97	14.18	10.33	13.40	13.41	12.72	14.38	15.54
MnO	0.23	0.21	0.18	0.18	0.14	0.20	0.20	0.19	0.21	0.23
MgO	28.52	31.35	6.07	4.74	5.52	7.89	7.39	6.62	6.66	5.23
CaO	6.13	5.40	9.43	8.00	8.69	10.79	10.45	10.85	10.54	9.36
Na_2O	0.42	0.44	2.54	2.70	3.16	2.23	2.35	2.49	2.39	2.72
K_2O	0.29	0.22	1.17	1.70	1.71	0.38	0.44	0.43	0.52	0.74
P_2O_5	0.08	0.05	0.18	0.25	0.28	0.09	0.10	0.11	0.11	0.16
CO_2	0.09	0.16	0.07	0.06	—	0.06	0.08	0.06	0.05	0.08
LOI	1.05	0.43	1.31	1.19	0.97	—	0.19	0.09	0.27	0.53
H_2O^+	0.04	0.03	0.01	0.02	0.03	0.03	0.03	0.02	0.02	0.02
Total	100.30	100.06	101.17	100.59	101.23	101.52	101.50	101.88	101.74	101.36
SiO_2 adj	42.908	42.824	51.698	51.864	53.451	49.045	48.947	49.606	49.492	50.738
TiO_2 adj	0.710	0.568	2.281	2.646	2.124	1.060	1.060	1.120	1.304	1.638
Al_2O_3 adj	3.308	3.255	14.040	14.350	15.049	15.510	16.242	16.431	15.018	14.310
Fe_2O_3 adj	4.441	3.968	4.485	5.125	3.900	4.174	4.224	4.074	4.599	5.233
FeO adj	12.432	11.184	7.744	8.273	5.847	8.420	8.387	7.886	8.939	9.432
MnO adj	0.233	0.213	0.182	0.182	0.141	0.202	0.202	0.192	0.212	0.233
MgO adj	28.944	31.791	6.127	4.786	5.556	7.967	7.464	6.681	6.731	5.289
CaO adj	6.221	5.476	9.518	8.078	8.747	10.896	10.555	10.951	10.652	9.466
Na_2O adj	0.426	0.446	2.564	2.726	3.181	2.252	2.374	2.513	2.415	2.751
K_2O adj	0.294	0.223	1.181	1.717	1.721	0.384	0.444	0.434	0.526	0.748
P_2O_5 adj	0.081	0.051	0.182	0.252	0.282	0.091	0.101	0.111	0.111	0.162
Q	—	—	4.978	6.156	4.422	—	—	0.517	1.091	3.999
Or	1.730	1.310	6.974	10.137	10.165	2.269	2.624	2.565	3.109	4.421
Ab	3.584	3.744	21.643	23.013	26.868	19.020	20.049	21.229	20.398	23.233
An	6.210	6.173	23.264	21.807	21.672	31.021	32.290	32.220	28.533	24.440
Ne	—	—	—	—	—	—	—	—	—	—
C	—	—	—	—	—	—	—	—	—	—
En	15.277	13.084	12.901	8.840	12.648	12.179	10.266	11.347	12.129	10.070
Fs	3.396	2.391	5.196	4.457	3.375	5.678	5.061	5.702	6.820	7.121
Hy-Mg	8.935	8.143	9.248	7.799	7.956	13.151	12.544	11.354	11.113	8.481
Hy-Fe	2.278	1.707	4.272	4.510	2.435	7.034	7.093	6.544	7.167	6.879
Fo	39.009	45.098	—	—	—	0.708	0.878	—	—	—
Fa	10.963	10.422	—	—	—	0.418	0.547	—	—	—
Mt	6.403	5.709	6.487	7.413	5.644	6.040	6.112	5.897	6.655	7.572
He	—	—	—	—	—	—	—	—	—	—
Il	1.341	1.071	4.322	5.014	4.027	2.010	2.009	2.124	2.472	3.105
Ap	0.187	0.117	0.421	0.584	0.654	0.210	0.234	0.257	0.257	0.375
Z	0.007	0.006	0.028	0.037	0.037	0.014	0.014	0.015	0.016	0.024
Tn	—	—	—	—	—	—	—	—	—	—
Cc	0.204	0.361	0.159	0.136	—	0.136	0.182	0.136	0.114	0.182
Cm	0.476	0.664	0.107	0.096	0.097	0.112	0.098	0.095	0.126	0.099
Mg#	80.583	83.517	58.512	50.768	62.878	62.779	61.336	60.162	57.306	49.989
FeO_t/MgO	0.568	0.464	1.922	2.692	1.684	1.528	1.633	1.729	1.943	2.674
Salic	11.524	11.227	56.859	61.113	63.127	52.310	54.963	56.531	53.131	56.093
Femic	84.206	85.234	37.230	33.576	32.710	41.540	39.449	37.266	39.536	36.107
CI	84.434	85.200	57.573	46.341	54.530	67.216	64.103	64.652	62.484	52.105
DI	5.314	5.054	33.595	39.306	41.455	21.289	22.673	24.311	24.598	31.653
SI	62.196	66.771	27.723	21.152	27.498	34.345	32.604	30.948	29.000	22.551
AR	1.163	1.166	1.378	1.494	1.519	1.222	1.235	1.241	1.259	1.345

For abbreviations used in "Rock Type", *see* Appendix 7; for other abbreviations, notes and explanations, *see* end of Appendix 3.

Appendix 3. Continued

Sample	**52**	**53**	**56**	**57a**	**57b**	**57f**	**98**	**100**	**139**	**244**
Rock Type	diabase sill	diabase sill	diabase sill	diabase sill	diabase sill	diabase sill	diabase sill	diabase sill	diabase sill	diabase sill
TAS Class	bslt, subalk	bslt, subalk	bslt, subalk	bslt, subalk	bslt, subalk	bslt, subalk	bslt, subalk	bslt, subalk	bslt, subalk	bslt, subalk
SiO_2	50.20	48.88	49.41	49.54	49.26	49.61	47.72	48.81	49.85	49.45
TiO_2	1.64	2.46	1.29	1.96	2.15	1.24	0.88	1.18	2.52	1.17
Al_2O_3	14.97	13.38	15.89	14.40	13.81	16.15	16.44	14.96	12.09	15.56
$Fe_2O_{3\,total}$	15.09	18.33	13.52	16.82	17.28	13.32	13.15	14.01	20.52	13.14
MnO	0.22	0.25	0.20	0.23	0.23	0.20	0.19	0.21	0.26	0.20
MgO	4.77	4.09	5.82	3.90	4.57	5.42	8.71	7.27	2.70	6.40
CaO	9.07	8.72	10.60	9.21	8.60	10.55	10.15	10.54	7.62	10.94
Na_2O	2.94	2.87	2.58	2.94	2.98	2.80	2.28	2.36	2.94	2.49
K_2O	0.85	0.76	0.52	0.74	0.90	0.49	0.34	0.45	1.11	0.44
P_2O_5	0.16	0.18	0.11	0.19	0.15	0.11	0.08	0.11	0.31	0.10
CO_2	0.09	0.10	0.06	0.08	0.08	0.11	0.09	0.10	0.09	0.10
LOI	0.58	0.45	0.18	0.11	0.19	0.56	0.07	0.14	0.13	0.25
H_2O^+	0.04	0.04	0.04	0.04	0.04	0.03	0.03	0.03	0.08	0.02
Total	101.37	101.50	101.49	99.75	101.45	100.87	101.75	101.49	100.82	101.34
SiO_2 adj	50.752	49.528	49.898	50.137	49.866	50.115	48.190	49.335	50.572	49.953
TiO_2 adj	1.658	2.493	1.303	1.984	2.176	1.253	0.889	1.193	2.556	1.182
Al_2O_3 adj	15.135	13.557	16.047	14.573	13.980	16.314	16.602	15.121	12.265	15.718
Fe_2O_3 adj	5.189	6.154	4.400	5.704	5.917	4.401	4.053	4.442	7.167	4.232
FeO adj	9.058	11.174	8.327	10.184	10.416	8.147	8.302	8.745	12.283	8.136
MnO adj	0.222	0.253	0.202	0.233	0.233	0.202	0.192	0.212	0.264	0.202
MgO adj	4.822	4.144	5.877	3.947	4.626	5.475	8.796	7.348	2.739	6.465
CaO adj	9.170	8.836	10.705	9.321	8.706	10.657	10.250	10.653	7.730	11.051
Na_2O adj	2.972	2.908	2.605	2.975	3.017	2.828	2.302	2.385	2.982	2.515
K_2O adj	0.859	0.770	0.525	0.749	0.911	0.495	0.343	0.455	1.126	0.444
P_2O_5 adj	0.162	0.182	0.111	0.192	0.152	0.111	0.081	0.111	0.314	0.101
Q	3.446	4.362	1.639	4.158	3.147	1.544	—	0.402	7.575	1.383
Or	5.076	4.547	3.103	4.426	5.380	2.924	2.019	2.687	6.652	2.623
Ab	25.100	24.542	22.009	25.124	25.465	23.876	19.354	20.139	25.175	21.236
An	25.371	21.607	30.498	24.150	21.857	30.293	33.739	29.151	16.714	30.225
Ne	—	—	—	—	—	—	—	—	—	—
C	—	—	—	—	—	—	—	—	—	—
En	8.804	8.499	11.060	8.498	8.914	10.695	8.961	11.974	6.058	12.354
Fs	6.384	8.414	6.489	8.369	7.433	6.566	3.778	6.159	9.989	6.580
Hy-Mg	7.907	6.356	9.490	5.873	7.362	8.650	11.434	12.714	3.999	10.343
Hy-Fe	6.577	7.218	6.387	6.635	7.041	6.091	5.531	7.502	7.563	6.319
Fo	—	—	—	—	—	—	4.331	—	—	—
Fa	—	—	—	—	—	—	2.309	—	—	—
Mt	7.509	8.899	6.369	8.253	8.557	6.366	5.839	6.427	10.367	6.122
He	—	—	—	—	—	—	—	—	—	—
Il	3.143	4.723	2.471	3.761	4.123	2.375	1.678	2.261	4.844	2.240
Ap	0.375	0.421	0.257	0.444	0.351	0.257	0.186	0.257	0.726	0.234
Z	0.024	0.027	0.016	0.029	0.024	0.017	0.016	0.011	0.044	0.016
Tn	—	—	—	—	—	—	—	—	—	—
Cc	0.204	0.227	0.136	0.182	0.182	0.250	0.203	0.227	0.204	0.227
Cm	0.079	0.159	0.074	0.097	0.164	0.096	0.620	0.089	0.089	0.098
Mg#	48.690	39.798	55.714	40.858	44.186	54.502	65.381	59.964	28.443	58.617
FeO_t/MgO	2.847	4.033	2.090	3.880	3.402	2.211	1.358	1.734	6.839	1.847
Salic	58.993	55.058	57.249	57.858	55.849	58.637	55.112	52.379	56.116	55.467
Femic	33.940	35.695	35.777	33.020	35.997	34.177	40.083	40.878	32.831	37.378
CI	49.903	44.394	61.005	46.596	46.244	59.424	65.412	63.889	32.584	64.121
DI	33.622	33.451	26.751	33.708	33.992	28.344	21.373	23.228	39.402	25.242
SI	21.057	16.477	27.040	16.754	18.588	25.649	36.964	31.435	10.416	29.667
AR	1.374	1.393	1.265	1.369	1.419	1.281	1.218	1.248	1.517	1.248

For abbreviations used in "Rock Type", ***see*** **Appendix 7; for other abbreviations, notes and explanations,** ***see*** **end of Appendix 3.**

Appendix 3. continued

Sample	**287**	**347**	**373**	**1019a**	**1019b**	**1019d**	**3031**
Rock Type	diabase sill	diabase sill	diabase sill	diabase sill	diabase sill	diabase sill	diabase sill
TAS Class	bslt, subalk	kom	bslt, alk	bslt, subalk	bslt, subalk	bslt, subalk	bslt, subalk
SiO_2	49.29	44.50	48.57	49.41	49.19	49.23	49.18
TiO_2	1.16	0.87	0.67	1.45	1.38	1.42	1.40
Al_2O_3	15.09	6.77	16.10	14.68	14.85	14.82	14.70
$Fe_2O_{3\,total}$	13.65	15.83	9.64	14.40	14.65	14.79	14.66
MnO	0.21	0.18	0.11	0.22	0.21	0.21	0.21
MgO	6.71	24.15	8.20	6.12	6.44	6.38	6.34
CaO	10.88	5.66	12.47	9.82	9.67	9.62	9.81
Na_2O	2.43	1.12	3.63	2.98	2.73	2.54	2.77
K_2O	0.45	0.65	0.34	0.68	0.61	0.71	0.56
P_2O_5	0.10	0.07	0.03	0.13	0.13	0.14	0.13
CO_2	0.03	0.19	0.20	0.10	0.13	0.14	0.22
LOI	0.05	4.84	2.85	0.65	0.53	0.49	0.43
H_2O^+	0.02	0.34	0.04	0.04	0.05	0.04	0.04
Total	101.33	99.67	101.50	101.35	101.50	101.26	101.42
SiO_2 adj	49.770	45.109	49.001	49.945	49.752	49.798	49.792
TiO_2 adj	1.171	0.882	0.676	1.466	1.396	1.436	1.417
Al_2O_3 adj	15.237	6.863	16.243	14.839	15.020	14.991	14.883
Fe_2O_3 adj	4.370	4.402	3.281	4.864	4.837	4.858	4.842
FeO adj	8.469	10.478	5.799	8.721	8.980	9.091	8.999
MnO adj	0.212	0.182	0.111	0.222	0.212	0.212	0.213
MgO adj	6.775	24.481	8.273	6.186	6.514	6.454	6.419
CaO adj	10.986	5.738	12.581	9.926	9.780	9.731	9.932
Na_2O adj	2.454	1.135	3.662	3.012	2.761	2.569	2.804
K_2O adj	0.454	0.659	0.343	0.687	0.617	0.718	0.567
P_2O_5 adj	0.101	0.071	0.030	0.131	0.131	0.142	0.132
Q	1.018	—	—	0.314	0.892	5.191	1.070
Or	2.684	3.874	2.024	4.060	3.644	3.372	3.346
Ab	20.735	9.535	22.095	25.430	23.304	17.243	23.645
An	29.178	11.599	26.785	24.885	26.702	21.618	26.258
Ne	—	—	4.763	—	—	—	—
C	—	—	—	—	—	—	—
En	12.969	9.900	21.032	11.904	10.452	8.807	10.701
Fs	6.948	2.064	6.245	6.711	5.930	—	6.156
Hy-Mg	10.839	12.516	—	9.856	11.340	8.670	10.973
Hy-Fe	6.662	2.994	—	6.373	7.379	—	7.240
Fo	—	30.437	7.562	—	—	—	—
Fa	—	8.024	2.839	—	—	—	—
Mt	6.326	6.338	4.742	7.036	6.995	—	6.996
He	—	—	—	—	—	3.854	—
Il	2.221	1.664	1.280	2.778	2.645	—	2.682
Ap	0.234	0.163	0.069	0.303	0.303	0.261	0.305
Z	0.015	0.012	0.007	0.022	0.020	0.017	0.021
Tn	—	—	—	—	—	2.797	—
Cc	0.068	0.429	0.454	0.227	0.295	0.253	0.499
Cm	0.103	0.452	0.104	0.101	0.098	23.055	0.108
Mg#	58.780	80.638	71.776	55.838	56.390	55.859	55.976
FeO_t/MgO	1.830	0.590	1.058	2.117	2.047	2.086	2.081
Salic	53.615	25.008	50.904	54.689	54.542	47.424	54.319
Femic	39.017	71.873	37.455	37.947	38.811	21.331	38.592
CI	64.748	72.162	79.714	57.469	57.194	46.691	57.030
DI	24.437	13.409	28.882	29.804	27.840	25.806	28.061
SI	30.082	59.485	38.735	26.357	27.475	27.244	27.163
AR	1.249	1.332	1.323	1.351	1.315	1.307	1.314

For abbreviations used in "Rock Type", *see* Appendix 7; for other abbreviations, notes and explanations, *see* this page.

Abbreviations:

$Fe_2O_{3\,total}$ = total iron expressed as Fe_2O_3; "adj" refers to adjusted data (anhydrous 100% adjusted basis); Mg# = 100 $Mg^{2+}/(Mg^{2+} + Fe^{2+})$, atomic; FeO_t = total iron expressed as FeO. Salic = sum of salic normative minerals; Femic = sum of femic normative minerals; CI = Crystallization Index; DI = Differentiation Index; SI = Solidification Index; AR = Alkalinity Ratio. n.d., not detected; —, not analyzed.

Rock types are presented according to total alkalis versus silica diagram (*after* Le Bas et al. 1986; Le Bas 1989, 2000) and CIPW norms are on an anhydrous 100% adjusted basis and using Fe_2O_3/FeO ratio *after* Middlemost (1989), using the SINCLAS computer program (Verma, Torres-Alvarado and Sotelo-Rodriguez 2002).

Purposely, 1 or 2 extra digits are reported for all calculated data.

Appendix 4:

Assay Results for Gold-Related Sampling.

Appendix 4. Assay results for gold-related sampling.

Field Number		35a	35b	60	116	124	124b	124c	142	143a
Lab Number		01TRH102	01TRH103	01TRH106	01TRH111	01TRH112	01TRH113	01TRH114	01TRH158	01TRH159
UTM East		424769	424769	425145	422467	423513	423445	423445	428481	428457
UTM North		5484468	5484468	5487221	5495656	5490059	5490000	5490000	5497476	5497368
UTM Zone		16	16	16	16	16	16	16	16	16
Belt		Quetico	Quetico	Quetico	SSB	SVB	SVB	SVB	SSB	SSB
Township		Kitto	Kitto	Kitto	Eva	Kitto	Kitto	Kitto	Summers	Summers
Rock Name		flds wacke	quartz vein	quartz vein	quartz vein	maf mtvolc	quartz vein	maf mtvolc	quartz vein	quartz vein
Description		diss, 5% fg pyrite	15% fg diss pyrite	trc chlorite	white qtz w/ mi chl in shrd chlc flds wacke	carbonatized w/ trc pods py/po	white qtz w/ mi chl in carbonatized shrd plwd bslt	cz plwd bslt adjacent to sample 113	trc sulphide, tur, chl next to IF	trc sulphide, tur, chl next to IF
	detection limit ppm									
Ag	*0.1*	n.d.	n.d.	n.d.	n.d.	n.d.	n.d.	n.d.	n.d.	n.d.
Au	*0.01*	n.d.	n.d.	n.d.	n.d.	n.d.	n.d.	n.d.	n.d.	n.d.
Be	*3*	n.d.	n.d.	n.d.	n.d.	n.d.	n.d.	n.d.	n.d.	n.d.
Co	*5*	37	40	22	9	47	n.d.	55	6	10
Cu	*5*	311	66	64	n.d.	98	n.d.	n.d.	22	n.d.
Mo	*8*	n.d.	n.d.	n.d.	n.d.	n.d.	n.d.	n.d.	n.d.	n.d.
Ni	*5*	14	148	40	20	89	n.d.	103	28	30
Sb	*0.1*	—	—	—	—	—	—	—	0.91	0.71
Sc	*1*	n.d.	18	5	3	30	n.d.	31	4	3
Sr	*1*	9	303	63	21	110	3	78	3	6
V	*5*	n.d.	136	63	26	268	7	267	47	24
W	*40*	n.d.	n.d.	n.d.	n.d.	n.d.	n.d.	n.d.	n.d.	n.d.
Zn	*2*	6	40	13	11	104	5	131	60	44

Field Number		143b	143c	143d	165a	165b	172a	172b	172c	173a
Lab Number		01TRH160	01TRH161	01TRH162	01TRH163	01TRH164	01TRH165	01TRH166	01TRH167	01TRH168
UTM East		428457	428457	428457	428510	428510	423143	423143	423143	423168
UTM North		5497368	5497368	5497368	5497301	5497301	5498910	5498910	5498910	5499018
UTM Zone		16	16	16	16	16	16	16	16	16
Belt		SSB	SSB	SSB	SSB	SSB	CVB	CVB	CVB	CVB
Township		Summers	Summers	Summers	Summers	Summers	Eva	Eva	Eva	Eva
Rock Name		quartz vein	quartz vein	flds wacke	flds wacke	quartz vein	quartz vein	maf mtvolc	maf mtvolc	quartz vein
Description		chl and trc v fg py	10% diss mg cubic py in chlc shear	10% diss mg cubic py in chlc shear	chlc shear w/ trc to 1% diss fg py	minor tur and chl	vuggy quartz w/ chl and trc hem	10 to 15 cm carb vein in carbonatized shear	carbonatized w/ pods of calcite and/or ankerite	5 cm vein, chlc rock w/ trc fg py
	detection limit ppm									
Ag	*0.1*	n.d.	n.d.	n.d.	n.d.	n.d.	n.d.	n.d.	n.d.	n.d.
Au	*0.01*	n.d.	n.d.	n.d.	n.d.	n.d.	n.d.	n.d.	n.d.	n.d.
Be	*3*	n.d.	n.d.	n.d.	n.d.	n.d.	n.d.	n.d.	n.d.	n.d.
Co	*5*	14	24	11	n.d.	n.d.	6	22	62	9
Cu	*5*	7	264	31	n.d.	n.d.	n.d.	10	195	8
Mo	*8*	n.d.	n.d.	n.d.	n.d.	n.d.	n.d.	n.d.	n.d.	n.d.
Ni	*5*	34	52	73	51	9	7	47	68	21
Sb	*0.1*	0.73	1.66	1.16	2.07	1.19	n.d.	0.17	0.41	1.27
Sc	*1*	3	8	12	2	2	2	7	29	7
Sr	*1*	40	6	18	82	160	15	61	57	43
V	*5*	47	69	71	n.d.	37	54	83	162	24
W	*40*	n.d.	n.d.	n.d.	n.d.	n.d.	n.d.	n.d.	n.d.	n.d.
Zn	*2*	34	83	130	93	16	19	169	131	31

For abbreviations used in "Rock Name" and "Description", *see* Appendix 7; n.d., not detected; —, not analyzed.

Appendix 4. Continued

Field Number		**35a**	**173b**	**194a**	**194b**	**207**	**207b**	**223**	**229a**	**229b**
Lab Number		**01TRH102**	**01TRH169**	**01TRH182**	**01TRH183**	**01TRH186**	**01TRH201**	**01TRH202**	**01TRH203**	**01TRH234**
UTM East		424769	423168	428312	428312	417806	417806	424563	424326	424326
UTM North		5484468	5499018	5497939	5497939	5492215	5492215	5499536	5503786	5503786
UTM Zone		16	16	16	16	16	16	16	16	16
Belt		Quetico	CVB	SSB	SSB	SVB	SSB	CVB	NVB	NVB
Township		Kitto	Eva	Summer	Summers	Kitto	Kitto	Eva	Dorothea	Dorothea
Rock Name		flds wacke	maf mtvolc	quartz vein	quartz vein	argillite	argillite	maf mtvolc	maf mtvolc	int mtvolc
Description		diss, 5% fg pyrite	carb shear w/ trc fg py	stockwork veins w/ carb and trc py	stockwork veins w/ carb and trc py	trc py and po along fractures	trc py and po along fractures	slf maf flow cut by fel prph fels dike	diss to patchy py and po	diss py in qtz vn
detection limit										
	ppm									
Ag	*0.1*	n.d.	n.d.	n.d.	n.d.	n.d.	n.d.	n.d.	n.d.	n.d.
Au	*0.01*	n.d.	n.d.	n.d.	n.d.	n.d.	n.d.	n.d.	trace	n.d.
Be	*3*	n.d.	n.d.	n.d.	n.d.	n.d.	n.d.	n.d.	n.d.	n.d.
Co	*5*	37	37	7	7	31	n.d.	32	n.d.	26
Cu	*5*	311	99	6	n.d.	81	n.d.	425	2839	53
Mo	*8*	n.d.	n.d.	n.d.	n.d.	n.d.	n.d.	n.d.	n.d.	n.d.
Ni	*5*	14	47	18	19	108	6	35	n.d.	85
Sb	*0.1*	—	2.98	0.95	1.26	—	—	—	—	—
Sc	*1*	n.d.	23	3	3	13	5	16	1	11
Sr	*1*	9	108	124	123	293	44	106	11	233
V	*5*	n.d.	244	27	28	128	n.d.	125	6	93
W	*40*	n.d.	56	n.d.	n.d.	n.d.	n.d.	n.d.	n.d.	n.d.
Zn	*2*	6	106	25	20	205	37	126	3	26

Field Number		**229c**	**261**	**262**	**263**	**357**	**359**	**364**	**369**	**371**
Lab Number		**01TRH235**	**01TRH204**	**01TRH206**	**01TRH205**	**01TRH237**	**01TRH238**	**01TRH240**	**01TRH241**	**01TRH242**
UTM East		424326	418102	418251	418644	423872	424022	424007	424395	424317
UTM North		5503786	5488463	5488657	5488869	5503578	5503758	5504541	5503855	5504012
UTM Zone		16	16	16	16	16	16	16	16	16
Belt		NVB	SVB	SVB	SVB	NVB	NVB	NVB	NVB	NVB
Township		Dorothea	Kitto	Kitto	Kitto	Dorothea	Dorothea	Dorothea	Dorothea	Dorothea
Rock Name		int mtvolc	maf mtvolc	quartz vein	quartz vein	fel porphyry	int mtvolc	qtz fel porphyry	int mtvolc	int mtvolc
Description		diss py in qtz vn	diss py and po and minor carb altn	5 to 10% black tur	minor mag and v fg py - possibly IF	blebby to frac filled py in chl altn	highly chlc mtx to tuff cut by gabbro dike	2% diss cg py	trc py in frac	quartz vein w/ trc to 1% cg sbhl py
detection limit										
	ppm									
Ag	*0.1*	n.d.	n.d.	n.d.	n.d.	n.d.	n.d.	n.d.	n.d.	n.d.
Au	*0.01*	trace	n.d.	n.d.	n.d.	n.d.	n.d.	n.d.	n.d.	n.d.
Be	*3*	n.d.	n.d.	n.d.	n.d.	n.d.	n.d.	n.d.	n.d.	n.d.
Co	*5*	n.d.	53	n.d.	14	43	24	11	38	21
Cu	*5*	4554	108	n.d.	130	1366	96	6	332	34
Mo	*8*	n.d.	n.d.	n.d.	n.d.	n.d.	n.d.	n.d.	n.d.	n.d.
Ni	*5*	6	87	n.d.	15	70	88	12	30	15
Sb	*0.1*	—	—	—	—	—	—	—	—	—
Sc	*1*	1	35	2	1	20	17	11	16	11
Sr	*1*	13	71	16	n.d.	164	99	95	94	57
V	*5*	11	286	27	11	169	102	19	162	125
W	*40*	n.d.	n.d.	n.d.	n.d.	n.d.	n.d.	n.d.	n.d.	n.d.
Zn	*2*	6	101	3	15	95	122	92	151	171

For abbreviations used in "Rock Name" and "Description", *see* Appendix 7; n.d., not detected; —, not analyzed.

Appendix 4. Continued

Field Number		**387**	**394**	**394b**	**396**	**415a**	**415b**	**415c**	**431**	**431b**
Lab Number		**01TRH243**	**01TRH244**	**01TRH245**	**01TRH246**	**01TRH257**	**01TRH258**	**01TRH259**	**01TRH260**	**01TRH261**
UTM East		420575	428580	428580	428790	424639	424639	424639	422858	422858
UTM North		5502710	5498022	5498022	5498245	5505279	5505279	5505279	5504281	5504281
UTM Zone		16	16	16	16	16	16	16	16	16
Belt		NVB	CSB	CSB	CVB	NVB	NVB	NVB	NVB	NVB
Township		Dorothea	Summers	Summers	Summers	Dorothea	Dorothea	Dorothea	Dorothea	Dorothea
Rock Name		granodiorite	quartz vein	quartz vein	maf mtvolc	quartz vein	quartz vein	maf mtvolc	int mtvolc	int mtvolc
Description		trc to 1% cg py along frac w/ chl altn	foliation parallel vn w/ Fe carb in unit 6c	foliationn parallel vn w/ Fe carb in unit 6c	foliation parallel vn w/ Fe carb in unit 6c chlc shr	quartz vein w/ 5 to 10% py along frac w/ chl	5 to 10% v fg py along frac w/ chl	shr wr next to Tyson vein w/ 10% diss v fg py	shrd w/ chl and gossanous possibly 5% py	shrd w/ chl and gossanous 5% mg to fg py
detection limit										
	ppm									
Ag	*0.1*	n.d.	n.d.	n.d.	n.d.	n.d.	n.d.	n.d.	n.d.	n.d.
Au	*0.01*	n.d.	n.d.	n.d.	n.d.	n.d.	n.d.	n.d.	n.d.	n.d.
Be	*3*	n.d.	n.d.	n.d.	n.d.	n.d.	n.d.	n.d.	n.d.	n.d.
Co	*5*	14	n.d.	n.d.	5	6	16	32	33	21
Cu	*5*	59	12	9	n.d.	48	86	80	167	210
Mo	*8*	n.d.	n.d.	n.d.	n.d.	n.d.	n.d.	n.d.	n.d.	n.d.
Ni	*5*	n.d.	10	11	13	14	22	60	119	83
Sb	*0.1*	—	—	—	—	—	—	—	—	—
Sc	*1*	5	2	2	3	2	10	17	14	15
Sr	*1*	46	95	59	169	25	32	14	26	12
V	*5*	n.d.	14	13	12	15	67	131	119	119
W	*40*	n.d.	n.d.	n.d.	n.d.	n.d.	n.d.	n.d.	n.d.	n.d.
Zn	*2*	181	18	17	19	37	103	78	200	133

Field Number		**439**	**444a**	**444b**	**444c**	**444d**	**446**	**447**	**456**	**1033**
Lab Number		**01TRH262**	**01TRH266**	**01TRH269**	**01TRH270**	**01TRH265**	**01TRH268**	**01TRH267**	**01TRH092**	**01TRH100**
UTM East		423469	429578	429578	429578	429578	430556	430040	425213	423134
UTM North		5503788	5499904	5499904	5499904	5499904	5499594	5499862	5497365	5495178
UTM Zone		16	16	16	16	16	16	16	16	16
Belt		NVB	CVB	CVB	CVB	CVB	CVB	CVB	SSB	SSB
Township		Dorothea	Summers	Summers	Summers	Summers	Summers	Summers	Eva	Eva
Rock Name		int tuff	maf mtvolc	quartz vein	quartz vein	maf mtvolc	maf mtvolc	chert	quartz vein	quartz vein
Description		bedded w/ mag-ch bed 5 to 10% v fg diss po and/or py	late qtz stringers w/ mg euhedral py	smass v fg apy py along vn w/ trc py	smass v fg apy fg subhedral mass py	smass-subhedral needles	2% diss py in vesicles	sulphides w/in IF	fg tuff	minor potassic alteration
detection limit										
	ppm									
Ag	*0.1*	n.d.	n.d.	n.d.	n.d.	n.d.	n.d.	n.d.	n.d.	n.d.
Au	*0.01*	n.d.	n.d.	0.13	0.08	0.01	n.d.	n.d.	1.75	n.d.
Be	*3*	n.d.	n.d.	n.d.	n.d.	n.d.	n.d.	n.d.	n.d.	n.d.
Co	*5*	41	41	18	26	15	35	37	n.d.	n.d.
Cu	*5*	384	118	19	7	9	61	50	96	n.d.
Mo	*8*	n.d.	n.d.	n.d.	n.d.	n.d.	n.d.	n.d.	n.d.	n.d.
Ni	*5*	91	14	11	11	12	88	99	n.d.	6
Sb	*0.1*	—	—	—	—	—	—	—	—	—
Sc	*1*	12	33	9	11	10	19	19	4	n.d.
Sr	*1*	119	46	25	12	17	106	59	123	17
V	*5*	82	242	63	97	69	143	135	7	10
W	*40*	n.d.	n.d.	n.d.	n.d.	n.d.	n.d.	n.d.	6934	n.d.
Zn	*2*	131	158	36	30	32	83	122	40	12

For abbreviations used in "Rock Name" and "Description", *see* Appendix 7; n.d., not detected; —, not analyzed.

Appendix 4. Continued

Field Number		1055	1056a	1056b	1057a	1057b	1057	1059	1060	1065
Lab Number		01TRH125	01TRH126	01TRH127	01TRH207	01TRH208	01TRH128	01TRH129	01TRH130	01TRH138
UTM East		424252	424116	424116	424279	424279	424264	424724	423841	422705
UTM North		5497023	5497302	5497302	5497553	5497553	5497441	5497122	5496963	5496637
UTM Zone		16	16	16	16	16	16	16	16	16
Belt		SSB	SSB	SSB	SSB	SSB	SSB	SSB	SSB	SSB
Township		Eva	Eva	Eva	Eva	Eva	Eva	Eva	Eva	Eva
Rock Name		quartz vein	quartz vein	quartz vein	quartz vein	quartz vein	quartz vein	quartz vein	quartz vein	flds wacke
Description		white qtz w/ K altn and trc py in flds wacke	white qtz w/ K altn and trc py in flds wacke	white qtz w/ K altn and trc py in flds wacke	Fe carb and/or chl and up to 1% fg diss apy	Fe carb and/or chl and up to 1% fg diss apy	white qtz w/ K altn and trc py in flds wacke	white qtz w/ K altn and trc py in flds wacke	white qtz w/ K altn and trc py in flds wacke	sulphides in quartz vein
detection limit										
	ppm									
Ag	*0.1*	n.d.	n.d.	n.d.	n.d.	n.d.	n.d.	n.d.	n.d.	n.d.
Au	*0.01*	n.d.	n.d.	n.d.	0.04	0.01	n.d.	n.d.	n.d.	n.d.
Be	*3*	n.d.	n.d.	n.d.	n.d.	n.d.	n.d.	n.d.	n.d.	n.d.
Co	*5*	7	17	n.d.	n.d.	5	6	15	n.d.	18
Cu	*5*	n.d.	180	18	7	11	45	21	9	n.d.
Mo	*8*	n.d.	n.d.	n.d.	n.d.	n.d.	n.d.	n.d.	n.d.	n.d.
Ni	*5*	20	44	n.d.	12	13	17	39	10	49
Sb	*0.1*	—	—	—	—	—	—	—	—	2.56
Sc	*1*	4	8	n.d.	2	4	3	7	2	8
Sr	*1*	91	156	71	100	166	60	181	104	146
V	*5*	31	66	n.d.	19	25	23	58	15	75
W	*40*	n.d.	n.d.	n.d.	n.d.	n.d.	n.d.	n.d.	n.d.	n.d.
Zn	*2*	24	68	10	17	27	27	36	17	55

Field Number		1088	1088b	1091	1092	1108	1110a	1110b	1115a	1115b
Lab Number		01TRH132	01TRH141	01TRH137	01TRH149	01TRH145	01TRH194	01TRH195	01TRH146	01TRH147
UTM East		426236	426236	425296	425870	422936	423784	423784	424572	424572
UTM North		5495653	5495653	5497235	5497705	5498622	5498876	5498876	5497897	5497897
UTM Zone		16	16	16	16	16	16	16	16	16
Belt		SSB	SSB	SSB	SSB	CVB	CVB	CVB	SSB	SSB
Township		Summers	Summers	Eva	Summers	Eva	Eva	Eva	Eva	Eva
Rock Name		quartz vein	quartz vein	quartz vein	quartz vein	int mtvolc	quartz vein	maf mtvolc	quartz vein	quartz vein
Description		qtz tur vein w/ sercite alteration	qtz tur vein	w/ sericite and chlorite altn	trc sulphides, carb altn, and minor tur	trc diss sulphides	trc sulphides	carb altn and trc sulphides	quartz vein near fold hinge - carb altn	quartz vein near fold hinge in IF-carb altn
detection limit										
	ppm									
Ag	*0.1*	n.d.	n.d.	n.d.	n.d.	n.d.	n.d.	n.d.	n.d.	n.d.
Au	*0.01*	trace	n.d.	trace	n.d.	n.d.	n.d.	n.d.	n.d.	n.d.
Be	*3*	n.d.	n.d.	n.d.	n.d.	n.d.	n.d.	n.d.	n.d.	n.d.
Co	*5*	5	14	n.d.	n.d.	52	10	52	8	6
Cu	*5*	n.d.	18	15	n.d.	75	7	n.d.	10	10
Mo	*8*	n.d.	n.d.	n.d.	n.d.	n.d.	n.d.	n.d.	n.d.	n.d.
Ni	*5*	12	45	10	7	217	44	358	21	13
Sb	*0.1*	0.47	0.59	2.26	2.94	1.47	—	—	1.58	2.69
Sc	*1*	3	7	2	1	22	3	17	4	3
Sr	*1*	82	130	177	22	65	23	73	303	147
V	*5*	28	55	19	16	166	20	113	20	14
W	*40*	n.d.	n.d.	n.d.	n.d.	n.d.	n.d.	n.d.	n.d.	n.d.
Zn	*2*	26	39	19	12	97	16	76	23	16

For abbreviations used in "Rock Name" and "Description", *see* Appendix 7; n.d., not detected; —, not analyzed.

Appendix 4. Continued

Field Number		**1121**	**1122**	**1128a**	**1128b**	**1154**	**1155**	**1156a**	**1156b**	**1162**
Lab Number		**01TRH133**	**01TRH134**	**01TRH135**	**01TRH136**	**01TRH170**	**01TRH171**	**01TRH172**	**01TRH173**	**01TRH174**
UTM East		423994	425259	430098	430098	428079	428162	428393	428393	422851
UTM North		5495808	5495975	5497034	5497034	5499013	5498970	5498968	5498968	5498853
UTM Zone		16	16	16	16	16	16	16	16	16
Belt		SSB	SSB	SSB	SSB	SSB	SSB	SSB	SSB	CVB
Township		Eva	Eva	Summers	Summers	Summers	Summers	Summers	Summers	Eva
Rock Name		quartz vein	quartz vein	quartz vein	quartz vein	quartz vein	quartz vein	quartz vein	quartz vein	maf mtvolc
Description		qtz tur vein	qtz tur w/ K and/or hem alteration	qtz tur vein	qtz tur vein	carb altn	carb altn next to IF	carb and pot and/or hem altn - fold hinge	carb altn in IF	hem and carb altn
detection limit										
	ppm									
Ag	*0.1*	n.d.	n.d.	n.d.	n.d.	n.d.	n.d.	n.d.	n.d.	n.d.
Au	*0.01*	n.d.	n.d.	n.d.	n.d.	n.d.	n.d.	n.d.	n.d.	n.d.
Be	*3*	n.d.	n.d.	n.d.	n.d.	n.d.	n.d.	n.d.	n.d.	n.d.
Co	*5*	9	n.d.	6	n.d.	n.d.	n.d.	6	n.d.	45
Cu	*5*	n.d.	n.d.	7	n.d.	n.d.	n.d.	9	n.d.	106
Mo	*8*	n.d.	n.d.	n.d.	n.d.	n.d.	n.d.	n.d.	n.d.	n.d.
Ni	*5*	43	8	23	n.d.	n.d.	12	15	15	66
Sb	*0.1*	0.51	0.83	0.21	0.12	1.85	0.97	8.74	2.16	0.67
Sc	*1*	5	2	4	n.d.	n.d.	3	3	2	28
Sr	*1*	121	107	69	8	20	19	13	280	63
V	*5*	35	32	34	6	n.d.	9	21	14	234
W	*40*	n.d.	n.d.	n.d.	n.d.	n.d.	n.d.	n.d.	n.d.	n.d.
Zn	*2*	30	19	18	5	15	29	24	26	89

Field Number		**1171**	**1172**	**1173**	**1176**	**1177a**	**1177b**	**1209**	**1216**	**1218a**
Lab Number		**01TRH175**	**01TRH176**	**01TRH177**	**01TRH187**	**01TRH254**	**01TRH255**	**01TRH189**	**01TRH188**	**01TRH191**
UTM East		416552	416017	416140	429026	429256	429256	423582	425081	425540
UTM North		5488890	5490411	5490670	5499158	5499271	5499271	5499916	5501019	5501156
UTM Zone		16	16	16	16	16	16	16	16	16
Belt		SVB	SVB	SVB	SVB	CVB	CVB	CVB	CVB	CVB
Township		Kitto	Kitto	Kitto	Kitto	Summers	Summers	Eva	Summers	Summers
Rock Name		maf mtvolc	maf mtvolc	maf mtvolc	maf mtvolc	maf mtvolc	maf mtvolc	maf mtvolc	maf mtvolc	maf mtvolc
Description		1 to 2% fg py - po pod in graphitic shear	white 10 cm quartz vein and IF	white 10 cm quartz vein and IF	trc sulphides	quartz vein w/ maf layers similar to Leitch Mine	quartz vein w/ maf layers similar to Leitch Mine	sulphides found in carb shear	cp present asoc w/ carb altn zone	trc sulphide in wall to vein
detection limit										
	ppm									
Ag	*0.1*	n.d.	n.d.	n.d.	n.d.	n.d.	n.d.	n.d.	n.d.	n.d.
Au	*0.01*	n.d.	n.d.	n.d.	n.d.	n.d.	n.d.	n.d.	n.d.	n.d.
Be	*3*	n.d.	n.d.	n.d.	n.d.	n.d.	n.d.	n.d.	n.d.	n.d.
Co	*5*	182	66	32	31	n.d.	7	31	58	17
Cu	*5*	228	280	133	84	n.d.	9	56	298	21
Mo	*8*	n.d.	n.d.	n.d.	n.d.	n.d.	n.d.	n.d.	n.d.	n.d.
Ni	*5*	211	126	69	81	n.d.	21	92	138	53
Sb	*0.1*	8.32	1.23	0.37	—	—	—	—	—	—
Sc	*1*	n.d.	37	16	15	n.d.	3	12	13	9
Sr	*1*	3	28	19	111	54	66	64	60	69
V	*5*	234	323	153	112	8	28	75	117	55
W	*40*	n.d.	n.d.	n.d.	n.d.	n.d.	n.d.	n.d.	n.d.	n.d.
Zn	*2*	31	161	93	69	5	28	119	173	59

For abbreviations used in "Rock Name" and "Description", *see* Appendix 7; n.d., not detected; —, not analyzed.

Appendix 4. Continued

Field Number		**1218b**	**1218c**	**1265**	**1372**	**1390a**	**1390b**	**1392**	**1394**	**1402**
Lab Number		**01TRH192**	**01TRH193**	**01TRH190**	**01TRH218**	**01TRH247**	**01TRH248**	**01TRH252**	**01TRH251**	**01TRH250**
UTM East		425540	425540	416583	420751	428708	428708	428735	425061	425184
UTM North		5501156	5501156	5488666	5503312	5500110	5500110	5499700	5504107	5504563
UTM Zone		16	16	16	16	16	16	16	16	16
Belt		CVB	CVB	SVB	NVB	CVB	NVB	CVB	CVB	NVB
Township		Summers	Summers	Kitto	Dorothea	Summers	Summers	Summers	Dorothea	Dorothea
Rock Name		quartz vein	gossan	maf mtvolc	fel porphyry	maf mtvolc	maf mtvolc	maf mtvolc	maf mtvolc	maf mtvolc
Description		trc sulphides	trc sulphides	trc sulphides	sulphide-rich intrusive	gossan, mass sulphide, old trench	gossan, mass sulphide, old trench	gossan, previously trenched	mass sulphides, carb shrd, old trench	large py crystals diss in rock
detection limit										
	ppm									
Ag	*0.1*	n.d.	n.d.	n.d.	n.d.	n.d.	n.d.	n.d.	n.d.	n.d.
Au	*0.01*	n.d.	n.d.	n.d.	n.d.	n.d.	n.d.	n.d.	n.d.	n.d.
Be	*3*	n.d.	n.d.	n.d.	n.d.	n.d.	n.d.	n.d.	n.d.	n.d.
Co	*5*	n.d.	n.d.	44	17	n.d.	11	30	21	23
Cu	*5*	n.d.	47	52	38	n.d.	n.d.	n.d.	11	16
Mo	*8*	n.d.	n.d.	n.d.	n.d.	n.d.	n.d.	n.d.	n.d.	n.d.
Ni	*5*	19	30	100	23	39	105	117	33	15
Sb	*0.1*	—	—	—	—	—	—	—	—	—
Sc	*1*	n.d.	n.d.	34	8	n.d.	n.d.	2	13	14
Sr	*1*	11	21	38	98	4	5	9	59	64
V	*5*	n.d.	n.d.	297	64	n.d.	n.d.	n.d.	113	154
W	*40*	n.d.	n.d.	n.d.	n.d.	n.d.	n.d.	n.d.	n.d.	n.d.
Zn	*2*	38	49	63	87	60	69	70	1123	87

Field Number		**1440**	**2080**	**2083**	**2124a**	**2124b**	**2125a**	**2125b**	**2125c**	**2153**
Lab Number		**01TRH263**	**01TRH156**	**01TRH148**	**01TRH150**	**01TRH151**	**01TRH152**	**01TRH153**	**01TRH154**	**01TRH180**
UTM East		430203	424603	424687	429016	429016	428970	428970	428970	423970
UTM North		5493555	5497049	5494161	5496582	5496582	5496732	5496732	5496732	5499613
UTM Zone		16	16	16	16	16	16	16	16	16
Belt		SVB	SSB	SSB	SSB	SSB	SSB	SSB	SSB	CVB
Township		Summers	Eva	Eva	Summers	Summers	Summers	Summers	Summers	Eva
Rock Name		maf mtvolc	quartz vein	flds wacke	quartz vein	flds wacke	quartz vein	flds wacke	quartz vein	quartz vein
Description		sulphides w/ rusty weathering	carb altn	diss fg cubic py	chl altd rock near quartz vein w/ trc sulphide	quartz vein w/ trc v fg sulphide	w/ tur and v fg sulphides	trc sulphides	tur and trc sulphides	sericite and carb altn
detection limit										
	ppm									
Ag	*0.1*	n.d.	n.d.	n.d.	n.d.	n.d.	n.d.	n.d.	n.d.	n.d.
Au	*0.01*	n.d.	n.d.	0.02	n.d.	n.d.	n.d.	n.d.	n.d.	n.d.
Be	*3*	n.d.	n.d.	n.d.	n.d.	n.d.	n.d.	n.d.	n.d.	n.d.
Co	*5*	30	6	22	15	22	n.d.	20	13	n.d.
Cu	*5*	365	n.d.	46	29	35	5	27	7	n.d.
Mo	*8*	n.d.	n.d.	n.d.	n.d.	n.d.	n.d.	n.d.	n.d.	n.d.
Ni	*5*	42	17	65	34	69	6	50	37	n.d.
Sb	*0.1*	—	0.51	0.78	0.6	0.74	0.44	0.59	0.63	n.d.
Sc	*1*	3	3	9	8	10	1	9	7	n.d.
Sr	*1*	8	128	399	98	277	68	214	205	1
V	*5*	18	24	94	77	89	24	83	66	n.d.
W	*40*	n.d.	n.d.	n.d.	n.d.	n.d.	n.d.	n.d.	n.d.	n.d.
Zn	*2*	559	29	79	69	79	11	68	65	n.d.

For abbreviations used in "Rock Name" and "Description", *see* Appendix 7; n.d., not detected; —, not analyzed.

Appendix 4. Continued

Field Number		**2161**	**2162**	**2169**	**2185**	**2192**	**2198**	**2250**	**2251**	**2262**
Lab Number		**01TRH178**	**01TRH200**	**01TRH179**	**01TRH181**	**01TRH197**	**01TRH196**	**01TRH198**	**01TRH209**	**01TRH227**
UTM East		422062	424914	425880	427507	416941	417694	416087	415990	417301
UTM North		5499033	5497764	5498840	5503916	5492343	5493102	5489018	5489617	5488822
UTM Zone		16	16	16	16	16	16	16	16	16
Belt		CVB	SSB	CVB	CSB	SSB	SSB	SVB	SVB	SVB
Township		Eva	Eva	Summers	Summers	Kitto	Kitto	Kitto	Kitto	Kitto
Rock Name		quartz vein	gossan	maf mtvolc	quartz vein	quartz vein	quartz vein	quartz vein	maf mtvolc	maf mtvolc
Description		py and mlc	highly weathered py and po	trc diss sulphides	bs qtz vn w/ chl ser altn	minor sulphides and chl altn	minor sulphides and chl altn	minor sulphides and chl altn	bs sulphides	sulphides
detection limit	*ppm*									
Ag	*0.1*	n.d.	n.d.	n.d.	n.d.	n.d.	n.d.	n.d.	n.d.	n.d.
Au	*0.01*	n.d.	n.d.	n.d.	n.d.	n.d.	n.d.	0.03	n.d.	n.d.
Be	*3*	n.d.	n.d.	n.d.	n.d.	n.d.	n.d.	n.d.	n.d.	n.d.
Co	*5*	14	8	34	5	n.d.	33	6	54	48
Cu	*5*	5102	n.d.	39	n.d.	8	184	n.d.	754	112
Mo	*8*	n.d.	n.d.	n.d.	n.d.	n.d.	n.d.	n.d.	n.d.	n.d.
Ni	*5*	22	53	167	14	11	70	12	52	71
Sb	*0.1*	0.12	—	1.61	0.75	—	—	—	—	—
Sc	*1*	8	8	13	2	3	8	3	5	34
Sr	*1*	23	20	89	51	53	175	12	3	63
V	*5*	17	46	94	14	24	68	10	26	278
W	*40*	n.d.	n.d.	n.d.	n.d.	n.d.	n.d.	n.d.	n.d.	n.d.
Zn	*2*	14	84	92	19	60	88	64	40	98

Field Number		**2321b**	**4023**	**5005**	**5006**	**5007**	**5008a**	**5008b**	**5010**	**5015**
Lab Number		**01TRH228**	**01TRH226**	**01TRH210**	**01TRH211**	**01TRH212**	**01TRH213**	**01TRH214**	**01TRH229**	**01TRH221**
UTM East		420297	421387	421256	421190	420919	420827	420827	429060	429645
UTM North		5506140	5506275	5511357	5511262	5511429	5511484	5511484	5493507	5493090
UTM Zone		16	16	16	16	16	16	16	16	16
Belt		NVB	NVB	NVB	NVB	NVB	NVB	NVB	SVB	SVB
Township		Dorothea	Dorothea	Dorothea	Dorothea	Dorothea	Dorothea	Dorothea	Summers	Summers
Rock Name		IF	gabbro	quartz vein	quartz vein	maf mtvolc	maf mtvolc	maf mtvolc	maf mtvolc	maf mtvolc
Description		shear, sulphides	gabbro w/ sulphides	qtz veinlets in shrd mtvolc - PLF	qtz veinlets in shrd carb and slf mtvolc - PLF	K/cz/slf altn w/minor qtz veinlets - PLF	slf w/ 1% fg diss py - PLF	slf-carb w/patches of fg py up to 0.5 cm - PLF	sulphides	sulphide w/in quartz-filled fracture
detection limit	*ppm*									
Ag	*0.1*	n.d.	n.d.	n.d.	n.d.	n.d.	n.d.	n.d.	n.d.	n.d.
Au	*0.01*	n.d.	n.d.	n.d.	n.d.	n.d.	n.d.	n.d.	0.08	n.d.
Be	*3*	n.d.	n.d.	n.d.	n.d.	n.d.	n.d.	n.d.	n.d.	n.d.
Co	*5*	27	50	9	n.d.	16	31	56	41	6
Cu	*5*	193	88	32	n.d.	n.d.	35	260	158	11
Mo	*8*	n.d.	n.d.	n.d.	n.d.	n.d.	n.d.	n.d.	n.d.	n.d.
Ni	*5*	29	35	16	12	47	99	58	57	8
Sb	*0.1*	—	—	—	—	—	—	—	—	—
Sc	*1*	6	34	3	4	7	11	10	32	3
Sr	*1*	36	72	126	28	114	96	91	38	2
V	*5*	45	326	23	27	59	94	81	290	29
W	*40*	n.d.	n.d.	n.d.	n.d.	n.d.	n.d.	n.d.	n.d.	n.d.
Zn	*2*	445	100	31	14	35	48	31	54	10

For abbreviations used in "Rock Name" and "Description", *see* Appendix 7; n.d., not detected; —, not analyzed.

Appendix 4. Continued

Field Number		**5027**	**5035**	**5058**	**5061**	**5064**
Lab Number		**01TRH230**	**01TRH231**	**01TRH220**	**01TRH222**	**01TRH219**
UTM East		428064	427095	427719	427321	427042
UTM North		5492868	5494088	5492538	5492366	5492550
UTM Zone		16	16	16	16	16
Belt		SVB	SVB	SVB	SVB	SVB
Township		Summers	Summers	Summers	Summers	Summers
Rock Name		gabbro	maf mtvolc	maf mtvolc	maf mtvolc	maf mtvolc
Description		IF w/ sulphides	sulphides	sulphide-rich mtvolc, carb altn	sulphide w/in qtz vein	sulphides, gossan-type fracture
detection limit						
	ppm					
Ag	*0.1*	n.d.	n.d.	n.d.	n.d.	n.d.
Au	*0.01*	n.d.	n.d.	n.d.	n.d.	0.03
Be	*3*	n.d.	n.d.	n.d.	n.d.	n.d.
Co	*5*	n.d.	37	n.d.	n.d.	44
Cu	*5*	153	n.d.	44	11	78
Mo	*8*	n.d.	n.d.	n.d.	n.d.	n.d.
Ni	*5*	22	54	24	7	69
Sb	*0.1*	—	—	—	—	—
Sc	*1*	5	36	5	n.d.	19
Sr	*1*	4	21	2	3	13
V	*5*	16	340	23	8	149
W	*40*	n.d.	n.d.	n.d.	n.d.	n.d.
Zn	*2*	109	173	235	7	70

Field Number		**5076**	**5078**	**5092**	**5093**	**5118**
Lab Number		**01TRH232**	**01TRH233**	**01TRH223**	**01TRH264**	**01TRH253**
UTM East		428014	427832	429046	429086	426808
UTM North		5494401	5494807	5494644	5494533	5500624
UTM Zone		16	16	16	16	16
Belt		SVB	SVB	SVB	SVB	CVB
Township		Summers	Summers	Summers	Summers	Summers
Rock Name		gabbro	maf mtvolc	maf mtvolc	IF	maf mtvolc
Description		gabbro w/ sulphides	sulphides	sulphide w/in qtz vein	sulphides in unit 5a	sulphides w/in mass mtvolc
detection limit						
	ppm					
Ag	*0.1*	n.d.	n.d.	n.d.	n.d.	n.d.
Au	*0.01*	0.03	n.d.	n.d.	0.31	n.d.
Be	*3*	n.d.	n.d.	n.d.	n.d.	n.d.
Co	*5*	51	25	19	15	41
Cu	*5*	103	39	234	80	n.d.
Mo	*8*	n.d.	n.d.	n.d.	n.d.	n.d.
Ni	*5*	102	72	42	28	53
Sb	*0.1*	—	—	—	—	—
Sc	*1*	32	11	12	3	20
Sr	*1*	140	565	27	2	60
V	*5*	293	96	112	23	205
W	*40*	n.d.	n.d.	n.d.	n.d.	n.d.
Zn	*2*	115	76	203	566	105

For abbreviations used in "Rock Name" and "Description", *see* Appendix 7; n.d., not detected; —, not analyzed.

Appendix 5:

Assay Results for Base Metals-Related Sampling.

Appendix 5. Assay results for base metals-related sampling.

Field Number		**15**	**35**	**204**	**229**	**229b**	**229c**	**261**	**357**
Lab Number		**01TRH101**	**01TRH102**	**01TRH184**	**01TRH203**	**01TRH234**	**01TRH235**	**01TRH204**	**01TRH237**
UTM East		424590	424769	424606	424326	424326	424326	418102	423872
UTM North		5490279	5484468	5503973	5503786	5503786	5503786	5488463	5503578
UTM Zone		16	16	16	16	16	16	16	16
Belt		Nipigon sills	Quetico Subprovince	CVB	NVB	NVB	NVB	SVB	NVB
Township		Kitto	Kitto	Dorothea	Dorothea	Dorothea	Dorothea	Kitto	Dorothea
Rock Name		diabase	quartz vein	maf mtvolc	maf mtvolc	int mtvolc	int mtvolc	maf mtvolc	fel porphyry
Description		massive, mg w/ altn along jnt and trc sulphide	15% fg diss py	qtz and carb amyg w/ minor py and trace diss py	diss to patchy py and po	diss py in qtz vein	diss py in qtz vein	diss py and po and mi carb altn	blebby to frac filled py in chl altn
	detection limit								
Ag	*0.1 ppm*	—	n.d.	n.d.	n.d.	n.d.	n.d.	n.d.	n.d.
Au[1]	*5 ppb*	—	—	—	—	—	—	—	—
Au[2]	*0.01 ppm*	—	n.d.	n.d.	n.d.	Trace	Trace	n.d.	n.d.
Be	*3 ppm*	n.d.	n.d.	n.d.	n.d.	n.d.	n.d.	n.d.	n.d.
Co	*5 ppm*	28	37	35	32	n.d.	n.d.	53	43
CO_2	*0.03 wt %*	—	—	—	—	—	—	—	—
Cu	*5 ppm*	260	311	150	425	2839	4554	108	1366
Mo	*8 ppm*	n.d.	n.d.	n.d.	n.d.	n.d.	n.d.	n.d.	n.d.
Ni	*5 ppm*	60	14	48	35	n.d.	6	87	70
Pd	*8 ppb*	—	—	—	—	—	—	—	—
Pt	*8 ppb*	—	—	—	—	—	—	—	—
S	*0.01 wt %*	—	—	—	—	—	—	—	—
Sb	*0.1 ppm*	—	—	—	—	—	—	—	—
Sc	*1 ppm*	10	n.d.	18	16	1	1	35	20
Sr	*1 ppm*	137	9	88	106	11	13	71	164
V	*5 ppm*	92	n.d.	174	125	6	11	286	169
W	*40 ppm*	n.d.	n.d.	n.d.	n.d.	n.d.	n.d.	n.d.	n.d.
Zn	*2 ppm*	44	6	78	126	3	6	101	95

For abbreviations used in "Rock Name" and "Description", *see* Appendix 7.
[1] MS–IAT 200; [2] gravimetric fire assay; n.d., not detected; —, not analyzed.

Appendix 5. Continued

Field Number		**362**	**371**	**387**	**413**	**431a**	**431b**	**439**	**443**
Lab Number		**01TRH239**	**01TRH242**	**01TRH074**	**01TRH256**	**01TRH260**	**01TRH261**	**01TRH262**	**01TRH091**
UTM East		423956	424317	420575	425378	422858	422858	423469	424778
UTM North		5504235	5504012	5502710	5504961	5504281	5504281	5503788	5504951
UTM Zone		16	16	16	16	16	16	16	16
Belt		NVB	NVB	NVB	NVB	NVB	NVB	NVB	NVB
Township		Dorothea	Dorothea	Dorothea	Dorothea	Dorothea	Dorothea	Dorothea	Dorothea
Rock Name		int mtvolc	int mtvolc	fels intrusive	maf lapilli tuff	int mtvolc	int mtvolc	int tuff	quartz vein
Description		up to 10% diss py chlc mtx	qtz vein w/ trace to 1% cg sbhl py	massive flow, fg	shrd volc w/ tabular frag of qtz and 5% diss py	shrd w/ chl and gossanous possibly 5% py	shrd w/ chl and gossanous 5% mg to fg py	bedded w/ mag-ch bed 5-10% v fg diss po and/or py	crack seal quartz vein
	detection limit								
Ag	*0.1 ppm*	n.d.	n.d.	—	n.d.	n.d.	n.d.	n.d.	—
Au[1]	*5 ppb*	—	—	n.d.	—	—	—	—	11.99
Au[2]	*0.01 ppm*	n.d.	n.d.	—	n.d.	n.d.	n.d.	n.d.	—
Be	*3 ppm*	n.d.	n.d.	n.d.	n.d.	n.d.	n.d.	n.d.	n.d.
Co	*5 ppm*	41	21	12	135	33	21	41	n.d.
CO_2	*0.03 wt %*	—	—	3.08	—	—	—	—	—
Cu	*5 ppm*	190	34	17	28708	167	210	384	n.d.
Mo	*8 ppm*	n.d.	n.d.	n.d.	n.d.	n.d.	n.d.	n.d.	3839
Ni	*5 ppm*	58	15	17	349	119	83	91	n.d.
Pd	*8 ppb*	—	—	n.d.	—	—	—	—	n.d.
Pt	*8 ppb*	—	—	n.d.	—	—	—	—	n.d.
S	*0.01 wt %*	—	—	0.08	—	—	—	—	—
Sb	*0.1 ppm*	—	—	—	—	—	—	—	—
Sc	*1 ppm*	14	11	5	25	14	15	12	n.d.
Sr	*1 ppm*	66	57	117	28	26	12	119	3
V	*5 ppm*	51	125	33	92	119	119	82	n.d.
W	*40 ppm*	n.d.	n.d.	n.d.	n.d.	n.d.	n.d.	n.d.	n.d.
Zn	*2 ppm*	344	171	87	1105	200	133	131	8

For abbreviations used in "Rock Name" and "Description", *see* Appendix 7.

[1] MS–IAT 200; [2] gravimetric fire assay; n.d., not detected; —, not analyzed.

Appendix 5. Continued

Field Number		**444**	**446**	**1108**	**1110a**	**1110b**	**1132**	**1171**	**1172**
Lab Number		**01TRH084**	**01TRH268**	**01TRH145**	**01TRH194**	**01TRH195**	**01TRH144**	**01TRH175**	**01TRH176**
UTM East		429578	430556	422936	423784	423784	429455	416552	416017
UTM North		5499904	5499594	5498622	5498876	5498876	5496537	5488890	5490411
UTM Zone		16	16	16	16	16	16	16	16
Belt		CVB	CVB	CVB	CVB	CVB	SSB	SVB	SVB
Township		Dorothea	Summers	Eva	Eva	Eva	Summers	Kitto	Kitto
Rock Name		gabbro	maf mtvolc	int mtvolc	quartz vein	maf mtvolc	feldspathic wacke	maf mtvolc	maf mtvolc
Description		massive, mg	2% diss py in vesicles	trc diss sulphides	trc sulphides	carb altn and trc sulphides	trc fg diss sulphides	1 to 2% fg py - po pod in graphitic shr	w/ 10 cm quartz vein and IF
	detection limit								
Ag	*0.1 ppm*	—	n.d.	n.d.	n.d.	n.d.	n.d.	n.d.	n.d.
Au[1]	*5 ppb*	n.d.	—	—	—	—	—	—	—
Au[2]	*0.01 ppm*	—	n.d.	n.d.	n.d.	n.d.	n.d.	n.d.	n.d.
Be	*3 ppm*	n.d.	n.d.	n.d.	n.d.	n.d.	n.d.	n.d.	n.d.
Co	*5 ppm*	51	35	52	10	52	21	182	66
CO_2	*0.03 wt %*	1.53	—	—	—	—	—	—	—
Cu	*5 ppm*	65	61	75	7	n.d.	28	228	280
Mo	*8 ppm*	n.d.	n.d.	n.d.	n.d.	n.d.	n.d.	n.d.	n.d.
Ni	*5 ppm*	26	88	217	44	358	68	211	126
Pd	*8 ppb*	n.d.	—	—	—	—	—	—	—
Pt	*8 ppb*	n.d.	—	—	—	—	—	—	—
S	*0.01 wt %*	n.d.	—	—	—	—	—	—	—
Sb	*0.1 ppm*	—	—	1.47	—	—	0.8	8.32	1.23
Sc	*1 ppm*	33	19	22	3	17	10	n.d.	37
Sr	*1 ppm*	89	106	65	23	73	451	3	28
V	*5 ppm*	355	143	166	20	113	87	234	323
W	*40 ppm*	n.d.	n.d.	n.d.	n.d.	n.d.	n.d.	n.d.	n.d.
Zn	*2 ppm*	129	83	97	16	76	76	31	161

For abbreviations used in "Rock Name" and "Description", *see* Appendix 7.

[1] MS–IAT 200; [2] gravimetric fire assay; n.d., not detected; —, not analyzed.

Appendix 5. Continued

Field Number		**1173**	**1189**	**1347**	**1383**	**1390a**	**1390b**	**1394**	**1402**
Lab Number		**01TRH177**	**01TRH185**	**01TRH217**	**01TRH249**	**01TRH247**	**01TRH248**	**01TRH251**	**01TRH250**
UTM East		416140	429947	420617	428928	428708	428708	425061	425184
UTM North		5490670	5502113	5506730	5500585	5500110	5500110	5504107	5504563
UTM Zone		16	16	16	16	16	16	16	16
Belt		SVB	CVB	NVB	CVB	CVB	CVB	NVB	NVB
Township		Kitto	Sandra	Dorothea	Summers	Summers	Summers	Dorothea	Dorothea
Rock Name		maf mtvolc	maf mtvolc	maf mtvolc	maf mtvolc	maf mtvolc	maf mtvolc	maf mtvolc	maf mtvolc
Description		w/ 10 cm quartz vein and IF	smass to diss py and po	sulphides, gossan-type fracture	sulphides in shear subbelt, old trench	gossan, mass sulphide, old trench	gossan, mass sulphide, old trench	mass sulphides, carb shrd, old trench	large py crystals diss in rock
	detection limit								
Ag	*0.1 ppm*	n.d.	n.d.	n.d.	n.d.	n.d.	n.d.	n.d.	n.d.
Au^1	*5 ppb*	—	—	—	n.d.	—	—	—	—
Au^2	*0.01 ppm*	n.d.	n.d.	n.d.	n.d.	n.d.	n.d.	n.d.	n.d.
Be	*3 ppm*	n.d.	n.d.	n.d.	n.d.	n.d.	n.d.	n.d.	n.d.
Co	*5 ppm*	32	14	18	76	n.d.	11	21	23
CO$_2$	*0.03 wt %*	—	—	—	—	—	—	—	—
Cu	*5 ppm*	133	7	112	2069	n.d.	n.d.	11	16
Mo	*8 ppm*	n.d.	n.d.	n.d.	n.d.	n.d.	n.d.	n.d.	n.d.
Ni	*5 ppm*	69	46	48	70	39	105	33	15
Pd	*8 ppb*	—	—	—	—	—	—	—	—
Pt	*8 ppb*	—	—	—	—	—	—	—	—
S	*0.01 wt %*	—	—	—	—	—	—	—	—
Sb	*0.1 ppm*	0.37	—	—	—	—	—	—	—
Sc	*1 ppm*	16	6	6	8	n.d.	n.d.	13	14
Sr	*1 ppm*	19	107	59	17	4	5	59	64
V	*5 ppm*	153	31	58	55	n.d.	n.d.	113	154
W	*40 ppm*	n.d.	n.d.	n.d.	n.d.	n.d.	n.d.	n.d.	n.d.
Zn	*2 ppm*	93	67	34	286	60	69	1123	87

For abbreviations used in "Rock Name" and "Description", *see* Appendix 7.

[1] MS–IAT 200; [2] gravimetric fire assay; n.d., not detected; —, not analyzed.

Appendix 5. Continued

Field Number		**1440**	**2080**	**2161**	**2251**	**2321**	**5093**	**5118**
Lab Number		**01TRH263**	**01TRH155**	**01TRH178**	**01TRH209**	**01TRH228**	**01TRH264**	**01TRH253**
UTM East		430203	424603	422062	415990	420297	429086	426808
UTM North		5493555	5497049	5499033	5489617	5506140	5494533	5500624
UTM Zone		16	16	16	16	16	16	16
Belt		SVB	SSB	CVB	SVB	NVB	SVB	CVB
Township		Summers	Eva	Eva	Kitto	Dorothea	Summers	Summers
Rock Name		maf mtvolc	diabase	quartz vein	maf mtvolc	IF	IF	maf mtvolc
Description		sulphides w/ rusty weathering	chill w/ trc sulphides	py and mlc	sulphides	shr, sulphides	sulphides in unit 5a	sulphides w/in mass mtvolc
	detection limit							
Ag	*0.1 ppm*	n.d.	n.d.	n.d.	n.d.	n.d.	n.d.	n.d.
Au[1]	*5 ppb*	—	—	—	—	—	—	—
Au[2]	*0.01 ppm*	n.d.	n.d.	n.d.	n.d.	n.d.	0.31	n.d.
Be	*3 ppm*	n.d.	n.d.	n.d.	n.d.	n.d.	n.d.	n.d.
Co	*5 ppm*	30	40	14	54	27	15	41
CO_2	*0.03 wt %*	—	—	—	—	—	—	—
Cu	*5 ppm*	365	14	5102	754	193	80	n.d.
Mo	*8 ppm*	n.d.	n.d.	n.d.	n.d.	n.d.	n.d.	n.d.
Ni	*5 ppm*	42	19	22	52	29	28	53
Pd	*8 ppb*	—	—	—	—	—	—	—
Pt	*8 ppb*	—	—	—	—	—	—	—
S	*0.01 wt %*	—	—	—	—	—	—	—
Sb	*0.1 ppm*	—	—	0.12	—	—	—	—
Sc	*1 ppm*	3	35	8	5	6	3	20
Sr	*1 ppm*	8	312	23	3	36	2	60
V	*5 ppm*	18	108	17	26	45	23	205
W	*40 ppm*	n.d.	n.d.	n.d.	n.d.	n.d.	n.d.	n.d.
Zn	*2 ppm*	559	795	14	40	445	566	105

For abbreviations used in "Rock Name" and "Description", *see* Appendix 7.

[1] MS–IAT 200; [2] gravimetric fire assay; n.d., not detected; —, not analyzed.

Appendix 6:

Assay Results for Platinum Group-Related Sampling.

Appendix 6. Assay results for platinum group-related sampling.

Field Number		**15a**	**15b**	**15c**	**15d**	**37**	**51a**	**51b**	**51c**
Lab Number		**01TRH013**	**01TRH014**	**01TRH015**	**01TRH120**	**01TRH104**	**01TRH001**	**01TRH002**	**01TRH107**
UTM East		424590	424590	424590	424590	424220	424944	424914	424914
UTM North		5490279	5490279	5490279	5490279	5483970	5485067	5485081	5485081
UTM Zone		16	16	16	16	16	16	16	16
Belt		Nipigon sills	Nipigon sills	Nipigon sills	Nipigon sills	Nipigon sills	Nipigon sills	Nipigon sills	Nipigon sills
Township		Kitto	Kitto	Kitto	Kitto	Kitto	Kitto	Kitto	Kitto
Rock Name		diabase	diabase	diabase	diabase	diabase	diabase	diabase	diabase
Description		mass, mg - base of quarry wall	mass, mg - ~20 m above base of wall	mass, mg - ~40 m above base of wall	mass, mg w/ altn along jnt and trc sulphide	mg w/ trc py in jnt next to contact w/ mtsed	mass, mg, near top of sill	mass, mg, mag prpc	v cg amp + pnk fel jnt filling w/ trc fg py, po
	detection limit								
Au[1]	*5 ppb*	n.d.	n.d.	n.d.	n.d.	n.d.	n.d.	n.d.	5.8
Au[2]	*0.73 ppb*	4.11	3.77	3.58	—	—	4.17	4.52	—
Co	*5 ppm*	62	61	56	38	48	59	55	56
CO_2	*0.03 wt %*	0.06	0.08	0.06	—	—	0.05	0.08	—
Cu	*5 ppm*	147	154	150	186	284	180	233	203
Ir	*0.04 ppb*	0.15	0.15	0.1	—	—	0.06	n.d.	—
Ni	*5 ppm*	154	148	120	87	35	106	61	34
Pd[1]	*8 ppb*	13.91	13.42	13.85	9.3	n.d.	15.76	12.33	17.42
Pd[2]	*0.11 ppb*	14.4	14.6	14.8	—	—	18.7	17.6	—
Pt[1]	*8 ppb*	12.16	12.16	10.03	8.25	n.d.	9.01	n.d.	n.d.
Pt[2]	*0.14 ppb*	12.8	12.6	10.4	—	—	10.2	7.44	—
Rh	*0.08 ppb*	0.78	0.81	0.74	—	—	0.76	0.66	—
Ru	*0.13 ppb*	0.46	0.44	0.32	—	—	0.29	n.d.	—
S	*0.01 wt %*	0.03	0.03	0.02	—	—	0.02	0.02	—
Sc	*1 ppm*	29	28	28	16	24	32	33	29
Sr	*1 ppm*	140	148	149	161	148	143	144	110
V	*5 ppm*	255	244	255	146	145	297	334	328
Zn	*2 ppm*	106	109	108	107	123	123	139	121

For abbreviations used in "Rock Name" and "Description", *see* Appendix 7.

[1] MS–IAT 200; [2] MS–NFA; n.d., not detected; —, not analyzed.

Appendix 6. Continued

Field Number		**52**	**53**	**56**	**56b**	**57a**	**57b**	**57c**	**57c**
Lab Number		**01TRH003**	**01TRH004**	**01TRH005**	**01TRH105**	**01TRH006**	**01TRH007**	**01TRH108**	**01TRH109**
UTM East		424794	424659	424307	424307	423985	423920	423991	423991
UTM North		5484969	5484851	5484556	5484556	5484302	5484276	5484303	5484303
UTM Zone		16	16	16	16	16	16	16	16
Belt		Nipigon sills	Nipigon sills	Nipigon sills	Nipigon sills	Nipigon sills	Nipigon sills	Nipigon sills	Nipigon sills
Township		Kitto	Kitto	Kitto	Kitto	Kitto	Kitto	Kitto	Kitto
Rock Name		diabase	diabase	diabase	diabase	diabase	diabase	diabase	diabase
Description		mass, mg, mag prpc	mass, cg	mass, mg	v cg jnt filling w/ trc fg py, po	mass, mg	mass, cg	v cg amp + pnk fel jnt filling w/ trc fg py, po	v cg amp + pnk fel jnt filling w/ trc fg py, po
	detection limit								
Au [1]	*5 ppb*	n.d.	9.23	n.d.	n.d.	n.d.	5.25	8.11	7.51
Au [2]	*0.73 ppb*	5.12	9.12	4.33	—	6.56	5.78	—	—
Co	*5 ppm*	54	65	53	41	58	62	56	58
CO_2	*0.03 wt %*	0.09	0.1	0.06	—	0.08	0.08	—	—
Cu	*5 ppm*	241	325	194	226	312	240	334	286
Ir	*0.04 ppb*	n.d.	n.d.	0.05	—	n.d.	n.d.	—	—
Ni	*5 ppm*	60	46	90	23	45	53	35	38
Pd [1]	*8 ppb*	21.33	43.16	18.67	n.d.	18.75	29.93	35.83	30.18
Pd [2]	*0.11 ppb*	21.9	43.4	19.4	—	28.5	29.6	—	—
Pt [1]	*8 ppb*	n.d.	13.01	10.61	n.d.	n.d.	9.31	11.94	11.37
Pt [2]	*0.14 ppb*	7.49	12.2	10.4	—	9.4	9.28	—	—
Rh	*0.08 ppb*	0.63	1.13	0.76	—	0.87	1.39	—	—
Ru	*0.13 ppb*	n.d.	0.16	0.24	—	n.d.	0.18	—	—
S	*0.01 wt %*	0.04	0.04	0.04	—	0.04	0.04	—	—
Sc	*1 ppm*	31	34	30	27	32	34	29	33
Sr	*1 ppm*	156	152	155	95	157	153	121	114
V	*5 ppm*	323	508	288	132	377	546	373	380
Zn	*2 ppm*	129	179	115	82	155	140	168	166

For abbreviations used in "Rock Name" and "Description", *see* Appendix 7.

[1] MS–IAT 200; [2] MS–NFA; n.d., not detected; —, not analyzed.

Appendix 6. Continued

Field Number		**57d**	**57e**	**57f**	**92**	**96**	**98**	**100**	**107**
Lab Number		**01TRH110**	**01TRH008**	**01TRH009**	**01TRH021**	**01TRH020**	**01TRH019**	**01TRH018**	**01TRH016**
UTM East		423997	423763	423695	419902	420313	420800	421185	421985
UTM North		548323	5484125	5484097	5490217	5489848	5489780	5489652	5496422
UTM Zone		16	16	16	16	16	16	16	16
Belt		Nipigon sills	Nipigon sills	Nipigon sills	Nipigon sills	Nipigon sills	Nipigon sills	Nipigon sills	Nipigon sills
Township		Kitto	Kitto	Kitto	Kitto	Kitto	Kitto	Kitto	Eva
Rock Name		diabase	diabase	diabase	pyroxenite	pyroxenite	diabase	diabase	diabase
Description		v cg amp + pnk fel jnt filling w/ trc fg py, po	mass, mg	mass, mg, near base	mass mg to cg w/ px phen	mass mg px rich	mass, mg, near top of sill	mass, mg, near base	mass, mg north-trending dike
	detection limit								
Au[1]	*5 ppb*	12.67	n.d.	n.d.	n.d.	n.d.	n.d.	n.d.	n.d.
Au[2]	*0.73 ppb*	—	3.67	3.84	—	—	—	—	—
Co	*5 ppm*	66	60	53	99	119	63	67	60
CO_2	*0.03 wt %*	—	0.06	0.11	0.12	0.31	0.09	0.1	0.06
Cu	*5 ppm*	293	167	183	47	31	162	126	103
Ir	*0.04 ppb*	—	0.16	n.d.	—	—	—	—	—
Ni	*5 ppm*	43	143	80	543	730	138	212	79
Pd[1]	*8 ppb*	50.47	15.48	11.71	n.d.	n.d.	14.52	12.47	n.d.
Pd[2]	*0.11 ppb*	—	16.8	18.3	—	—	—	—	—
Pt[1]	*8 ppb*	19.96	11.94	n.d.	14.98	n.d.	11.2	18.15	n.d.
Pt[2]	*0.14 ppb*	—	12.6	7.91	—	—	—	—	—
Rh	*0.08 ppb*	—	0.84	0.67	—	—	—	—	—
Ru	*0.13 ppb*	—	0.5	0.21	—	—	—	—	—
S	*0.01 wt %*	—	0.03	0.03	0.03	0.03	0.03	0.03	0.07
Sc	*1 ppm*	34	26	30	21	24	30	22	34
Sr	*1 ppm*	111	161	163	267	124	142	150	184
V	*5 ppm*	508	245	281	157	124	277	198	277
Zn	*2 ppm*	170	110	118	122	110	117	105	128

For abbreviations used in "Rock Name" and "Description", *see* Appendix 7.

[1] MS–IAT 200; [2] MS–NFA; n.d., not detected; —, not analyzed.

Appendix 6. Continued

Field Number		**137**	**137b**	**138**	**139**	**139b**	**140**	**202**	**208**
Lab Number		**01TRH121**	**01TRH122**	**01TRH123**	**01TRH017**	**01TRH124**	**01TRH067**	**01TRH089**	**01TRH049**
UTM East		424502	424502	424357	418383	418383	421285	425210	418108
UTM North		5485266	5485266	5485295	5496235	5496235	5497392	5504067	5492022
UTM Zone		16	16	16	16	16	16	16	16
Belt		Nipigon sills	Nipigon sills	Nipigon sills	Nipigon sills	Nipigon sills	SSB	NVB	Nipigon sills
Township		Kitto	Kitto	Kitto	Eva	Eva	Eva	Dorothea	Kitto
Rock Name		diabase	diabase	diabase	Diabase	pyroxenite	gabbro	maf mtvolc	diabase
Description		v cg amp + pnk fel along jnt	mg w/ trc po, py	v cg amp + pnk fel along jnt w/ trc po	Mass mg, w/ aligned px grains	cg w/ trc cp	mass, mg, w/ ep and fel	mg	mg mass contact w/ mtsed
	detection limit								
Au[1]	*5 ppb*	5.55	n.d.	8.35	14.61	7.03	n.d.	n.d.	n.d.
Au[2]	*0.73 ppb*	—	—	—	—	—	—	—	1.73
Co	*5 ppm*	67	58	56	58	69	43	30	54
CO_2	*0.03 wt %*	—	—	—	0.09	—	0.94	4.23	0.07
Cu	*5 ppm*	302	282	398	647	356	43	11	162
Ir	*0.04 ppb*	—	—	—	—	—	—	—	0.05
Ni	*5 ppm*	53	59	36	24	45	65	48	83
Pd[1]	*8 ppb*	26.33	17.53	31.67	n.d.	49.16	n.d.	n.d.	n.d.
Pd[2]	*0.11 ppb*	—	—	—	—	—	—	—	0.26
Pt[1]	*8 ppb*	n.d.	n.d.	9.4	12.27	9.95	n.d.	n.d.	n.d.
Pt[2]	*0.14 ppb*	—	—	—	—	—	—	—	0.7
Rh	*0.08 ppb*	—	—	—	—	—	—	—	n.d.
Ru	*0.13 ppb*	—	—	—	—	—	—	—	n.d.
S	*0.01 wt %*	—	—	—	0.08	—	0.02	0.01	0.01
Sc	*1 ppm*	34	31	29	31	36	19	17	24
Sr	*1 ppm*	107	130	129	141	112	461	88	497
V	*5 ppm*	656	507	379	191	631	135	157	342
Zn	*2 ppm*	160	131	157	200	176	102	84	142

For abbreviations used in "Rock Name" and "Description", *see* Appendix 7.

[1] MS–IAT 200; [2] MS–NFA; n.d., not detected; —, not analyzed.

Appendix 6. Continued

Field Number		**225**	**229**	**240**	**241**	**242**	**243**	**244**	**259**
Lab Number		**01TRH054**	**01TRH063**	**01TRH043**	**01TRH042**	**01TRH038**	**01TRH037**	**01TRH062**	**01TRH044**
UTM East		424517	424326	417099	416727	416958	416812	419860	417410
UTM North		5499839	5503786	5486830	5487103	5487794	5487918	5492669	5487839
UTM Zone		16	16	16	16	16	16	16	16
Belt		CVB	NVB	Nipigon sills	Nipigon sills	SVB	SVB	Nipigon sills	SVB
Township		Eva	Dorothea	Kitto	Kitto	Kitto	Kitto	Kitto	Kitto
Rock Name		basalt	rhyolite	pyroxenite	pyroxenite	maf mtvolc	maf mtvolc	diabase	gabbro
Description		very highly slf, mass, v fg	mass,fel qtz prph, possibly flow dome	mg mass w/ 10 to 30% ol	mg mass w/ 10 to 30% ol	mass flow	mass flow, fel prpc	mg, mass	mass, mg to fg, fel prph, possibly a flow
	detection limit								
Au [1]	*5 ppb*	n.d.	n.d.	n.d.	n.d.	n.d.	n.d.	n.d.	n.d.
Au [2]	*0.73 ppb*	—	—	1.75	1.22	—	—	4.26	—
Co	*5 ppm*	n.d.	13	145	138	59	55	56	53
CO_2	*0.03 wt %*	3.65	1.32	0.1	0.18	0.57	3.52	0.1	4.5
Cu	*5 ppm*	n.d.	23	56	52	109	101	151	105
Ir	*0.04 ppb*	—	—	2.72	2.49	—	—	0.06	—
Ni	*5 ppm*	9	10	1155	998	68	134	102	106
Pd [1]	*8 ppb*	n.d.	n.d.	8.36	n.d.	n.d.	n.d.	15.3	n.d.
Pd [2]	*0.11 ppb*	—	—	9.5	7.54	—	—	16.3	—
Pt [1]	*8 ppb*	n.d.	n.d.	n.d.	n.d.	n.d.	n.d.	n.d.	n.d.
Pt [2]	*0.14 ppb*	—	—	15	9.58	—	—	8.14	—
Rh	*0.08 ppb*	—	—	1.08	0.81	—	—	0.64	—
Ru	*0.13 ppb*	—	—	1.86	1.06	—	—	0.28	—
S	*0.01 wt %*	0.01	0.01	0.06	0.05	0.21	0.04	0.02	0.02
Sc	*1 ppm*	6	6	12	15	38	35	31	30
Sr	*1 ppm*	70	37	172	143	95	109	149	113
V	*5 ppm*	n.d.	32	101	106	315	252	282	213
Zn	*2 ppm*	45	31	131	127	129	107	105	83

For abbreviations used in "Rock Name" and "Description", *see* Appendix 7.

[1] MS–IAT 200; [2] MS–NFA; n.d., not detected; —, not analyzed.

Appendix 6. Continued

Field Number		**267**	**276**	**287**	**330**	**347a**	**347b**	**368**	**373**
Lab Number		**01TRH047**	**01TRH048**	**01TRH065**	**01TRH069**	**01TRH070**	**01TRH236**	**01TRH093**	**01TRH071**
UTM East		418080	418374	424385	425949	418295	418295	424453	418121
UTM North		5488043	5491669	5497047	5504567	5487385	5487385	5504053	5506292
UTM Zone		16	16	16	16	16	16	16	16
Belt		SVB	Nipigon sills	Nipigon sills	NVB	Nipigon sills	Nipigon sills	NVB	Nipigon sills
Township		Kitto	Kitto	Dorothea	Sandra	Kitto	Kitto	Dorothea	Dorothea
Rock Name		granodiorite	ferrosyenite	diabase	int volc	pyroxenite	diabase	fels mtvolc	diabase
Description		mg fel in a fg groundmass of qtz - fel	mg mass, pink fel, minor qtz and c mag	mg, mass	mass, fg	mass, fg chill	v fg chilled diabase w/ trc diss po, py near unit 10i ct	fg tuff	mass flow, fg
	detection limit								
Au[1]	*5 ppb*	n.d.	n.d.	n.d.	n.d.	n.d.	n.d.	7.12	n.d.
Au[2]	*0.73 ppb*	—	—	—	—	—	—	—	—
Co	*5 ppm*	13	54	62	23	119	47	22	52
CO_2	*0.03 wt %*	3.37	0.06	0.03	2.89	0.19	—	1.18	0.2
Cu	*5 ppm*	n.d.	290	153	53	237	82	52	23
Ir	*0.04 ppb*	—	—	—	—	—	—	—	—
Ni	*5 ppm*	13	74	111	48	1335	112	13	190
Pd[1]	*8 ppb*	n.d.	n.d.	15.66	8.92	282.76	13.8	n.d.	14.31
Pd[2]	*0.11 ppb*	—	—	—	—	—	—	—	—
Pt[1]	*8 ppb*	n.d.	n.d.	10	n.d.	157.57	n.d.	n.d.	10.47
Pt[2]	*0.14 ppb*	—	—	—	—	—	—	—	—
Rh	*0.08 ppb*	—	—	—	—	—	—	—	—
Ru	*0.13 ppb*	—	—	—	—	—	—	—	—
S	*0.01 wt %*	n.d.	0.02	0.02	0.01	0.34	—	0.2	0.04
Sc	*1 ppm*	3	21	33	11	15	27	13	27
Sr	*1 ppm*	101	537	152	83	58	244	123	127
V	*5 ppm*	38	364	300	101	134	278	155	169
Zn	*2 ppm*	39	119	124	88	89	56	60	32

For abbreviations used in "Rock Name" and "Description", *see* Appendix 7.

[1] MS–IAT 200; [2] MS–NFA; n.d., not detected; —, not analyzed.

Appendix 6. Continued

Field Number		**385**	**386**	**388**	**388b**	**398**	**408**	**408b**	**410**
Lab Number		**01TRH072**	**01TRH073**	**01TRH075**	**01TRH076**	**01TRH077**	**01TRH078**	**01TRH079**	**01TRH080**
UTM East		420608	420610	420265	420265	429070	423647	423647	421716
UTM North		5503257	5503164	5502452	5502452	5498910	5502907	5502907	5502261
UTM Zone		16	16	16	16	16	16	16	16
Belt		NVB	NVB	NVB	NVB	CVB	NVB	NVB	NVB
Township		Dorothea	Dorothea	Dorothea	Dorothea	Summers	Dorothea	Dorothea	Dorothea
Rock Name		int mtvolc	maf mtvolc	maf mtvolc	int intrusive	maf mtvolc	diabase	gabbro	int mtvolc
Description		mass flow, fg	mass, fg to mg	mass, fg to mg	mass flow, fg	mass, mg	mg	mass, fg	mass
	detection limit								
Au [1]	*5 ppb*	n.d.	n.d.	n.d.	n.d.	n.d.	n.d.	n.d.	n.d.
Au [2]	*0.73 ppb*	—	—	—	—	—	—	—	—
Co	*5 ppm*	14	27	53	19	20	61	25	14
CO_2	*0.03 wt %*	2.81	5.05	7.06	4.25	0.17	0.12	0.17	0.43
Cu	*5 ppm*	28	12	29	38	25	102	61	n.d.
Ir	*0.04 ppb*	—	—	—	—	—	—	—	—
Ni	*5 ppm*	24	54	76	27	46	77	12	24
Pd [1]	*8 ppb*	n.d.	n.d.	n.d.	n.d.	n.d.	n.d.	n.d.	n.d.
Pd [2]	*0.11 ppb*	—	—	—	—	—	—	—	—
Pt [1]	*8 ppb*	n.d.	n.d.	n.d.	n.d.	n.d.	n.d.	n.d.	n.d.
Pt [2]	*0.14 ppb*	—	—	—	—	—	—	—	—
Rh	*0.08 ppb*	—	—	—	—	—	—	—	—
Ru	*0.13 ppb*	—	—	—	—	—	—	—	—
S	*0.01 wt %*	0.1	n.d.	0.15	n.d.	n.d.	0.12	0.03	n.d.
Sc	*1 ppm*	9	14	18	9	11	35	21	9
Sr	*1 ppm*	101	83	102	86	223	177	162	178
V	*5 ppm*	64	101	186	73	95	282	45	76
Zn	*2 ppm*	82	86	182	117	58	126	136	53

For abbreviations used in "Rock Name" and "Description", *see* Appendix 7.

[1] MS–IAT 200; [2] MS–NFA; n.d., not detected; —, not analyzed.

Appendix 6. Continued

Field Number		**413**	**430**	**432**	**456**	**1008**	**1019a**	**1019b**	**1019c**
Lab Number		**01TRH081**	**01TRH082**	**01TRH083**	**01TRH092**	**01TRH085**	**01TRH010**	**01TRH011**	**01TRH119**
UTM East		425378	422990	422813	425213	424447	424651	424651	424651
UTM North		5504961	5504031	5504423	5497365	5495595	5490737	5490737	5490737
UTM Zone		16	16	16	16	16	16	16	16
Belt		NVB	NVB	NVB	SSB	Archean dike	Nipigon sills	Nipigon sills	Nipigon sills
Township		Dorothea	Dorothea	Dorothea	Eva	Eva	Kitto	Kitto	Kitto
Rock Name		maf mtvolc	maf mtvolc	maf mtvolc	quartz vein	diabase	diabase	diabase	diabase
Description		mass flow	mass flow, fg	mass, fg	fg tuff	mass flow	v fg chill - lower contact	mass, mg - 0.5 m above chill	mg w/ trc po, py in frac 2.0 m above lower chill
	detection limit								
Au[1]	*5 ppb*	n.d.	n.d.	n.d.	1000	n.d.	n.d.	n.d.	n.d.
Au[2]	*0.73 ppb*	—	—	—	—	—	3.77	3.71	—
Co	*5 ppm*	27	53	50	n.d.	81	57	59	58
CO_2	*0.03 wt %*	6.55	0.28	0.53	—	0.09	0.1	0.13	—
Cu	*5 ppm*	13	42	127	96	82	167	177	232
Ir	*0.04 ppb*	—	—	—	—	—	n.d.	0.07	—
Ni	*5 ppm*	49	140	112	n.d.	63	102	118	112
Pd[1]	*8 ppb*	n.d.	n.d.	n.d.	n.d.	n.d.	16.45	17.72	16.22
Pd[2]	*0.11 ppb*	—	—	—	—	—	17.2	18.8	—
Pt[1]	*8 ppb*	n.d.	n.d.	n.d.	n.d.	n.d.	n.d.	9.77	8.33
Pt[2]	*0.14 ppb*	—	—	—	—	—	6.81	9.28	—
Rh	*0.08 ppb*	—	—	—	—	—	0.62	0.75	—
Ru	*0.13 ppb*	—	—	—	—	—	0.3	0.35	—
S	*0.01 wt %*	n.d.	0.03	0.11	—	0.27	0.04	0.05	—
Sc	*1 ppm*	14	26	27	4	42	29	29	26
Sr	*1 ppm*	114	140	102	123	358	145	147	141
V	*5 ppm*	117	204	206	7	728	293	289	262
Zn	*2 ppm*	100	124	97	40	147	104	116	107

For abbreviations used in "Rock Name" and "Description", *see* Appendix 7.

[1] MS–IAT 200; [2] MS–NFA; n.d., not detected; —, not analyzed.

Appendix 6. Continued

Field Number		**1019d**	**1033**	**1052**	**1053**	**1080**	**1082**	**1084a**	**1084**
Lab Number		**01TRH012**	**01TRH100**	**01TRH116**	**01TRH117**	**01TRH139**	**01TRH143**	**01TRH140**	**01TRH142**
UTM East		424651	423134	424136	423987	426049	426089	426125	426125
UTM North		5490737	5495178	5485555	5485862	5495143	5494896	5494492	5494492
UTM Zone		16	16	16	16	16	16	16	16
Belt		Nipigon sills	SSB	Nipigon sills	Nipigon sills	SSB	SSB	SSB	SSB
Township		Kitto	Eva	Kitto	Kitto	Summers	Summers	Summers	Summers
Rock Name		diabase	quartz vein	diabase	diabase	diabase	diabase	diabase	diabase
Description		mass, mg - 1.75 m above chill	minor pot altn	cg w/ trc cp	fg w/ trc sulphide, posy chill contact w/ Quetico Subprovince	sulphides by contact w/ mtsed	trc sulphides by contact w/ mtsed	trc fg sulphides	chill margin
	detection limit								
Au [1]	*5 ppb*	n.d.	n.d.	5.52	n.d.	n.d.	n.d.	n.d.	n.d.
Au [2]	*0.73 ppb*	4.36	—	—	—	—	—	—	—
Co	*5 ppm*	62	n.d.	54	45	56	56	56	53
CO_2	*0.03 wt %*	0.14	—	—	—	—	—	—	—
Cu	*5 ppm*	220	n.d.	220	150	66	75	58	66
Ir	*0.04 ppb*	n.d.	—	—	—	—	—	—	—
Ni	*5 ppm*	119	6	48	71	52	56	55	60
Pd [1]	*8 ppb*	27.11	n.d.	23.29	20.46	n.d.	n.d.	n.d.	n.d.
Pd [2]	*0.11 ppb*	28.7	—	—	—	—	—	—	—
Pt [1]	*8 ppb*	n.d.	n.d.	8.93	n.d.	n.d.	n.d.	n.d.	n.d.
Pt [2]	*0.14 ppb*	6.99	—	—	—	—	—	—	—
Rh	*0.08 ppb*	0.73	—	—	—	—	—	—	—
Ru	*0.13 ppb*	0.3	—	—	—	—	—	—	—
S	*0.01 wt %*	0.04	—	—	—	—	—	—	—
Sc	*1 ppm*	30	n.d.	29	21	34	34	35	31
Sr	*1 ppm*	149	17	134	153	168	173	173	202
V	*5 ppm*	300	10	362	230	297	298	291	272
Zn	*2 ppm*	139	12	127	97	111	119	114	90

For abbreviations used in "Rock Name" and "Description", *see* Appendix 7.

[1] MS–IAT 200; [2] MS–NFA; n.d., not detected; —, not analyzed.

Appendix 6. Continued

Field Number		1117	1171	1173	1195	1196	1198	1199	1264
Lab Number		01TRH131	01TRH046	01TRH045	01TRH050	01TRH051	01TRH052	01TRH053	01TRH036
UTM East		424431	416552	416140	416096	416249	416438	416639	416918
UTM North		5495278	5488890	5490670	5492500	5492644	5492698	5492729	5488202
UTM Zone		16	16	16	16	16	16	16	16
Belt		Archean dike	SVB	SVB	Nipigon sills	Nipigon sills	Nipigon sills	Nipigon sills	SVB
Township		Eva	Kitto	Kitto	Kitto	Kitto	Kitto	Kitto	Kitto
Rock Name		diabase	maf mtvolc	maf mtvolc	pyroxenite	pyroxenite	pyroxenite	pyroxenite	maf mtvolc
Description		sulphides and unknown green mineral	plwd flow, var	mass flow	cg phen of px in a mg groundmass	cg phen of px in a mg groundmass	cg phen of px in a mg groundmass	mg mass w/ 10 to 30% ol	mass flow
	detection limit								
Au[1]	*5 ppb*	n.d.	n.d.	n.d.	n.d.	n.d.	5.5	n.d.	n.d.
Au[2]	*0.73 ppb*	—	—	—	2.95	1.08	7.42	1.77	—
Co	*5 ppm*	62	44	59	102	49	98	59	60
CO_2	*0.03 wt %*	—	1.7	1.25	0.14	n.d.	0.08	0.13	0.39
Cu	*5 ppm*	30	20	64	80	64	94	74	387
Ir	*0.04 ppb*	—	—	—	3.03	0.18	2.02	n.d.	—
Ni	*5 ppm*	43	70	209	546	73	459	65	211
Pd[1]	*8 ppb*	n.d.	n.d.	n.d.	n.d.	n.d.	n.d.	n.d.	n.d.
Pd[2]	*0.11 ppb*	—	—	—	4.96	2.2	2.93	n.d.	—
Pt[1]	*8 ppb*	n.d.	n.d.	n.d.	9.41	n.d.	n.d.	n.d.	n.d.
Pt[2]	*0.14 ppb*	—	—	—	10.3	8.05	5.78	n.d.	—
Rh	*0.08 ppb*	—	—	—	0.7	0.14	0.38	n.d.	—
Ru	*0.13 ppb*	—	—	—	0.42	0.04	0.34	n.d.	—
S	*0.01 wt %*	—	n.d.	0.01	0.05	0.03	0.05	0.14	0.12
Sc	*1 ppm*	30	34	26	26	19	28	34	30
Sr	*1 ppm*	258	65	80	197	607	202	246	111
V	*5 ppm*	340	246	242	170	255	193	286	211
Zn	*2 ppm*	163	94	96	133	82	106	104	91

For abbreviations used in "Rock Name" and "Description", *see* Appendix 7.

[1] MS–IAT 200; [2] MS–NFA; n.d., not detected; —, not analyzed.

Appendix 6. Continued

Field Number		**1266**	**1266b**	**1267**	**1268**	**1269**	**1370**	**2033**	**2053**
Lab Number		**01TRH032**	**01TRH057**	**01TRH027**	**01TRH028**	**01TRH026**	**01TRH086**	**01TRH115**	**01TRH118**
UTM East		415880	415880	416152	416265	415538	420978	418727	422972
UTM North		5489335	5489335	5491046	5490833	5492452	5503573	5496081	5486969
UTM Zone		16	16	16	16	16	16	16	16
Belt		SVB	SVB	SSB	SVB	Nipigon sills	NVB	Nipigon sills	Nipigon sills
Township		Kitto	Kitto	Kitto	Kitto	Kitto	Dorothea	Kitto	Kitto
Rock Name		maf mtvolc	maf mtvolc	flds wacke	maf mtvolc	pyroxenite	int mtvolc	diabase	diabase
Description		mass flow, cg, gabbroic textured	mass flow	10 to 30 cm beds interbedded w/ arg and silt	mass flow	mg mass w/ 10 to 30% ol	mg to cg	v cg amp + pnk fel	mg w/ cg pods and chl frac fillings
	detection limit								
Au[1]	*5 ppb*	n.d.	n.d.	n.d.	n.d.	11.89	n.d.	35.75	n.d.
Au[2]	*0.73 ppb*	—	—	—	—	—	—	—	—
Co	*5 ppm*	51	56	33	50	121	22	69	54
CO_2	*0.03 wt %*	0.11	0.05	0.87	2.89	0.18	3.35	—	—
Cu	*5 ppm*	149	86	66	90	31	12	663	141
Ir	*0.04 ppb*	—	—	—	—	—	—	—	—
Ni	*5 ppm*	73	91	279	52	735	56	26	99
Pd[1]	*8 ppb*	n.d.	n.d.	n.d.	n.d.	n.d.	n.d.	63.14	16.86
Pd[2]	*0.11 ppb*	—	—	—	—	—	—	—	—
Pt[1]	*8 ppb*	12.06	8.24	n.d.	n.d.	n.d.	n.d.	46.44	10.52
Pt[2]	*0.14 ppb*	—	—	—	—	—	—	—	—
Rh	*0.08 ppb*	—	—	—	—	—	—	—	—
Ru	*0.13 ppb*	—	—	—	—	—	—	—	—
S	*0.01 wt %*	n.d.	0.01	0.02	0.08	0.03	0.07	—	—
Sc	*1 ppm*	37	46	11	41	24	10	37	26
Sr	*1 ppm*	52	68	321	62	124	121	109	130
V	*5 ppm*	247	267	92	349	131	86	340	279
Zn	*2 ppm*	89	95	74	140	107	118	190	131

For abbreviations used in "Rock Name" and "Description", *see* Appendix 7.

[1] MS–IAT 200; [2] MS–NFA; n.d., not detected; —, not analyzed.

Appendix 6. Continued

Field Number		**2077**	**2080**	**2156**	**2244**	**2246**	**2247**	**2248**	**2249**
Lab Number		**01TRH157**	**01TRH155**	**01TRH068**	**01TRH041**	**01TRH040**	**01TRH039**	**01TRH035**	**01TRH034**
UTM East		423282	424603	421515	416643	416566	416716	416721	416426
UTM North		5496663	5497049	5499047	5487270	5487575	5487585	5488568	5488693
UTM Zone		16	16	16	16	16	16	16	16
Belt		Archean dike	SSB	CVB	Nipigon sills	Nipigon sills	Nipigon sills	SVB	SVB
Township		Eva	Eva	Eva	Kitto	Kitto	Kitto	Kitto	Kitto
Rock Name		diabase	diabase	gabbro	pyroxenite	pyroxenite	pyroxenite	maf mtvolc	maf mtvolc
Description		contact w/ mtsed	chill w/ trc sulphides	mg to fg mass flow	mg mass w/ 10 to 30% ol	mg mass w/ 10 to 30% ol	mg mass w/ 10 to 30% ol	mass flow	plwd flow, amyg
	detection limit								
Au [1]	*5 ppb*	7.13	n.d.	n.d.	n.d.	n.d.	n.d.	n.d.	n.d.
Au [2]	*0.73 ppb*	—	—	—	—	1.21	—	—	—
Co	*5 ppm*	37	40	27	147	143	123	60	54
CO_2	*0.03 wt %*	—	—	0.18	0.23	0.33	0.41	0.5	3.2
Cu	*5 ppm*	119	14	n.d.	31	50	37	n.d.	n.d.
Ir	*0.04 ppb*	—	—	—	—	2.84	—	—	—
Ni	*5 ppm*	18	19	70	1066	1040	801	167	114
Pd [1]	*8 ppb*	n.d.	n.d.	n.d.	n.d.	n.d.	n.d.	n.d.	n.d.
Pd [2]	*0.11 ppb*	—	—	—	—	3.85	—	—	—
Pt [1]	*8 ppb*	n.d.	n.d.	n.d.	n.d.	n.d.	n.d.	n.d.	n.d.
Pt [2]	*0.14 ppb*	—	—	—	—	6.83	—	—	—
Rh	*0.08 ppb*	—	—	—	—	0.56	—	—	—
Ru	*0.13 ppb*	—	—	—	—	1.04	—	—	—
S	*0.01 wt %*	—	—	0.01	0.06	0.05	0.05	n.d.	n.d.
Sc	*1 ppm*	33	35	18	12	11	20	30	38
Sr	*1 ppm*	179	312	214	153	156	132	81	71
V	*5 ppm*	78	108	134	96	93	119	242	333
Zn	*2 ppm*	159	795	51	117	132	111	108	86

For abbreviations used in "Rock Name" and "Description", *see* Appendix 7.

[1] MS–IAT 200; [2] MS–NFA; n.d., not detected; —, not analyzed.

Appendix 6. Continued

Field Number		**2250**	**2250**	**2251**	**2253**	**2254**	**2256**	**2258**	**2259**
Lab Number		**01TRH033**	**01TRH058**	**01TRH031**	**01TRH029**	**01TRH030**	**01TRH025**	**01TRH024**	**01TRH023**
UTM East		416087	416087	415990	416046	416303	415749	415522	416010
UTM North		5489018	5489018	5489617	5490035	5491282	5491843	5492590	5492901
UTM Zone		16	16	16	16	16	16	16	16
Belt		SVB	SVB	SVB	SVB	SVB	Nipigon sills	Nipigon sills	Nipigon sills
Township		Kitto	Kitto	Kitto	Kitto	Kitto	Kitto	Kitto	Kitto
Rock Name		maf mtvolc	maf mtvolc	maf mtvolc	maf mtvolc	maf mtvolc	pyroxenite	pyroxenite	pyroxenite
Description		mass flow	mass flow	mass flow	plwd flow, amyg	plwd flow, amyg	cg phen of px in a mg groundmass	mg mass w/ 10 to 30% ol	mg mass w/ 10 to 30% ol
	detection limit								
Au[1]	*5 ppb*	n.d.	n.d.	n.d.	n.d.	n.d.	n.d.	n.d.	n.d.
Au[2]	*0.73 ppb*	—	—	—	—	—	—	—	—
Co	*5 ppm*	58	50	69	52	57	122	127	135
CO_2	*0.03 wt %*	0.11	1.59	1.44	1.11	0.49	0.17	0.18	0.16
Cu	*5 ppm*	61	94	17	125	23	57	23	38
Ir	*0.04 ppb*	—	—	—	—	—	—	—	—
Ni	*5 ppm*	185	81	151	57	98	827	854	862
Pd[1]	*8 ppb*	9.28	n.d.	n.d.	n.d.	n.d.	n.d.	n.d.	n.d.
Pd[2]	*0.11 ppb*	—	—	—	—	—	—	—	—
Pt[1]	*8 ppb*	11.11	n.d.	n.d.	n.d.	n.d.	n.d.	n.d.	n.d.
Pt[2]	*0.14 ppb*	—	—	—	—	—	—	—	—
Rh	*0.08 ppb*	—	—	—	—	—	—	—	—
Ru	*0.13 ppb*	—	—	—	—	—	—	—	—
S	*0.01 wt %*	n.d.	0.01	n.d.	0.02	0.03	0.05	0.03	0.04
Sc	*1 ppm*	29	34	31	41	34	17	21	18
Sr	*1 ppm*	109	109	126	65	101	186	131	102
V	*5 ppm*	185	244	304	328	271	132	103	100
Zn	*2 ppm*	103	209	140	116	118	115	110	118

For abbreviations used in "Rock Name" and "Description", *see* Appendix 7.

[1] MS–IAT 200; [2] MS–NFA; n.d., not detected; —, not analyzed.

Appendix 6. Continued

Field Number		**2260**	**2321**	**3001**	**3002**	**3005**	**3025**	**3025b**	**3027**
Lab Number		**01TRH022**	**01TRH087**	**01TRH060**	**01TRH061**	**01TRH059**	**01TRH055**	**01TRH199**	**01TRH056**
UTM East		416383	420297	419157	419047	419575	415783	415783	417107
UTM North		5493528	5506140	5491909	5491882	5491815	5492140	5492140	5494150
UTM Zone		16	16	16	16	16	16	16	16
Belt		Nipigon sills	NVB	Nipigon sills	Nipigon sills	Nipigon sills	Nipigon sills	Nipigon sills	Nipigon sills
Township		Kitto	Dorothea	Kitto	Kitto	Kitto	Kitto	Kitto	Kitto
Rock Name		pyroxenite	gabbro	pyroxenite	pyroxenite	pyroxenite	pyroxenite	pyroxenite	pyroxenite
Description		mg mass w/ 10 to 30% ol	mass, mg	mg mass w/ 10 to 30% ol	cg phen of px in a mg groundmass	cg phen of px in a mg groundmass	mg mass w/ 10 to 30% ol	trc fg diss po	mg mass w/ 10 to 30% ol
	detection limit								
Au[1]	*5 ppb*	n.d.	n.d.	n.d.	n.d.	n.d.	n.d.	n.d.	n.d.
Au[2]	*0.73 ppb*	—	—	1.56	2.45	0.91	—	—	—
Co	*5 ppm*	134	107	124	107	137	141	146	147
CO_2	*0.03 wt %*	0.23	0.07	0.1	0.07	0.09	0.32	—	0.16
Cu	*5 ppm*	40	32	61	126	55	30	55	24
Ir	*0.04 ppb*	—	—	3.69	2.56	3.5	—	—	—
Ni	*5 ppm*	899	645	687	583	862	995	1047	1035
Pd[1]	*8 ppb*	n.d.	n.d.	22.93	n.d.	n.d.	n.d.	n.d.	n.d.
Pd[2]	*0.11 ppb*	—	—	24	4.72	0.291	—	—	—
Pt[1]	*8 ppb*	n.d.	n.d.	16.87	n.d.	n.d.	n.d.	n.d.	n.d.
Pt[2]	*0.14 ppb*	—	—	19.8	8.83	1.16	—	—	—
Rh	*0.08 ppb*	—	—	1.33	0.47	0.46	—	—	—
Ru	*0.13 ppb*	—	—	0.6	0.51	0.64	—	—	—
S	*0.01 wt %*	0.05	0.01	0.06	0.03	0.04	0.05	—	0.03
Sc	*1 ppm*	16	21	23	24	17	15	15	15
Sr	*1 ppm*	42	6	132	212	129	102	130	113
V	*5 ppm*	92	127	138	148	98	111	126	80
Zn	*2 ppm*	123	125	135	124	127	126	126	117

For abbreviations used in "Rock Name" and "Description", *see* Appendix 7.

[1] MS–IAT 200; [2] MS–NFA; n.d., not detected; —, not analyzed.

Appendix 6. Continued

Field Number		**3031**	**4003**	**4003b**	**4006**	**4009**	**4016**	**5000**
Lab Number		**01TRH088**	**01TRH215**	**01TRH216**	**01TRH224**	**01TRH225**	**01TRH090**	**01TRH064**
UTM East		422140	422545	422545	421650	422432	421043	421625
UTM North		5511363	5510370	5510370	5508641	5507917	5506137	5510954
UTM Zone		16	16	16	16	16	16	16
Belt		Nipigon sills	Nipigon sills	Nipigon sills	Nipigon sills	Nipigon sills	NVB	NVB
Township		Dorothea	Dorothea	Dorothea	Dorothea	Dorothea	Dorothea	Dorothea
Rock Name		diabase	diabase	diabase	diabase	diabase	gabbro	gabbro
Description		mass flow, fg	trc to 1% diss py and cp: Pd showing	trc to 1% diss py and cp: Pd showing	diabase w/ sulphides	diabase w/ sulphides	quartz vein	cg, mass w/ v cg px amp phen
	detection limit							
Au [1]	*5 ppb*	8.51	5.94	6.42	7.02	n.d.	n.d.	n.d.
Au [2]	*0.73 ppb*	—	7.78	—	—	—	—	—
Co	*5 ppm*	61	60	68	67	70	52	55
CO_2	*0.03 wt %*	0.22	—	—	—	—	0.09	0.64
Cu	*5 ppm*	189	302	247	258	289	54	143
Ir	*0.04 ppb*	—	n.d.	—	—	—	—	—
Ni	*5 ppm*	115	54	59	46	57	43	115
Pd [1]	*8 ppb*	23.27	29.2	36.98	48.16	31.07	n.d.	n.d.
Pd [2]	*0.11 ppb*	—	32	—	—	—	—	—
Pt [1]	*8 ppb*	10.24	n.d.	9.14	12.71	n.d.	n.d.	n.d.
Pt [2]	*0.14 ppb*	—	9.08	—	—	—	—	—
Rh	*0.08 ppb*	—	0.62	—	—	—	—	—
Ru	*0.13 ppb*	—	n.d.	—	—	—	—	—
S	*0.01 wt %*	0.04	—	—	—	—	0.13	0.04
Sc	*1 ppm*	29	34	36	36	36	37	34
Sr	*1 ppm*	138	143	133	119	113	68	159
V	*5 ppm*	295	306	456	623	851	345	243
Zn	*2 ppm*	116	146	152	173	171	90	127

For abbreviations used in "Rock Name" and "Description", *see* Appendix 7.
[1] MS–IAT 200; [2] MS–NFA; n.d., not detected; —, not analyzed.

Appendix 7:

Glossary of Abbreviations and Acronyms Used in This Report.

Appendix 7. Glossary of abbreviations and acronyms used in this report.

A

ab	albite
act	actinolite
AEM	airborne electromagnetic survey
Ag	silver
AGPH	airborne geophysics
alk	alkali
alms	aluminous
alng	along
altd	altered
altn	alteration
AMAG	airborne magnetic survey
amp	amphibole
amyg	amygdaloidal
and	andesite
ank	ankerite
ap	apatite
apy	arsenopyrite
arg	argillite
argn	arginite
As	arsenic
asb	asbestos
asoc	associated
atg	antigorite
Au	gold
aug	augite
ave	average
ax	axinite

B

BBA	Bish Bay assemblage
BGB	Beardmore–Geraldton Belt
BIF	banded iron formation
blcd	bleached
blst	blasting
bn	bornite
bnd	band
bndd	banded
bpmt	beep mat
bs	basaltic
bsad	basaltic andesite
bslt	basalt
bsn	basanite
bt	biotitic
bx	breccia
bxd	brecciated

C

c	carbonate
Ca	calcium
cal	calcite
calc	calc-silicate
carb	carbonate
cg	coarse grained
ch	chert
chl	chlorite
chlc	chloritic
chr	chromite
chty	cherty
cld	chloritoid
CSB	central metasedimentary subbelt
cngl	conglomerate
Co	cobalt
conc	concentration
cp	chalcopyrite
Cr	chromium
crd	cordierite
ct	contact
Cu	copper
CVB	central metavolcanic subbelt
cz	carbonatized

D, E, F

DDH	diamond drill hole
DHRC	drill hole reverse circulation
diss	disseminated

EM	electromagnetic survey
EOH	end of hole
ep	epidote

Fe	iron
fel	feldspar
fels	felsic
fg	fine grained
flds	feldspathic
flt	fault
frac	fracture

G

g	grams
gb	gabbro
gchm	geochemistry
gmap	geological mapping
geo	geology
geo-map	geology map
gn	galena
gp	gypsum
gphys	geophysics
gr	graphite
grd	ground
grid	gridding

grt	garnet
grun	grünerite
gwke	greywacke

H, I, J, K, L

hbl	hornblende
hem	hematite
hfl	hornfels
HFSE	high field strength element(s)
HREE	heavy rare earth element(s)
ICP–AES	inductively coupled plasma atomic emission spectroscopy
ICP–MS	inductively coupled plasma mass spectrometry
IF	iron formation
int	intermediate
intr	intrusion
IP	induced polarization
ir	ironstone
ireg	irregular
jas	jasper
jnt	joint
K	potassium
kfs	potassium feldspar
kom	komatiite
lm	limonite
lnct	line cutting
LOI	loss-on-ignition
LREE	light rare earth element(s)
ls	limestone

M, N, O

m	metre
maf	mafic
mag	magnetite
mag-s	magnetic survey
mass	massive
mb	marble
meim	meimechite
mg	medium grained
Mg	magnesium
mgnt	magnetometer
mi	minor
mlc	malachite
mnzd	mineralized
mo	molybdenite
Mo	molybdenum
MORB	mid-ocean ridge basalt
mtld	mottled
mtsed	metasediments
mtvolc	metavolcanic
mtx	matrix
NFA–ICP–MS	nickel fire assay – inductively coupled plasma mass spectrometry
Ni	nickel
NSB	northern metasedimentary subbelt
num	numerous
NVB	northern metavolcanic subbelt
obs	observed
occ	occasional
ol	olivine

P

Pb	lead
pct	pectolite
Pd	palladium
PGE	platinum group element
phen	phenocryst
pl	plagioclase
PLF	Paint Lake Fault
plwd	pillowed
p-mag	proton magnetometer
pn	pentlandite
pnk	pink
po	pyrrhotite
posy	possibly
pot	potassic
PP	past producer
PPA	Poplar Point assemblage
ppm	parts per million
prd	peridotite
prpc	porphyritic
prph	porphyry
prsp	prospecting
pryc	propylitic
Pt	platinum
px	pyroxene
py	pyrite

Q, R

qcv	quartz-carbonate vein
qv	quartz vein
qtz	quartz
REE	rare earth element(s)
rx	rock

S

S	sulphur
sbhl	subhedral
sch	schist
sd	siderite
sect	section
seds	sediments
ser	sericite
sh	shale

she	scheelite
shr	shear
shrd	sheared
si	silica
silt	siltstone
slf	silicified
SM	sulphide-mineralization
smass	semi-massive
SSB	southern metasedimentary subbelt
smp	sampling
sp	sphalerite
spec-hem	specular hematite
spn	sphene
SP-s	self-potential survey
srp	serpentine
ss	sandstone
str	stringer
strg	strong
strp	stripping
subalk	subalkali
sulf	sulphide
SVB	southern metavolcanic subbelt

T, V, W, Z

TAS	total alkali-silica [classification]
tep	tephrite
tlc	talc
tr	tremolite
trc	trace
trnch	trenching
TS	thin section
tur	tourmaline
v	very
var	variolitic
VLEM	vertical loop electromagnetic survey
VLF-EM	very low frequency electromagnetic survey
vn	vein
vnlt	veinlet
volc	volcanic
vrbl	variable
W	tungsten
w/	with
w/in	within
wh	white
wkly	weakly
wr	wallrock
XRF	X-ray fluorescence
zeol	zeolite
Zn	zinc
?	data questionable

References

Anglin, C.D. and Franklin, J.M. 1985. Gold mineralization in the Beardmore–Geraldton area of northwestern Ontario: structural considerations and the role of iron formation; *in* Current Research, Part A, Geological Survey of Canada, Paper 85-1A, p.193-201.

Bald, R. 1982. Diamond drill log for Ternosky-Rentz Property holes TR-82-1, 2, 3, 4, 5, 6 Gold Fields Mining Corp.; Thunder Bay Resident Geologist's Office, assessment file AFRI# 42E12SW0079.

Bardoux, M., Jébrak, M., Goulet, M., Morin, D., Giguère, C. and Zadeh, H. 1990. Metallogenesis of the Cadillac shear zone in the McWatters area, Abitibi belt, Canada; abstract *in* Proceedings, 8th IAGOD Symposium, in conjunction with Mineral deposit modeling international conference, Ottawa, Ontario, p.A260.

Barnes, S.J., Boyd, R., Korneliussen, A., Nilsson, L-P., Often, M., Pedersen, R.B. and Robins, B. 1987. The use of mantle normalization and metal ratios in discriminating between the effects of partial melting, crystal fractionation and sulphide segregation on platinum group elements, gold, nickel and copper: examples from Norway; *in* Geo-Platinum '87, Elsevier, Barking, United Kingdom, p.113-143.

Barnes, S.J., Couture, J.-F., Swayer, E.W. and Bouchaib, C. 1993. Nickel-copper occurrences in the Belleterre–Angliers Belt of the Pontiac Subprovince and the use of Cu-Pd ratios in interpreting platinum group element distributions; Economic Geology, v.88, p.1402-1418.

Barrett, T.J. and Fralick, P.W. 1985. Sediment redeposition in Archean iron formation: examples from the Beardmore–Geraldton greenstone belt, Ontario; Journal of Sedimentary Petrology, v.55, p.205-212.

——— 1986. Resedimentation associated with the gold bearing banded iron formation in the Geraldton–Beardmore greenstone belt, Ontario; Ontario Geological Survey, Open File Report 5577, 27p.

Batiza, R. and White, J.D.L. 2000. Submarine lavas and hyaloclastite; *in* Encyclopedia of volcanoes, Academic Press, San Diego, California, p.361-381.

Bell, R. 1870. Report on the geology of the northwest side of Lake Superior, and of the Nipigon District; *in* Reports on Ontario 1865–1886, Geological and Natural History Survey of Canada, *reprinted from* Geological Survey of Canada, Reports of Progress 1866–1869, p.313-364.

Benedict, P.C. and Titcomb, J.A. 1947. Geology of the Northern Empire Mine; The Canadian Institute of Mining and Metallurgy Bulletin, v.50, p.412-423.

——— 1948. Northern Empire Mine; *in* Structural geology of Canadian ore deposits, Canadian Institute of Mining and Metallurgy, Jubilee Volume, p.389-399.

Bent, H. 1989a. The Sturgeon River diamond drill project, Dorothea Township, Ontario; for Glen Auden Resources Limited, Shango Resources Ltd, January 20, 1989; Thunder Bay Resident Geologist's Office, assessment file AFRI# 52H09NE0007.

——— 1989b. Geological report of the Summers Township property, Summers Township, Thunder Bay Mining Division, Ontario; Thunder Bay Resident Geologist's Office, assessment file AFRI# 42E12SW0034.

Binney, P. and Barrie, T. 1990. Kamiskotia area; *in* Geology and ore deposits of the Timmins District, Ontario, Field Trip 6, 8th IAGOD Symposium, Geological Survey of Canada, Open File Report 2161, p.52-65.

Brown, G.H. 1995. Precambrian geology, Oliver and Ware townships; Ontario Geological Survey, Report 294, 48p.

Bruce, E.L. and Laird, H.C. 1937. The western part of the Sturgeon River area; Ontario Department of Mines, Annual Report 1936, v.45, pt.2, p.60-117.

Carstens, H. 1965. Axinite in the Norwegian Caledonides: Contributions to the mineralogy of Norway, No. 32; Norsk Geologisk Tidsskrift, v.45, p.397-415.

Carter, M.W. 1983. McComber and Vincent townships, District of Thunder Bay; *in* Summary of Field Work and Other Activities 1983, Ontario Geological Survey, Miscellaneous Paper 116, p.32-36.

——— 1987. Geology of McComber and Vincent townships, District of Thunder Bay; Ontario Geological Survey, Open File Report 5648, 144p.

Cas, R.A.F. 1992. Submarine volcanism: eruption styles, products and relevance to understanding the host-rock successions to volcanic-hosted massive sulphide deposits; Economic Geology, v.87, p.511-541.

Cas, R.A.F. and Wright, J.V. 1987. Volcanic successions: modern and ancient; Allen and Unwin, London, United Kingdom, 528p.

Clemmer, S.G. 1984. Magnetic survey of the Undersill Lake property, Eva and Summers townships, Thunder Bay Mining Division; Thunder Bay Resident Geologist's Office, assessment file AFRI# 52H09SE0008.

Coleman, A.P. 1907. Iron ranges east of Lake Nipigon, Ontario; Ontario Bureau of Mines, Annual Report, v.16, pt.1, p.105-135.

Cowan, M.F. 1984. Report on the geology of the Patter Lake claims, TB768664 to TB768675, TB732037 to TB732042, Irwin Township, Thunder Bay Mining Division, Ontario, December, 1984; Thunder Bay Resident Geologist's Office, assessment file AFRI# 42E12NW0069.

Cox, K.G., Bell, J.D. and Pankhurst, R.J. 1978. The interpretation of igneous rocks; Allen and Unwin, London, United Kingdom, 450p.

Cunnison, K.M. and Pyke, D.L. 2001. Geological report for East West Resources Corporation and Canadian Golden Dragon Resources Ltd. on the Hele Township property, Thunder Bay Mining Division, Ontario, December 17, 2001; Thunder Bay Resident Geologist's Office, assessment file 52A15-2.22612.

Davis, D.W. and Sutcliffe, R.H. 1985. U-Pb ages from the Nipigon plate and northern Lake Superior; Geological Society of America Bulletin, v.96, p.1572-1579.

Dawson, G.M. 1895. Summary report on the operations of the Geological Survey for the year 1894 [dated 1895]; Geological Survey of Canada, Annual Report 1894, v.7, p.1A-124A.

——— 1901. Summary report on the operations of the Geological Survey for the year 1898 [dated 1899]; Geological Survey of Canada, Annual Report 1898, v.11, p.1A-208A.

Deer, W.A., Howie, R.A. and Zussman, J. 1966. An introduction to the rock forming minerals; John Wiley and Sons Inc., New York, p.93.

——— 1986. Rock forming minerals: disilicates and silicates, 2nd ed.; Longman, Scientific and Technical, London, United Kingdom, v.1B, p. 603-623.

Devaney, J.R. and Williams, H.R. 1989. Evolution of an Archean subprovince boundary: a sedimentological and structural study of part of the Wabigoon–Quetico boundary in northern Ontario; Canadian Journal of Earth Sciences, v.26, p.1013-1026.

DeWolfe, J.C. 2001. Preliminary geological investigation of Dorothea and Sandra townships: evaluating potential for structurally hosted mesothermal gold mineralization; Ontario Geological Survey, Open File Report 6059, 16p.

Dubé, B. and Guha, J. 1993. Factors controlling the occurrence of ferro-axinite within Archean gold-copper-rich quartz veins: Cooke mine, Chibougamau area, Abitibi greenstone belt; The Canadian Mineralogist, v.31, p.905-916.

Dudas, F.O. and Rogan, P.T. 1997. Isotopic evidence for the role of crustal melts in the genesis of granophyre in diabase dykes; abstract *in* AGU Spring Meeting, American Geophysical Union, EOS, v.78, no.17, p.S333.

Duggan, B.M. 2002. The geology and potential mineralization of the Kitto Township Proterozoic layered ultramafic intrusion in Beardmore, Ontario; unpublished BSc thesis, Queen's University, Kingston, Ontario, 65p.

East–West Resource Corporation 2000. Annual Report 2000 of East West Resource Corporation [dated September 15, 2000].

Ehlers, E.G. and Blatt, H. 1982. Petrology igneous, sedimentary, and metamorphic: W.H. Freeman and Company, New York, 732p.

Fekete, M. 1992. Assessment report for work completed on the Summers property, Freewest Resources Inc., Summers Township, Thunder Bay Mining Division, Ontario; Thunder Bay Resident Geologist's Office, assessment file AFRI# 42E12SW0046.

——— 1995. Final submission report, OPAP OP95-282, Morgan extension project, Beardmore–Geraldton area, Thunder Bay Mining Division, Summers Township, January 6, 1995; Thunder Bay Resident Geologist's Office, assessment file AFRI# 42E12SW0052.

Ferguson, S.A. 1967a. Leitch Gold Mines Limited, surface plan of eastern part of property, parts of Eva and Summers townships, District of Thunder Bay; Ontario Department of Mines, Preliminary Map P.484, scale 1:6000.

——— 1967b. Leitch Gold Mines Limited, subsurface No.1, 900-foot level, subsurface No.2, 4525 foot level, parts of Eva and Summers townships, District of Thunder Bay; Ontario Department of Mines, Preliminary Map P.485, scale 1:6000.

Ferguson, S.A., Groen, H.A. and Haynes, R. 1971. Gold deposits of Ontario: part 1, districts of Algoma, Cochrane, Kenora, Rainy River and Thunder Bay; Ontario Department of Mines, Mineral Resources Circular No.13, 315p.

Fisher, R.V. and Schminke, H.-U. 1984. Pyroclastic rocks; Springer-Verlag, Berlin, 472p.

Floyd, P.A. and Winchester, J.A. 1978. Identification and discrimination of altered and metamorphosed volcanic rocks using immobile elements; Chemical Geology, v.21, p.291-306.

Fralick, P., Wu, J. and Williams, H.R. 1992. Trench and slope basin deposits in an Archean metasedimentary belt, Superior Province, Canadian Shield; Canadian Journal of Earth Sciences, v.29, p.2551-2557.

Gasper, L.M. and Inverno, C.M.C. 2000. Mineralogy and metasomatic evolution of distal strata-bound scheelite skarns in the Riba de Alva Mine, northeastern Portugal; Economic Geology, v.95, p.1259-1275.

Getling, R.V. 1965. Axinite from the Kyzyl–Espe deposit; Zapiski Vserossiīskogo Mineralogicheskogo Obshchestva (St. Petersburg, Russia), v.94, p.607-612 [in Russian].

Goettel, T. 1998. Report on the exploration project on the Lafontaine option for Explorations Minières du Nord Ltée, March 7, 1998; Thunder Bay Resident Geologist's Office, assessment files 52H09SE and 42E12SW MEI-025.

Goldbrook Explorations 1996. 21 Creek Property, Thunder Bay Mining Division; Thunder Bay Resident Geologist's Office, assessment file AFRI# 42E12SW0013.

Goldcliff Resource Corporation. 2002. The Hedley Basin Project – skarn and intrusive gold deposits http://www.goldcliff.ca/hedleyreport.htm (web page accessed July 29, 2002).

Goodman, D.C. 1997. Speke Point project: final report: Kitto Township, Thunder Bay Mining Division; Thunder Bay Resident Geologist's Office, assessment file 52H09SE MEI-026.

Goodman, H.G. 1997. Final submission: Morgan South extension project, Beardmore–Geraldton area, Summer Township, Thunder Bay Mining Division; Thunder Bay Resident Geologist's Office, assessment file 42E12SW MEI-056.

Goodman, H.G., Jr. 1991. Report on Minefinders and Gustafson properties, Thunder Bay Mining Division; Thunder Bay Resident Geologist's Office, assessment file AFRI# 42E13SW0016.

——— 1994. Report on Morgan Extension, Summers Township, Thunder Bay Mining Division; Thunder Bay Resident Geologist's Office, assessment file AFRI# 42E12SW0025.

Goodman, H.K. 1997. Speke Point project: final report, Kitto Township, Thunder Bay Mining Division; Thunder Bay Resident Geologist's Office, assessment file 52H09SE MEI-026.

Gorton, M.P. and Schandl, E.S. 2000. From continents to island arcs: a geochemical index of tectonic setting for arc-related and within-plate felsic to intermediate volcanic rocks; The Canadian Mineralogist, v.38, p.1065-1073.

Graham, R.J. 1987. Interim progress report on the exploration of the Spooner Gold Mine property, Parklane Technologies, Summers Township, Thunder Bay Mining Division, Ontario; Thunder Bay Resident Geologist's Office, assessment file AFRI# 42E12SW0961.

Grew, E.S. 1996. Borosilicates (exclusive of tourmaline) and boron in rock-forming minerals in metamorphic environments; Mineralogical Society of America, Reviews in Mineralogy, v.33, p.387-502.

Gupta, V.K. 1991. Shaded image of total magnetic field of Ontario, west-central sheet; Ontario Geological Survey, Map 2585, scale 1:1 000 000.

Hall, P. 1990. Minerals of the Mount Cleveland Mine, Luina, Tasmania; Australian Mineralogist, v.5, no.3, p.82-92.

Hart T.R. 1984. The geochemistry and petrogenesis of a metavolcanic and intrusive sequence in the Kamiskotia area; Timmins, Ontario; unpublished MSc thesis, University of Toronto, Toronto, Ontario, 179p.

Hart, T.R. and MacDonald, C.A. 2000. Geology of the Heaven Lake greenstone belt, central Wabigoon Subprovince; *in* Summary of Field Work and Other Activities 2000, Ontario Geological Survey, Open File Report 6032, p.17-1 to 17-8.

Heaman, L.M. 1997. Global mafic magmatism at 2.45 Ga: remnants of an ancient large igneous province?; Geology, v.25, p.299-302.

Hofmann, A.W. 1988. Chemical differentiation of the Earth: the relationship between mantle, continental crust, and oceanic crust; Earth and Planetary Science Letters, v.90, p.297-314.

Holt, L. 1995. Assessment work, Summers Township, Thunder Bay Mining Division; Thunder Bay Resident Geologist's Office, assessment file AFRI# 42E12SW0002.

Hopkins, A. 1959. Report on a geological survey on the Hopkins–Nipigon gold prospect, Dorothea Township, Thunder Bay Mining Division; Thunder Bay Resident Geologist's Office, assessment file AFRI# 52H09NE0021.

Houghton, F. and Cox, N. 1995. Nortoba prospect, Dorothea Township, Thunder Bay Mining Division; Thunder Bay Resident Geologist's Office, assessment file AFRI# 52H09NE0008.

Hunt, D.S. 1989. Diamond drill log for Metalore Joint Venture holes 405-018, -019, -020, -021 Placer Dome Inc.; Thunder Bay Resident Geologist's Office, assessment file AFRI# 42E12NW0147.

Hurst, M.E. 1935. Vein formation at Porcupine, Ontario; Economic Geology, v.30, p.103-127.

Jackson, P. 1985. Minerals of the tin mines; *in* Minerals of Tasmania, Combined Mineralogical Societies seminar, p.64-80.

Jébrak, M., Mineau, R., Bardoux, M. and Goulet, N. 1991. Boron cycle in the Abitibi greenstone belt, and compositional variations in tourmaline associated gold deposits; *in* Greenstone gold and crustal evolution; Geological Association of Canada and GAC Mineral Deposits Division, NUNA Conference Volume, p.177.

Kehlenbeck, M.M. 1983. Structural studies in the Beardmore–Geraldton area; *in* Summary of Field Work 1983, Ontario Geological Survey, Miscellaneous Paper 116, p.201-203.

Kerrich, R. and Wyman, D.A. 1997. Review of developments in trace-element fingerprinting of geodynamic settings and their implications for mineral exploration; Australian Journal of Earth Sciences, v.44, p.465-487.

Kilbourne, M.W. 1987. Geological report on the Summers Township property for Stratmin, Summers Township, Thunder Bay Mining Division; Thunder Bay Resident Geologist's Office, assessment file AFRI# 42E12SW0061.

Knox, W.P. 1981. VLF-EM and magnetometer surveys, Ternowsky–Rentz property, for Gold Field Resources Canada, Summers Township, Thunder Bay Mining Division; Thunder Bay Resident Geologist's Office, assessment file AFRI# 42E12SW0082.

Koch, J.A. 1956. The Frisco Mine, Chihuahua, Mexico; Economic Geology, v.51, p.1-40.

Kowalski, B. 1989. Report on geological mapping survey, Sturgeon River grid, Sandra Township, Ontario for Metalore Resources Limited, July through September 1988, volume one, February, 1989; Thunder Bay Resident Geologist's Office, assessment file AFRI# 42E12NE0026.

——— 1995. Geological survey on the Undersill property, Summers Township, Thunder Bay Mining Division; Thunder Bay Resident Geologist's Office, assessment file AFRI# 42E12NW0003.

Kristjansson, L.H. and Thorleifson, F.J. 1987. Quaternary geology of the Beardmore–Geraldton area, District of Thunder Bay; Ontario Geological Survey, Miscellaneous Paper 132, p.368-373.

——— 1991. Quaternary geology and drift prospecting, Beardmore–Geraldton area, Ontario; Geological Survey of Canada, Memoir 435, 146p.

Kurshakova, L.D. 1968. Metasomatism and other physical-chemical processes in petrology; Publishing House Nauka, Moscow, p.289-311.

Lafontaine, A. 1991. Owner's report on the property of Andres LaFontaine, 1991 work program; Thunder Bay Resident Geologist's Office, assessment file AFRI# 42E12SW0010.

——— 1999. Lafontaine–Minnow Lake property, Summers Township, Thunder Bay Mining Division; Thunder Bay Resident Geologist's Office, assessment file 52H09NE.

Lafontaine, A. and Lafontaine, S. 1995a. Report on the Lafontaine–Eva Lake property, Eva Township, Thunder Bay Mining Division; Thunder Bay Resident Geologist's Office, assessment file AFRI# 52H09NE0009.

——— 1995b. Report of work by traditional prospecting, Eva Township, Thunder Bay Mining Division; Thunder Bay Resident Geologist's Office, assessment file AFRI# 52H09NE0010.

——— 1996. Report on the Lafontaine–Eva Lake property, Eva Township, Thunder Bay Mining Division; Thunder Bay Resident Geologist's Office, assessment file 52H09NE MEI-038.

——— 1997. Report on the Lafontaine–Eva Lake property, Eva Township, Thunder Bay Mining Division; Thunder Bay Resident Geologist's Office, assessment file 52H09NE MEI-037.

Laird, H.C. 1937. The western part of the Sturgeon River area (Sturgeon River – Beardmore section); Ontario Department of Mines, Annual Report 1936, v.45, pt.2, p.60-117.

Lamble, B.C. 1959. Letter to Nortoba Mines Limited; Thunder Bay Mining Division; Thunder Bay Resident Geologist's Office, assessment file 52H09NE0015.

Lassila, P. 1995. Report of exploration of the Dorothea Gold property, Dorothea Township, Ontario; Thunder Bay Resident Geologist's Office, assessment file AFRI# 42E12NW0103.

——— 1996. Report on 1996 exploration of the Dorothea Gold property; Thunder Bay Resident Geologist's Office, assessment file AFRI# 42E12NE0233.

——— 1998. The report of the 1997 exploration on the Dorothea Gold property by Poplar Point Explorations Inc., Dorothea Township, Ontario; Thunder Bay Resident Geologist's Office, assessment file 52H09NE MEI-039.

——— 2000. 1999 Prospecting on the Dorothea Gold property, Dorothea Township, Ontario; Thunder Bay Resident Geologist's Office, assessment file 52H09NE.

Lavoie, C. 1987. Magnetic survey on the property owned by Stratmin, Summers Township, Thunder Bay Mining Division; Thunder Bay Resident Geologist's Office, assessment file AFRI# 42E12SW0057.

Lawson, G.E. 1986. Geological investigations in the Oxaline Lake area, near Jellicoe, northern Ontario; unpublished BSc thesis, Brock University, St. Catharines, Ontario, 50p.

LeBas, M.J. 1989. Nephelinitic and basanitic rocks; Journal of Petrology, v.30, p.1299-1312.

——— 2000. IUGS reclassification of the high-Mg and picritic volcanic rocks; Journal of Petrology, v.42, p.1467-1470.

LeBas, M.J., LeMaitre, R.W., Streckeisen, A. and Zanettin, B. 1986. A chemical classification of volcanic rocks on the total alkali-silica diagram; Journal of Petrology, v.27, p.745-750.

LeMaitre, R.W., Bateman, P., Dubek, A., Keller, J., Lameyre, J., LeBas, M.J., Sabine, P.A., Sorensen, H., Streckeisen, A., Woolley, A.R. and Zanettin, B. 1989. A classification of igneous rocks and glossary of terms. Recommendations of the International Union of Geological Sciences subcommission on the systematics of igneous rocks; Blackwell Scientific Publications, Oxford, United Kingdom, 193p.

Lesher, C.M., Goodwin, A.M., Campbell, I.H. and Gorton, M.P. 1986. Trace-element geochemistry of ore-associated and barren, felsic metavolcanic rocks in the Superior Province, Canada; Canadian Journal of Earth Sciences, v.23, p.222-237.

Lesher, C.M. and Stone, W.E. 1996. Exploration geochemistry of komatiites; *in* Trace element geochemistry of volcanic rocks: applications for massive sulphide exploration, Geological Association of Canada, Short Course Notes Volume 12, p.153-204.

Lightfoot, P.C., Hawkesworth, C.J., Olshefsky, K., Green, T., Doherty, W. and Keays, R.R. 1997. Geochemistry of Tertiary tholeiites and picrites from Qeqertarssuaq (Disko Island) and Nuussuaq, West Greenland with implications for the mineral potential of comagmatic intrusions; Contributions to Mineralogy and Petrology, v.128, p.139-163.

Lightfoot, P.C., Keays, R.R. and Doherty, W. 2001. Chemical evolution and origin of nickel sulphide mineralization in the Sudbury Igneous Complex, Ontario, Canada; Economic Geology, v.96, p.1855-1875.

Lightfoot, P.C., Sutcliffe, R.H. and Doherty, W. 1991. Crustal contamination identified in Keweenawan Osler Group tholeiites, Ontario: a trace element perspective; Journal of Geology, v.99, p.739-760.

Lottermoser, B.G. 1992. Rare earth elements and hydrothermal ore formation processes; Ore Geology Reviews, v.7, p.25-41.

Lumpkin, G.R. and Ribbe, P.H. 1979. Chemistry and physical properties of axinites; American Mineralogist, v.64, p.635-645.

MacAdam, R. 1992. Report on the Princess property, Eva Township, Thunder Bay Mining Division; Thunder Bay Resident Geologist's Office, assessment file AFRI# 52H09SE0005.

MacEachern, P. 1989. Diamond drill log for Project No.402 – Archie Lake Option holes 402-001, -002, -003, -004, -005 Placer Dome Inc.; Thunder Bay Resident Geologist's Office, assessment file AFRI# 42E12SW0050.

Mackasey, W.O. 1970a. Geology of Eva Township, District of Thunder Bay, Ontario Department of Mines, Preliminary Map P.601, scale 1:15 840.

——— 1970b. Geology of Summers Township, District of Thunder Bay, Ontario Department of Mines, Preliminary Map P.602, scale 1:15 840.

——— 1975. Geology of Dorothea, Sandra and Irwin townships, District of Thunder Bay, Ontario Division of Mines, Report 122, 83p.

——— 1976. Geology of Walters and Leduc townships, District of Thunder Bay; Ontario Division of Mines, Report 149, 58p.

Mason, J. and White, G. 1986. Gold occurrences, prospects, and deposits of the Beardmore–Geraldton area, districts of Thunder Bay and Cochrane; Ontario Geological Survey, Open File Report 5630, v.1 and v.2, 670p.

McDonough, W.F. and Sun, S.-S. 1995. The composition of the earth; Chemical Geology, v.120, p.223-253.

McKay, G.A., Cormie, A.M. and Coulson, C.J. 1948. Leitch Mine; *in* Structural geology of Canadian ore deposits, Canadian Institute of Mining and Metallurgy, Jubilee Volume, p.385-389.

Middlemost, E.A.K. 1989. Iron oxidation ratios, norms and the classification of volcanic rocks; Chemical Geology, v.77, p.19-26.

Morin, D., Jébrak, M., Bardoux, M. and Goulet, N. 1993. Pontiac metavolcanic rocks within the Cadillac tectonic zone, McWatters Township, Abitibi Belt, Quebec; Canadian Journal of Earth Sciences, v.30, p.1521-1531.

Nakamura, N. 1974. Determination of REE, Ba, Fe, Mg, Na, and K in carbonaceous and ordinary chondrites; Geochimica et Cosmochimica Acta, v.38, p.757-775.

Naldrett, A.J., Duke, J.M., Lightfoot, P.C. and Thompson, J.F.H. 1984. Quantitative modelling of the segregation of magmatic sulphides: an exploration guide; Canadian Institute of Mining and Metallurgy, Bulletin, v.77, no.864, p.46-55.

Naldrett, A.J. and Lightfoot, P.C. 1993. Ni-Cu-PGE ores of the Noril'sk region, Siberia: a model for giant magmatic sulfide deposits associated with flood basalts; *in* Giant ore deposits, Society of Economic Geologists, Special Publication Volume 2, p.81-123.

Nekrasov, I.Y. and Kashirtseva, G.A. 1975. Hydrothermal synthesis of stanniferous axinite; Doklady of the Academy of Sciences of the USSR, Earth Sciences Section, v.222, p.440-443.

Nelson, B. 1989. Report on the geology, geochemistry, VLF-EM–magnetic surveys and diamond drilling, Eva Township, Thunder Bay Mining Division; Thunder Bay Resident Geologist's Office, assessment file AFRI# 52H09SE0002.

O'Brien, M.S. 1985. A detailed geological study of the mafic metavolcanic rocks north of Poplar Lodge, Ontario; unpublished BSc, thesis, Lakehead University, Thunder Bay, Ontario, 86p.

Oja, R.V. 1970. Report on the properties of Meridian Mining and Exploration Company, Thunder Bay Mining Division; Thunder Bay Resident Geologist's Office, assessment file, AFRI# 52H09NE0022 and 8104.

Ontario Geological Survey 1998. Airborne magnetic and electromagnetic surveys, processed data and derived products: Geraldton–Tashota area; Ontario Geological Survey, Data Sets 1031 and 1032.

——— 1999. Ontario drill hole database; Ontario Geological Survey, Data Set 13.

——— 2000. Mineral deposit inventory of Ontario (version 2–July 2000); Ontario Geological Survey, Digital Data.

——— 2002. Phoenix Bedrock Mapping Project: whole rock lithogeochemical and assay data, mineral deposit information, and diamond drill hole compilation of the Kitto, Eva, Summers, Dorothea, and Sandra townships, Beardmore area, northwestern Ontario; Ontario Geological Survey, Miscellaneous Release—Data 105.

Osmani, I.A. 1991. Proterozoic mafic dike swarms in the Superior Province of Ontario; *in* Geology of Ontario, Ontario Geological Survey, Special Volume 4, Part 1, p.661-681.

Ozaki, M. 1972. Chemical composition and occurrence of axinite; Kumamoto Journal of Scientific Geology, v.9, p.1-34.

Paul, D. 1988. Diamond drill log for Edda Resources – Mill City Gold holes BRD-88-01, -02, -03, -04, -05, -07 E.H. van Hees Geological Services Inc.; Thunder Bay Resident Geologist's Office, assessment file AFRI# 42E12NW0150.

Pearce, J.A. 1982. Trace element characteristics of lavas from destructive plate boundaries; *in* Andesites, orogenic andesites and related rocks, John Wiley and Sons, Chichester, United Kingdom, p.525-548.

Percival, J. and Sullivan, R.W. 1988. Age constraints on the evolution of the Quetico Belt, Superior Province, Ontario; *in* Radiogenic and Isotopic Studies: Report 2, Geological Survey of Canada, Paper 88-2, p.97-107.

Pettijohn, F.J. 1975. Sedimentary rocks, 3rd ed.; Harper & Row, Publishers, Inc., New York, 628p.

Pringle, I.J. and Kawachi, Y. 1980. Axinite mineral group in low-grade regionally metamorphosed rocks in southern New Zealand; American Mineralogist, v.65, p.1119-1129.

Pudifin, A.D. 1987. Report on exploration program, Parquet Resources (Holmwood Option), Sandra and Meader townships, Thunder Bay Mining Division; Thunder Bay Resident Geologist's Office, assessment file AFRI# 42E12NW0160.

Pye, E.G., Harris, F.R., Fenwick, K.G. and Baillie, J. 1966. Tashota–Geraldton sheet, Thunder Bay and Cochrane districts; Ontario Department of Mines, Map 2102, scale 1:253 440.

Ray, G.E. and Dawson, G.L. 1994. The geology and mineral deposits of the Hedley gold skarn district, southern British Columbia; British Columbia Ministry of Energy, Mines and Petroleum Resources, Bulletin 87, 156p.

Reilly, B.A. 1988. Structural analysis of the Paint Lake deformation zone, northern Ontario; Uunpublished MSc thesis, Brock University, St. Catharines, Ontario, 182p.

Reilly, B.A. and Williams, H.R. 1986. Structural geology of the Paint Lake Fault systems in Walters, Leduc, and Legault townships of northeastern Ontario; Geological Association of Canada – Mineralogical Association of Canada, Program with Abstracts, v.11, p.117.

——— 1987. Spatial and temporal relationships of C'-fabric within the Paint Lake deformation zone, northwestern Ontario; Geological Association of Canada – Mineralogical Association of Canada, Program with Abstracts, v.12, p.83.

Rennick, M.W. 1988. Report on the Cryderman Gold Inc., Sand River property, Eva Township, Thunder Bay Mining Division; Thunder Bay Resident Geologist's Office, assessment file AFRI# 52H09NE0004.

Richardson, W. 1988. Report on a VLF-EM survey and magnetic survey, Undersill claims, Eva Township, Thunder Bay Mining Division; Thunder Bay Resident Geologist's Office, assessment file AFRI# 52H09SE0006.

Robert, F. 1996. Quartz-carbonate vein gold; *in* Geology of Canadian mineral deposit types, Geological Survey of Canada, Geology of Canada, no.8, p.350-366.

Robinson, S.D. 1983. An axinite vein cutting amphibolite, Bishop Corners, Frontenac County, Ontario; unpublished BSc thesis, Queen's University, Kingston, Ontario, 40p.

Sabina, A.P. 1987. Rocks and minerals for the collector, La Ronge – Creighton, Saskatchewan, Flin Flon – Thompson, Manitoba; Geological Survey of Canada, Miscellaneous Report 42, p.54-55.

——— 1991. Rocks and minerals for the collector, Sudbury to Winnipeg; Geological Survey of Canada, Miscellaneous Report 49, p.143.

——— 1992. Rocks and minerals for the collector, the Alaska Highway: Dawson Creek, British Columbia to Yukon/Alaska border; Geological Survey of Canada, Miscellaneous Report 50, p.21-22.

——— 2000. Rocks and minerals for the collector, Cobalt–Belleterre–Timmins, Ontario and Quebec; Geological Survey of Canada, Miscellaneous Report 57, p.43-44, p.48-49, p.78-79, p.82, p.100, p.141-143, p.158-161, p.167.

Sandar, G.W. 1984. Report on the combined helicopter-borne gamma ray spectrometer survey, on behalf of Metalore Sources Limited: in the Beradmore area, northwestern Ontario, September 28, 1984; Thunder Bay Resident Geologist's Office, assessment file AFRI# 42E12NE0045.

Sanero, E. and Gottardi, G. 1968. Nomenclature and crystal chemistry of axinites; American Mineralogist, v.53, p.1407-1411.

Satterly, J. 1977. A catalogue of the Ontario localities represented by the mineral collection of the Royal Ontario Museum; Ontario Geological Survey, Miscellaneous Paper 70, p.54.

Scime, V.J. 1989. Geophysical report on the Spooner property, Parklane Technologies, Summers Township, Thunder Bay Mining Division; Thunder Bay Resident Geologist's Office, assessment file AFRI# 42E12SW0053.

Serdyuchenko, D.P. and Makarov, V.N. 1971. New data on magnesium-iron axinite from Pechenga and on the chemical composition of axinite in general; Doklady of the Academy of Sciences of the USSR, Earth Sciences Section, v.197, p.128-130.

Shanks, W.S. 1990. Geology of the Eva and Summers townships, District of Thunder Bay; *in* Summary of Field Work and Other Activities 1990, Ontario Geological Survey, Miscellaneous Paper 151, p.111-116.

——— 1993. Geology of Eva and Summers townships, District of Thunder Bay; Ontario Geological Survey, Open File Report 5821, 93p.

Smith, D. and Silver, C.T. 1975. Potassic granophyre associated with Precambrian diabase, Sierre Ancha, central Arizona; Geological Society of America Bulletin, v.86, p.503-573.

Sonnet, P. and Verkaeren, J. 1989. Scheelite-, malayaite-, and axinite-bearing skarns from El Hammam, central Morocco; Economic Geology, v.83, p.575-590.

Speed, A.A. and Craig, S. 1992. Beardmore–Geraldton historical research project; Ontario Geological Survey, Open File Report 5823, 283p.

Sproule, R.M. 1987. Report to Legion Resources Limited on their property in Summers Township, District of Thunder Bay, Ontario, April, 1987; Thunder Bay Resident Geologist's Office, assessment file AFRI# 42E12SW0065.

Stott, G.M. 1984. Lake Nipigon sheet, Thunder Bay District; Ontario Geological Survey, Preliminary Map P.257 (revised), scale 1:126 720.

Sun, S.-S. and McDonough, W.F. 1989. Chemical and isotopic systematics of oceanic basalts: implications for mantle compositions and processes; *in* Magmatism in the ocean basins, Geological Society, Special Publication No. 42, p.313-345.

Sutcliffe, R.H. 1981. Geology of the Wabigoon–Quetico Subprovince boundary in the Lake Nipigon area, District of Thunder Bay; *in* Summary of Field Work, Ontario Geological Survey, Miscellaneous Paper 100, p.26-29.

——— 1982a. Precambrian geology of the Wabigoon–Quetico Subprovince boundary, Grand Bay sheet, District of Thunder Bay; Ontario Geological Survey, Preliminary Map 2528, scale 1:50 000.

——— 1982b. Precambrian geology of the Wabigoon–Quetico Subprovince boundary, Shakespeare Island sheet, District of Thunder Bay; Ontario Geological Survey, Preliminary Map 2529, scale 1:50 000.

——— 1982c. Precambrian geology of the Wabigoon–Quetico Subprovince boundary, Orient Bay sheet, District of Thunder Bay; Ontario Geological Survey, Preliminary Map 2530, scale 1:50 000.

——— 1982d. Precambrian geology of the Wabigoon–Quetico Subprovince boundary, Black Sturgeon Lake sheet, District of Thunder Bay; Ontario Geological Survey, Preliminary Map 2531, scale 1:50 000.

——— 1986. Proterozoic rift-related igneous rocks at Lake Nipigon, Ontario; unpublished PhD thesis, University of Western Ontario, London, Ontario, 325p.

——— 1987. Petrology of Middle Proterozoic diabases and picrites from Lake Nipigon, Canada; Contributions to Mineralogy and Petrology, v.96, p.201-211.

——— 1991. Proterozoic geology of the Lake Superior area; *in* Geology of Ontario, Ontario Geological Survey, Special Volume 4, Part 1, p.405-484.

Sutcliffe, R.H. and Greenwood, R.C. 1985. The geology of Eva and Kitto townships ultramafic intrusion; Figure 1, scale 1:50 000; *in* Precambrian geology of the Lake Nipigon area, Livingstone Point sheet, District of Thunder Bay; Ontario Geological Survey, Preliminary Map P.2839, scale 1:50 000.

Teare, P.S. 1937. Summary report of examination of Montmorr Gold Mines Ltd., Eva Township, Thunder Bay Mining Division; Thunder Bay Resident Geologist's Office, assessment file AFRI# 52H09NE0012.

Thompson, W.H. 1972. Duncanex Resources: Jones–Sijpkens property, diamond drill logs, Summers Township, Thunder Bay Mining Division; Thunder Bay Resident Geologist's Office, assessment file AFRI# 42E12SW0100.

Thorsteinson, D. 1984. Diamond drill log for Summers property hole S84-1, Thorlo Gold Finders Inc.; Thunder Bay Resident Geologist's Office, assessment file AFRI# 42E12SW0077.

Tomlinson, K.Y. 1996. The geochemistry and tectonic setting of Early Precambrian greenstone belts, northern Ontario, Canada; unpublished PhD thesis, University of Portsmouth, Portsmouth, United Kingdom, 287p.

Tomlinson, K.Y., Hall, R.P., Hughes, D.J. and Thurston, P.C. 1996. Geochemistry and assemblage accretion of metavolcanic rocks in the Beardmore–Geraldton greenstone belt, Superior Province; Canadian Journal of Earth Sciences, v.33, p.1520-1533.

Tomlinson, K.Y., Davis, D.W., Percival, J.A., Hughes, D.J. and Thurston, P.C. 1999. Neoarchean supracrustal development in the central Wabigoon subprovince: Nd isotope data and U/Pb geochronology; *in* Western Superior Transect, Lithoprobe Report 70, Lithoprobe Secretariat, University of British Columbia, Vancouver, British Columbia, p.147-155.

Tough, S. and Gledhill, T. 1979. Report on Cryderman (Sand River) property for Camel Resources, Eva Township, Thunder Bay Mining Division; Thunder Bay Resident Geologist's Office, assessment file AFRI# 52H09SE0010.

TVX Normandy 2002. Operations, New Britannia Mine, February 4, 2002. http://www.tvxgold.com/properties/mines/newb.htm (web pages accessed July 29, 2002).

Tyson, A.E. 1945. Report on gold belts in the Little Long Lac – Sturgeon River district; Canadian Mining Journal, v.66, p.839-850.

Vallance, T.G. 1966. A contact metamorphic axinite paragenesis at London Bridge, near Queanbeyan, N.S.W.; Journal and Proceedings of the Royal Society of New South Wales, v.99, p.57-67.

Verma, S.P., Torres-Alvarado, I.S. and Sotelo-Rodriguez, Z.T. 2002. SINCLAS: standard igneous norm and volcanic rock classification system; Computers and Geosciences, v.28, p.711-715.

Wanless, R.K. and Loveridge, W.D. 1978. Rubidium-strontium isochron age studies: Report 2 (Canadian Shield); Geological Survey of Canada, Paper 77-14, 70p.

Waring, H.G. 1937. Report on Murphy claims, Eva and Summers townships, Thunder Bay Mining Division; Thunder Bay Resident Geologist's Office, assessment file AFRI# 52H09SE0012.

Williams, H.R. 1986. Structural studies in the Beardmore–Geraldton belt, northern Ontario; *in* Geoscience Research Programs, Summary of Research 1985-86, Ontario Geological Survey, Miscellaneous Paper 130, p.138-146.

——— 1987a. Ontario Geoscience Research Grant Program, Grant #242: Structural studies in the Wabigoon and Quetico subprovinces; Ontario Geological Survey, Open File Report 5668, 163p.

——— 1987b. Structural studies in the Beardmore–Geraldton belt and in the Quetico and Wawa subprovinces; *in* Summary of Field Work and Other Activities 1987, Ontario Geological Survey, Miscellaneous Paper 137, p.90-92.

——— 1989. Geological studies in the Wabigoon, Quetico, and Abitibi–Wawa subprovinces, Superior Province of Ontario, with an emphasis on the structural development of the Beardmore–Geraldton belt; Ontario Geological Survey, Open File Report 5724, 189p.

——— 1991. Quetico Subprovince; *in* Geology of Ontario, Ontario Geological Survey, Special Volume 4, Part 1, p.383-403.

Wilson, A.W.G. 1910. Geology of the Nipigon Basin, Ontario; Canada Department of Mines, Geological Survey Branch, Memoir 1, 152p.

Wood, D.A. 1980. The application of a Th–Hf–Ta diagram to problems of tectonomagmatic classification and to establishing the nature of crustal contamination of basaltic lavas of the British Tertiary volcanic province; Earth and Planetary Science Letters, v.50, p.11-30.

Wood, D.H. 1996a. Geology and geochemistry of the Partizan Zn-Pb skarn deposit, Dal'neggorsk, Primorye, Russian Far East; unpublished MSc thesis, Washington State University, Pullman, Washington, 91p.

——— 1996b. Geology and geochemistry of the Ftoroy Sovietskiy Mine (Partizan Zn-Pb skarn deposit), Dal'negorsk, Primorye, Russian Far East; Geological Society of America, Abstracts with Programs, v.28, no.7, p.A151.

Wood, D.H., Palmer, M.R., Carpenter, S.B. and Nosenko, N.A. 1997. Preliminary geological and geochemical results from the studies of the Dal'negorsk borosilicate skarn deposit, Dal'negorsk, Primorye region, Russian Far East; Geological Society of America, Abstracts with Programs, v.29, no.6, p.A62.

Yta, M., Moreno-Tovar, R., Cordoba-Mendez, D.A. and Patiyo-Cardona, F. 1996. Mineral events at the Zimapan mining district, Hidalgo, Mexico; Geological Society of America, Abstracts with Programs, v.28, no.7, p.A475.

Zamudio, J.A. 1986. Mineralogy and paragenesis of vein and manto deposits at the Frisco Mine, Chihuahua, Mexico; unpublished MSc thesis, University of Colorado, Boulder, Colorado, 96p.

Zoltai, S.C. 1967. Glacial features in the north-central Lake Superior region, Ontario, Canada; Canadian Journal of Earth Sciences, v.4, p.515-528.

Metric Conversion Table

Conversion from SI to Imperial			**Conversion from Imperial to SI**		
SI Unit	*Multiplied by*	*Gives*	*Imperial Unit*	*Multiplied by*	*Gives*
			LENGTH		
1 mm	0.039 37	inches	1 inch	**25.4**	mm
1 cm	0.393 70	inches	1 inch	**2.54**	cm
1 m	3.280 84	feet	1 foot	**0.304 8**	m
1 m	0.049 709	chains	1 chain	20.116 8	m
1 km	0.621 371	miles (statute)	1 mile (statute)	**1.609 344**	km
			AREA		
1 cm^2	0.155 0	square inches	1 square inch	**6.451 6**	cm^2
1 m^2	10.763 9	square feet	1 square foot	**0.092 903 04**	m^2
1 km^2	0.386 10	square miles	1 square mile	2.589 988	km^2
1 ha	2.471 054	acres	1 acre	0.404 685 6	ha
			VOLUME		
1 cm^3	0.061 023	cubic inches	1 cubic inch	**16.387 064**	cm^3
1 m^3	35.314 7	cubic feet	1 cubic foot	0.028 316 85	m^3
1 m^3	1.307 951	cubic yards	1 cubic yard	0.764 554 86	m^3
			CAPACITY		
1 L	1.759 755	pints	1 pint	0.568 261	L
1 L	0.879 877	quarts	1 quart	1.136 522	L
1 L	0.219 969	gallons	1 gallon	**4.546 090**	L
			MASS		
1 g	0.035 273 962	ounces (avdp)	1 ounce (avdp)	28.349 523	g
1 g	0.032 150 747	ounces (troy)	1 ounce (troy)	**31.103 476 8**	g
1 kg	2.204 622 6	pounds (avdp)	1 pound (avdp)	**0.453 592 37**	kg
1 kg	0.001 102 3	tons (short)	1 ton (short)	**907.184 74**	kg
1 t	1.102 311 3	tons (short)	1 ton (short)	**0.907 184 74**	t
1 kg	0.000 984 21	tons (long)	1 ton (long)	**1016.046 908 8**	kg
1 t	0.984 206 5	tons (long)	1 ton (long)	**1.016 046 90**	t
			CONCENTRATION		
1 g/t	0.029 166 6	ounce (troy)/ ton (short)	1 ounce (troy)/ ton (short)	34.285 714 2	g/t
1 g/t	0.583 333 33	pennyweights/ ton (short)	1 pennyweight/ ton (short)	1.714 285 7	g/t

OTHER USEFUL CONVERSION FACTORS

	Multiplied by	
1 ounce (troy) per ton (short)	31.103 477	grams per ton (short)
1 gram per ton (short)	0.032 151	ounces (troy) per ton (short)
1 ounce (troy) per ton (short)	20.0	pennyweights per ton (short)
1 pennyweight per ton (short)	0.05	ounces (troy) per ton (short)

Note: Conversion factors which are in bold type are exact. The conversion factors have been taken from or have been derived from factors given in the Metric Practice Guide for the Canadian Mining and Metallurgical Industries, published by the Mining Association of Canada in co-operation with the Coal Association of Canada.

M46

MAPS NOT FILMED

CARTES NON REPRODUITES

micromedia
a division of IHS Canada

20 Victoria Street
Toronto, Ontario M5C 2N8
Tel.: (416) 362-5211
Toll Free: 1-800-387-2689
Fax: (416) 362-6161
Email: info@micromedia.on.ca